Hyperglycaemia in acute ischaemic stroke: Brain imaging studies in a rodent model of stroke

Lisa Roy

BSc (Hons), MRes

Submitted in fulfilment of the requirements for the degree of Doctor of Philosophy to the Institute of Neuroscience and Psychology, College of Medical, Veterinary and Life Sciences, University of Glasgow

September, 2015

Abstract

Hyperglycaemia on admission is a frequent finding in acute ischaemic stroke patients. This post-stroke hyperglycaemia (PSH) is associated with a poor clinical outcome independent of age and stroke severity. Evidence from clinical stroke studies indicates that hyperglycaemia is associated with a worse outcome in non-diabetic compared to diabetic stroke patients, but the mechanisms underlying this association are poorly understood. Previous in-house studies reported that hyperglycaemia, at clinically-relevant blood glucose levels, exacerbated the evolution of early ischaemic damage in a non-diabetic rat stroke model, indicating that the detrimental effects of hyperglycaemia occur early following the onset of focal cerebral ischaemia. In ischaemic stroke the severity and duration of ischaemia are the major determinants of acute brain damage and therefore a potential mechanism by which hyperglycaemia exacerbates ischaemic damage could be through an influence on tissue perfusion. The studies in this thesis aimed to test the hypothesis that hyperglycaemia exacerbates early ischemic damage by increasing the severity of the cerebral blood flow (CBF) deficit. Initial studies were performed to optimise a rodent model with clinically relevant blood glucose levels before and after focal cerebral ischaemia induced by permanent middle cerebral artery occlusion (MCAO). This animal model was then used in subsequent studies to assess the effect of hyperglycaemia on the CBF deficit after MCAO. The CBF deficit was assessed using two different methods: ^{99m}Tc-HMPAO blood flow autoradiography and MRI perfusion imaging. Each method offered its own advantages, for example, ^{99m}Tc-HMPAO autoradiography produces blood flow images with high spatial resolution enabling detailed semi-quantitative region of interest analysis and MRI perfusion imaging allowed repeated, quantitative CBF measurements at multiple time points after stroke. In addition, the use of MRI enabled concurrent diffusion weighted images to be acquired in order to assess the evolution of acute ischaemic damage and final T_2 defined infarct volume. The results demonstrate that hyperglycaemia exacerbates acute ischaemic damage induced by MCAO but not the perfusion deficit as measured by both ^{99m}Tc-HMPAO autoradiography and MRI. These findings suggest that the primary mechanism of hyperglycaemia-associated ischaemic damage is not mediated by an increase in the severity of ischaemia. Alternatively, the harmful effects of hyperglycaemia may

be predominantly mediated in the brain parenchyma. However Western blot analysis of ischaemic brain tissue showed that glucose treatment resulted in only minor changes in the levels of the calpain substrates MAP2 and αII-spectrin. Thus, the predominant mechanism exacerbated by hyperglycaemia does not appear to be calpain-mediated proteolysis, raising the possibility that hyperglycaemia affects many different mechanisms simultaneously.

Table of Contents

List of Tables

List of Figures

Chapter 1

Chapter 2

Chapter 5

Chapter 6

Acknowledgements

First and foremost I would like to thank my supervisors, Dr Debbie Dewar and Professor Mhairi Macrae for their continued support, encouragement and guidance over the past 4 years. It has been greatly appreciated and I can't thank you both enough. I would also like to extend my thanks to Dr Chris McCabe for his help and guidance throughout my PhD and during my thesis write-up. In addition I would also like to thank the Medical Research Council for funding this research.

I would like to say a massive thank you to all the staff at the Wellcome Surgical Institute and the Glasgow experimental MRI centre: Lindsay Gallagher, Linda Carberry, Ann Marie Colquhoun, Jim Mullin and William Holmes for all their help and support over the last 4 years. In particular I would like to thank Linda Carberry who cut all of the brain tissue for my autoradiography study and to Lindsay Gallagher who helped generate the 2 hour MCAO tissue in Chapter 6. Also, many thanks to Dr Mark McLaughlin for teaching me the Western blot technique and for his help and support during the final year of my PhD.

I would also like to thank some of the students who have contributed to this research. Thank you to MRes student Kathleen MacDonald who did the ROI analysis in Chapter 4 and also MRes student Evelina Avizaite and BMedSci student Michael Burns who did the MAP2 analysis in Chapter 6.

I would also like to thank my fellow students at the University of Glasgow: Emma R, Dave, Ashleigh, Emma B, Emma M, Vicky, Tristan, Mass, and Mariana. Thank you so much for keeping spirits high and for making my PhD such an enjoyable experience.

I also have to thank my wonderful family and my amazing fiancé John for all of their love, encouragement and support over these last few years. I could never have completed this without you guys.

Finally, I want to say thank you to my amazing Dad, Alfred Roy who passed away last year. Without him this would never have been possible. I dedicate this thesis to him.

Author's Declaration

I declare that, except where explicit reference is made to the contribution of others, this dissertation is the result of my own work and has not been submitted for any other degree at the University of Glasgow or any other institution.

Lisa Roy

Published Manuscripts

Tarr, D., Graham, D., **Roy, L. A**., Holmes, W. M., McCabe, C., Macrae, I. M., Muir, K., Dewar, D. (2013). Hyperglycaemia accelerates apparent diffusion coefficient-defined lesion growth after focal cerebral ischaemia in rats with and without features of the metabolic syndrome. J Cereb Blood Flow Metab, 33, 1556-63.

Abstracts

Roy, L. A., Macrae, I, M., Dewar, D. (2012). Hyperglycaemia and animal models of stroke. The Integrative Mammalian Biology Symposium, University of Glasgow.

Roy, L. A., Tarr, D., Muir, K., Macrae, I, M., Dewar, D. (2012). The effects of hyperglycaemia on ischaemic damage in different rat models of focal cerebral ischaemia. Scottish Neuroscience Group meeting 2012. University of Dundee.

Roy, L. A., Holmes, W. M., Muir, K., Macrae, I, M., Dewar, D. (2014). Exacerbation by hyperglycemia of lesion growth after focal cerebral ischemia is not due to greater severity of the initial cerebral blood flow deficit. Society for Neuroscience, Washington DC.

List of Abbreviations

1x T-TBS	1xTris-buffered saline containing Tween-20
^{99m}Tc-HMPAO	Technetium- 99m hexamethylpropyleamine oxime
ADC	apparent diffusion coefficient
AMPA	α-amino-3-hydroxyl-5-methyl-4-isoxazole-propionate
ASL	arterial spin labelling
ATP	adenosine triphosphate
AUC	area under the curve
BCA	bicinchoninic acid
Ca^{2+}	calcium ion
CBF	cerebral blood flow
CBV	cerebral blood volume
CCA	common carotid artery
CPP	cerebral perfusion pressure
CT	computed tomography
DEFUSE	diffusion and perfusion imaging evaluation for understanding stroke evolution trial
DIAS	Desmoteplase in acute ischaemic stroke trial
DD	distal diathermy
DTT	dithiothreitol
DWI	diffusion weighted imaging
ECA	external carotid artery
ECG	electrocardiogram
ECL	enhanced chemi-luminescence
EPI	echo planar imaging
ffSHRSP	fructose fed spontaneously hypertensive stroke-prone rats
FMZ	flumazenil
GIST-UK	Glucose Insulin in Stroke Trial UK
HB	homogenate buffer
HMW	high molecular weight
HRP	horseradish peroxidise
HT	haemorrhagic transformation
IAP	[^{14}C]-iodoantipyrine
ICA	internal carotid artery

ICV	inferior cerebral vein
ILF	intraluminal filament
IP	intraperitoneal
KX	ketamine/xylazine
LDL	low density lipoprotein
MABP	mean arterial blood pressure
MAP2	microtubule associated protein 2
MAPs	microtubule-associated proteins
MCA	middle cerebral artery
MCAO	middle cerebral artery occlusion
MRI	magnetic resonance imaging
MTT	mean transit time
Na^+/K^+-ATPase	sodium-potassium adenosine triphosphatase
NCX	sodium-calcium exchanger
NHS	National Health Service
NINDS	National Institute of Neurological Disorders and Stroke
NMDA	*N*-methyl-D-aspartate
NO	nitric oxide
OD	optical density
$PaCO_2$	arterial carbon dioxide tension
PAI-1	plasminogen activator inhibitor type 1
PaO_2	arterial oxygen tension
pCASL	pseudo-continuous arterial spin labelling
PCT	perfusion computed tomography
PET	positron emission tomography
PI	perfusion imaging
PIDs	peri-infarct depolarisations
PI-DWI mismatch	perfusion-diffusion mismatch
PSH	post-stroke hyperglycaemia
RARE	rapid acquisition with refocused echoes
RM-2way ANOVA	repeated measures two-way analysis of variance
RNS	reactive nitrogen species
ROI	region of interest
ROS	reactive oxygen species
rt-PA	recombinant tissue plasminogen activator

SAINT I	Stroke–Acute Ischaemic NYX Treatment I
SBDPs	spectrin breakdown products
SD	Sprague Dawley rat
SDS-PAGE	sodium dodecyl sulphate polyacrylamide gel electrophoresis
SHINE	Stroke Hyperglycaemia Insulin Network Effort
SHRSP	spontaneously hypertensive stroke prone rat
SE-EPI	Spin Echo-Echo Planar Imaging
STAIR	Stroke Therapy Academic Industry Roundtable
TE	echo time
TGC	tight glycaemic control
THIS	treatment of hyperglycaemia in acute stroke trial
TIA	transient ischaemic attacks
TR	repetition time
TTC	2,3,5-triphenyltetrazolium chloride
WKY	Wistar Kyoto rat

Chapter 1 - Introduction

1. Introduction

1.1 Stroke

1.1.1 Incidence and classification

Stroke is the fourth most common cause of death in the UK and the second worldwide. In the UK there are approximately 152,000 strokes per year which leads to approximately 40,000 deaths (Stroke.org.uk, 2015). The death rate from stroke varies between countries and regions, with parts of Scotland having some of the highest in the UK (Townsend et al., 2014). Between 1990 and 2010, the incidence of stroke fell across the UK, in part due to improvements in stroke prevention and increasing awareness of healthy living (Krishnamurthi et al., 2013). However, it is projected that the incidence of stroke will increase in the coming decades in developed countries due to the ageing population and expected increase in population size (Truelsen et al., 2006).

The majority of strokes are not fatal and as a result stroke is the largest cause of severe disability. More than half of stroke survivors are left with a disability and a third are dependent on others for tasks of daily living (Stroke.org.uk, 2015). Stroke is therefore a huge burden on the National Health Service (NHS) and economy. From the most recent academic and National Audit office's analyses, the estimated health and social care costs of stroke to the UK are approximately £4.4 billion per year (Stroke.org.uk, 2015). When taking into account informal care costs and those to the wider economy this figure approaches £9 billion (Saka et al., 2009). Despite the huge economic burden of stroke, stroke research in the UK is extremely underfunded compared to diseases with similar economic burden such as cancer and heart disease. For example, the social and healthcare costs of coronary heart disease and stroke were similar in 2012 yet the UK research spend for stroke was less than a third of that on coronary heart disease (Luengo-Fernandez et al., 2015).

The World Health Organisation's definition of stroke is: "rapidly developing clinical signs of focal (or global) disturbance of cerebral function, lasting more than 24 hours or leading to death, with no apparent cause other than that of vascular origin" (WHO, 1988). Transient ischaemic attacks (TIA) have the same

clinical features of stroke but symptoms can resolve within 24 hours. A TIA should be considered as a warning sign of stroke or other cardiovascular complications given that 15 to 30% of cerebral infarctions are preceded by a TIA (Hankey and Warlow, 1999, Rothwell and Warlow, 2005).

The vascular mechanisms leading to stroke can be classified as ischaemic and haemorrhagic. Haemorrhagic strokes account for 15% of all cases of stroke and occur when a blood vessel ruptures either within the brain (intracerebral haemorrhage) or on the surface of the brain (subarachnoid haemorrhage). Due to the leakage of blood into the brain tissue at high pressures, haemorrhagic strokes are generally more severe and are associated with a higher rate of mortality compared with ischaemic strokes ((SSNAP), 2014).

Ischaemic strokes are more common than haemorrhagic strokes, accounting for 85% of all stroke cases. Ischaemic stroke results from a sudden reduction in blood flow to an area of the brain. The reduction in cerebral blood flow (CBF) results from the formation of a blood clot which can arise in one of two ways: associated with an atherosclerotic plaque in a damaged artery within or leading to the brain (thrombotic stroke), or a clot that forms elsewhere in the body which then travels to the brain where it blocks a cerebral artery (embolic stroke). Blood clots (emboli) which form in the heart account for 18-25% of all ischaemic strokes (Figure 1.1) (Arboix, 2014). The cause of the cardiac embolus is most commonly atrial fibrillation but can also arise in many other conditions including; dilated cardiomyopathy, endocarditis and patent foramen ovale (Arboix, 2010). Compared with other ischaemic stroke subtypes, cardioembolic stroke has the highest rate of in-hospital mortality (Murtagh and Smalling, 2006, Arboix, 2014).

Ischaemic stroke arising from an atherosclerotic plaque is the most common, accounting for approximately 50% of all ischaemic strokes (Warlow et al., 2003). Atherosclerotic plaques develop when the inner lining of a blood vessel, the endothelium, becomes damaged due to underlying factors such as hypertension or hypercholesterolemia. Damage to the endothelium eventually leads to endothelial dysfunction and the accumulation of substances such as cholesterol, fats and cellular debris at the site of damage. This initiates an inflammatory response and leads to the infiltration of inflammatory cells that interact with

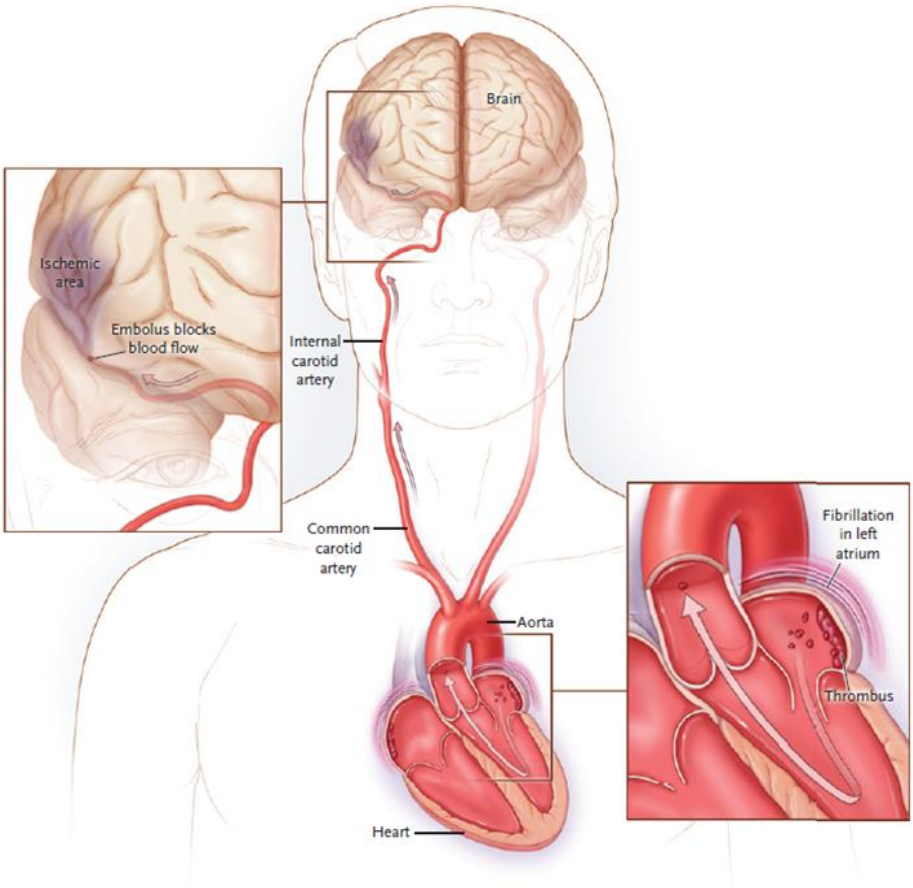

Figure 1.1. Ischaemic stroke arising from a cardiac embolus. Stroke arising from a cardiac embolus accounts for around a quarter of all cases of ischaemic stroke. Cardiac emboli can result from a number of conditions including: atrial fibrillation, dilated cardiomyopathy, endocarditis and patent foramen ovale. Reproduced with permission from (Go, 2009), Copyright Massachusetts Medical Society.

low density lipoprotein (LDL) cholesterol and are converted into macrophages. The macrophages engulf LDL and by doing so are transformed into foam cells which accumulate and form the basis of the atherosclerotic plaque. Over time, plaques can increase in size, narrowing the blood vessel and restricting the flow of blood (Figure 1.2). The atherosclerotic plaque can rupture, leading to the formation of a thrombus, which can occlude the vessel and prevent the flow of blood (Figure 1.2).

Ischaemic strokes can also arise from lacunar or small vessel occlusions. This subtype of stroke accounts for a quarter of all ischaemic stroke cases and results from the occlusion of one of the deep penetrating arteries by microatheroma or lipohyalinosis (Jickling et al., 2011). These vessels are small and highly susceptible to damage induced by conditions such as hypertension. Brain injury from lacunar strokes is smaller than other stroke subtypes and as such they are generally associated with more favourable outcomes (Petty et al., 2000).

The signs and symptoms of ischaemic stroke can vary depending of the vascular territory affected. The most common, visible signs of stroke include: facial weakness, hemiparesis of the left or right limbs (upper and lower) and slurred speech. These signs are featured in the acronym, FAST- Face Arm Speech Time established in the UK to inform the public on how to recognize the signs of stroke and to understand the importance of emergency treatment. Other symptoms of stroke include: a sudden severe headache, blurred vision or loss of sight, and sudden confusion.

1.1.2 Risk factors

1.1.2.1 Non-modifiable Risk factors

Age, gender, race and ethnicity are examples of non-modifiable risk factors for stroke. Whilst it is not possible to modify such factors, they can be used to identify those patients that are most at risk and who might benefit from preventative treatment.

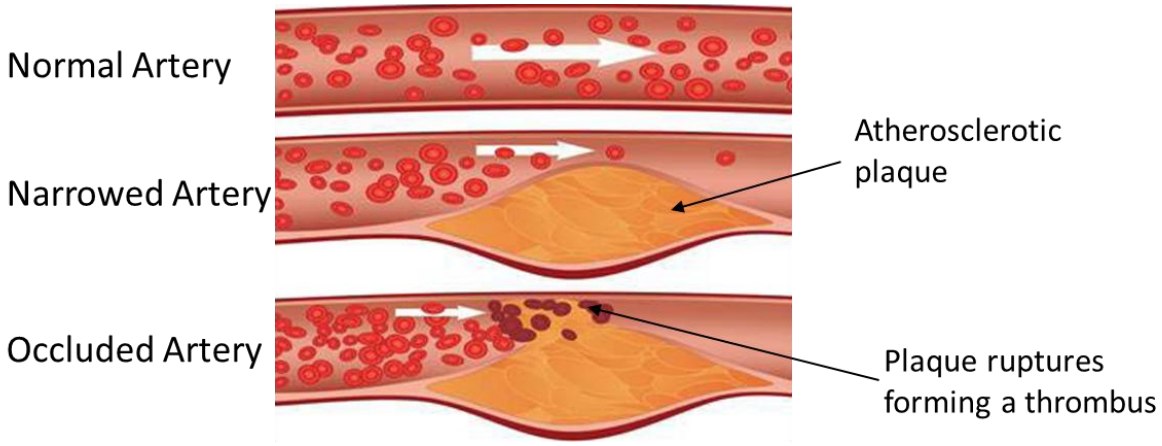

Figure 1.2. Ischaemic stroke arising from an atherosclerotic plaque. The top image illustrates a normal artery with normal CBF. Damage to the endothelium initiates an inflammatory process which ultimately leads to the formation of a fibrous atherosclerotic plaque within the vessel wall. The plaque causes the artery to become narrowed and restricts blood flow (middle image). Over time, the plaque can continue to grow and occlude the vessel itself or it can rupture resulting in the formation of a thrombus. The thrombus can occlude the artery which will obstruct the flow of blood resulting in an ischaemic stroke (bottom image) (Adapted (with permission) from (Stroke.org.uk, 2015)).

Age is the most important risk factor for stroke. The chance of having a stroke doubles for each decade after the age of 55 in both men and woman (AHA/ASA, 2012, Stroke.org.uk, 2015). Estimates from the Framingham study, a long-term ongoing cardiovascular study, show that by the age of 75, 1 in 5 women and 1 in 6 men will have a stroke (Seshadri et al., 2006). Men have a 25% risk of having a stroke at an earlier age compared to women, but because women live longer than men there are more total incidences of stroke in women (Stroke.org.uk, 2015).

1.1.2.2 Modifiable risk factors.

A larger number of risk factors for stroke are potentially modifiable (Figure 1.3). A recent study found that modifiable risk factors accounted for more than 80% of all strokes (O'Donnell et al., 2010). Hypertension is the leading modifiable risk factor for stroke, contributing to over 50% of strokes. Hypertension is defined as systolic/diastolic blood pressures consistently greater than 140/90mmHg and is a common problem, affecting approximately 10 million people in the UK (Stroke.org.uk, 2015).

Diabetes is another major risk factor for the development of stroke and occurs when there is too much glucose in the blood (hyperglycaemia). There are two main types of diabetes: type 1 and type 2. Type 1 diabetes occurs when the body is not able to produce enough insulin to adequately regulate blood glucose levels. Normally, blood glucose levels range from between 4-6mmol/L when fasting. However in patients with type 1 (and type 2) diabetes fasting blood glucose levels are 7.0mmol/L or greater (Diabetes.co.uk). Type 2 diabetes is the most common and occurs when the body is ineffective at using the insulin it produces or when it is unable to produce enough insulin. There are over 3.3 million people in the UK registered as diabetic and it is estimated that another 850,000 people have undiagnosed diabetes (Stroke.org.uk, 2015). People who have diabetes (type 1 and type 2) are twice as likely to have a stroke compared to nondiabetics (Stroke.org.uk, 2015).

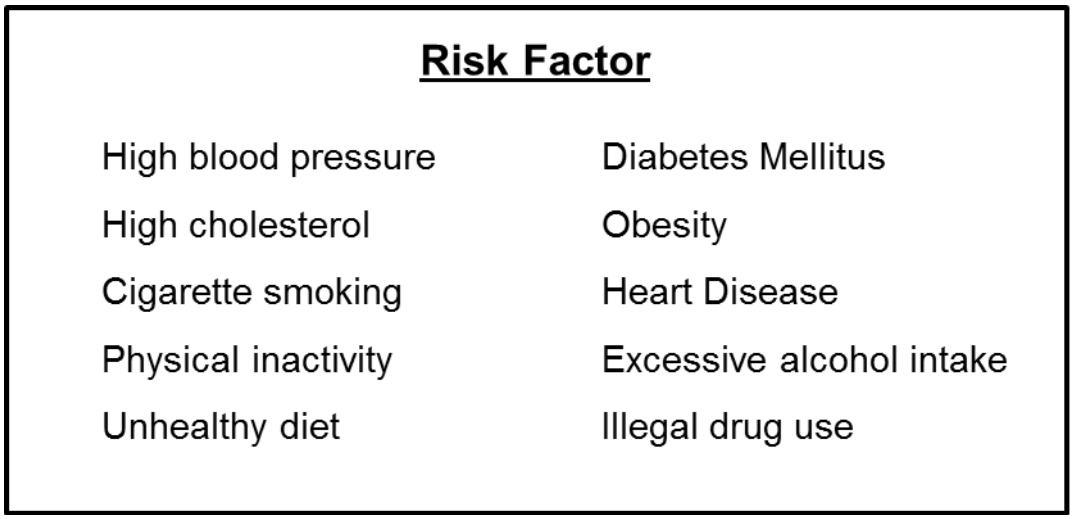

Figure 1.3. Potentially modifiable risk factors for stroke.

Chronically elevated glucose levels contribute to the build-up of atherosclerotic plaques in blood vessels, this can be particularly damaging to small blood vessels, including capillaries, and may explain why diabetic patients display a greater tendency for lacunar stroke (Hill, 2014). The increased risk of stroke in diabetic patients could, in part, be due to an increase in fibrinogen, a glycoprotein that is involved in the formation of blood clots. Increased plasma concentrations of fibrinogen have been reported in type 2 diabetic patients (Barazzoni et al., 2000) and this hyperfibrinogenemia is associated with an increased risk of cardiovascular and cerebrovascular disease (Kannel et al., 1987).

Conditions of abnormal glucose metabolism such as: prediabetes, insulin resistance and impaired fasting glucose, are also considered as important risk factors for stroke and a high incidence of these conditions is reported among ischaemic stroke patients (Urabe et al., 2009).

1.1.3 Pathophysiology of ischaemic stroke

The reduction in blood flow arising from an ischaemic stroke restricts the delivery of essential substrates to the territory of the occluded vessel. This in turn initiates a cascade of deleterious biochemical and cellular events which converge to mediate brain damage. The pathological processes in this cascade develop over hours and even days after the onset of ischaemia (Figure 1.4). This section will focus on the early events in this cascade, which are excitotoxicity, oxidative stress and peri-infarct depolarisations.

1.1.3.1 Bioenergetic failure and excitotoxicity

The brain has a relatively high energy demand: the weight of the brain makes up just 2% of the total body mass but it uses around 20% of the oxygen and 25% of the glucose consumed by the entire body. Despite this, the brain has a limited capacity to store energy and is reliant on a continuous blood supply to deliver the essential substrates it needs to function. Consequently, the brain is highly vulnerable to ischaemia. When CBF is reduced during ischaemic stroke the delivery of oxygen and glucose is restricted and this leads to the rapid failure of the brains normal process for adenosine triphosphate (ATP) production:

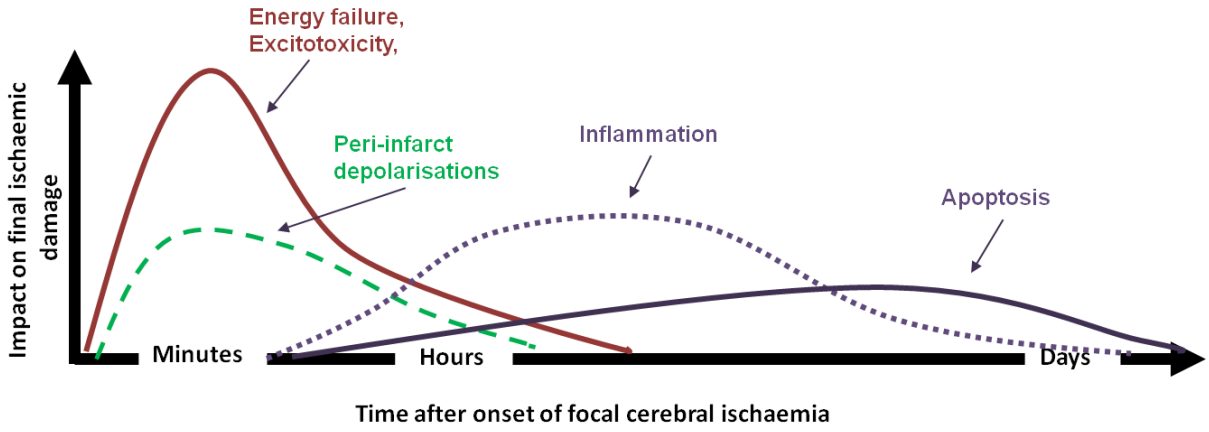

Figure 1.4. Simplified temporal profile of the major pathological mechanisms underlying focal cerebral ischaemia and their impact on ischaemic damage. Figure adapted from: (Dirnagl et al., 1999).

oxidative phosphorylation (Dirnagl et al., 1999). This leads to a profound decrease in cellular ATP production and depletion of cellular ATP levels. In addition, the lack of oxygen during focal ischaemia leads to the anaerobic metabolism of glucose and the build-up of lactate. An increase in lactate levels leads to intracellular acidification and further depletion of ATP. Diminished ATP levels causes the sodium-potassium adenosine triphosphatase (Na^+/K^+-ATPase) pump function to fail. This leads to the rapid loss of ionic gradients and the depolarisation of neurons and glia (Martin et al., 1994, Katsura et al., 1994). This in turn results in the activation of somatodendritic and presynaptic voltage-gated calcium channels and the subsequent spontaneous release of excitatory amino acids, primarily glutamate, into the extracellular space (Brouns and De Deyn, 2009). At the same time, presynaptic reuptake of glutamate is reduced which further increases the extracellular concentration of glutamate. The rise in extracellular glutamate concentration leads to the pathological activation of glutamate receptors, inducing a type of neuronal insult called excitotoxicity.

There are two main groups of excitatory glutamate receptors - ionotropic NMDA, AMPA and kainate receptors and metabotropic glutamate receptors (mGluRs) - in the central nervous system (CNS). Ionotropic receptors are named after the agonists that activate them: NMDA (*N*-methyl-D-aspartate), AMPA (α-amino-3-hydroxyl-5-methyl-4-isoxazole-propionate), and kainic acid. All of the ionotropic receptors are nonselective cation channels that allow the influx of sodium ions and the efflux of potassium ions. However, during ischaemia when the Na^+/K^+-ATPase fails, the influx of sodium ions is much greater than the efflux of potassium which results in the passive inflow of water into the cells leading to cytotoxic oedema. This can affect perfusion of brain tissue in surrounding areas and may also lead to increases in intracranial pressure and vascular compression (Dirnagl et al., 1999). The NMDA family of glutamate receptors are permeable to calcium and the excessive activation of NMDA receptors during ischaemia leads to the massive influx of calcium (Ca^{2+}) into the cell. In addition, the activation of mGluRs causes calcium to be released from intracellular stores, via phospholipase C and Ins(1,4,5)*P*3 signalling, which contributes to the calcium overload during excitotoxicity (Dirnagl et al., 1999). The rise in intracellular calcium is toxic to neurons and initiates a series of deleterious events including the generation of free radicals and the activation of proteolytic enzymes that

degrade proteins, membranes and nucleic acids. These events lead to neuronal cell death through necrosis but excitotoxic mechanisms can also induce delayed cell death via apoptosis.

1.1.3.2 Ischaemia-induced activation of calpain

Activation of the proteolytic enzyme, calpain is one of the key excitotoxic events to occur after ischaemia due to calcium overload. Calpains are a family of ubiquitous calcium sensitive cysteine proteases with a wide range of important physiological functions including: cytoskeletal alterations, cell cycle and differentiation processes, synaptic function and memory formation (Lynch and Baudry, 1984, Chan and Mattson, 1999a, Goll et al., 2003, Denny et al., 1990). Under normal physiological conditions the activity of calpain is increased by transient, localized increases in the concentration of cytosolic calcium and tightly regulated by an endogenous inhibitor, calpastatin. However, the profound increase in cytosolic calcium, which occurs following the massive release of glutamate during ischaemia, overwhelms the endogenous regulation of calpain leading to pathological calpain activity and calpain-mediated brain injury (Neumar et al., 2001).

Cleavage of the sodium-calcium exchanger (NCX) is considered to be an important mechanism by which the activation of calpain contributes to ischaemic damage. Sodium-calcium exchangers are antiporter membrane proteins that use the outward sodium gradient generated by the Na^+/K^+ ATPase to transport one calcium ion out of the cell and 3 sodium ions into the cell, and in doing so help to maintain the cells normal, low calcium concentration. Using an in vitro model of ischaemia, Bano et al (2005), found that calpain-mediated cleavage of the NCX inactivated the ionic exchange activity of the pump resulting in the retention of intracellular Ca^{2+}, prolonged calpain activation and neurotoxicity. These effects were reversed by over-expression of the calpain inhibitor, calpastatin (Bano et al., 2005). Further to this, studies have shown that inhibition of calpain reduces ischaemic damage, indicating that calpains are important mediators of ischaemic brain damage (Hong et al., 1994a, Hong et al., 1994b, Li et al., 1998).

1.1.3.3 Oxidative stress

Oxidative stress has been implicated as an important mediator of neuronal cell death after cerebral ischaemia (Niizuma et al., 2009, Sugawara and Chan, 2003, Chan, 2001). Following ischaemia, and in particular reperfusion, free radicals such as superoxide, hydrogen peroxide and hydroxyl radicals, are generated via a number of different mechanisms (Nakashima et al., 1999, Schaller and Graf, 2004). However, reactive oxygen species (ROS) generated from mitochondria are considered to be the primary source of free radical generation during ischaemia. In addition to ROS, reactive nitrogen species (RNS) also contribute to tissue damage during ischaemia. High levels of nitric oxide (NO) are produced during ischaemia via the calcium-dependent activation of the constitutive neuronal nitric oxide synthase and by the activation of inducible nitric oxide synthase in inflammatory cells (Castillo et al., 2000). NO reacts with superoxide producing the highly reactive peroxynitrite radical. Reactive oxygen and nitrogen species induce a wide array of cellular effects including: inactivation of enzymes, release of calcium ions from intracellular stores, protein denaturation, lipid peroxidation and damage to the cytoskeleton and DNA (Brouns and De Deyn, 2009). They can also lead to an increase in blood brain barrier permeability through the activation of matrix metalloproteinases (MMP), in particular matrix metalloproteinase 9 (Rosenberg et al., 1998, Montaner et al., 2003), which contributes to the development of vasogenic oedema.

1.1.3.4 Peri-infarct depolarisations

Peri-infarct depolarisations (PIDs) are secondary mechanisms that can contribute to the expansion of the ischaemic lesion. In the severely hypoperfused tissue of the ischaemic lesion (ischaemic core) cells undergo anoxic depolarisation and are unable to repolarise and go on to die. However, in the moderately hypoperfused tissue bordering the ischaemic core, termed the ischaemic penumbra, the cells are able to repolarise but at the cost of high energy consumption. Once repolarised, these cells have the ability to depolarise again in response to high extracellular glutamate and potassium concentrations. This process can be repeated and repetitive depolarisations are called peri-infarct depolarisations. The occurrence of PIDs has been well documented in animal stroke models where an increase in the frequency of PIDs is associated with

greater infarct growth (Back et al., 1996, Gill et al., 1992, Strong et al., 2000). This phenomenon has also been demonstrated in human stroke patients and may contribute to delayed ischaemic damage (Nakamura et al., 2010).

1.1.3.5 Necrotic and apoptotic cell death

During ischaemic stroke, brain cells can die via two distinct processes: necrosis or apoptosis. There are several factors that govern which process predominates including: the severity and nature of the stimulus and cell type and maturity (Brouns and De Deyn, 2009).

Necrotic cell death is the predominant cell death mechanism that occurs in the tissue at the core of the ischaemic lesion which suffers the most severe reduction in blood flow (Dirnagl et al., 1999). Necrotic cell death in the ischaemic core occurs within minutes to hours after stroke onset and when cells die through this mechanism they release more glutamate and toxins into the extracellular environment which can affect surrounding neuronal and glial cells.

Apoptosis, or programmed cell death, is the form of cell death which predominates in the peri-infarct brain tissue (Dirnagl et al., 1999), occurring within hours and can last for days after ischaemia onset. Apoptosis may be initiated by caspase-dependent or caspase-independent pathways although caspase-dependent pathways are primarily involved in mediating cell death following focal cerebral ischaemia. Caspase-dependent apoptosis is mediated by the release of cytochrome C from the mitochondria. This facilitates the formation of the apoptosome complex which contains the cytosolic protein Apaf-1 and procaspase 9. The formation of the apoptosome complex promotes the activation of caspases, a family of cysteine proteases, which upon activation cleave a number of downstream substrates, including other “executioner” caspases, DNA repair enzymes, and cytoskeletal proteins. Caspase-3 is one of the executioner caspases activated during brain ischaemia and its activation is considered to be a critical step in apoptosis. This is supported by the fact that pharmacological inhibition or genetic disruption of caspase-3 reduces ischaemic injury (Endres et al., 1998, Le et al., 2002).

1.1.4 Animal models of ischaemic stroke

Animal models of stroke provide a valuable tool for studying the complex pathophysiology of stroke and for testing novel therapeutic agents. The middle cerebral artery (MCA) is the cerebral vessel most commonly occluded in human ischaemic stroke (Treadwell and Thanvi, 2010), and pre-clinical studies reflect this as occlusion of the MCA is the most commonly used method to induce ischaemic stroke in animals. The MCA can be occluded using various surgical methods which vary in their ability to model human disease. The two methods of middle cerebral artery occlusion (MCAO) which are commonly used to induce focal cerebral ischaemia in the rat in our research group are: the intraluminal filament (ILF) method and the distal diathermy (DD) MCAO method.

1.1.4.1 Intraluminal filament method

The ILF method of MCAO, first described by Koizumi et al (1986) and later modified by Longa et al (1989), is the most commonly used method for studying ischaemic stroke in rats and mice. This method involves the exposure of the common carotid artery through a midline incision in the neck and dissection and exposure of the internal and external carotid arteries. The MCA is occluded by inserting a filament into the internal carotid artery and advancing it until it lodges in the narrow proximal anterior cerebral artery blocking the origin of the MCA. Filaments can be made in-house using nylon monofilaments (Dermalon) or can be purchased from Doccol Corporation. Ischaemic damage induced using the ILF method can be extensive, causing damage to the caudate nucleus and other subcortical structures, as well as significant damage to the cortex. The typical pattern of ischaemic damage induced by the intraluminal filament method is shown on the T_2-weighted magnetic resonance images in Figure 1.5 (Reid, 2012). A major advantage of this method is the potential to induce both permanent and transient occlusion of the MCA by leaving the filament in place or removing it after a specified. Also, MCAO surgery using the intraluminal filament method does not require a craniotomy and can be done in a high throughput manner. The major disadvantage of this method is the low reproducibility in lesion size and high rate of subarachnoid haemorrhage development (Schmid-Elsaesser et al., 1998).

1.1.4.2 Distal diathermy method

The distal diathermy method of MCAO involves the exposure of the MCA via a craniotomy followed by direct occlusion of the MCA using diathermy forceps to electrocoagulate the blood within the exposed portion of the vessel, thereby disrupting the structural integrity of the artery. This method of MCAO was adapted from work by Robinson et al (1975) and Tamura et al (1981) who demonstrated that the extent of ischaemic damage is dependent of the position and length of the occluded vessel (Robinson et al., 1975, Tamura et al., 1981a). Occluding the distal stem of the MCA (above the lenticulostriate arteries) and its main cortical branches produces smaller lesions localised to the cerebral cortex in comparison to those induced by proximal MCA occlusion which produces both cortical and subcortical ischaemic damage. The smaller lesions produced by distal MCAO are advantageous as they are more relevant to human stroke (Carmichael, 2005) and also the craniectomy reduces the deleterious consequences of brain swelling and thereby reduces post-surgical mortality rates. Disadvantages of this method are that the craniotomy requires an acquired degree of neurosurgical skill and longer preparation time compared to other models. T_2-weighted magnetic resonance images demonstrating the typical pattern of ischaemic damage induced by distal diathermy MCAO are shown in Figure 1.6.

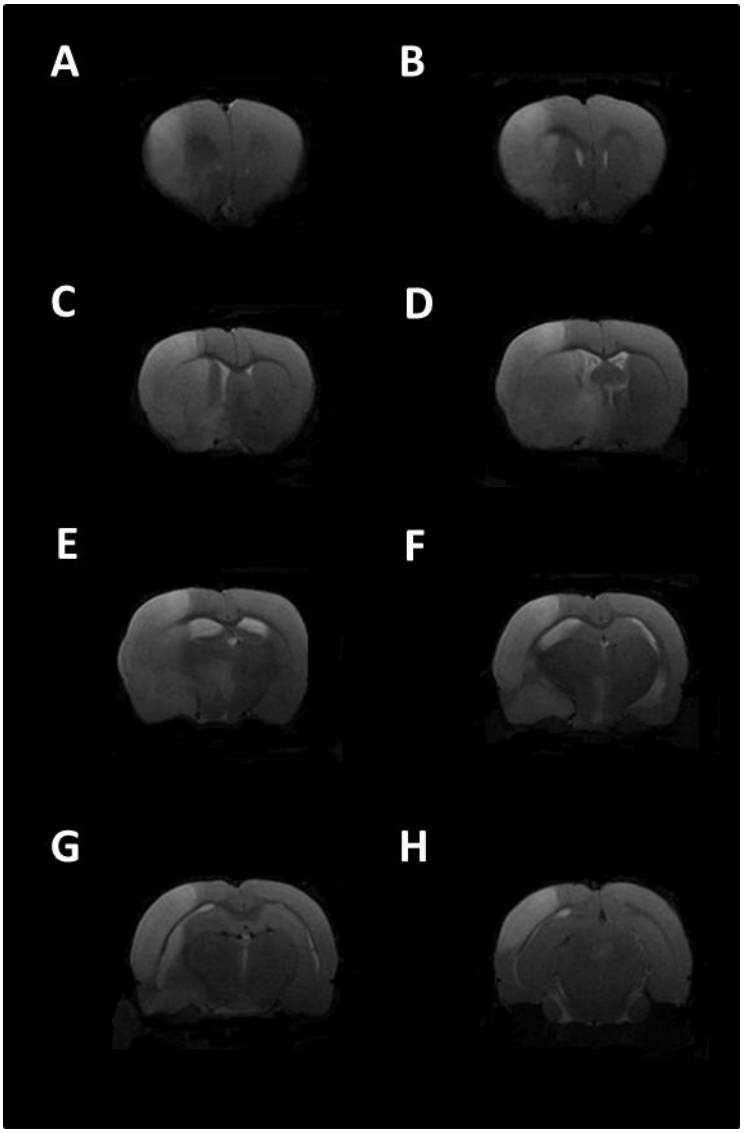

Figure 1.5. MRI RARE T_2-weighted coronal brain images depicting ischaemic damage in Wistar Kyoto rats 24 hours after permanent MCAO induced by the intraluminal filament method. Images: rostral (A) to caudal (H). Ischaemic damage on T_2 images appears hyperintense and incorporates both cortical and subcortical brain regions. Images courtesy of Dr Emma Reid (Reid, 2012).

Figure 1.6. MRI RARE T_2-weighted coronal brain images demonstrating ischaemic damage 24 hours after permanent MCAO induced by the distal diathermy method in adult, male Wistar rats. Images: rostral (A) to caudal (H). Ischaemic damage on T_2 images appears hyperintense and is primarily restricted to the cortex.

1.2 The ischaemic penumbra

1.2.1 Cerebral blood flow

Due to high oxygen consumption, the brain requires tight regulation of blood flow for survival. In normotensive adults CBF is maintained relatively constant at around 55ml/100g/min by cerebral autoregulation. Autoregulation refers to the physiological mechanisms (myogenic, neurogenic and metabolic) that maintain CBF at a constant level during changes in cerebral perfusion pressure (CPP) provided CPP is within the range of 50-150mmHg (Figure 1.7). Above and below this limit, autoregulatory mechanisms fail and CBF passively follows changes in mean arterial pressure and intracranial pressure. When CPP falls below the lower limit, cerebral ischaemia ensues.

1.2.2 Cerebral blood flow alteration in focal cerebral ischaemia

Following stroke there is a topographical gradient of cerebral blood flow reduction across the territory of the supplied artery. The end-artery territory has the most severe reduction in blood flow and tissue within this region is referred to as the ischaemic core. The profound or complete loss of CBF in the ischaemic core leads to irreversible tissue damage and this tissue will rapidly progress to infarction. The brain tissue at the periphery of this core - termed the ischaemic penumbra, experiences a less severe reduction in CBF as this region receives collateral flow from alternative routes, mostly via the circle of Willis or leptomeningeal anastomoses (Shuaib et al., 2011). Tissue within the ischaemic penumbra is functionally impaired but does not immediately progress to infarction and therefore has the capacity to regain normal function if blood flow is promptly restored. In addition to the ischaemic core and penumbra, there are some areas of tissue which experience a modest reduction in CBF which are not expected to become incorporated into the infarct. This tissue is called benign oligaemic tissue and it may not be completely safe from ischaemic damage as modest reductions in CBF, in conjunction with pathological conditions such as hyperglycaemia or hypotension, could induce progressive damage.

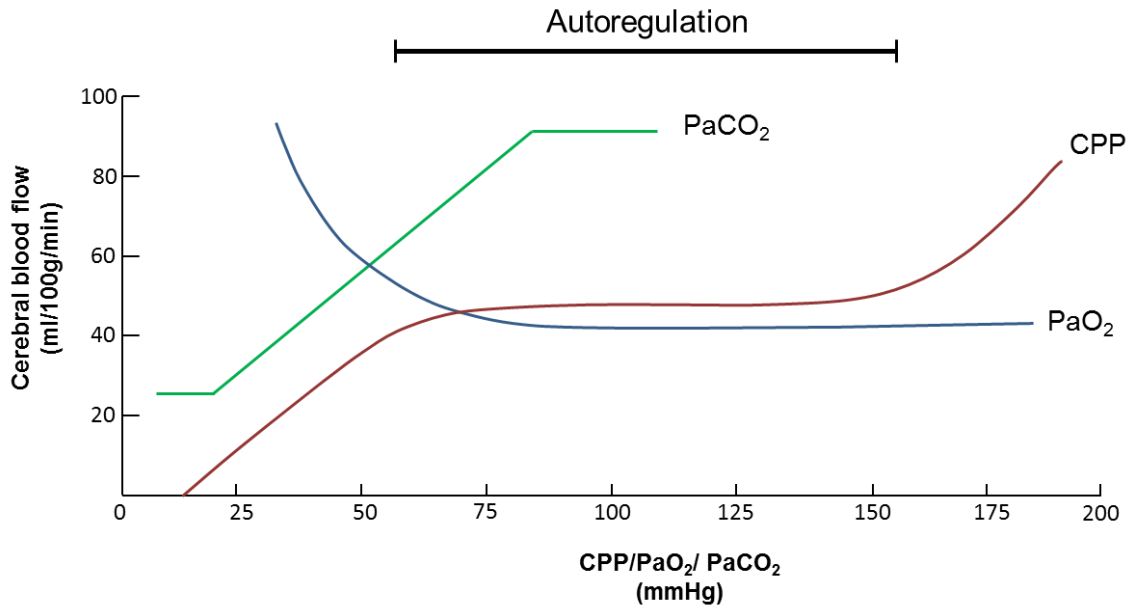

Figure 1.7. Cerebrovascular autoregulation in health and the influence of arterial blood gasses and CPP. CBF is maintained at a relatively constant level by autoregulation when CPP is within the range of 50-150mmHg. Out with the upper and lower limits of this range, at the point of maximal vasodilation and vasoconstriction, autoregulation is lost. Hypercapnia and hypoxia cause blood vessels to dilate, leading to an increase in CBF whereas hypocapnia causes vasoconstriction and a decrease in blood flow. PaO_2, $PaCO_2$ partial pressures of oxygen/carbon dioxide in arterial blood. Figure adapted from (Shardlow and Jackson, 2011).

CBF thresholds for the ischaemic core and penumbra were first described by Lindsay Symon and colleagues in the 1970's using a baboon model of focal cerebral ischaemia. They examined cortical-evoked responses to varying degrees of ischaemia and identified three different regions when CBF was progressively lowered:

1. Benign oligaemic tissue in which cerebral function (somato-sensory evoked potentials) was normal despite a reduction in CBF from normal.

2. Ischaemic penumbra tissue, where cerebral function was impaired at ~20ml/100g/min.

3. Ischaemic core where cerebral function was abolished at around 6-10ml/100g/min.

They also showed that the functional impairment in the ischaemic penumbra could be restored with an increase in CBF (Symon et al., 1977). From these experiments the ischaemic penumbra was defined as: a region of functionally impaired but structurally intact hypoperfused tissue that is potentially viable. The definition of the ischaemic penumbra has evolved over the past 30-40 years due to advances in neuroimaging and a revised definition defines it as:

"Ischaemic tissue which is functionally impaired and is at risk of infarction and has the potential to be salvaged by reperfusion and/or other strategies. If it is not salvaged this tissue is progressively recruited into the infarct core which will expand with time into the maximal volume originally at risk" (Donnan et al., 2007).

In addition, Donnan et al (2007) established a set of criteria to define the ischaemic penumbra (Figure 1.8)(Donnan et al., 2007). CBF thresholds to define the ischaemic core and ischaemic penumbra tissue have also been defined in human stroke (Figure 1.9)(Powers et al., 1985, Hakim et al., 1989, Baron et al., 1984). Some of the brain imaging methods used to identify the ischaemic penumbra in human stroke will be discussed in the following section.

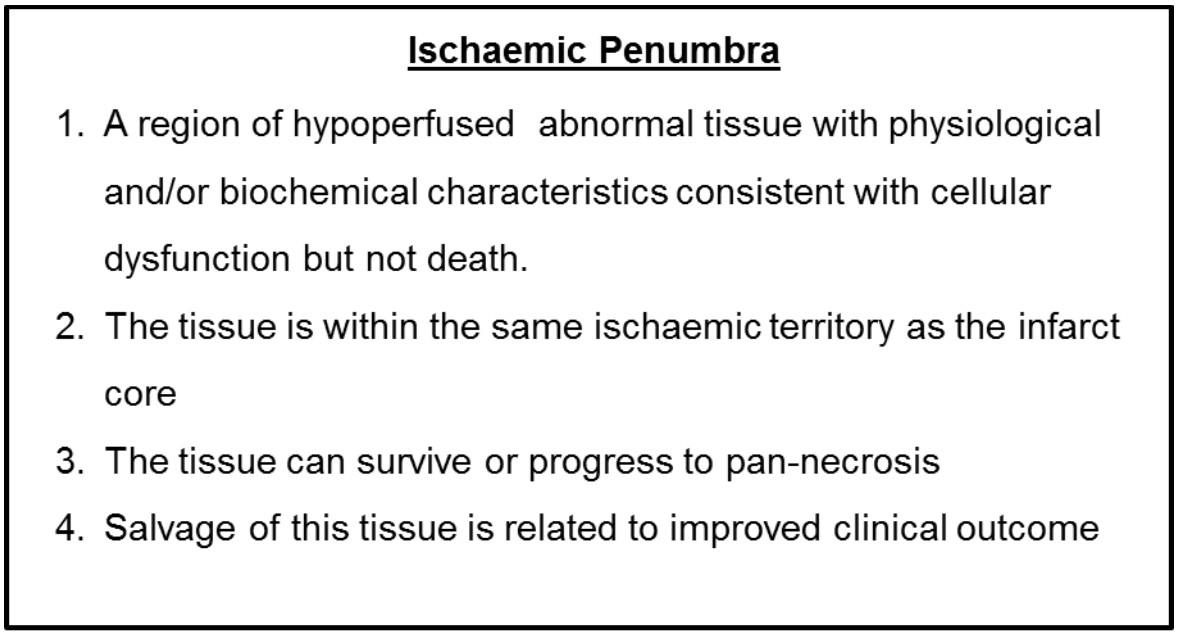

Figure 1.8. Criteria for defining the ischaemic penumbra. (Donnan et al., 2007).

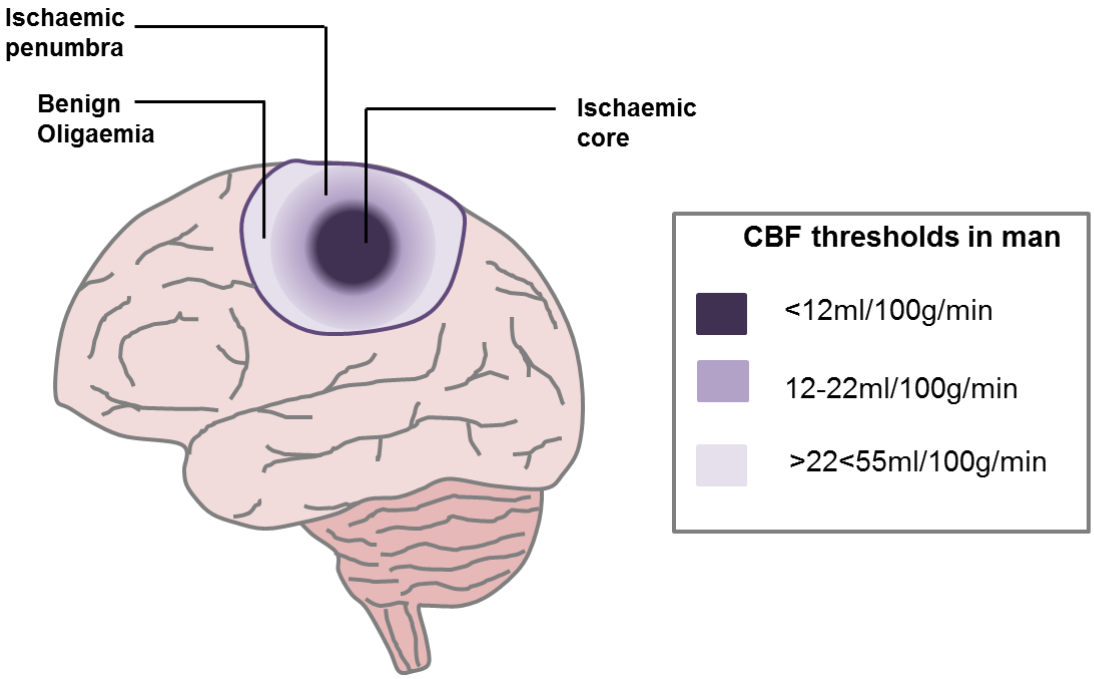

Figure 1.9. Ischaemic core and penumbra. Following occlusion of a cerebral artery, most commonly the middle cerebral artery, the region with the most severe reduction in blood flow is referred to as the ischaemic core. In humans, this region corresponds to a region with CBF below a value of approximately 12ml/100g/min. At the periphery of this ischaemic core there is a region with less severely reduced blood flow termed the ischaemic penumbra. Blood flow within this region can range from 12-22ml/100g/min. Benign oligaemic tissue is hypoperfused tissue in which CBF is above 22ml/100g/min that does not progress to infarction. CBF values from: (Heiss, 2000) .

1.2.3 Imaging the ischaemic penumbra

The identification of potentially salvageable penumbra tissue is hugely important in clinical and preclinical stroke research. Clinically it can be used to identify patients who are most likely to benefit from treatment. Therapeutics for stroke are limited and although many neuroprotective strategies have shown efficacy in animal models of stroke there has been a failure to translate these results to the clinic. One contributing factor could be that many clinical studies included patients with no salvageable tissue, those patients that are least likely to benefit from treatment. Therefore identification of potentially viable penumbra tissue could allow new stroke therapies to be assessed in comparable patient groups, which in turn could aid translation from bench to bedside. Identification of the penumbra in preclinical research is equally important as it enables the efficacy of new neuroprotective strategies to be assessed. Magnetic resonance imaging (MRI) is the favoured imaging modality in the preclinical setting although perfusion computed tomography (PET) is considered to be the gold standard for imaging the ischaemic penumbra clinically. However developments in MRI have led to an increase in the use of this technique to identify potentially viable tissue in the clinical setting. Computed tomography (CT) is the most widely accessible and cost effective technique for diagnosing ischaemic stroke and the use of perfusion CT (PCT) to identify the ischaemic penumbra is being used increasingly. As such, PCT is likely to become one of the most widely used techniques for identifying the penumbra. The use of these three imaging modalities to identify the ischaemic penumbra will be discussed in the following sections.

1.2.3.1 Positron emission tomography

PET imaging of the penumbra involves the intravenous administration of a positron emitting radioisotope bound to a tracer ligand. The PET system detects the gamma rays emitted by the tracer and produces an image of the tracer's distribution in the brain. The presence of the ischaemic penumbra was first demonstrated in ischaemic stroke patients using PET with the ^{15}O inhalation technique (Baron et al., 1981). Using this method the penumbra was defined as a region of hypoperfused tissue (CBF>12-22ml/100g/min) with preserved

neuronal function ($CMRO_2$ >65μmol/100g/min) and increased oxygen extraction fraction (80-100% above the normal 40%)(Heiss, 2003).

The penumbra is a dynamic process and the flow values within the tissue deemed the ischaemic penumbra may vary depending on the time elapsed since stroke onset. This stressed the need for a marker of neuronal integrity that could be used to distinguish between irreversibly damaged and potentially viable tissue regardless of variations in CBF over time. This led to the use of ^{11}C-flumazenil (FMZ), a ligand for the benzodiazepine receptor subunit of the $GABA_A$ receptor, that was found to be a useful marker of neuronal integrity since $GABA_A$ receptors are abundant in neuronal tissue and are sensitive to ischaemic damage (Alicke and Schwartz-Bloom, 1995). FMZ-PET imaging studies have demonstrated that the FMZ ligand can be reliably used to distinguish between irreversibly damaged (decreased FMZ binding) and penumbra (preserved FMZ binding/morphological integrity) tissue early after acute stroke (Heiss et al., 2000). Other PET tracers such as ^{18}F-fluromisonidazole have also been used to identify penumbra tissue. ^{18}F-fluromisonidazole is a hypoxia tracer and the uptake of the tracer specifically occurs in viable hypoxic tissue (Read et al., 1998).

Although PET is an effective tool for imaging the ischaemic penumbra it has a number of disadvantages which make it impractical for clinical use. Firstly, PET requires arterial cannulation for tracer administration and arterial blood sampling is necessary for CBF quantitation, both of which can restrict its use when thrombolytic therapy is planned. Secondly, the radioactive dose used limits the amount of times a patient can undergo PET imaging and therefore it is not suitable for studies requiring repeated measurements. Lastly, PET imaging is expensive and therefore it is not available in many stroke units around the world. Consequently, MRI and CT perfusion imaging are the preferred imaging modalities for imaging the ischaemic penumbra in the clinical setting.

1.2.3.2 Perfusion computed tomography

Perfusion computed tomography is the most widely accessible imaging tool for identifying the ischaemic penumbra and its advantages over other imaging methods include short imaging times and lower costs. PCT involves the

intravenous administration of an iodinated contrast agent and defines the penumbra based on changes in cerebral blood volume (CBV), CBF and mean transit time (MTT). CBV is defined as the volume of flowing blood for a given volume of brain and is measured in units of ml per 100g of tissue. MTT is measured in seconds and defines the mean time it takes for a volume of blood to transit a given volume of tissue. In normally perfused tissue perfusion is symmetrical with higher CBF and CBV in grey compared to white matter. During ischaemic stroke the severe reduction in CBF, and loss of autoregulation, leads to a decrease in CBV and a prolonged MTT in the core of the ischaemic lesion. The tissue at the periphery of the ischaemic core also has a prolonged MTT but only moderately reduced CBF and almost normal or increased CBV (due to preserved cerebral autoregulation). Various definitions have been proposed to estimate the ischaemic penumbra using different CBF, CBV and MTT thresholds. A systematic review of all three PCT parameters found that a CBV threshold of 2ml/100g most accurately defined the infarct core and a MTT threshold ≥145% of normal most accurately describes the tissue at risk of infarction (Wintermark et al., 2006). Using these thresholds, the ability of PCT to identify the ischaemic penumbra has been validated against MRI measurements of perfusion-diffusion mismatch (Schaefer et al., 2008). Therefore although MR is currently the preferred imaging method to evaluate core and penumbra, PCT is likely to become one of the most widely used imaging modalities due the high accessibility to computed tomography in stroke care units.

1.2.3.3 Identifying the penumbra using MRI perfusion-diffusion mismatch

Diffusion weighted imaging (DWI) is an established MRI technique that can accurately identify ischaemic tissue injury within minutes after stroke onset (Moseley et al., 1990, Yoneda et al., 1999). DWI of acute stroke is based on the restricted diffusion of water molecules caused by ischaemia induced membrane dysfunction and cytotoxic oedema. The restricted diffusion of protons leads to high signal intensity on DWI maps and can be quantitatively assessed using the apparent diffusion coefficient (ADC). ADC is a physiological measure of the rate of water movement through the brain tissue and is measured in units of mm^2/sec. On ADC maps, regions of restricted diffusion have lower ADC values compared to regions with normal diffusion and appear hypointense. MRI Perfusion imaging (PI) measures capillary blood flow and can be performed by a

bolus contrast technique or an arterial spin labelling (ASL) technique (Figure 1.10). The latter technique is less invasive as it does not require the administration of a contrast agent and instead uses electromagnetically labelled arterial blood water as an endogenous blood flow tracer. However it is not as widely used as it is more difficult to perform. The mismatch between regions of diffusion and perfusion abnormality during acute ischaemic stroke has been used to estimate the ischaemic penumbra. This perfusion-diffusion mismatch (PI-DWI mismatch) model developed from the observation that the diffusion lesion evolved over time to encompass the PI defined lesion in the absence of reperfusion (Baird et al., 1997, Warach et al., 2000). According to the PI-DWI mismatch model, the DWI lesion is taken to represent the ischaemic core, tissue that will progress to infarction regardless of reperfusion. The PI lesion, which is typically larger than the DWI lesion, represents hypoperfused tissue and the mismatch between them, is taken to represent the ischaemic penumbra.

The PI-DWI mismatch model has been widely used to identify the ischaemic penumbra in acute ischaemic stroke patients. Darby et al (1999) reported that approximately 70% of patients studied within 24 hours of symptom onset had a PI-DWI mismatch (Darby et al., 1999). Serial MRI studies have demonstrated the presence of mismatch tissue beyond 24 hours after stroke in some patients (Markus et al., 2004, Heiss et al., 1992), indicating that the time-window available for salvage of this tissue may be longer than the originally proposed time window of 3-6 hours.

Several clinical studies have shown that patients with PI-DWI mismatch benefit from acute thrombolytic therapy (DIAS, DEFUSE, DEFUSE 2, EPITHET, DEDAS). The phase II Desmoteplase in acute ischaemic stroke trial (DIAS) recruited only patients that had at least a 20% PI-DWI mismatch. Using this criterion they found that patients treated with Desmoteplase within 9 hours of symptom onset had a higher rate of reperfusion and significantly improved clinical outcome compared to placebo treatment (Hacke et al., 2005). In the diffusion and perfusion imaging evaluation for understanding stroke evolution (DEFUSE) study, patients were not selected based on PI-DWI mismatch. However this study showed that early reperfusion (within 3-6 hours after symptom onset) with intravenous alteplase

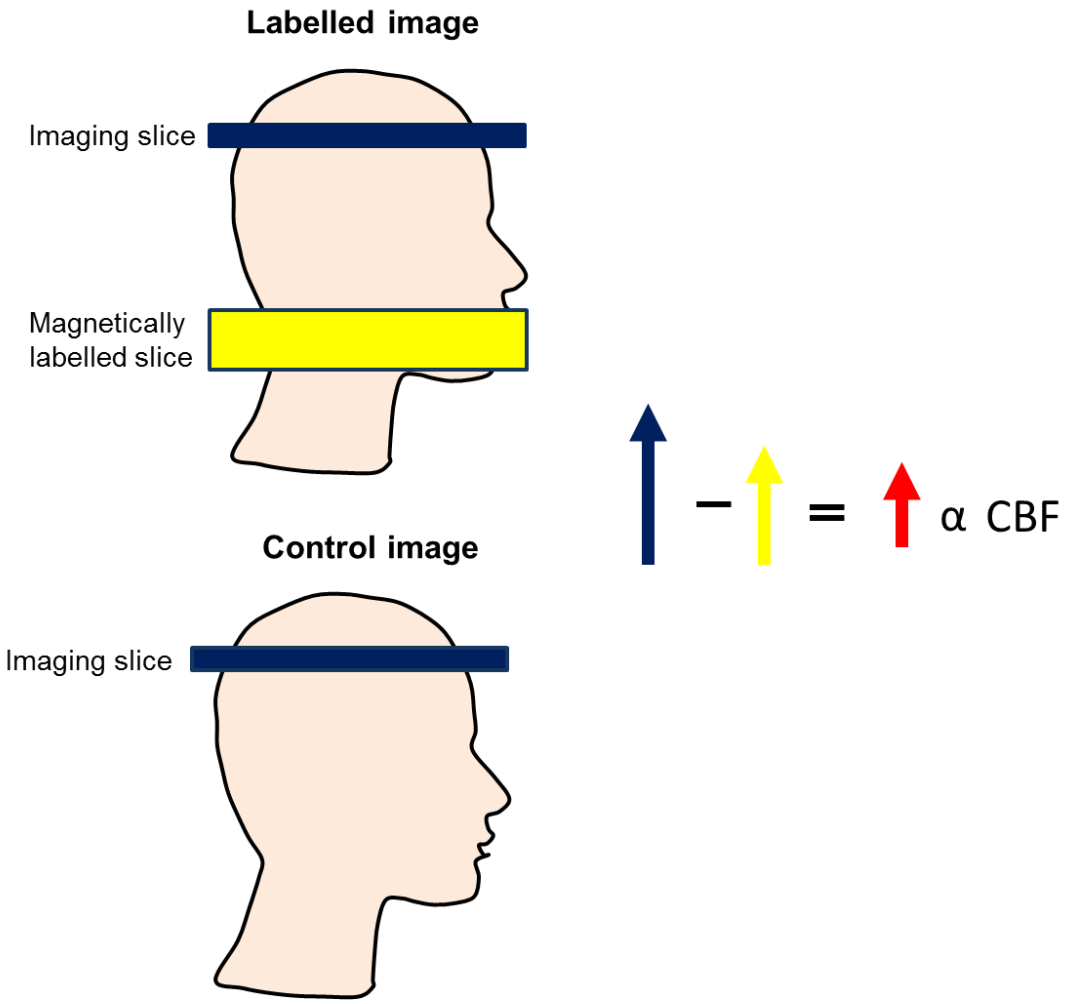

Figure 1.10. Diagram showing a summary of the arterial spin labelling technique. This technique uses electromagnetically labelled arterial blood water as an endogenous blood flow tracer. Two separate images are captured, one with magnetic labelling of arterial blood water (labelled image) and one without (control image). Subtraction of labelled images from control images removes the signal from the static tissue leaving only the signal from the magnetically labelled blood which provides a relative measure of perfusion that is proportional to blood flow. Figure adapted from: http://fmri.research.umich.edu.

was associated with favourable clinical outcomes in patients with mismatch tissue compared to those without (Albers et al., 2006). These studies demonstrate that the PI-DWI mismatch model can be successfully used to identify potentially salvageable tissue and in turn, those patients that are likely to benefit from thrombolytic therapy. However it may not always be reliable. There is evidence from animal studies and cases in humans reporting that the diffusion lesion can be temporarily or completely reversed following early reperfusion with thrombolytic therapy (Kidwell et al., 2000, Hasegawa et al., 1994). Thus, the diffusion lesion may not only include irreversibly damaged tissue, as defined by the mismatch model. There is also evidence that the perfusion lesion includes some benign oligaemic tissue and therefore does not always correctly identify tissue at risk of infarction (Rose et al., 2004, Sobesky et al., 2005). In order to address this problem, attempts have been made to establish diffusion and perfusion viability thresholds that can differentiate between regions that will proceed to infarction and salvageable penumbral tissue. However, at present there is no clear consensus on where to set perfusion and diffusion thresholds in order to define mismatch tissue in both clinical and preclinical studies (Campbell and Macrae, 2015).

The MRI PI-DWI mismatch model has also been used to assess the temporal evolution of ischaemic penumbra tissue in animal models of focal cerebral ischaemia. In a rodent model of permanent MCAO, Meng et al (2004) examined the temporal evolution of the PI-DWI mismatch. They showed that the diffusion lesion expands over time to incorporate the larger perfusion lesion and that this corresponded with a reduction in the volume of PI-DWI mismatch tissue over time (Meng et al., 2004). Meng and colleagues found that by 3 hours after permanent MCAO the ADC-derived lesion had fully evolved suggesting that the time window for penumbral salvage is short. The same group also examined the temporal evolution of PI-DWI mismatch tissue following transient MCAO (60 minute occlusion period). They found that the infarct volume measured 24 hours after transient MCAO was significantly smaller than the acute diffusion lesion measured 3 hours after MCAO (Meng et al., 2004). This indicated that reperfusion following transient MCAO may have successfully salvaged penumbral tissue. The animals used by Meng and colleagues were normotensive Sprague Dawley rats but similar studies have also been performed in hypertensive rat

strains (Reid et al., 2012, McCabe et al., 2009, Letourneur et al., 2011). Compared to control Wistar Kyoto (WKY) rats, the size of the initial diffusion lesion was significantly greater in spontaneously hypertensive stroke prone (SHRSP) rats resulting in smaller volumes of PI-DWI mismatch tissue early after the onset of permanent MCAO.

1.2.4 Salvaging the ischaemic penumbra

Since the discovery of the penumbra and the potential to halt or even reverse neurological damage the main goal of ischaemic stroke therapy has been to salvage this tissue. Tissue in the penumbra can be salvaged by restoring blood flow to the affected tissue and improving collateral flow. Current therapies for stroke are limited and the available recanalization strategies include: blood clot thrombolysis with intravenous recombinant tissue plasminogen activator (rt-PA, alteplase), or surgical clot removal with endovascular devices (mechanical thrombectomy). The latter is a highly specialised treatment that is not widely available as it is only performed in hospitals which have experience in using these devices. However, in cases where this method has been used, substantial neurological improvements have been documented (Pereira et al., 2013, San Roman et al., 2012, Rohde et al., 2011).

Thrombolysis with rt-PA is the most effective treatment for ischaemic stroke but despite this, less than 10% of all stroke patients currently receive it (ISD_Scotland, 2014). This is mainly due to the narrow window of opportunity for treatment and the increased risk of haemorrhage with rt-PA use. In the first instance, thrombolysis treatment with rt-PA was licensed for use within 3 hours of stroke onset after the National Institute of Neurological Disorders and Stroke (NINDS) trial found that patients that received rt-PA within 3 hours of stroke symptom onset had improved clinical outcomes compared to placebo treated patients (NINDS, 1995). The time window for rt-PA therapy has since been extended out to 4.5 hours after stroke onset (Hacke et al., 2008), but the number of patients receiving it remains low. Attempts have been made to improve this figure for example, the advertising campaign FAST, which aims to educate the public on identifying stroke symptoms and stresses the importance of seeking emergency treatment, has led to an increase in the number of patients arriving within the therapeutic time window (ISD_Scotland, 2014). In

addition, the number of patients receiving rt-PA could be improved by the use of imaging techniques, rather than relying on the time from symptom onset, to identify those patients with penumbral tissue - those who are most likely to benefit from treatment. Indeed, the potential for selecting patients who might benefit from thrombolysis treatment beyond the 4.5 hour time window has been demonstrated clinically (Albers et al., 2006, Davis et al., 2008, Lansberg et al., 2012). At present, the use of MRI PI-DWI mismatch to select patients that may benefit from rt-PA administered 4.5-9 hours after stroke onset or in patients with wake-up stroke is being tested in a phase 3 clinical trial (ECAS4-ExTEND). Extending the time window for thrombolysis treatment is an important method by which clinical outcomes may be improved. Ischaemic stroke is a highly heterogeneous disease and therefore each patient's time window for treatment can vary. Furthermore, imaging studies have demonstrated the presence of potentially salvageable tissue up to 48 hours after symptom onset in some patients (Markus et al., 2004, Read et al., 2000, Heiss et al., 1992).

As well as recanalisation therapy, these patients may also benefit from neuroprotective interventions. Neuroprotective agents have been developed in an attempt to save neurons from irreversible injury, thereby preserving the ischaemic penumbra and extending the therapeutic time window for reperfusion therapies. However, despite numerous neuroprotective strategies showing efficacy in animal models of focal cerebral ischaemia, at present no neuroprotective therapies have demonstrated efficacy in human stroke. There are a number of experimental factors which could have contributed to the failure of neuroprotective agents to translate from animal models to the clinic. One such factor is the use of mostly young, healthy animals in preclinical studies. This is not representative of the clinical stroke population, in which the majority of patients are elderly and have any number of underlying medical conditions such as diabetes and hypertension that can influence prognosis. Hyperglycaemia can also influence prognosis and is a potential target for therapeutic intervention.

1.3 Hyperglycaemia and Stroke

Hyperglycaemia is a frequent finding in patients admitted to hospital with a suspected stroke: arising in over 60% of stroke patients with no previous history of diabetes and in 90% of diabetics (Muir et al., 2011). This post-stroke hyperglycaemia (PSH) is recognised as a predictor of mortality and disability independent of age, stroke type and severity. Melamed and colleagues were one of the first groups to report on the significance of hyperglycaemia in acute stroke, demonstrating that hyperglycaemia was associated with significantly higher in-hospital mortality rates compared to normoglycaemic stroke patients (Melamed, 1976). Many more clinical stroke studies have also reported a similar association between hyperglycaemia and worse clinical outcomes (Table 1.1)(Berger and Hakim, 1986, Weir et al., 1997, Melamed, 1976, Kiers et al., 1992b, Baird et al., 2003, Parsons et al., 2002). This association was reviewed in a meta-analysis which reported that hyperglycaemia was associated with an increased relative risk of in-hospital mortality and poor functional outcomes after stroke (Capes et al., 2001). Interestingly, the results from this meta-analysis revealed that the unadjusted relative risk of in-hospital mortality and poor functional outcome was higher in non-diabetic stroke patients compared to those with a known history of the condition. A more recent study also found that hyperglycaemia was independently associated with infarct growth and neurological deterioration in non-diabetic but not diabetic stroke patients (Shimoyama et al., 2014). Thus the adverse effects of hyperglycaemia may vary between diabetic and non-diabetic stroke patients. This is interesting as it suggests that there may be differences in the injury mechanisms induced by acute hyperglycaemia at the time of stroke onset compared to chronic hyperglycaemia (as in the case of diabetes). Understanding these mechanisms will be important in terms of the future management and treatment of patients with PSH, as well as the identification of new therapeutic targets.

Study	Definition of hyperglycaemia (mmol/L)	Outcome
Melamed et al (1976)	>6.7 (fasting)	Hyperglycaemia was associated with an increase in stroke severity (determined by stroke type, location and frequency of comatose patients) and risk of in-hospital mortality
Berger & Hakim (1986)	>5.6 (fasting)	Ischaemic stroke patients with hyperglycaemia developed more pronounced oedema and had an increased risk of mortality
Kiers et al (1992)	>7.8 (fasting)	Hyperglycaemia was associated with larger lesion sizes, worse neurological outcomes and higher mortality
Weir et al (1997)	≥8.0 (non-fasting)	Hyperglycaemia was associated with shorter survival times and higher mortality
Baird et al (2003)	≥8.0 (non-fasting)	Persisting hyperglycaemia was associated with infarct expansion and worse clinical outcomes following clinical assessments
Parsons et al (2002)	≥8.0 (non-fasting)	Acute hyperglycaemia was correlated with reduced salvage of perfusion-diffusion mismatch tissue from infarction, greater final infarct size, and worse functional outcomes following clinical assessments

Table 1.1. Clinical studies demonstrating an association between hyperglycaemia and worse clinical outcomes.

The temporal profile of blood glucose levels after stroke is complex and varies from patient to patient. For example in some patients blood glucose levels are only elevated on admission, returning to normal after 24 hours. In others, hyperglycaemia may not be present on admission but may occur at some point during the first 72 hours after stroke (Allport et al., 2006). In addition, patients can show persistent hyperglycaemia, in which blood glucose levels are elevated on admission and remain elevated at 24 hours or longer after stroke (Yong and Kaste, 2008). The outcome from stroke may vary depending on the temporal profile of blood glucose levels. For example, Yong et al (2008) found that persistent hyperglycaemia was associated with worse neurological outcomes and an increased risk of mortality at 90 days, whereas hyperglycaemia only on admission was not associated with any parameters of worse outcome. This will have an impact on the design of any future clinical trials for the treatment of PSH, as this data indicates that only patients with persistent hyperglycaemia may benefit from treatment.

1.3.1 Etiology of post-stroke hyperglycaemia

Although hyperglycaemia is associated with increased mortality and disability in ischaemic stroke patients the underlying etiology of PSH is not fully understood. Many initial studies proposed that hyperglycaemia after acute ischaemic stroke arises from a stress reaction following a more severe stroke, leading to the activation of the hypothalamic-pituitary-adrenal axis and the subsequent release of stress hormones such as cortisol and catecholamines (O'Neill et al., 1991, Tracey et al., 1993, Tracey and Stout, 1994). However, the stress response is disputed since later studies failed to demonstrate an association between hyperglycaemia, stress hormone levels and stroke severity (van Kooten et al., 1993, Allport et al., 2006). The neuroanatomical location of the infarct has also been associated with elevated glucose levels after ischaemic stroke. Allport et al (2004) reported that infarcts affecting the insular cortex predicted PSH (Allport et al., 2004), whilst others do not support an association between PSH and a neuroanatomical trigger for PSH (Moreton et al., 2007, Kiers et al., 1992a). PSH might also be explained by the uncovering of underlying latent diabetes or a form of dysglycaemia as it has been reported that over 50% of stroke survivors diagnosed as having PSH were diabetic or had impaired glucose tolerance or metabolic syndrome 12 weeks after stroke (Gray et al., 2004).

1.3.2 Management of hyperglycaemia in ischaemic stroke

There are no firm guidelines for the management of hyperglycaemia in acute ischaemic stroke. Guidelines from the European Stroke Initiative recommend intervention with insulin when blood glucose levels exceed 10mmol/L. However the optimum strategy will vary depending on the individual patient and the characteristics of the care-unit setting. Insulin treatment regimens are considered labour intensive, requiring consistent bedside glucose monitoring due to the potential for hypoglycaemia (Gray et al., 2007), which should be avoided as severe hypoglycaemia can exacerbate ischaemic damage (Zhu and Auer, 2004).

Some clinical trials have reported that tight glycaemic control (TGC) with intensive insulin regimens leads to better long-term outcomes in patients with myocardial infarction or other critical illnesses (Malmberg et al., 1995, Gibson et al., 2009). However, others such as NICE-SUGAR found that TGC in critically ill patients can increase the risk of adverse events (Finfer et al., 2009). Relatively few clinical trials have examined the effectiveness of TGC protocols in the acute stroke setting and currently there is no significant evidence that TGC improves patient outcome (Ntaios et al., 2014). The largest clinical trial to date is the UK Glucose Insulin in Stroke Trial (GIST-UK). GIST-UK investigated the effects of TGC with glucose-potassium-insulin (GKI) infusion therapy versus saline infusion in hyperglycaemic patients presenting within 24 hours of stroke onset with blood glucose levels between 6.0-17.0mmol/L. The data from GIST-UK indicate that there was no improvement in mortality rates or secondary outcome measures in patients treated with GKI compared to saline, however the results were inconclusive (Gray et al., 2007). This is because the study failed to recruit the number of patients it set out to (only 933 out of 2355) and was therefore underpowered to be able to make accurate conclusions about clinical outcome. In addition, although the reduction in blood glucose levels between insulin and saline groups was clinically significant, the reduction was small: mean blood glucose was 0.57mmol/L lower than control. However, the extent of the blood glucose reduction may not influence patient outcome because in a smaller study, the treatment of hyperglycaemia in acute stroke (THIS) trial, in which a larger reduction of 3.6mmol/L from control was observed in patients treated with intravenous insulin, there was again no improvement in patients treated

with insulin (Bruno et al., 2008). In the GRASP trial, which was a safety study and was therefore not powered to determine efficacy, exploratory efficacy analysis revealed that the TGC group had slightly better outcomes than controls (Johnston et al., 2009), and therefore supports further investigation of TGC for patients with PSH. Whether insulin treatment can reduce mortality rates and improve clinical outcome in patients with PSH therefore remains to be determined.

1.3.3 Pathophysiology of hyperglycaemia in ischaemic stroke

The mechanisms by which hyperglycaemia mediates its harmful effects during ischaemia have not been fully elucidated. Possible mechanistic explanations include: reduction in CBF, impaired recanalisation and increased reperfusion injury, increased lactic acidosis, enhancing excitotoxicity and increased oxidative stress and inflammation. These have mostly been investigated in animal models of stroke as only a few clinical studies have addressed the pathophysiological mechanisms associated with hyperglycaemia.

1.3.3.1 Reduced CBF

In the normal rat brain, an intraperitoneal injection of glucose to induce severe hyperglycaemia (plasma glucose: 39mmol/L) induced a 24% reduction in regional CBF (Duckrow, 1995). The reduction in CBF could not be fully explained by an increase in plasma osmolality as the injection of mannitol to induce a similar blood osmolality induced only a 10% reduction in regional CBF. In rodent models of global and focal ischaemia, moderate hyperglycaemia (blood glucose ~20mmol/L) induced a progressive reduction in CBF after the induction of ischaemia (Kawai et al., 1998). Similarly in cats, after 3 hours of focal cerebral ischaemia, moderate hyperglycaemia (plasma glucose ~20mmol/L) induced a 70% reduction in CBF after occlusion of the MCA compared with a lesser reduction of 34% in normoglycaemic animals (Wagner et al., 1992). If hyperglycaemia reduces CBF following ischaemic stroke this could lead to a significantly larger volume of hypoperfused tissue and subsequently to greater ischaemic damage and neurological deficits.

One way in which hyperglycaemia may reduce CBF is through altering the reactivity of the cerebral microcirculation. Mayhan and colleagues examined the response of rat cerebral arterioles *In Vivo* to various agonists (acetylcholine, histamine, NMDA and nitroglycerin) in the presence of increasing concentrations of glucose. They found that in the presence of glucose concentrations of 20 and 25mmol/L the dilation of the cerebral arterioles to the agonists acetylcholine, histamine and NMDA was inhibited but the response to nitroglycerin, a non-endothelium dependent agonist, was not (Mayhan and Patel, 1995). This indicated that acute exposure to high glucose impairs endothelium dependent (NO-mediated) vasodilation. Thus, elevated blood glucose levels may reduce CBF by impairing NO-mediated vasodilation. This is comparable to the reported effects of diabetes on the cerebrovasculature. Normally, exposure to 5% carbon dioxide (CO_2) following normocapnia in healthy, non-diabetic patients causes cerebral blood vessels to dilate, resulting in an increase in CBF. However this CO_2-induced increase in CBF is markedly attenuated in diabetics, in which the endothelial production of NO is known to be reduced (Dandona et al., 1978, Griffith et al., 1987, Lin et al.). In addition, the hyperglycaemia-mediated increase in ROS production (see below), can neutralise NO in the vessel wall which can further compromise cerebrovascular reactivity (Garg et al., 2006). Together this suggests that hyperglycaemia may reduce CBF by impairing NO production or reducing its availability.

1.3.3.2 Pre-stroke hyperglycaemia

As previously mentioned, over 50% of patients without a history of diabetes presenting with PSH are found to have diabetes or a related disorder of glucose metabolism at follow-up (3 months after stroke) (Gray et al., 2004). It is therefore highly possible that prior to their stroke, these patients had elevated blood glucose levels that could have induced morphological changes in the cerebrovasculature leading to neurovascular dysfunction. This is a condition in which the normal blood flow increases during neural activity are suppressed and is thought to be caused by the production of ROS at the level of the vascular endothelium (Moskowitz et al., 2010, Iadecola and Davisson, 2008). Morphological and functional changes might also occur in cerebral capillaries and this has been found to occur in conditions which pre-dispose to stroke such as aging, hypertension and diabetes (Bell and Ball, 1981, Tagami et al., 1990,

Junker et al., 1985, McCuskey and McCuskey, 1984). The role of such capillary changes in the aetiology and pathophysiology of stroke is uncertain at present. It is hypothesised that constriction of capillary pericytes (contractile cells that wrap around the endothelium of capillaries) during ischaemia could block the flow of blood and may explain the lack of reperfusion (no-reflow phenomenon) that occurs in some patients (Yemisci et al., 2009, Ostergaard et al., 2013). Prior to stroke, changes in capillary morphology could disturb the passage of blood through capillary beds, affecting local oxygen delivery. This could contribute to the abnormal CBF responses found in neurovascular dysfunction. During ischaemia this could be detrimental to the ischaemic penumbra where the survival of tissue depends on effective oxygen extraction to compensate for the reduced perfusion (Ostergaard et al., 2013).

1.3.3.3 Impaired recanalisation and increased reperfusion injury

Hyperglycaemia is associated with lower recanalisation rates in ischaemic stroke patients treated with rt-PA (Ribo et al., 2005). This may be caused by a decrease in plasma fibrinolytic activity and elevated plasma levels of plasminogen activator inhibitor type 1 (PAI-1), which have been reported to occur in both acute (Pandolfi et al., 2001) and chronic hyperglycaemic states (Auwerx et al., 1988, Juhan-Vague et al., 1989). Both a decrease is plasma fibrinolytic activity and increased levels of PAI-1 can reduce the thrombolytic activity of rt-PA and impair its ability to recanalise occluded blood vessels. The lower recanalization rates in stroke patients with PSH may explain the worse outcome observed in these patients as this could prevent the restoration of blood flow to the potentially viable tissue in the ischaemic penumbra causing this tissue to become incorporated into the infarct.

Evidence from animal models of transient focal cerebral ischaemia indicates that hyperglycaemia may exacerbate reperfusion injury (Nedergaard, 1987, Huang et al., 1996a, Kamada et al., 2007, Wei et al., 1997). Reperfusion injury is the tissue damage caused by the restoration of blood to previously ischaemic tissue and is believed to be caused by the generation of ROS upon restoration of CBF. Hyperglycaemia may exacerbate reperfusion injury by increasing the production of free-radicals during reperfusion (Wei et al., 1997). This could lead to microvascular damage which in turn could impair the return of blood flow to the

tissue even after recanalization. Evidence from animal stroke studies supports this hypothesis as studies have shown that the restoration of regional CBF to pre-ischaemic levels following transient focal cerebral ischaemia was impaired in hyperglycaemic but not normoglycaemic animals (Kawai et al., 1997b, Wei et al., 2003).

1.3.3.4 Lactic acidosis

During ischaemia, the reduction in CBF and the resulting lack of oxygen delivery causes a shift from aerobic to anaerobic metabolism of glucose. This leads to the production of lactic acid. The level of lactic acid production is dependent on the amount of glucose available. Therefore, elevated blood glucose levels during ischaemia leads to increased levels of lactic acid and subsequently intracellular acidosis in the brain tissue. Tissue acidosis may lead to greater ischaemic brain injury through enhancing the production of free radicals, activation of endonucleases leading to DNA fragmentation and altering gene expression or protein synthesis (Siesjo et al., 1996). Excessive lactate production may also cause the hypoperfused, yet potentially viable tissue in the ischaemic penumbra to progress to infarction. Evidence from clinical and experimental studies supports this. Parsons et al (2002) measured brain lactate levels, using magnetic resonance spectroscopy, in patients with PSH with evidence of perfusion-diffusion mismatch tissue. They found that higher blood glucose levels were associated with increased lactate production in the ischaemic brain, which in turn was associated with reduced salvage of mismatch tissue. In addition, Anderson et al reported that severe hyperglycaemia (plasma glucose: 28mmol/L) worsened tissue acidosis and mitochondrial function in the ischaemic penumbra after permanent focal cerebral ischaemia in rabbits. Infarct volume was significantly greater in hyperglycaemic animals compared to controls and this supports the hypothesis that tissue acidosis leads to the recruitment of ischemic penumbra into infarction. In the normal brain, despite the fact that lactate is considered to be potentially toxic, it is now recognised that lactate may be a valuable energy substrate for neurons in cases of high energy demand (Pellerin, 2010). Moreover, lactate metabolism is also recognised as an important substrate for ATP production during ischaemia (Pellerin and Magistretti, 1994) and therefore may be crucial for survival of the ischaemic penumbra. Furthermore, reducing brain lactate levels in patients with PSH did not influence

infarct growth (McCormick et al., 2010), indicating that brain lactic acidosis is not the only mediator of brain injury in hyperglycaemic ischaemia.

1.3.3.5 Hyperglycaemia-mediated increase in excitotoxicity

Hyperglycaemia may exacerbate the excitotoxic response after ischaemia. Following both global and focal cerebral ischaemia in rodents, the rise in extracellular glutamate levels in the ischaemic cerebral cortex was reported to be significantly greater in hyperglycaemic compared to normoglycaemic animals (Li et al., 2000b, Wei and Quast, 1998, Choi et al., 2010). Furthermore, the increase in extracellular glutamate levels correlated with an increase in ischaemic brain injury (Wei and Quast, 1998). Increased extracellular glutamate levels during ischaemia could lead to an increase in glutamate receptor stimulation which in turn may lead to significantly greater levels of intracellular Ca^{2+} resulting in more Ca^{2+} mediated cell death. The increase in Ca^{2+} may also increase the activation of calcium-dependent proteolytic enzymes which can also lead to increased brain injury. In particular, an increase in the activation of the calcium-dependent cysteine protease calpain has been reported in a rat model of chronic hyperglycaemia (Smolock et al., 2011).

1.3.3.6 Increased oxidative stress and inflammation

Hyperglycaemia is linked to increased oxidative stress following ischaemia. The production of ROS during ischaemia increases in the presence of elevated glucose levels, particularly in combination with reperfusion (Tsuruta et al., 2010). Hyperglycaemia can increase the production of superoxide through the enzyme NADPH oxidase. During ischaemia/reperfusion, elevated glucose levels helps to sustain the production of NADPH, a substrate for the production of ROS, through the pentose phosphate pathway (Tang et al., 2012). The increase in superoxide production during hyperglycaemic ischaemia can disrupt the blood brain barrier leading to increased vasogenic oedema (Kamada et al., 2007).

Hyperglycaemia has also been found to have a profound effect on the inflammatory response after ischaemia. In particular, hyperglycaemia has been shown to increase several transcription pathways that increase the migration of inflammatory cells such as leukocytes into the injured brain (Li et al., 2013). The migration of circulating leukocytes into the brain is thought to amplify

inflammatory signalling pathways which in turn will enhance ischaemic damage (Wang et al., 2007). In addition, the infiltration of leukocytes into the brain following transient focal ischaemia is enhanced under hyperglycaemic ischaemia (Lin et al., 2000).

1.3.4 Hyperglycaemia and animal models of stroke

Understanding the pathophysiology of hyperglycaemia in animal focal cerebral ischaemia models could help to inform the design of future clinical trials. However, the findings from animal studies show conflicting results. Most studies are consistent with the clinical findings, reporting that hyperglycaemia increases ischaemic damage in both permanent (Decourtenmyers et al., 1988, Huang et al., 1996b, Prado et al., 1988) and transient (Huang et al., 1996b, Nedergaard, 1987, Gisselsson et al., 1999) models of focal cerebral ischaemia. Whereas others have shown that hyperglycaemia may be beneficial by decreasing the extent of ischaemic damage following experimental stroke (Zasslow et al., 1989, Ginsberg et al., 1987, Kraft et al., 1990). Data from a recent systematic review of studies assessing the effects of hyperglycaemia on infarct size in animal models of MCAO found that most of the previous studies report clinically irrelevant models of hyperglycaemia (MacDougall and Muir, 2011). This is because in the vast majority of studies included in that review hyperglycaemia was induced by either the streptozotocin (STZ) model of type I diabetes or by extremely high glucose/dextrose infusions. The different methods will be discussed in the subsequent sections.

1.3.4.1 Streptozotocin model of hyperglycaemia

Streptozotocin causes hyperglycaemia by destroying the insulin producing beta cells of the pancreas leading to diminished insulin release and failure to control blood glucose levels. Due to its high toxicity to pancreatic beta cells STZ is commonly used to simulate experimental type I diabetes and therefore has limited pathophysiological relevance to the type of diabetes (type 2), and the insulin resistant phenotype, commonly observed in acute ischaemic stroke patients (O'Donnell et al., 2010, Rothwell et al., 2004, Gray et al., 2004). Despite this, the STZ model of hyperglycaemia has been widely used to study the effects of hyperglycaemia in global and focal cerebral ischaemia models. In the

systematic review by MacDougall and Muir, animals in which hyperglycaemia was induced by STZ had higher glucose levels and larger infarcts compared to animals in which hyperglycaemia was induced by glucose infusions (MacDougall and Muir, 2011). Glucose values exceeding 20mmol/L are typical of STZ induced hyperglycaemia, with values approaching or greater than 30mmol/L in some studies (Bomont and MacKenzie, 1995, Quast et al., 1997). In clinical studies patients are generally considered to have post stroke hyperglycaemia if blood glucose levels on admission are greater than 6.0-8.0mmol/L (Scott et al., 1999b, Gray et al., 2007, Shimoyama et al., 2014), with blood glucose levels rarely exceeding 15mmol/L (Scott et al., 1999a). Therefore hyperglycaemia induced by STZ would be considered severe and not typical of the clinical scenario.

1.3.4.2 Hyperglycaemia induced by glucose administration

Glucose administration has also been widely used to study the effects of hyperglycaemia in experimental stroke models. Glucose administration protocols vary amongst studies with regards to the route and timing of administration, dose used and the frequency of dosing. Due to the variation in protocols it is difficult to interpret what effect hyperglycaemia induced by glucose loading has on stroke outcome.

In permanent MCAO models glucose administration to induce hyperglycaemia has produced divergent results. In one of the earliest studies performed in cats, hyperglycaemia (~30mmol/L) was reported to reduce ischaemic injury in a study in which a 50% glucose infusion was administered before permanent ischaemia to induce hyperglycaemia (Zasslow et al., 1989). However in other studies, which have also used permanent MCAO models, hyperglycaemia induced by intraperitoneal injection of a 50% glucose solution before ischaemia had no influence on infarct size (Nedergaard et al., 1987, Slivka, 1991). In another study, a 20% glucose solution administered 2 hours prior- and 2 hours post-MCAO in rats increased infarct volume after permanent MCAO (Bomont and MacKenzie, 1995). In contrast to permanent MCAO models, results of glucose-induced hyperglycaemia on ischaemic damage are more consistent following transient MCAO, with the majority of studies reporting that hyperglycaemia exacerbates ischaemic damage (Gisselsson et al., 1999, Martin et al., 2006, Liu et al., 2007, Wei et al., 2003, Tan et al., 2015).

A wider range of glucose values, between 13-31mmol/L are reported in hyperglycaemic animals following glucose administration, with an average of ~23mmol/L. Glucose values exceeding 20mmol/L are not typically seen in patients with PSH, with one study reporting values >17mmol/L in fewer than 2% of patients (Scott et al., 1999a). In the GIST-UK clinical trial, patients with admission hyperglycaemia had only mild to moderate increases in plasma glucose levels compared to normoglycaemic patients (normoglycaemia: ~4-6mmol/L). In GIST-UK hyperglycaemia was defined as having a plasma glucose concentration between 6.0-17.0mmol/L. The median plasma glucose level in hyperglycaemic patients receiving GKI therapy was 7.6mmol/L, indicating a mild increase compared to normal levels (4-6mmol/L) (Gray et al., 2007). Results from experimental rodent studies, in which the majority of studies report blood glucose levels in excess of 20mmol/L, are therefore difficult to interpret as they are not typical of clinical scenarios with stroke patients. The establishment of an animal model with clinically relevant glucose values is therefore essential for future assessment of hyperglycaemia in experimental stroke.

1.3.5 Summary

Post-stroke hyperglycaemia is common and is associated with increased mortality and poor clinical outcomes. In addition, it is associated with an increased risk of intracerebral haemorrhage in patients treated with rt-PA, the only licensed thrombolytic therapy for ischaemic stroke. Several clinical trials have investigated the treatment of PSH with insulin but to date there is no clear evidence that insulin treatment improves patient outcome. The pathogenic mechanisms underlying the harmful effects of hyperglycaemia in ischaemic stroke are poorly understood. Understanding these mechanisms could help to guide the development of new therapies for treating PSH, as well as the optimal time-window for therapeutic intervention. The majority of the mechanistic proposals to date have been inferred from animal models that are not representative of the clinical picture of PSH. Therefore there is a need for further studies with relevant animal models. One potential mechanism by which hyperglycaemia may exacerbate ischaemic damage is through an influence on perfusion. The studies in this thesis aimed to test the hypothesis that hyperglycaemia leads to a significantly larger volume of hypoperfused tissue,

and subsequently to greater ischaemic damage, using an animal model of clinically relevant hyperglycaemia.

1.4 Thesis Aims

1. To optimise a clinically relevant animal model for studying the effects of hyperglycaemia in experimental ischaemic stroke.

2. To determine the effects of clinically relevant levels of hyperglycaemia on the severity of the initial blood flow deficit using ^{99m}Tc-HMPAO blood flow autoradiography and MRI perfusion imaging. MRI was also used to assess the effects of hyperglycaemia on acute lesion growth, perfusion-diffusion mismatch tissue and infarct size after permanent MCAO.

3. To determine if excitotoxicity induced brain injury pathways play a role in hyperglycaemia-mediated damage by examining the protein levels of calpain substrates in ischaemic brain tissue.

Chapter 2 - Methods

2.

2.1 ARRIVE guidelines

All experiments in this thesis were performed with strict adherence to the National Centre for the Replacement, Refinement and Reduction of Animals in Research (NC3R's) ARRIVE (Animal Research; Reporting *In Vivo* Experiments) guidelines *(*https://www.nc3rs.org.uk/**arrive-guidelines)**.

2.2 Animals

Adult male Sprague-Dawley, Fischer 344 or Wistar rats were obtained from Harlan laboratories UK and housed in an animal care facility at the University of Glasgow. On arrival to the University all rats were acclimatised for 1 week before experimentation. Rats were housed in groups of 2-4 rats per cage and were maintained on a 12:12 hour light:dark cycle. Water and food (standard rat chow) were available *ad libitum* until the day before surgery when food was removed at the end of the day for fasting. All experiments were performed under license from the UK Home Office (Personal license number 60/12152, working under Project license numbers 60/3759 and 60/4449). All surgical procedures in Chapters 3-5 were carried out by Lisa Roy. In Chapter 6 Lindsay Gallagher (Personal license number 60/713) assisted with surgery.

2.2 Surgery

Aseptic techniques were maintained throughout all surgical procedures. All rats were fasted for 18 hours prior to surgery. Fasting was essential as the anaesthetic used in this technique induced hyperglycaemia in fed rats but not fasted rats (in-house observation; (Saha et al., 2005). On the day of surgery, rats were weighed in the animal housing unit before being transferred to the operating theatre.

2.2.1 Induction and maintenance of general anaesthesia

Anaesthesia was induced in an anaesthetic gas chamber, with 5% isoflurane (Baxter Healthcare Ltd, UK) administered in a 30:70% oxygen:nitrous oxide mixture. The depth of anaesthesia was assessed using the withdrawal reflex,

where the footpad of a hind limb was tightly squeezed to evoke withdrawal of the foot. When the rat showed no reflex the animal was considered deeply anaesthetised and it was therefore appropriate to proceed with surgery. The withdrawal reflex was assessed regularly throughout the surgical period to determine if the anaesthetic dose required adjustment.

Once deeply anaesthetised the rat was immediately transferred to a designated area within the laboratory and the fur overlying any planned incision sites was removed using electric clippers (Wella, Germany) and cleared using a handheld vacuum (Black & Decker, USA). The rat was then transferred to the operating table and artificially ventilated via one of two methods: oral intubation or surgical tracheotomy.

Surgical tracheotomy

In experiments where rats were not recovered following surgery a tracheotomy was performed. Upon transfer to the operating table the rat was positioned on its back and a facemask was used to deliver isoflurane at a reduced dose of 2-3% in the same gaseous mixture as previously stated. The neck area, which was previously shaved, was cleaned with 70% alcohol. An incision was made through the skin and fascia of the neck using blunt ended scissors and the underlying musculature was divided by blunt dissection to expose the trachea. The connective tissue surrounding the trachea was carefully separated using small round forceps and two ligatures of 2-0 thread (Davis & Geck, UK) were threaded under the trachea and loosely tied around the proximal and distal ends of the exposed trachea, approximately 1.5cm apart. A small incision was made between rings of tracheal cartilage using microscissors (World Precision Instruments, UK) and a ventilation tube (Linton Instruments, UK) was quickly inserted into the trachea and advanced down the trachea, towards the bronchi, approximately 2cm. Prior to insertion of the ventilation tube, a ruler was used to measure 2cm from the bottom of the tube and this distance was marked on the tube using a permanent marker pen. When inserting the tube into the trachea, care was taken to ensure that it was not advanced beyond this mark as this could lead to obstruction of one of the bronchi. The ventilation tube was then quickly connected to the ventilator (Ugo Basile, Linton Instruments, UK) where the stroke volume was set to ~3ml at a frequency of 45 strokes per minute to maintain anaesthesia. The two ligatures at the proximal and distal

ends of the trachea were then tied firmly around the trachea and ventilation tube to hold it in place and the neck was stitched using 4-0 silk suture (Softsilk™, Covidien, USA).

Oral Intubation

In experiments where rats were recovered following surgery oral intubation was performed for artificial ventilation using a simplified rat intubation method (Jou et al., 2000). Following the initial induction of anaesthesia, animals were transferred to a cork board. A loop of 4-0 silk thread (Softsilk™, Covidien, USA) attached to the board was placed around the incisors of the animal and used to lift the animal into a raised position at an approximate angle of 45°. A fibre optic light (Schott, USA) was positioned over the neck of the animal and the tongue was pulled to one side. An intubation wedge made from a 2ml plastic syringe (BD Plastipak™, Spain, Figure 2.1C) was inserted into the mouth of the rat with the bottom of the wedge touching the rat's tongue and the roof touching its palate. The wedge was fixed firmly in the oropharyngeal cavity by natural pressure from the incisors. The wedge was held in a thumb and index finger grip and the tip of the wedge was elevated causing expansion of the oropharyngeal cavity and allowing visualisation of the vocal cords and trachea. A 16 gauge catheter, 45mm in length with a 70mm long wire stylet (MillPledge Veterinary, UK) was used as the endotracheal tube. The 5mm long sharp tip of the stylet was cut off to produce a blunt ended guide wire (Figure 2.1A). The wings of the 16 gauge catheter were also removed to enable the catheter to pass through the intubation wedge (Figure 2.1B). Under illumination of the fibre optic light the catheter attached to the guide wire was directed into the trachea. The guide wire was removed and the catheter was then further advanced 1-2cm into the trachea. The intubation wedge was then carefully removed with the aid of a cotton bud to hold the catheter in place. The catheter was then connected to a ventilator at a stroke volume of 3-4ml and a frequency of 55-60 strokes per minute. The dose of isoflurane delivered to the ventilator was set to between 2.5 and 3% to maintain anaesthesia. Condensation in the intubation tube and chest expansion and collapse synchronous with the ventilator provided confirmation that the intubation tube was correctly inserted into the trachea. The intubation tube was then secured in place by stitching it to the side of the mouth using 4-0 silk suture.

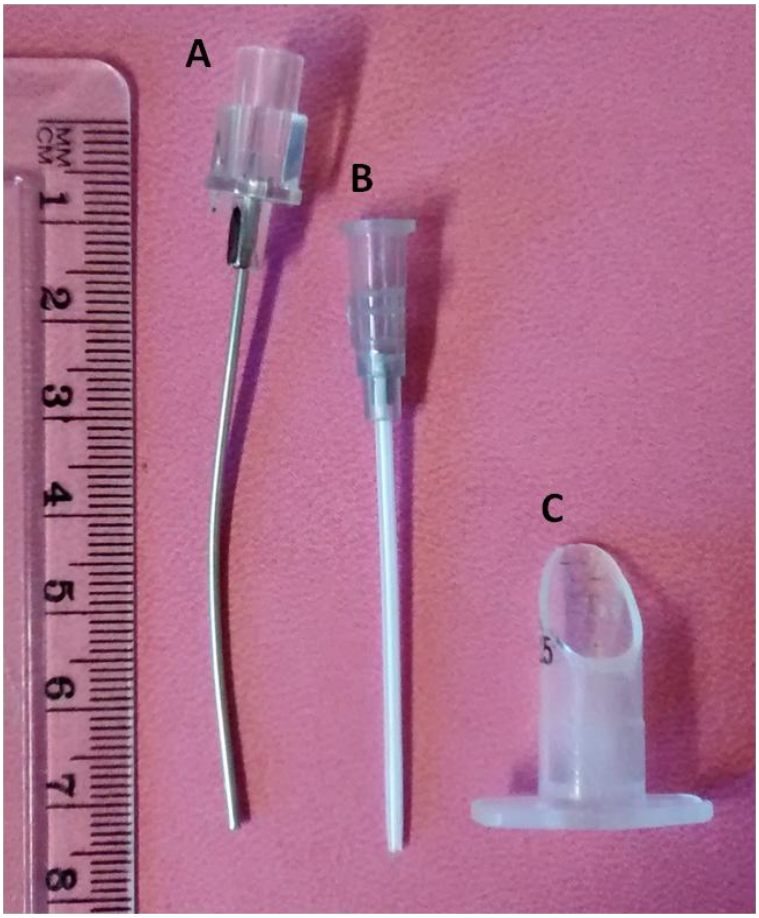

Figure 2.1. Rat intubation kit. Composed of a guide wire made from a blunt-ended 70mm long wire stylet (A), a 16 gauge catheter (B) and an intubation wedge prepared from a 2ml syringe (C).

2.2.2 Blood vessel cannulation

In all experiments the right femoral artery was cannulated to allow for continuous recording of mean arterial blood pressure (MAPB) and monitoring of blood gases and blood glucose. The rats' hind limbs were secured to the corkboard using masking tape (Tesa, Germany) to prevent movement during cannulation. The ventral abdomen and inner thigh region, which was previously shaved, was disinfected with 70% alcohol. A small incision was made in the skin and fascia over the region of the femoral vessels using blunt ended scissors. The femoral artery was carefully isolated from the femoral vein and saphenous nerve (~10mm section) using small curved and straight-edged forceps.

A 4-0 silk thread was securely fastened around the distal end of the artery and a second 4-0 thread was loosely tied around the proximal end. Tension was applied to the proximal and distal ties by using masking tape to secure the ends of the ties to the corkboard. Using microscissors, a small incision was made in the artery, mid-way between the two ties. A 30cm length of polythene catheter (external diameter 0.96mm; internal diameter 0.58mm, Smiths Medical International Ltd) attached to a 1ml syringe filled with 1% heparinised saline (1000units/ml, Wockhardt UK Ltd, UK) was then inserted into the vessel using right-angled forceps. Tension on the proximal tie was then released to allow the catheter to be advanced further into the vessel, ~1-2cm, before securing the catheter in place with the proximal tie. Before securing the distal tie, blood was withdrawn into the syringe to ensure that the catheter was inserted correctly. Excess thread was then removed and the wound was closed with a 4-0 suture to prevent the tissue from drying out. The catheter was connected to a blood pressure transducer which in turn was connected to a computer where physiological parameters including MABP and heart rate were recorded (Biopac, Acknowledge).

The femoral cannulation procedure was also performed on the right femoral vein for radioisotope administration in Chapter 4.

2.3 Focal Cerebral Ischaemia

2.3.1 Intraluminal filament model of middle cerebral artery occlusion

Permanent occlusion of the middle cerebral artery (MCA) was performed using the intraluminal filament model which was first described by Koizumi et al (1986) and later modified (Longa et al., 1989). All surgery was performed under a light operating microscope (Zeiss, Germany). Where a tracheotomy was performed for artificial ventilation the common carotid artery (CCA) was isolated through the incision site used for exposing the trachea. Where artificial ventilation was achieved through tracheal intubation the neck area was firstly shaved and disinfected with 70% alcohol before a midline incision was made through the skin and fascia in the neck region overlying the trachea. The soft tissues were carefully pulled apart and retracted to expose the left CCA. Using curved and straight-edged forceps the left CCA was carefully dissected free from surrounding nerves. A 4-0 silk thread was securely tied around the CCA ~15mm below the bifurcation of the external carotid artery (ECA) and the internal carotid artery (ICA), tying off the vessel at this point. A 4-0 silk thread was loosely tied around the CCA immediately below the bifurcation of the ECA and ICA. A loose tie was placed around the ECA above the occipital artery branch but below the ascending pharyngeal artery branch. Another loose tie was placed around the occipital artery and a separate tie was place around the ICA. The pterygopalatine artery was isolated and tied off at its bifurcation from the ICA using a 4-0 silk thread (Figure 2.2). Blood flow through the ECA, ICA and occipital arteries was ceased by applying tension to the ties. This was achieved by using masking tape to secure the ties to the corkboard.

The intraluminal filament was prepared from a length of 3-0 or 4-0 nylon monofilament (Dermalon, Sherwood Medical, USA). A small bulb was created at one end of the filament using a cauterising pen (Aaron Medical, FL, USA). The diameter of the bulb was measured and this was used to select filaments for use based upon the weight of the animal. The length of the filament was also measured and a bend was introduced at a point of 20mm from the bulb. This was introduced to ensure that the filament occluded the vessel at the origin of the MCA.

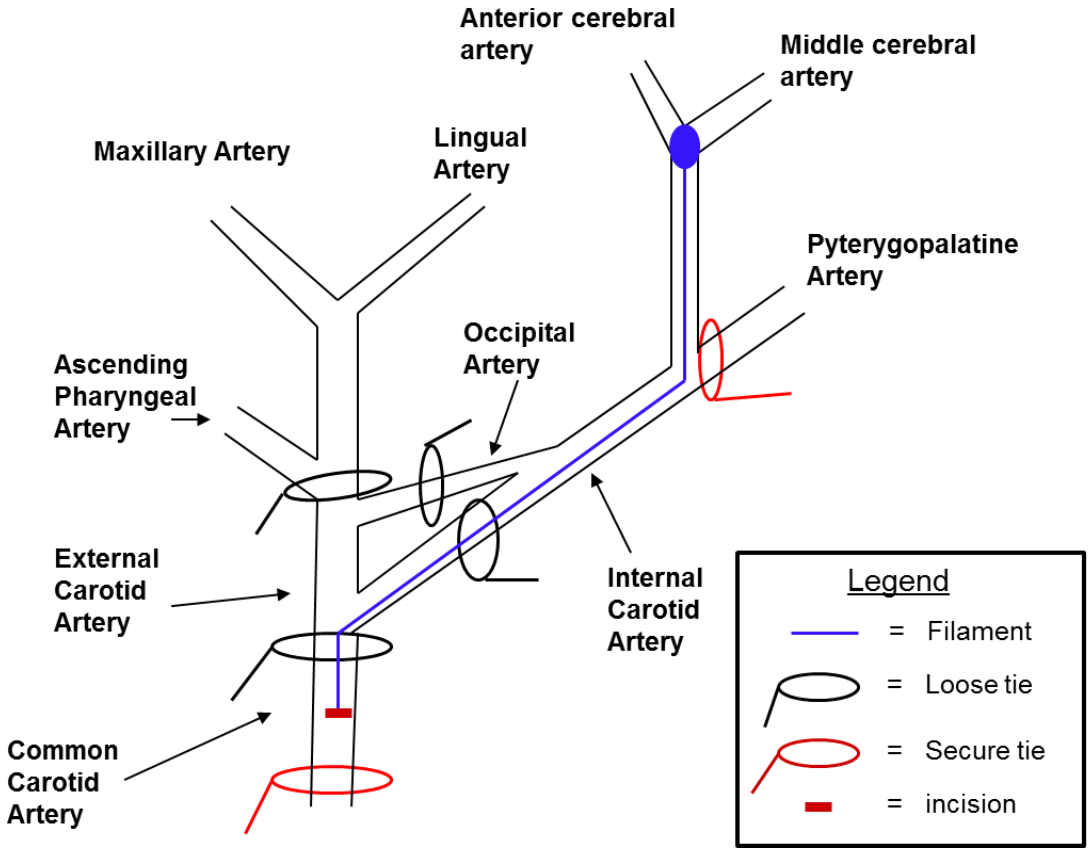

Figure 2.2. Diagram illustrating the intraluminal filament model of MCAO. The proximal end of the common carotid artery is tied off with a secure tie (red) and loose ties (black) are placed around the external carotid artery at the bifurcation with the internal carotid artery and where it meets the ascending pharyngeal artery. Loose ties are also placed around the occipital and internal arteries and a secure tie around the pytergopalatine artery. Tension is placed on these ties to cease blood flow during insertion of the filament. A small incision is made in the common carotid artery and the filament (blue) is advanced along the internal carotid artery until it lodges in the narrow proximal anterior cerebral artery, where it blocks the origin on the middle cerebral artery. The filament can be left in place for permanent MCAO or can be removed after a specified time to produce transient MCAO.

A small incision was made between the two ties on the CCA using microscissors and a filament was introduced through the incision and gently advanced through the ICA to the origin of the MCA where the filament meets slight resistance. After correct insertion of the filament, the loose ties around the ICA and CCA were tied firmly around the filament to hold it in place. Tension in the remaining loose ties was released and the ties were removed. The secure tie around the pytergopalatine artery was carefully removed using needle point forceps. The filament was left in position for 24 hours in order to occlude blood flow and induce a stroke within the MCA territory. The wound was closed using a 4-0 silk suture.

2.3.2 Distal diathermy model of MCAO

Following oral or tracheal intubation the rat was positioned laterally so that the left side of the head was clearly visible. The left eye was sutured closed with a 6-0 suture (SoftsilkTM, Covidien, USA) to prevent it from drying out and the whiskers were carefully taped over to one side. The area between the left eye and auditory canal was shaved and wiped clean with 70% alcohol. Using sharp-ended scissors, a small incision was made at the midpoint between the auditory canal and the left orbit, and the underlying connective tissue and muscle was dissected until the skull was clearly visible. Retractors were used to pull back the muscle in order to expose an area of the skull approximately 5mm^2. Small pieces of absorbent sponge (Surgiswabs, John Weiss International, UK) were carefully placed within the working area to protect the muscle and surrounding connective tissue from drilling. A craniectomy was performed on the exposed skull using a dental drill (Volvere Vmax, Nakanishi Inc) and a round diamond bur (Wright Cottrell, UK). Drilling was performed across the entire area of exposed skull in an up and down motion and took approximately 30 minutes to complete. The craniectomy site was regularly flushed with sterile saline (0.9%, Baxter Healthcare Ltd) during this time to prevent over-heating. Drilling was continued until the MCA and inferior cerebral vein (ICV) were visible through the skull. The remaining layer of bone was removed using needle point forceps. A dura hook, constructed in-house by bending the tip of a 21 gauge needle, was used to pierce the dura mater over a region with no visible blood vessels. Starting from this point the dura mater was carefully removed using needle point forceps and any bleeding from small vessels of the dura mater or those surrounding the MCA was

ceased by flushing the area with sterile saline. If bleeding continued then absorbent sponge was used to apply gentle pressure or the vessels were electrocoagulated using bipolar diathermy forceps (110mm angled, Eschmann, UK). The point at which the MCA crosses the ICV was identified and the entire portion of the MCA above and below the ICV was electrocoagulated with diathermy forceps (Figure 2.3). This was carried out under saline to prevent the diathermy forceps from sticking to the vessel. Mean arterial blood pressure was reduced to ~70mmHg during the diathermy step by increasing the concentration of isoflurane to 3.5%. MABP was reduced to this level for approximately 10 minutes and this step dramatically reduced bleeding from the surrounding cerebral vasculature. Complete occlusion of the MCA was confirmed by cutting the vessel using microscissors. Following this the absorbent sponges and retractors were removed from the craniectomy site and a small piece of haemostatic gauze (Surgicel, Ethicon, Johnson & Johnson Medical Ltd 2011) soaked in saline was placed inside the cavity before the muscle was closed over. The wound was then sutured using a 4-0 silk suture and the eye suture was removed.

2.3.3 Physiological monitoring

Throughout the period of anaesthesia a number of physiological variables were monitored and details of these variables were recorded at regular intervals. Body temperature was maintained at 37°C using an external heat lamp and recorded using a rectal thermometer (Physitemp, New Jersey, USA). A blood sample was taken at the beginning of each experiment (immediately after femoral artery cannulation) and at each hour from this point for the duration of the experiment for the measurement of blood pH, arterial oxygen tension (PaO_2) and arterial carbon dioxide tension ($PaCO_2$). A blood sample (~100µl) was withdrawn from the femoral artery cannula into a glass capillary tube and the tube was immediately taken to the blood gas analyser (Rapidlab 248/348, Siemens). The animal's temperature at the moment the sample was obtained was entered into the analyser and the blood gas analyser adjusted the blood gas and pH values according to the animal's temperature.

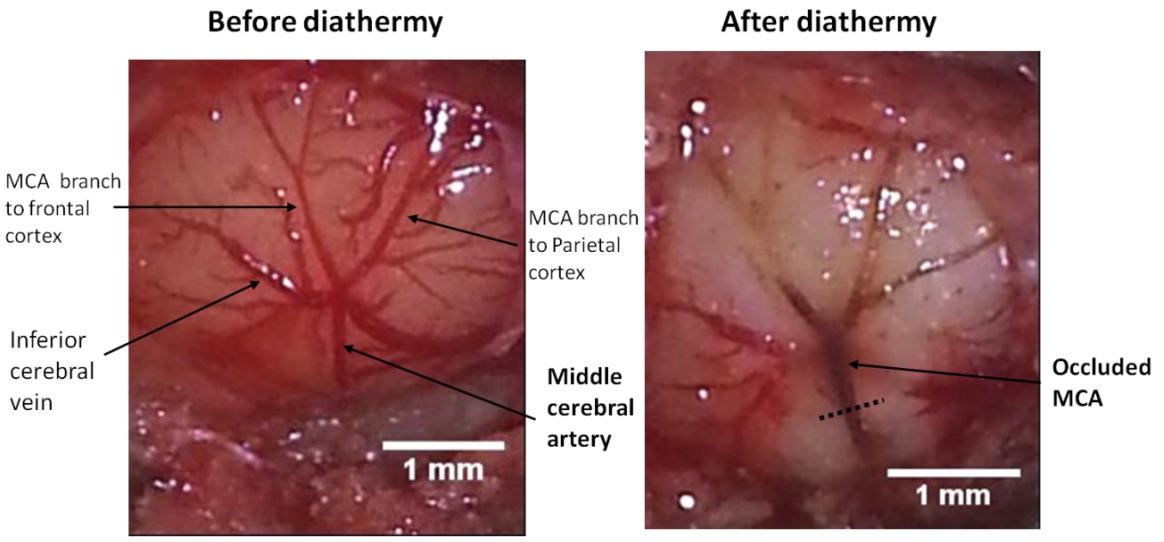

Figure 2.3. Images of the middle cerebral artery before and after the diathermy step performed during the distal diathermy MCAO model. The left image shows the MCA prior to the diathermy step. The inferior cerebral vein regularly crosses the MCA and this can be used as a point of reference when occluding and cutting the vessel. The right image shows the MCA after diathermy where approximately 2mm of the vessel is occluded. The dotted line indicates where the vessel is cut to confirm complete occlusion.

Blood gases and blood pH were maintained within a defined range ($paCO_2$ 35-45mmHg, pH 7.35-7.45) by adjusting the output parameters of the ventilator. PaO_2 values were higher than the normal physiological range of 80-100mmHg due to the high percentage (30%) of oxygen used to ventilate the animals. Blood pressure was monitored by connecting a femoral artery catheter to a blood pressure transducer which was connected to a computer in combination with an MP150 Biopac system (Biopac systems Inc, USA) and Acknowledge software (Linton) used to display mean arterial, systolic and diastolic blood pressure and heart rate throughout surgery. During all surgical procedures MABP was maintained within the range of 85-100mmHg by adjusting the isoflurane concentration.

2.3.4 Animal recovery from surgery

At the end of surgical procedures where animals were recovered from surgery for 24 hours, the arterial cannula was removed and the small incision in the artery was closed over using diathermy forceps. The wound was flushed with sterile saline and closed using 4-0 suture. The isoflurane concentration was decreased to 0% and the animals were ventilated with 100% oxygen until they became responsive to foot pinching and started to breathe without the ventilator. At this point the animal was disconnected from the ventilator and the intubation tube was removed. The animal was supplemented with 50% oxygen via a facemask until breathing became steady and the animal started to regain consciousness. At this point the animal was transferred to a clean cage lined with soft absorbent pads containing softened food and water available *ad libitum*. The cage was transferred to a recovery room maintained at ~25°C and the animal was housed there until it was killed at 24 hours. The animal was closely monitored for at least 2 hours post-surgery and details of the animals condition were recorded on animal recovery sheets.

2.4 Induction of hyperglycaemia and glucose measurements

In all experiments rats were randomly assigned to a vehicle or glucose treatment group using a randomization plan generator (http://www.randomization.com). Glucose treated rats received a 15% glucose solution (10ml/Kg), by intraperitoneal (IP) injection, 10 minutes before MCAO. A fresh glucose solution was prepared for each experiment by dissolving 1.5g of D-glucose (Sigma-Aldrich, USA) in 10ml distilled water. Vehicle treated rats received the equivalent volume of distilled water.

Blood and plasma glucose levels were measured regularly during experiments. Blood glucose levels were measured using the Accu-Chek® Aviva test strip system. To measure blood glucose using this system a test strip was placed in the meter and then a drop of blood, withdrawn from the femoral artery cannula, was placed at the tip of the test strip. The glucose value in mmol/L was displayed on the meter and was recorded. To ensure the results were reliable a control test was performed regularly and each time a new box of test strips was opened using Accu-Chek® Aviva control solutions in accordance with the manufacturer's instructions.

Plasma glucose levels were measured using a GM9 plasma glucose analyser (Analox Instruments Ltd, UK). To measure plasma glucose levels using the plasma glucose analyser a small amount of blood (~100µl) was withdrawn from the femoral artery cannula into a microcentrifuge tube. The microcentrifuge tube was centrifuged at 1000rpm for 2 minutes to separate the blood into its various components and plasma was inserted into the plasma glucose analyser using a pipette. The plasma glucose analyser utilizes an enzymatic assay to determine the plasma glucose concentration in mmol/L, which the machine produced a printout of. Before each use the glucose analyser was calibrated using an 8.0mmol/L glucose standard (Analox Instruments, UK). Although both blood and plasma glucose levels were measured in most studies, only blood glucose results are presented in this thesis. Plasma glucose levels tended to be higher than blood glucose levels as shown in Table 2.1, and this was expected because it is known clinically that the glucose content of plasma is approximately 12% higher than whole blood (Diabetes.co.uk). In one study

included in this thesis (Chapter 4) the glucose content of plasma ranged from between 9-28% above blood values (Table 2.1).

Time (min) relative to MCAO	Blood glucose (mmol/L)	Plasma glucose (mmol/L)	% difference
-20	7.1	8.8	24
0	13.2	14.4	9
30	13.1	16.3	24
60	11.9	15.3	28

Table 2.1. Comparison of blood and plasma glucose levels. Mean blood and plasma glucose levels measured in a group of Wistar rats (n=11) measured at baseline (-20 minutes) and 0, 30 and 60 minutes after MCAO. This group of rats received a 15% glucose solution (10ml/kg) 10 minutes before MCAO. The difference between blood and plasma glucose levels is expressed as a % of blood glucose values.

2.5 2,3,5-triphenyltetrazolium chloride staining and quantifying ischaemic damage

2,3,5-triphenyltetrazolium chloride (TTC) has been used for decades to identify regions of ischaemic tissue damage and has been validated for assessing infarct volume 24 hours after the induction of cerebral ischaemia (Bederson et al., 1986). TTC is a water soluble salt which is reduced by dehydrogenase enzymes to a lipid soluble, deep red formazan. Normal undamaged tissue will appear deep red after TTC staining as the mitochondria, which contain the necessary enzymes to reduce TTC, are still intact. Damaged tissue will remain unstained after TTC staining as the mitochondrial systems become incapacitated. Therefore in TTC stained brain slices from rats subjected to MCAO, the unstained regions depict the area of ischaemic damage (Figure 2.4). For TTC processing of the brain the animal was deeply anaesthetised at 24 hours post-MCAO using 5% isoflurane before decapitation. The brain was then rapidly removed and immersed in saline at 1-2°C. The brain was wrapped in tin foil and placed in the freezer at -20°C for 20 minutes. After this time the brain was placed into a rat brain matrix (World Precision Instruments, UK) and sectioned into 2 mm slices using microtome blades. The slices were incubated in a pre-warmed solution of 2% TTC (Sigma-Aldrich, Switzerland) in phosphate buffered saline at 37°C for 15 minutes. The sections were then removed from the TTC solution and fixed in 4% paraformaldehyde (PAM, VWR International, Belgium) overnight prior to imaging. For each brain, digital images of six, 2mm thick slices were captured using a digital camera. The areas of the infarct, ipsilateral (ischaemic) and contralateral (non-ischaemic) hemispheres were measured on both faces of each slice using image analysis software (ImageJ, http://rsb.info.nih.gov.ij). Infarct volume was calculated by summing the individual areas and multiplying by the slice thickness. Infarct volume was corrected for ipsilateral brain swelling (Swanson et al., 1990), by computing the volume of each hemisphere and using the following equation:

Corrected infarct volume =	Volume of contralateral hemisphere	-	(Volume of ipsilateral hemisphere – lesion volume)

Figure 2.4. Representative image of a rat brain slice stained with TTC. Cerebral ischaemia was induced using the distal diathermy model of permanent MCAO. The unstained region represents ischaemic damage.

2.6 Preparation of ^{99m}Tc-HMPAO for autoradiography

Technetium- 99m hexamethylpropyleamine oxime (^{99m}Tc-HMPAO) is an established radiopharmaceutical for the study of regional CBF both clinically and experimentally. Clinically ^{99m}Tc-HMPAO is used as a tracer to study rCBF using single photon emission computed tomography (SPECT). ^{99m}Tc-HMPAO is also used experimentally to assess CBF in animals using autoradiography (Baskerville et al., 2012). ^{99m}Tc-HMAPO autoradiography was used in Chapter 4 to assess the reduction in CBF 1 hour after MCAO. The isotope used in this study, [^{99m}Tc] pertechnetate, has a half life for gamma emission of 6.03 hours. Radiation protection measures were put in place during this experiment and all contaminated material was handled with caution and disposed of in accordance with the University of Glasgow's radiation protection policy.

2.6.1 Reconstitution of Ceretec kit

HMPAO is supplied in small single use vials under the trade name Ceretec™ (GE Healthcare, UK). Each vial contains a freeze-dried mixture of 0.5mg exametazime (HMPAO), 7.6µg stannous chloride dehydrate and 4.5mg sodium chloride. For the purpose of experimental rodent work, each vial of Ceretec™ was reconstituted in 1ml 0.9% sterile saline and 4 x 250µl aliquots were stored in sterile nitrogen filled vials at -50°C until further use.

2.6.2 Preparation and administration of ^{99m}Tc-HMPAO

On the day of the experiment ^{99m}Tc-HMPAO was prepared using fresh generator eluted sodium [^{99m}Tc] pertechnetate ordered from the dispensary at the Western Infirmary hospital, Glasgow. 500Mbq in 1ml of 0.9% saline was ordered in for a reference injection time of 1pm. If there was any deviation from this reference time the activity of the isotope at a certain time was calculated using the following exponential decay equation:

$$A(t) = A_0 e^{-\lambda t}$$

Where A(t)= activity at certain time; A0 = activity at reference time; -λ = decay constant (ln2 (0.693) / t1/2); t1/2 = half life.

Approximately 10 minutes before the planned injection time an aliquot of Ceretec (HMPAO) was removed from the freezer and transferred to a 1.5ml eppendorf tube. The reducing agent stannous chloride (7µg/ml) was added to the tube to stabilise the reagent. The volume of ^{99m}Tc-pertechnetate containing an activity of 280Mbq was calculated and this volume was added to the tube containing the aliquot of HMPAO. The contents of the tube were thoroughly mixed and the volume of ^{99m}Tc-HMPAO required to produce a dose of 225Mbq (~0.6ml) was withdrawn from the tube into a 1ml syringe. This step was carried out under a fume hood in a designated radioisotope laboratory. The syringe containing 225Mbq ^{99m}Tc-HMPAO was then placed in a lead lined container and transferred to the operating theatre.

2.7 Magnetic Resonance Imaging

MRI scanning took place at the Glasgow experimental MRI centre (GEMRIC) based within the University of Glasgow. MRI scanning was performed by staff within the centre: Jim Mullin, Dr Chris McCabe and Dr William Holmes, and technical assistance was provided by Lindsay Gallagher.

2.7.1 Magnet specifications

Animals were scanned using a Bruker Biospec 7T/30cm system with a gradient coil (internal diameter=121mm, 400mT/m) and a 72mm birdcage resonator (diffusion weighted imaging, perfusion imaging) or Bruker Pharmascan 7T/30cm system with a gradient coil (internal diameter=121mm, 400mT/m) and a 72mm birdcage resonator (T_2-weighted Imaging).

2.7.2 Physiological monitoring during MRI scanning

Following surgery to induce MCAO rats were immediately transferred to the MRI scanner and placed prone in a Perspex rat cradle and the head was restrained using tooth and ear bars. A linear phased array surface receiver coil (2cm diameter) was placed above the head of the animal. Body temperature was monitored using a rectal thermocouple and maintained within physiological range (37±0.5°C) using a temperature controlled water jacket. MABP was monitored via the femoral artery catheter attached to a blood pressure transducer, which was in turn connected to Biopac software. In some animals

electrocardiogram (ECG) leads were positioned onto the ventral surface of the chest and the left hind limb before animals were placed in the scanner. ECG leads were attached for cardiac gating during perfusion imaging when motion artefacts appeared in some scans. ECG gating allows for stop motion imaging by acquiring data only during a specified portion of the cardiac cycle (typically during diastole when the heart is not contracting) leading to improved perfusion images.

2.7.3 Diffusion Weighted Imaging

Diffusion-weighted imaging was performed each hour post-MCAO for 4 hours to assess the evolution of the ischemic lesion.

Technical specifications

Spin Echo-Echo Planar Imaging (SE-EPI) diffusion-weighted scans consisted of eight contiguous coronal slices of 1.5mm thickness which were generated with an in-plane resolution of 260μm. The field of view was 25 x 25mm^2 and the matrix size was 96 x 96mm. The gradient strengths (B values) were 0 and 1000 s/mm^2 and gradient directions were x, y and z. The repetition time (TR) was 4000.3ms and the echo time (TE) was 22.5ms.

Image Processing

Quantitative ADC maps (mm^2/sec) were generated for each of the 8 contiguous coronal slices throughout the brain (Figure 2.5). Raw datasets were initially processed using Paravision v5 (Bruker Biospin). Subsequent analysis of ADC maps was carried out using ImageJ (http://rsb.info.nih.gov.ij) software. To calculate ADC lesion volume an abnormal diffusion threshold was applied to all ADC maps. ADC threshold values are described in detail in Chapter 5.

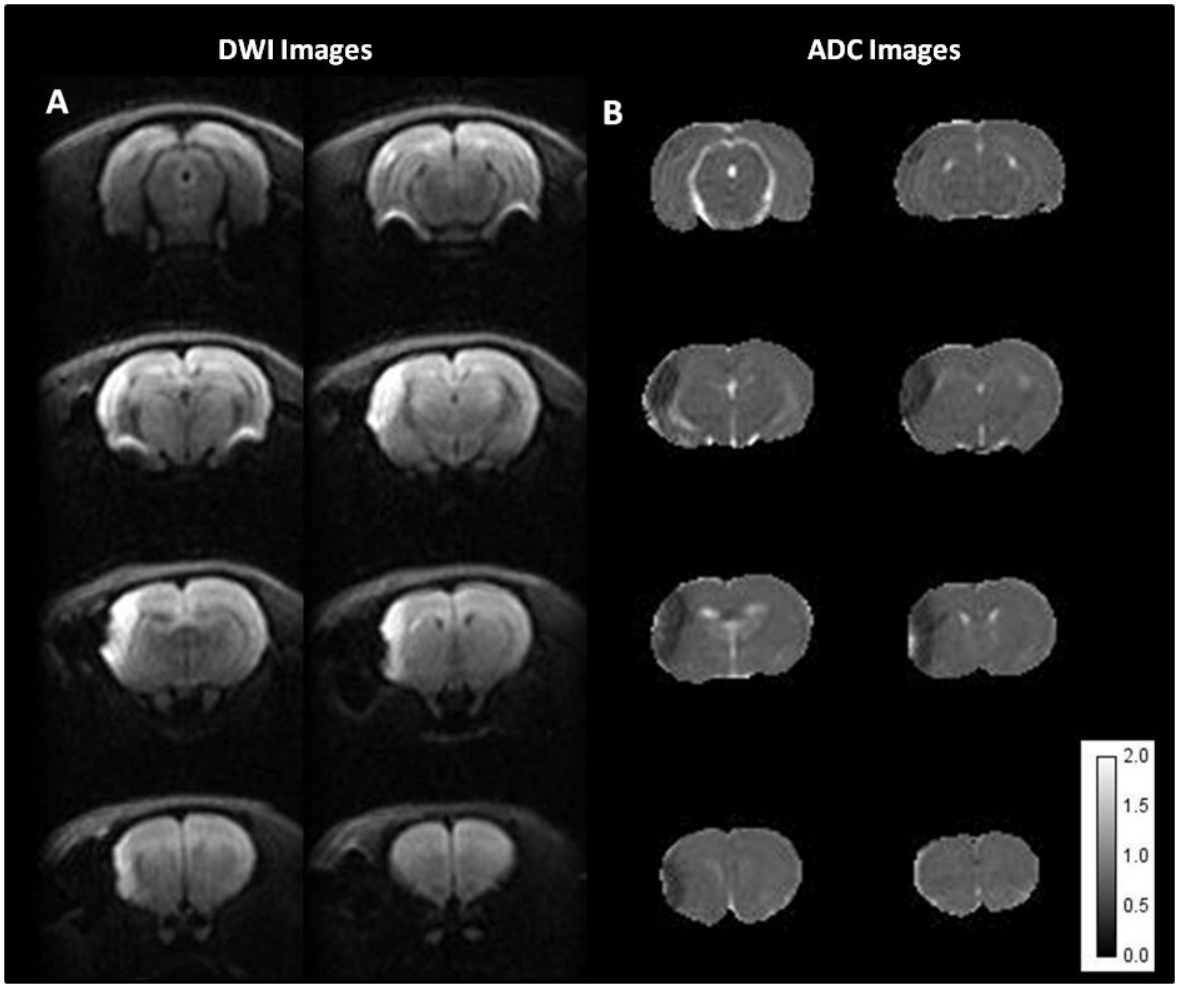

Figure 2.5. DWI images of 8 coronal slices from a rat brain 4 hours after permanent MCAO. B. The equivalent ADC maps for the 8 DWI images. The region of ischaemic damage appears bright on DWI maps and dark on ADC maps. Scale bar - ADC values expressed as 0-2 x10^{-3} mm^2/sec.

2.7.4 Perfusion imaging

Perfusion Imaging was performed each hour post MCAO for 4 hours to assess the perfusion deficit.

Technical specifications

Quantitative imaging of CBF (expressed as ml/100g/min) was carried out on 6 coronal slices within the MCA territory (slices 2-7 of DWI scan) during ischaemia using a form of pseudo-continuous arterial spin labelling (pCASL) based on a train of adiabatic inversion pulses (Baskerville et al., 2012). The sequence employs a SE-EPI imaging module (TE 20ms,TR 7000ms, matrix 96 x 96, FOV 25 x 25mm^2, slice thickness 1.5mm, 16 averages, 4 shots) preceded by 50 hyperbolic secant inversion pulses in a 3 second train (Baskerville et al., 2012, Moffat et al., 2005). Inversion pulse frequency offset and gradient strength were set to provide 10mm label/control bands centred at ±30mm from the centre of the imaging slice. A T_1-weighted image was also acquired each hour for four hours using an EPI inversion recovery sequence (TE=20ms, TR=10000ms, matrix=96x96, FOV=25x25mm, slice thickness 1.5mm, 16 averages, 4 shots, using 16 inversion times from 200ms to 7700ms). Quantitative CBF maps in ml/100g/min were calculated using the following formula for continuous labelling (Williams et al., 1992):

$$CBF = \frac{\lambda}{T1} \frac{S^{control} - S^{label}}{2\alpha S^{control}}$$

Where α is the inversion pulse efficiency (0.79 taken from Moffat et al, 2005), λ is the blood tissue partition function (assumed to be 0.9). $S^{control}$ and S^{label} are the signal intensity from the control and labelled images acquired with inversion pulses applied above the head and in the neck respectively.

Image processing

CBF maps were generated for 6 contiguous slices throughout the brain. Raw data sets were processed using ImageJ software. To quantify the CBF images the labelled pCASL images were first subtracted from the averaged control images (Subtracted pCASL, Figure 2.6A) and the resulting image was divided by the control image to generate a relative CBF map (Normalised pCASL, Figure 2.6B).

Fully quantitative CBF maps (Figure 2.6D) were generated by dividing the relative CBF map by the T1 values generated from the T1 map (Figure 2.6C). A perfusion deficit map was produced by applying an abnormal perfusion threshold to the CBF map (Figure 2.6E). An absolute perfusion threshold of 30ml/100g/ml was applied to pCASL images. Details of the perfusion threshold are described in Chapter 5.

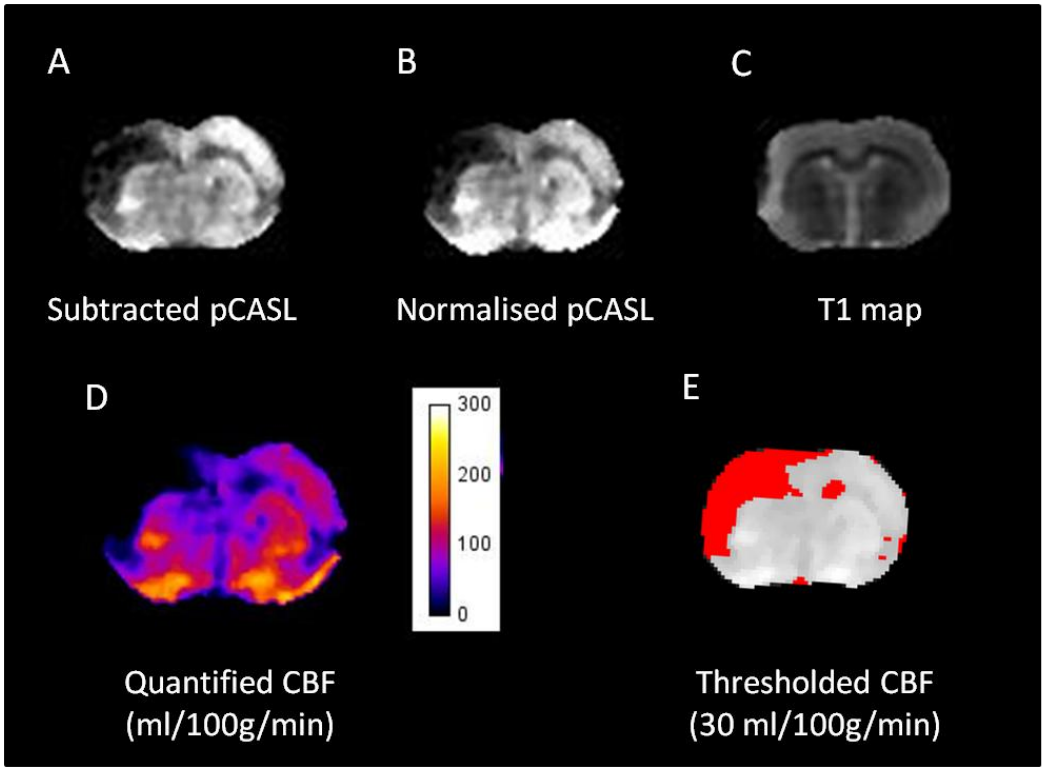

Figure 2.6. Images from the different steps involved in the post-processing of pCASL images to produce quantitative CBF maps. Colour bar units, ml/100g/min, red shading in (E), CBF below 30ml/100g/min.

2.7.5 T_2-Weighted Imaging

T_2-weighted imaging was performed at 24 hours post-MCAO to calculate infarct volume.

Technical specifications

A RARE (rapid acquisition with refocused echoes) T_2 weighted sequence (effective TE: 46.8ms, TR: 5000s; in plane resolution of 97 um; 16 slices of 0.75mm thickness) was used to determine infarct volume 24 hours post MCAO (Figure 2.7).

Image processing

The infarct was defined as the hyperintense area on T_2-weigted images. ImageJ was used to measure the area of the hyperintense region on each of the 16 slices in mm^2. Infarct volume was calculated by summing the total area across the 16 slices and multiplying by the slice thickness. The areas of the ipsilateral and contralateral hemispheres on each slice were also measured and these were used to calculate the volume of each hemisphere. Infarct volume was corrected for oedema using published equations (see below) that take into account both the compression of the contralateral hemisphere (Gerriets et al., 2004), and swelling of the ipsilateral hemisphere (Swanson et al., 1990).

To correct infarct volume for swelling of the ipsilateral hemisphere the following equation was used:

Corrected infarct volume = Volume of contralateral hemisphere - (Volume of ipsilateral hemisphere – lesion volume)

To account for compression of the contralateral hemisphere a correction factor was established using the following equation:

Compression factor = (ipsilateral volume + contralateral volume)/(2 x contralateral volume)

To correct infarct volume for both ipsilateral swelling and compression of the contralateral hemisphere the following equation was used:

Infarct Volume = Corrected lesion volume x Compression Factor

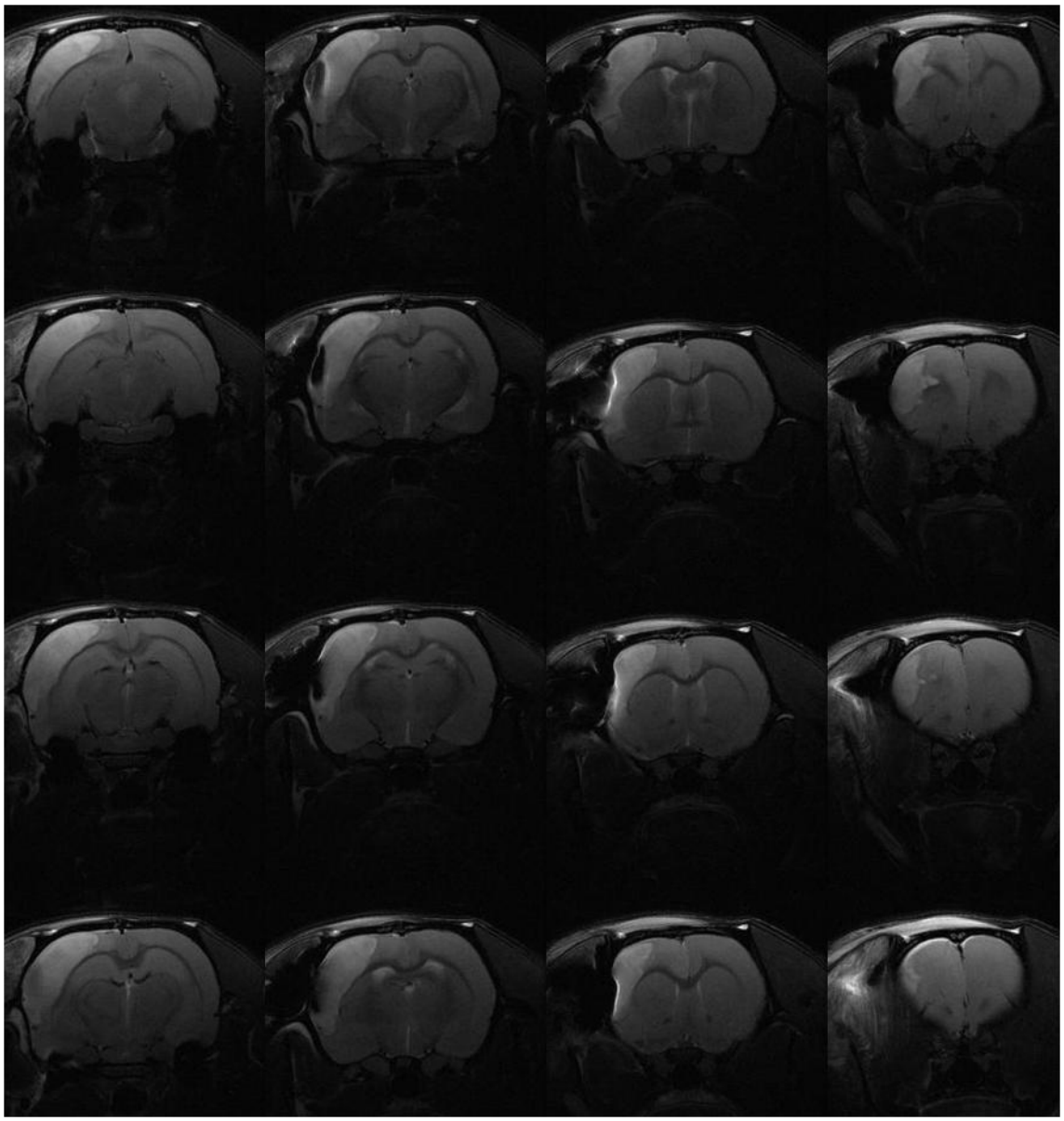

Figure 2.7. T_2-weighted images of 16 coronal slices from a rat brain imaged 24 hours after permanent MCAO. Ischaemic damage appears bright on T_2-weighted images. From top-bottom and left to right the coronal sections lie caudal-rostral.

2.8 Protein Analysis

2.8.1 Materials

All materials in this section were purchased from either Sigma-Aldrich or BioRad Laboratories unless otherwise stated:

Sigma-Aldrich, UK
Sucrose, HEPES, protease inhibitor cocktail, sodium orthovanadate, sodium pyrophosphate, sodium chloride, Tris-base, Tween 20, Ponceau S solution ethylenediaminetetraacetic acid, phenylmethylsulfonyl fluoride.

BioRad Laboratories Inc, UK
2x Laemmli sample buffer, dithiothreitol (DTT), pre-cast 4-20% polyacrylamide mini-protean TGX gels and Criterion TGX gels, precision plus protein standards, 10x Tris/Glycine/SDS running buffer, Trans-Blot turbo mini and midi transfer packs, Clarity Western ECL substrate.

2.8.2 Preparation of rat brain tissue lysates

Brain tissue lysates were prepared from the ipsilateral cortex of rats in which permanent MCAO was induced for 2 or 24 hours. To obtain the ipsilateral cortex samples rats were euthanized by decapitation and the brains were rapidly removed from the skull and placed onto a chilled glass plate. The olfactory bulbs and cerebellum were removed and discarded and the remaining cerebrum was dissected into four: ipsilateral cortex, contralateral cortex, ipsilateral subcortex and contralateral subcortex. Each sample was placed into a sterile eppendorf tube and snap frozen in liquid nitrogen. Samples were stored at -80°C until for later use.

Prior to tissue homogenisation, a homogenate buffer (HB, Table 2.2), supplemented with a protease inhibitor cocktail (Table 2.3) was prepared and pre-chilled on ice. Approximately 0.4g of ipsilateral cortex brain tissue was transferred to a 15ml tube and homogenised in 2ml HB using a Ultra-Turrax T8 blender (IKA Labortechnick, USA). Homogenates were centrifuged at 1000rpm for 20 minutes at 4°C, using a Beckman TL-100 centrifuge to remove debris.

Reagent	Concentration
Sucrose	250mM
Hepes	10mM
Sodium orthovanadate	1mM
Sodium pyrophosphate	1mM
EDTA	1mM
PMSF	0.2mM

Table 2.2. Tissue homogenisation buffer. The buffer was supplemented with a protease inhibitor cocktail (Sigma, UK). The desired volume of HB was prepared in distilled water. Ethylenediaminetetraacetic acid (EDTA), phenylmethylsulfonyl fluoride (PMSF).

Component	Inhibitory Property	Concentration
AEBSF	Serine proteases	104mM
Aprotinin	Serine proteases	80µM
Bestatin	Aminpeptidases	4mM
E-64	Cystein proteases	1.4mM
Leupeptin	Serine & cystein proteases	2mM
Pepstain A	Acid proteases	1.5mM

Table 2.3. Protease inhibitor cocktail (100X). A 1X dilution of the protease inhibitor cocktail was added to the tissue homogenisation buffer.

The resulting supernatant was transferred to a fresh centrifuge tube and centrifuged at 30,000 rpm for 30 minutes at 4°C. After this second, high speed spin, the resulting supernatant (cytosolic fraction) was removed and stored at -20°C until required. The pellet (membrane fraction) was resuspended in HB and centrifuged at 30,000 rpm for 30 minutes at 4°C. The resulting supernatant was discarded and the pellet was resuspended in HB and stored at -20°C until required.

2.8.3 Protein assay

The protein concentration in the brain tissue fractions from each rat was determined using the Pierce bicinchoninic acid (BCA) protein assay kit (Fisher Scientific, UK). This method is an adaptation of the Lowry method (Smith et al., 1985), and relies on the reduction of Cu^{2+} to Cu^{1+} by protein in an alkaline medium. This biuretic reaction generates a purple chromagen that is proportional to the amount of protein at a specific absorbance of 562nm.

Protein assays were performed using a 96 well plate. For each plate 25µl of blank standard (distilled water) and bovine serum albumin (BSA) protein standards: 25, 125, 250, 500, 750, 1000, 1500 (µg/ml), and 5µl of each sample were loaded in duplicate. 200µl of working reagent (mixture of reagent A&B from BCA kit in a 50:1 ratio) was added to each well and plates were covered and incubated at 37°C for 30 minutes. The absorbance of the plate was read on a standard spectrophotometer (Cecil Instruments, UK). The protein concentration of the samples was determined using a standard curve of the 562nm absorbance measurements for each albumin standard concentration (µg/ml) and correcting for the amount of sample loaded (Figure 2.8). The average 562nm absorbance measurement of the blank standard was subtracted from all standard and sample replicates prior to constructing the standard curve.

2.8.4 Sodium dodecyl sulphate polyacrylamide gel electrophoresis (SDS-PAGE)

To prepare samples for SDS-PAGE the desired amount of protein was determined from the protein concentration obtained from the BCA protein assay. Samples were mixed (1:1) with 2x Laemmli sample buffer containing 0.1M DTT and made up to a final volume with distilled water. Samples were prepared in equal

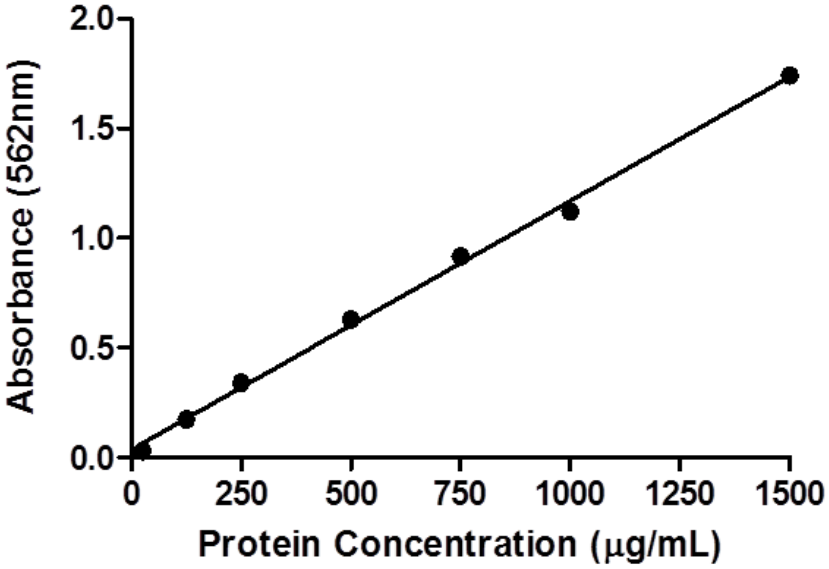

Figure 2.8. Typical standard curve using BCA protein assay

volumes and with equal amounts of protein (10µg/well). Samples were denatured in a water bath at 95°C for 4 minutes prior to loading the samples on to gels. Heating proteins in the presence of DTT linearises the proteins by disrupting protein disulphide bonds and the presence of SDS, an anionic detergent, imparts a negative charge which facilitates their migration towards the anode during PAGE.

Samples were loaded on to 1.0mm thick pre-cast 4-20% polyacrylamide mini-PROTEAN TGX gels (10 well) or Criterion™ TGX gels (18 or 26 well, BioRad Laboratories, UK). 5µl of Precision Plus Protein™ standards (10-250kD) were loaded into the first well of each gel and the samples were added to the other wells. Empty wells were loaded with a volume of sample buffer equal to the volume of the samples. 10 well gels were run in 1x Tris/Glycine/SDS running buffer in a BioRad Mini-PROTEAN® tetra Cell at 140 volts. 18 or 26 well gels were run in 1x Tris/Glycine/SDS running buffer in a Biorad Criterion™ Cell at 200 volts. Both cells were connected to a BioRad PowerPac Basic and gels were run until the blue dye had reached the bottom of the gel (approximately 1 hour).

2.8.5 Gel Staining

Following SDS-PAGE gels were removed from their plastic cassettes and transferred to a clean plastic tray and washed three times, for 5 minutes each time, with distilled water. Gels were stained with 20ml Coomassie blue stain (SimplyBlueTM SafeStain, Invitrogen, UK) for 1 hour with gentle agitation. Gels were initially de-stained in distilled water for 1 hour followed by a second overnight wash. Gels were then placed in a fixing solution containing 50% methanol and 10% glacial acetic acid overnight and stored in a 5% glacial acetic acid solution. The stained gels were dried using a gel dryer (BioRad, UK). Gel staining with Coomassie blue allows the visualisation of proteins as blue bands (Figure 2.9), and this reflects the strong covalent binding of the dye with the proteins on the gel (which is proportional to the amount of protein).

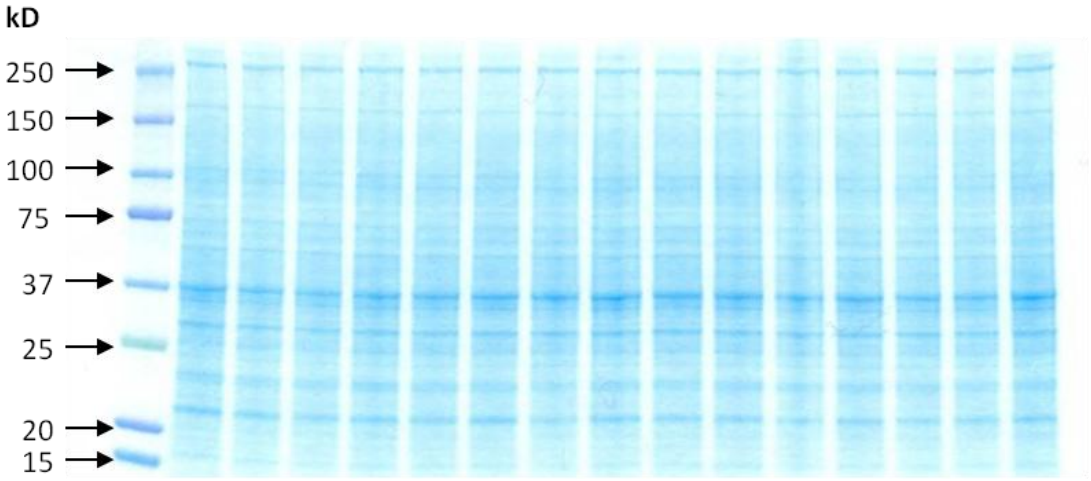

Figure 2.9. Image of a gel stained with Coomassie blue. Protein molecular weight standards were run in the left hand lane. In each subsequent lane 10µg of ischaemic cortex brain tissue, collected 2 hours post-MCAO from rats that were hyperglycaemic or normoglycaemic at the time of MCAO, was run.

2.8.6 Western blot

Following SDS-PAGE gels were removed from their cassettes, the wells were removed using a scalpel blade and the gels were washed in distilled water for 5 minutes. The Trans-blot Turbo system from BioRad was used for the transfer step. Gels were placed onto a nitrocellulose membrane which is a component of the transfer packs which are supplied with the system. Mini (7 x 8.5cm) transfer packs were used for 10 well gels and midi (8.5 x 13.5cm) transfer packs were used for 18 and 26 well gels. The packs were assembled in one of the transfer cassettes according to the manufacturer's instructions and the proteins were transferred using the turbo option on the system which takes 7 minutes. Following transfer membranes were quickly removed from the cassettes and stained with Ponceau S solution to confirm the successful transfer of proteins from the gel onto the membrane. Following removal of the Ponceau S solution, membranes were washed in distilled water for 5 minutes followed by two 5 minute washes in 1x Tris-buffered saline containing Tween-20 (1x T-TBS, Table 2.4). Membranes were blocked with 5% milk powder in 1x T-TBS for 1 hour then incubated overnight at 4°C in a primary antibody. The primary antibodies used in this thesis were: monoclonal mouse anti-spectrin (MAB1622, Millipore, UK), polyclonal rabbit anti-MAP2 (ab32454, Abcam, UK) both at a 1/200,000 dilution and monoclonal mouse anti-beta Actin (ab8224, Abcam, UK) at a 1:400,000 dilution. Primary antibodies were prepared in 5% milk powder in 1x T-TBS. After the overnight incubation membranes were washed in 1x T-TBS three times for 10 minutes each and were incubated for 1 hour in a horseradish peroxidise (HRP) conjugated secondary antibody. For the spectrin and ß-actin antibodies a polyclonal goat anti-mouse HRP conjugated secondary antibody was used (P0447, Dako, UK). For the MAP2 antibody a polyclonal goat anti-rabbit HRP conjugated secondary antibody was used (P0448, Dako, UK). Both secondary antibodies were diluted 1/10,000 (5% milk powder in 1x T-TBS). Membranes were then washed three times as before.

Reagent	Amount
Tris-Base	60.2g
Sodium Chloride	87.7g
Tween 20	10ml

Table 2.4. T-TBS (10X) recipe. The reagents were dissolved in 700ml distilled water and the pH was adjusted to 7.4 with concentrated hydrochloric acid before making up to 1 litre with distilled water. 1 litre of 1x T-TBS was prepared by diluting 10x T-TBS 1:10 in distilled water.

2.8.7 ECL detection and signal quantification

BioRad's Clarity Western enhanced chemi-luminescence (ECL) substrate was used in this study. Membranes were incubated in 2-4ml of the reagent for 1 minute and excess reagent was removed by placing blots between two sheets of filter paper. Membranes were placed in clear plastic wrap and exposed to X-ray film (hyperfilm™ECL™, Amersham Biosciences, UK) in a light tight cassette for a range of exposure times (between 1 and 60 seconds) and developed using an automatic film processor (Xograph Healthcare, UK). Membranes were also visualised using the BioRad Chemidoc MP system and Image Lab software (BioRad, UK). This system uses a high-resolution charge coupled device camera to produce a digital image of the membrane and therefore does not require the use of x-ray film.

The x-ray film images were scanned to produce a digital image and examples of an x-ray image and a BioRad Chemidoc image from the same membrane are shown in Figure 2.10. The x-ray images became saturated after an exposure time of 1 second which made it impossible to analyse the results. Therefore only images from the Biorad Chemidoc system were analysed in this thesis.

To estimate the amount of protein in each sample images were analysed using ImageJ. The rectangular selection tool in this software was used to select a band of interest on the image and a plot profile of the grey levels that represent the relative density over the area of each band was generated. The area under each peak was quantified and the values were expressed in arbitrary units of optical density (OD).

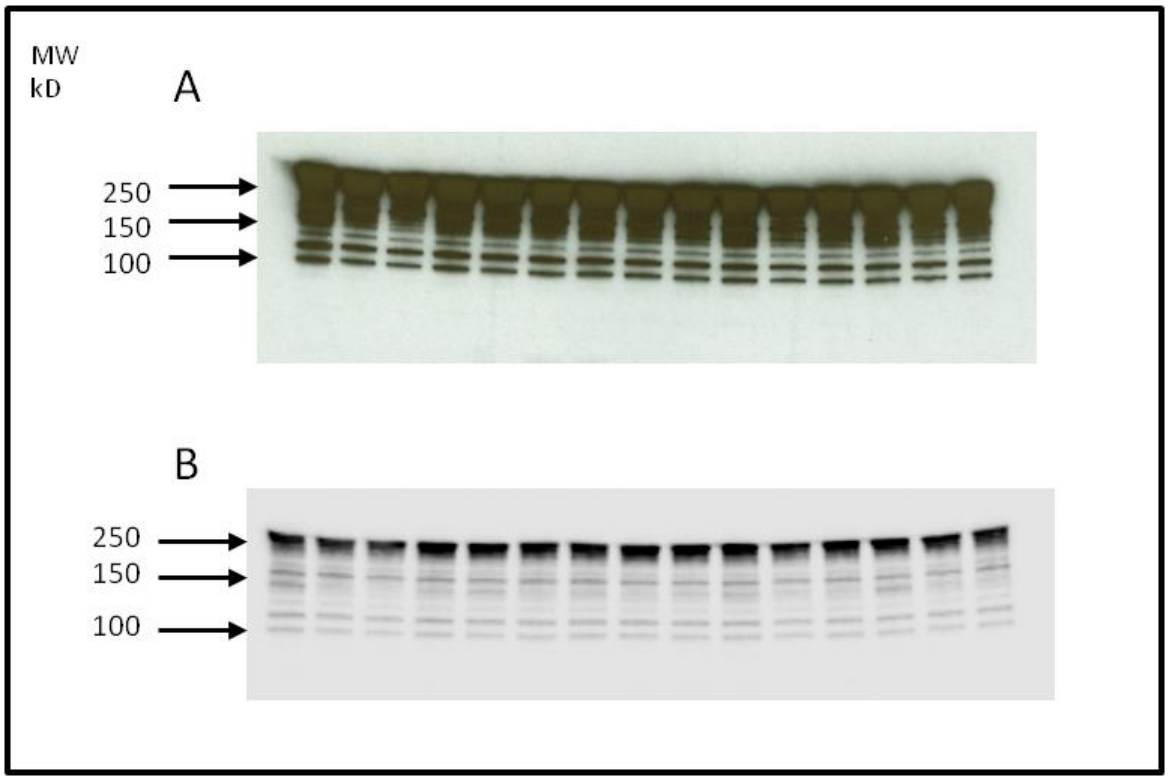

Figure 2.10. Western blot imaging methods. A. Images of a western blot produced using X-ray film. The membrane was exposed to the film for 1 second and the bands at 280kD and 150kD appear saturated. B. Image of the same blot produced using the BioRad Chemidoc system which automatically determines the exposure time (7 seconds in this case). The bands in this image are not saturated. The primary antibody for this blot was mouse anti-αIIspectrin (1:200,000).

Chapter 3 – Establishing a rodent model of clinically relevant hyperglycaemia

3.

3.1 Introduction

3.1.1 Animal models of hyperglycaemia in experimental stroke research

It is widely accepted that hyperglycaemia is associated with increased mortality and disability ischaemic stroke patients (Capes et al., 2001, Parsons et al., 2002). The findings from animal models however show diverging results. Most studies are consistent with the clinical findings, reporting that hyperglycaemia increases ischaemic damage in both permanent (Decourtenmyers et al., 1988, Huang et al., 1996b, Prado et al., 1988) and transient (Huang et al., 1996b, Nedergaard, 1987, Gisselsson et al., 1999) models of focal cerebral ischaemia, whereas others have shown that hyperglycaemia may be beneficial by decreasing the extent of ischaemic damage following experimental stroke (Zasslow et al., 1989, Ginsberg et al., 1987, Kraft et al., 1990). Data from a recent systematic review of studies assessing the effects of hyperglycaemia on infarct size in animal models of MCAO found that most of the previous studies report clinically irrelevant models of hyperglycaemia (MacDougall and Muir, 2011). This is because in previous studies hyperglycaemia was induced by either streptozotocin injection, which is a method used to induce experimental type I diabetes and thus does not reflect the most common type of diabetes, type 2, observed in acute stroke patients (Air and Kissela, 2007). In addition hyperglycaemia was also induced using glucose loading protocols that induced extremely high glucose levels that are rarely observed in patients with PSH. Therefore the development of a model with clinically relevant blood glucose values for the assessment of PSH is important for future experimental studies.

3.1.2 Rodent model of clinically relevant hyperglycaemia

3.1.2.1 Method of inducing hyperglycaemia

Recent data established from in-house studies showed that administering a 15% glucose solution IP to Wistar Kyoto (WKY) rats or fructose fed spontaneously hypertensive stroke-prone (ffSHRSP) rats 10 minutes before MCAO produced blood glucose levels of ~12mmol/L at the time of MCAO (Tarr et al., 2013). In

rats that received a vehicle solution at the same time blood glucose levels at the onset of MCAO ranged from 5-6mmol/L. In an acute MRI study using both rat strains hyperglycaemia, induced using the above method, was shown to increase the diffusion weighted lesion as early as 1 hour post-MCAO when compared to rats that received vehicle treatment. This level of hyperglycaemia is within the range of glucose values considered hyperglycaemic in the GIST-UK clinical trial (6-17mmol/L) and thus hyperglycaemia at clinically relevant levels was shown to increase ischaemic damage after MCAO. Further studies performed in-house using this same method to induce hyperglycaemia in Sprague Dawley (SD) rats showed that glucose treatment significantly increased infarct volume 24 hours after permanent MCAO (Tarr, 2012). Prior to glucose or vehicle treatment and MCAO, baseline blood glucose values measured in SD rats were approximately 5-7mmol/L. Following vehicle or glucose treatment at 1 hour post-MCAO blood glucose values remained at baseline levels in vehicle treated rats but rose to ~16mmol/L in animals that received glucose treatment. Blood glucose values in hyperglycaemic SD rats were higher than those observed in hyperglycaemic WKY and ffSHRSP rats but the values could still be considered clinically relevant (Gray et al., 2007). Together these data showed that administering an IP injection of a 15% glucose solution 10 minutes before MCAO produced blood glucose levels that were clinically relevant and that caused exacerbation of ischaemic damage. It was therefore decided to use this method to induce hyperglycaemia.

3.1.2.2 Rat strain

In ischaemic stroke patients hyperglycaemia is associated with a worse outcome in non-diabetic patients compared to those with a history of diabetes mellitus (Capes et al., 2001). In a more recent study Shimoyama et al (2014), confirmed this reporting that hyperglycaemia was associated with infarct volume growth and neurological deterioration in non-diabetic patients but not those with a diagnosis of diabetes (Shimoyama et al., 2014). These findings suggest that hyperglycaemia may be more harmful to specific sub-groups of ischaemic stroke patients and evidence from experimental studies using rodent models of stroke support this. Tarr et al (2013), investigated the effects of hyperglycaemia on lesion growth and infarct volume in rats with and without features of the metabolic syndrome (Tarr et al., 2013). Hyperglycaemia accelerated acute lesion growth in both rat strains but only increased infarct volume at 24 hours

post-MCAO in rats without features of the metabolic syndrome. A potential explanation for this could be due to the increased sensitivity to ischaemia in the rats with metabolic syndrome resulting in a severe initial lesion that makes it difficult to detect an increase induced by acute glucose treatment.

Together the data from both clinical and experimental stroke studies suggests that the effects of hyperglycaemia are worse in the absence of any underlying co-morbidities. To try and reflect these findings a normotensive rat strain was selected for future studies investigating the mechanisms responsible for the deleterious effects of hyperglycaemia in ischaemic stroke. The SD rat is an out-bred rat strain commonly used in medical research which is considered a standard, normotensive rat strain. Hyperglycaemia, has been previously shown to increase infarct volume in SD rats (Tarr, 2012). Therefore this strain of rat was selected for Study 1 which aimed to establish a rodent model in which ischaemic damage is increased by hyperglycaemia, at clinically relevant levels.

However, in Study 1 the blood glucose levels observed pre- and post-MCAO in normoglycaemic SD rats (vehicle group) were higher than previously recorded levels in this strain (Tarr, 2012). The high blood glucose levels suggest that the rats are hyperglycaemic before and after treatment and therefore describing the blood glucose levels in rats that receive vehicle treatment as “normoglycaemic” would be inaccurate. In a second study (Study 2) blood glucose levels were measured in different breeding colonies of SD rats: SDF and SDG, and in two other normotensive rats strains, Wistar and Fischer-344 rats, to determine which strain had glucose values which closely resembled normoglycaemic levels (target glucose range of GIST-UK: 4-7mmol/L)(Gray et al., 2007). Rats from the strain in which blood glucose values closely resembled normoglycaemic levels could then be used in subsequent mechanistic studies.

3.1.3 Study aims

To study the pathophysiological mechanisms leading to the increased infarct volume in hyperglycaemic rats, two studies were performed for the purpose of optimising a suitable rat model:

Study 1: Investigate the effect of hyperglycaemia on infarct volume following permanent MCAO in the Sprague Dawley rat

To develop an animal model in which ischaemic damage is induced in the presence of hyperglycaemia at clinically relevant levels.

Study 2: Compare glucose values pre- and post-MCAO in different rat strains

To identify a rat strain with clinically relevant 'normal' glucose values before and after MCAO.

3.2 Methods

All animals were obtained from Harlan Laboratories (UK) and housed in an animal care facility at the University of Glasgow. All experiments were carried out on adult male rats (250-400g) and all animals were maintained on a 12:12 hour light/dark cycle. Water and food were freely available until the night before surgery when rats were fasted overnight with free access to water.

3.2.1 The effect of acute hyperglycaemia on infarct volume following permanent MCAO in the Sprague Dawley rat (Study 1)

Adult male Sprague Dawley rats were randomly assigned to vehicle and glucose treatment groups using an online randomization plan generator. Rats were anaesthetised with 5% isoflurane, intubated and mechanically ventilated with 2.5% isoflurane in a 70% nitrous oxide and 30% oxygen mixture. The left femoral artery was cannulated for continuous recording of mean arterial blood pressure and monitoring of blood pH, $PaCO_2$ and PaO_2. Blood gases, with the exception of PaO_2, were maintained within normal physiological range throughout the experiment by adjusting the ventilator settings. The high percentage of oxygen used to maintain physiological stability resulted in PaO_2 values that were higher than the normal physiological range. Body temperature was maintained at 37±0.5°C using an external heat source and recorded using a rectal thermometer. Permanent focal cerebral ischaemia was achieved by occluding the left MCA using the ILF method as described in Chapter 2.3.1. The filament was left in position for 24 hours in order to permanently reduce blood flow within the MCA territory. Blood and plasma glucose levels were measured 20 minutes before MCAO (baseline) and 0, 10, 40 and 60 minutes post-MCAO as described in Chapter 2.4. Ten minutes prior to inserting the filament animals received an IP injection of vehicle or glucose solution (10ml/Kg) as described in Chapter 2.4. Animals were recovered for 24 hours following surgery and infarct volume was measured at 24 hours post-MCAO using TTC staining as described in Chapter 2.5.

3.2.2 Comparison of blood glucose values pre- and post-MCAO in different rat strains (Study 2)

Sprague Dawley colony F (SDF, n=4), Sprague Dawley colony G (SDG, n=4), Fischer 344 (n=7) and Wistar rats (n=6) were used in this study. The rats were anaesthetised with 5% isoflurane, intubated and mechanically ventilated with 2.5% isoflurane in a 70% nitrous oxide and 30% oxygen mixture. The left femoral artery was cannulated for continuous recording of MABP and monitoring of blood pH, $paCO_2$ and paO_2. Body temperature was maintained at 37°C using an external heat source and recorded using a rectal thermometer. Permanent focal cerebral ischaemia was achieved by occluding the distal portion of the MCA using the diathermy method adapted from Tamura et al (1981) as described in Chapter 2.3.2. Blood glucose levels were measured 20 minutes before occlusion of the MCA to obtain a baseline measurement and at 1 hour post-MCAO as described in Chapter 2.4. All glucose measurements were taken while the animals were under anaesthesia. In this study rats did not receive a vehicle or glucose injection and infarct volume was not measured. Rats were recovered for 24 hours following induction of focal cerebral ischaemia as described in Chapter 2.3.4. At 24 hours post-MCAO rats were deeply anaesthetised with 5% isoflurane and brains were removed, sectioned and stained with TTC. The animals in this study contributed to the training of the investigator (LR) in the distal diathermy method of MCAO therefore TTC staining was only performed to confirm successful occlusion of the MCA.

A separate group of Wistar rats (n=6) underwent identical surgery to that described above but these rats received a 15% glucose solution 10 minutes prior to MCAO. Blood glucose values were measured at baseline (20 minutes pre-MCAO) at the onset of MCAO (0 minutes post-MCAO) and at each hour for 4 hours post-MCAO. Infarct volume was not measured in these rats and therefore after the final glucose measurement at 4 hours post-MCAO the rats were killed using an overdose of isoflurane.

3.2.3 Statistical analysis

In Study 1 the blood glucose data were plotted over time and the area under the curve (AUC) was calculated. The blood glucose data measured over the first 60 minutes of MCAO were analysed using a repeated measures 2-way ANOVA with Bonferroni post-test. AUC data were analysed using an unpaired Student's t-test. Physiological variables, baseline blood glucose levels (Study 1) and infarct volume (were also analysed using an unpaired Student's t-test. In Study 2 baseline blood glucose data (scatterplots) were analysed using a 1-way ANOVA with Tukey's test for multiple comparisons. Also, blood glucose data in a group of Wistar rats was plotted over time and, as a summary measure, the values at baseline and 240 minutes post-MCAO were analysed using a paired Student's t-test. Data are expressed as mean ± standard deviation or scatterplots with the mean indicated.

3.3 Results

3.3.1 The effect of hyperglycaemia on infarct volume induced by intraluminal filament MCAO in the Sprague Dawley rat

3.3.1.1 Mortality and excluded animals

A total of 24 Sprague Dawley rats were included in Study 1. Three rats (two from the glucose treatment group and one from the vehicle group) died during the 24 hour recovery period. The brains of these rats were examined and showed signs of a subarachnoid haemorrhage. Two rats from the vehicle group died during MCAO surgery. One rat from the glucose group was excluded because of damage to the brain tissue. The final group sizes for analysis were n=9 for both the vehicle and glucose groups.

3.3.1.2 Physiological Variables

The physiological variables measured were all within the normal physiological range, except PaO_2 which was elevated by increasing the % inspired oxygen to maintain physiological stability during general anaesthesia. There were no significant differences in body weight, MABP, temperature, blood PaO_2, $PaCO_2$ or pH measurements between vehicle or glucose treated rats (Table 3.1).

Group	Weight (g)	MABP (mmHg)	$PaCO_2$ (mmHg)	PaO_2 (mmHg)	pH	Temperature (°C)
Vehicle (n=9)	303 ± 17	87 ± 4	40 ± 8	125 ± 16	7.4 ± 0.1	37 ± 0.1
Glucose (n=9)	296 ± 24	86 ± 3	45 ± 15	120 ± 37	7.4 ± 0.1	37 ± 0.1

Table 3.1. Pilot study 1 physiological variables. Body weight was measured prior to MCAO; MABP and temperature expressed as mean over entire surgical period; pH, $PaCO_2$, PaO_2 measured at the onset of MCAO. Values are mean ± standard deviation. There were no significant differences in any of the variables between the two groups (unpaired Student's t-test).

3.3.1.3 Blood glucose levels

Blood glucose levels were measured prior to glucose or vehicle treatment (baseline) and at 0, 10, 40 and 60 minutes post-MCAO. Mean baseline blood glucose levels were similar between groups (vehicle, 8.6 ± 8mmol/l; glucose, 8.0 ± 3.6mmol/l, P=0.4, Figure 3.1A). These values were higher than those recorded in previous glucose studies using Sprague Dawley rats (Tarr, 2012), with values >10mmol/L in some animals.

Following a single IP injection of either vehicle or 15% glucose solution blood glucose levels remained stable around baseline values in the vehicle group and rose to a mean level of ~16mmol/L in the glucose group at the onset of MCAO (Figure 3.1B). Glucose values in the glucose treatment group remained at this elevated level for the duration of the 60 minute measurement period. In order to test if there were differences between the two groups at each time point the data were analysed using a repeated measures 2-way ANOVA with Bonferroni's post-test. The blood glucose levels in the glucose treatment group at the onset of MCAO and at each time point post-MCAO were significantly higher than vehicle treated rats. As a summary measure the area under the blood glucose curve was established for each rat in each group (Figure 3.1C). The AUC data demonstrate that the rats that received glucose treatment have a significantly greater blood glucose level during the first hour of MCAO compared to those that received vehicle treatment (vehicle, 695±75mmol.min.L^{-1}; glucose, 1288±126mmol.min.L^{-1}, P<0.0001).

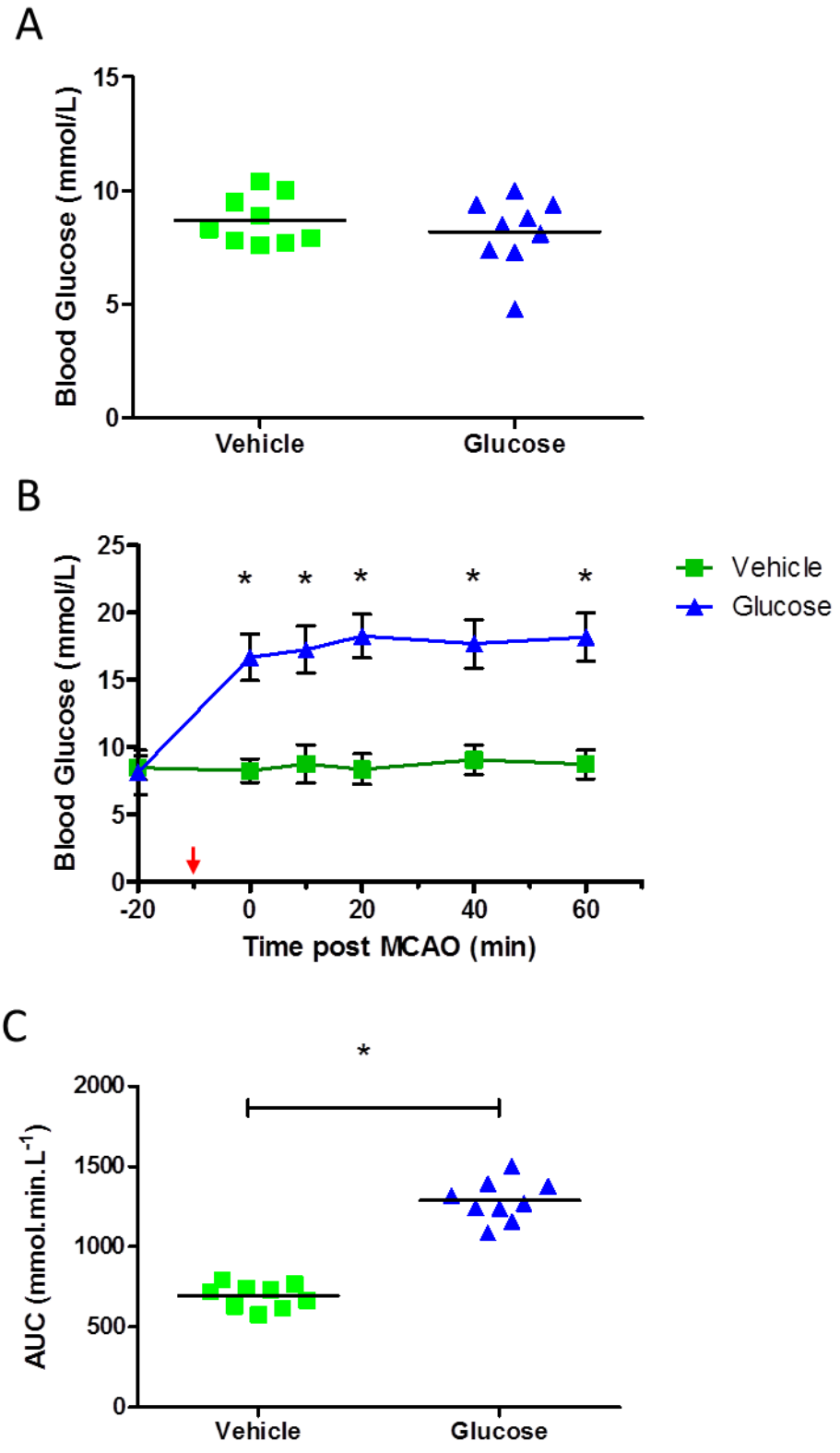

Figure 3.1. Blood glucose data from Study 1. Baseline blood glucose levels measured 20 minutes before ILF MCAO in SD rats (A). Data are presented as scatter plot with the line indicating the mean. There were no differences between groups (P=0.4, unpaired Student's t-test). The blood glucose response to a vehicle or 15% glucose solution in SD rats (n=9 per group) during the first 60 minutes of ILF-MCAO presented as the temporal profile (B) and area under the curve (C). The data in B) are presented as mean ± standard deviation. *P<0.0001 compared with vehicle group using repeated measures 2-way ANOVA. The data in C) are presented as scatter plot with the line indicating the mean. The red arrow in B indicates the time of glucose or vehicle administration. *P<0.0001 compared with vehicle group using Student's unpaired t-test.

3.3.1.4 Infarct Volume

Infarct volume was measured 24 hours after ILF MCAO using TTC staining and corrected for ipsilateral brain swelling as described in Chapter 2.5. Representative TTC stained sections from the median animal of each group are presented in Figure 3.2A. The unstained region on each slice represents the area of ischaemic damage. In both groups the area of ischaemic damage induced by MCAO encompassed almost the entire ipsilateral hemisphere. A scatterplot showing the infarct volume data for individual animals in each group is presented in Figure 3.2B. Mean infarct volume was 234.4±145mm^3 in the vehicle group and 332.5±149mm^3 in the glucose group. The difference in infarct size between the two groups was not statistically significant (p= 0.2). Within each group there was notable variation in infarct volume measurements and this is reflected in the large standard deviation values.

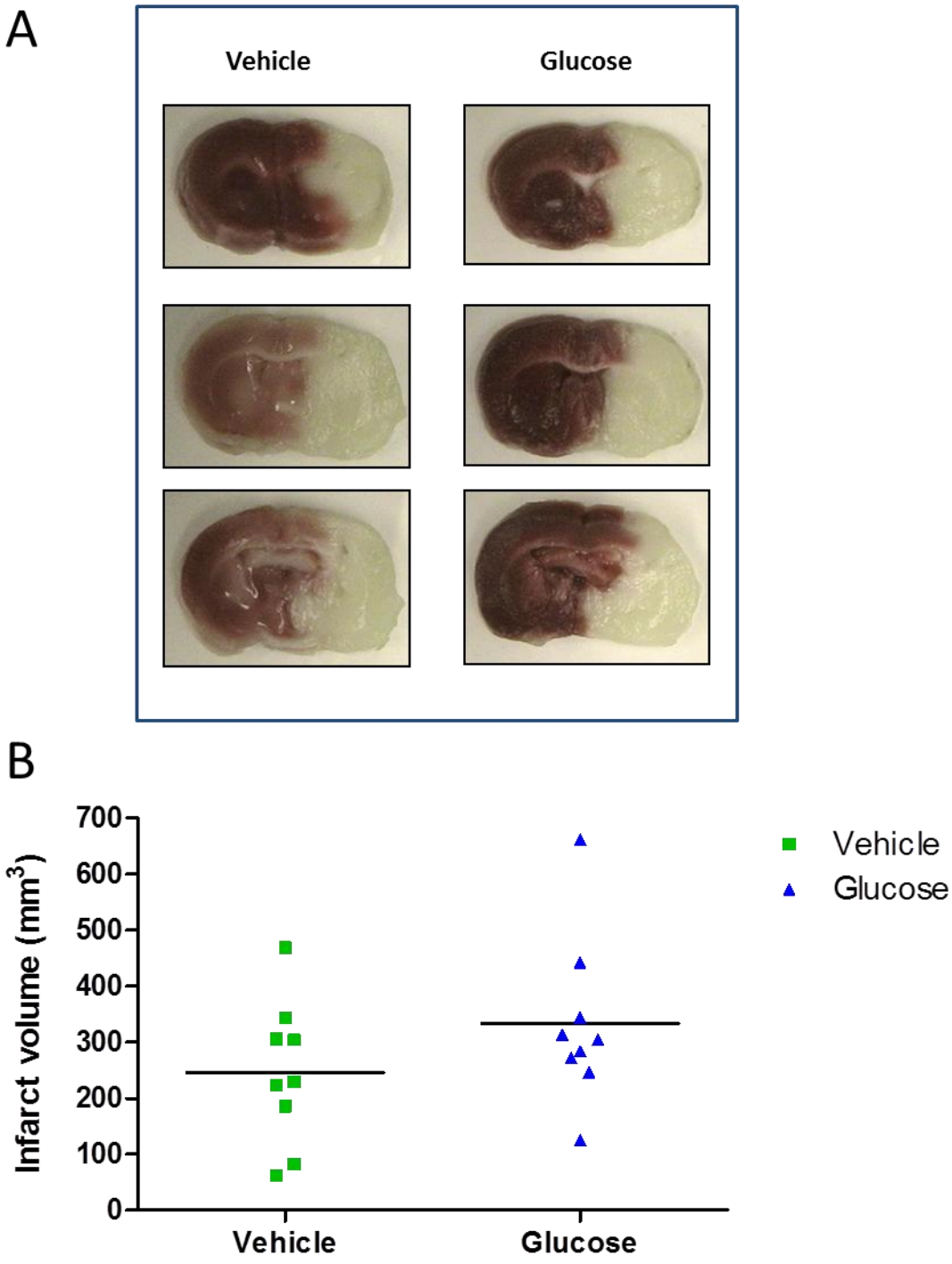

Figure 3.2. Infarct volume data from Study 1. A. Photographs illustrating three coronal sections of rat brain slices stained with TTC 24 hours after ILF MCAO from the median rat of each group. B. Scatter plot illustrating infarct volume 24 hours after ILF MCAO, in vehicle (n=9) and glucose (n=9) treated Sprague Dawley rats. The horizontal line represents the mean. The difference in infarct size between the two groups was not statistically significant (P=0.2, unpaired Student's t-test).

3.3.2 Comparison of blood glucose values pre- and post-MCAO in different rat strains

In Study 1 the blood glucose values measured pre- and post-MCAO in normoglycaemic SD rats were higher than previously observed in this rat strain, indicating that the rats were hyperglycaemic before treatment. To determine if there might be a possible breeding issue within this strain blood glucose levels were measured in rats from two different breeding colonies of SD rats: SDF and SDG, pre- and post-MCAO. In addition, blood glucose levels were measured in two other normotensive rat strains: Wistar and Fischer-344, to determine if another strain had glucose values that were within the target normoglycaemic glucose range.

3.3.2.1 Mortality and excluded animals

A total of 8 Sprague Dawley rats were included in this study. Four died during recovery from anaesthesia or during the 24 hour recovery period. Blood glucose data were collected from all 8 rats and therefore no SD rats were excluded. Nine Fischer-344 rats were included: two rats died shortly after the induction of anaesthesia (suspected overdose of anaesthetic) and two died during the 24 hour recovery period following surgery. The two that died following the induction of anaesthesia were excluded. A total of 12 Wistar rats were included in the study. Two Wistar rats died following recovery from surgery but the glucose measurements from these rats were included in the study. The final group sizes for analysis were n=4 for SDF and SDG groups, n=7 for the Fischer-344 group and n=6 per group in each of the two separate studies using Wistar rats.

3.3.2.2 Blood glucose levels pre- and post MCAO in different strains

In order to identify a rat strain with clinically relevant normoglycaemic blood glucose levels (target glucose range: 4-7mmol/L), blood glucose levels were measured in two different breeding colonies of Sprague Dawley (SDF and SDG), Fischer-344 and Wistar rats 20 minutes pre-MCAO and 60 minutes post-MCAO. At baseline, blood glucose levels were relatively high in all groups in comparison to the target blood glucose range of 4-7mmol/L. Mean baseline blood glucose values were 8.3, 8.6, 6.9 and 8.6mmol/L in SDF, SDG, Fischer-344 and Wistar rats respectively (Figure 3.3, top). In order to test the hypothesis that there

were strain differences the data were analysed using a 1-way ANOVA with Tukey's multiple comparisons correction separately at each time point following MCAO. At baseline there were no significant differences in blood glucose levels between strains. Mean blood glucose levels 60 minutes post-MCAO were 9.3, 8.5, 6.4 and 5.7mmol/L in SDF, SDG, Fischer-344 and Wistar rats respectively (Figure 3.3, bottom). The blood glucose levels in Wistar rats at 60 minutes post-MCAO were significantly lower than the levels in SDF and SDG rats and blood glucose levels in Fischer-344 rats were significantly lower than SDF rats.

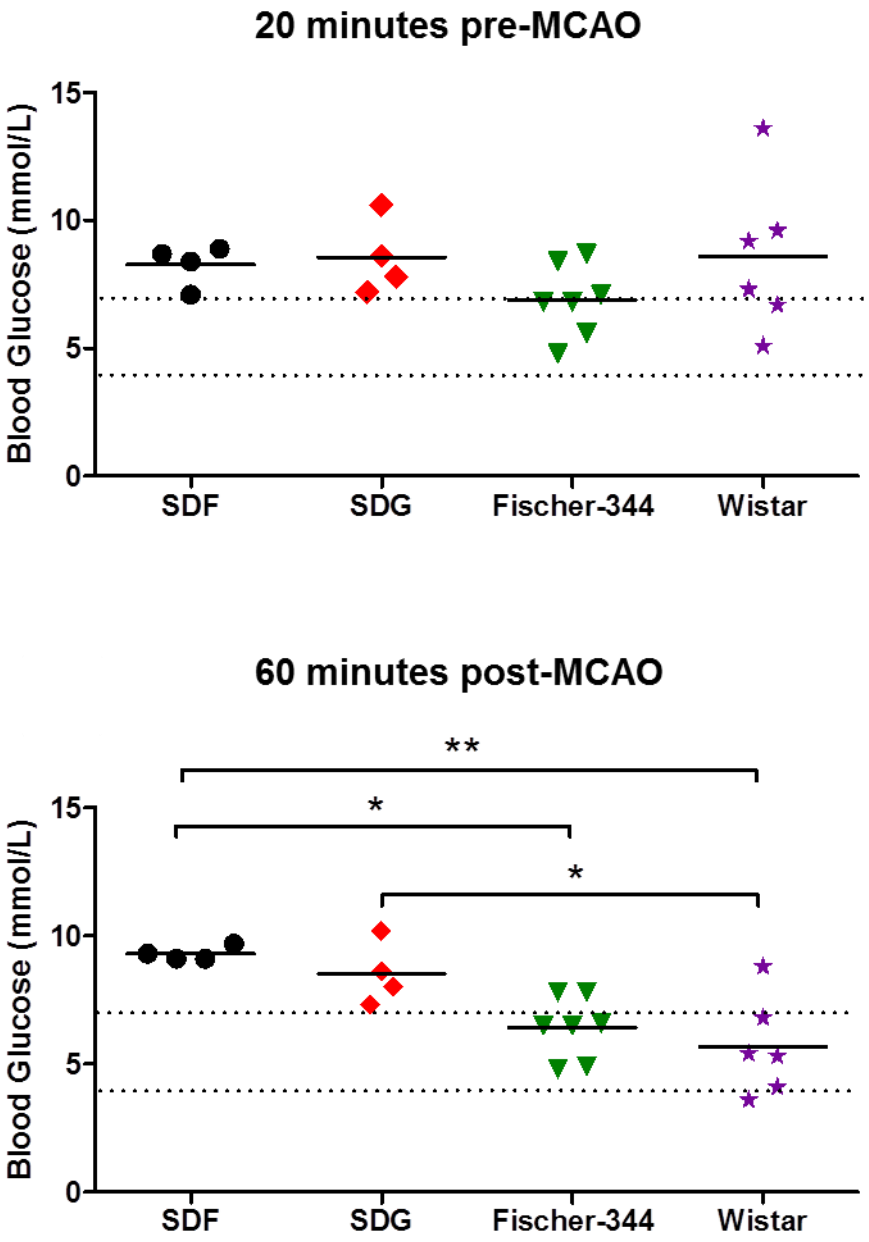

Figure 3.3. Blood glucose data pre- and post-MCAO in different rat strains. Blood glucose values in two separate breeding colonies of Sprague Dawley (SDF & SDG, n=4 per colony), Fischer-344 (n=7) and Wistar rats (n=6) at 20 minutes pre-MCAO and 60 minutes post-MCAO. The dotted lines on each graph represent the target blood glucose range for normoglycaemic rats: 4-7mmol/L. Data are presented as scatterplots where the line indicates the mean. Data analysed using 1-way ANOVA with Tukey's multiple comparisons test. *P<0.05, **P<0.01.

3.3.2.3 Blood glucose levels in Wistar rats

Although Fischer-344 rats displayed glucose values within the target blood glucose range of 4-7mmol/L, pre- and post-MCAO, two rats from this strain died following the induction of anaesthesia whereas there were no such deaths in any of the other strains. Further consideration was therefore given to the Wistar strain as this strain displayed mean blood glucose levels within the target range at 1 hour post-MCAO and the scatterplot of the individual blood glucose values for each Wistar rat at baseline showed that there were some rats with values within or close to the target blood glucose range. Consequently Wistar rats were included in a separate study where MCAO was induced using the DD method and glucose levels were measured at baseline and at each hour for 4 hours post-MCAO. All rats received a 15% glucose solution in this study. The mean blood glucose level at baseline in this group of rats was 6.3mmol/L (Figure 3.4). Following glucose treatment mean blood glucose levels rose to ~12mmol/L and remained at this elevated level for 4 hours post-MCAO. The difference between blood glucose levels measured at baseline and 4 hours post-MCAO was statistically significant (Figure 3.4B, P=0.004).

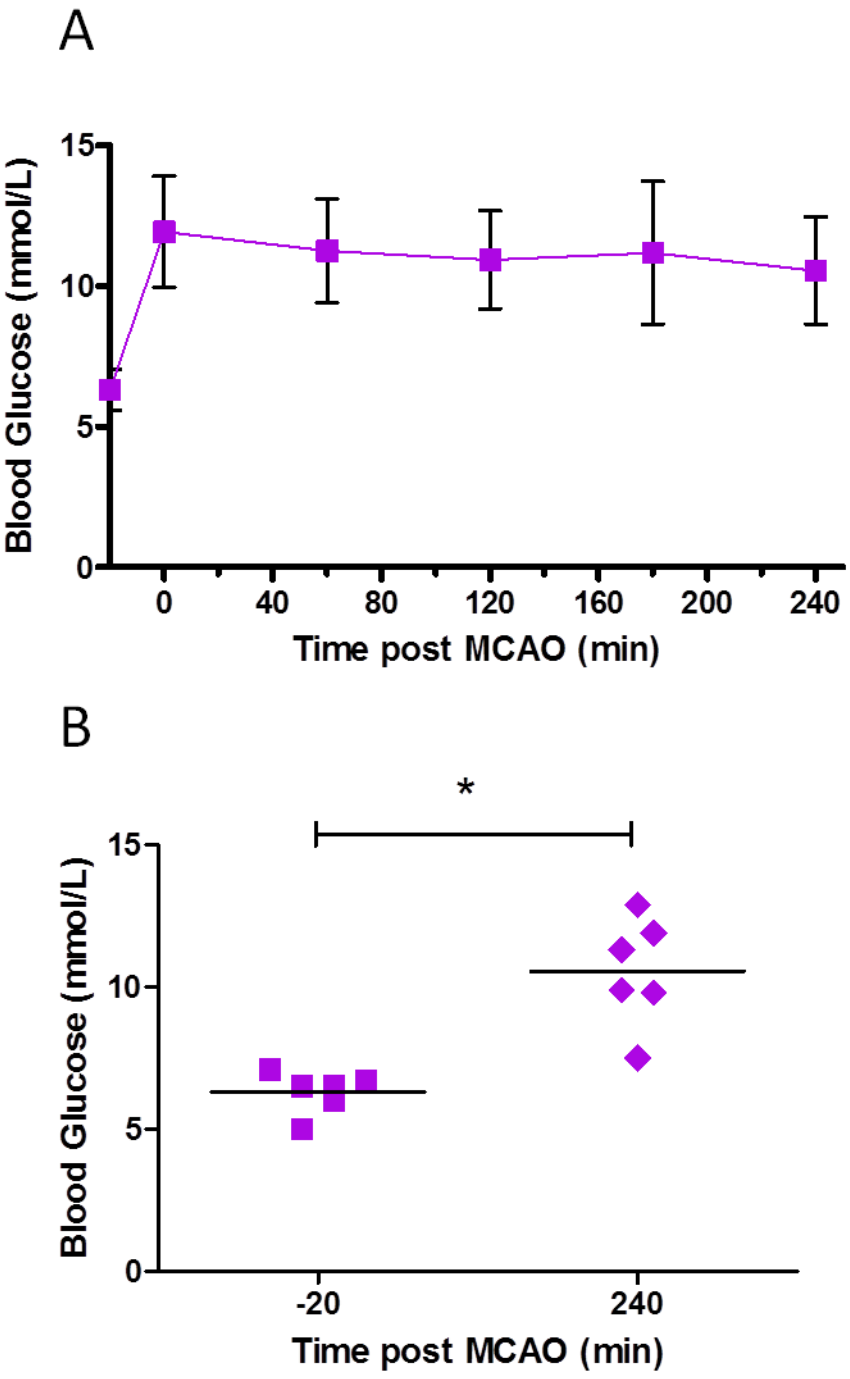

Figure 3.4. Blood glucose levels in Wistar rat strain. A. Blood glucose values measured at baseline (20 minutes pre-MCAO) and at each hour for 4 hours after DD MCAO in Wistar rats (n=6). Glucose was administered IP 10 minutes prior to MCAO. Data are presented as mean ± standard deviation. B. As a summary measure blood glucose levels at baseline and at 240 minutes (4 hours) post-MCAO were compared. Data are presented as scatterplot with the line indicating the mean. *P<0.01 compared with baseline (-20 minutes) using Student's paired t-test.

3.4 Discussion

The studies included in this chapter were performed to establish a rodent model with clinically relevant glucose levels to be used in future studies assessing the pathophysiological mechanisms of hyperglycaemia in ischaemic stroke. They demonstrate that administering a 15% glucose solution, ten minutes prior to permanent intraluminal filament occlusion of the MCA, to Sprague Dawley rats has no significant effect on infarct volume at 24 hours post-MCAO. The Sprague Dawley rats included in this study displayed blood glucose levels pre- and post-MCAO that were higher than those previously observed in this strain. Subsequent glucose studies using different normotensive rat strains identified the Wistar strain as an alternative for future studies.

3.4.1 Hyperglycaemia did not increase infarct volume in SD rats following permanent ILF MCAO (Study 1)

The aim of the first study was to establish a rodent model in which hyperglycaemia, at a clinically relevant level, exacerbates ischaemic damage. This was important because although many studies have investigated the effects of hyperglycaemia in animal models of stroke, few studies reported model systems with blood glucose concentrations relevant to those observed in clinical practice. Previous in-house data have shown that hyperglycaemia (12mmol/L), exacerbates ischaemic damage in Sprague Dawley rats at 24 hours following the induction of permanent MCAO (Tarr, 2012). In the previous study the MCA was occluded using the DD method, an invasive surgical method which does not allow for reperfusion. The aim of the first study was therefore to try and reproduce this result in Sprague Dawley rats using the same method to induce hyperglycaemia as the previous study but using a different method of MCAO: the ILF method. This method of MCAO does not require a craniectomy and is therefore less invasive compared to the DD method and subsequently requires less preparation time allowing for a higher throughput. It can also produce both permanent and transient MCAO as the intraluminal filament can either be left in place (permanent MCAO) or removed after a specified time to achieve reperfusion (transient). The effects of hyperglycaemia on ischaemic damage may be different in the absence and presence of reperfusion and using a model

that can produce both permanent and transient MCAO provides the opportunity to study both and draw comparisons.

3.4.1.1 Hyperglycaemia did not exacerbate ischaemic damage

In Study 1 the ILF method was used to induce permanent MCAO in male SD rats that were either normo- or hyperglycaemic at the time of MCAO. Although hyperglycaemic animals tended to have larger infarcts than normoglycaemic animals (Figure 3.2B) the difference between the two groups was not statistically significant. The scatter plot presentation of the infarct volume data revealed that there was substantial variation in infarct measurements within each group. There are a number of experimental factors that can affect the size and distribution of ischaemic damage induced by ILF MCAO. For example, deviations in body temperature and the blood partial pressure of CO_2 can significantly affect infarct volume and therefore physiological variables were closely monitored in this study to keep them within the normal physiological range. There were no differences in any of the physiological variables (Table 3.1) measured between the two groups that could have significantly influenced the results. Features of the filament used to occlude the MCA, such as the length of filament inserted and bulb size, can also have a major influence on infarct size. Filaments were inserted approximately 20mm along the ICA until slight resistance was met. At this point the filament was considered to be correctly inserted and left in place for 24 hours. However, the only way to ensure that the filament has successfully occluded the MCA is to measure CBF in a region of the brain supplied by the MCA. Measuring CBF, using a technique such as laser doppler flowmetry during ILF MCAO could help to reduce variability as criteria could be set so that animals that do not display a specified percentage reduction in CBF from baseline are excluded. The volume of ischaemic damage can also be influenced by the diameter of the bulb on the intraluminal filament and this should be matched to the weight of the animal. Incorrect matching of filament bulb sizes alongside the inherent variation in the cerebral vasculature between rats is probably one of the major factors contributing to the variation in infarct volume in this study. Any future studies utilizing this method would need to consider this when calculating group sizes and should also use laser doppler flowmetry to continuously measure CBF in the MCA brain territory to ensure that the vessel is successfully occluded.

Different methods of MCAO were considered before planning future studies. This is because hyperglycaemia, induced using the same protocol described in this Chapter, has repeatedly been shown to increase infarct volume 24 hours post-MCAO in different rat strains where the MCA was permanently occluded using the distal diathermy method (Tarr, 2012). The size and location of ischaemic damage induced by distal MCAO differs considerably to that induced by the ILF method. Permanent occlusion of the MCA using the ILF method tends to produce large infarcts encompassing both cortical and subcortical regions (Figure 3.2A). For example in Study 1 infarct volumes, measured 24 hours after ILF MCAO, for the median animal of each group were 230mm^3 and 304mm^3 in vehicle and glucose groups respectively. Conversely, occluding the distal portion of the MCA produces infarcts localised to the cerebral cortex and as such infarcts induced by DD MCAO tend to be smaller than those induced by the ILF method e.g. mean infarct volumes measured 24 hours after DD MCAO in hyperglycaemic WKY and SD rats were 150mm^3 and 167mm^3 respectively (Tarr, 2012). The larger infarcts induced by ILF MCAO could present a problem as they might restrict the ability to detect any harmful effect of hyperglycaemia on infarct size due to a "ceiling effect". This means that the level of ischaemic damage may be at its maximum regardless of glycaemic status. Data from a transient MCAO study demonstrates this effect as neuronal damage was found to be significantly increased in hyperglycaemic rats after 15 and 30 minutes of ILF MCAO compared to normoglycaemic rats, but there was no significant difference between normo- and hyperglycaemic animals after 60 minutes MCAO (Gisselsson et al., 1999). The volume of neuronal damage increased as the duration of ischaemia increased and therefore the extent of damage induced after 60 minutes may be maximal and as a result it's not possible to detect additional damage induced by hyperglycaemia. A similar effect may have occurred in Study 1.

Furthermore, the widespread ischaemic damage caused by ILF MCAO produces complex motor, sensory, autonomic and cognitive deficits. Hypothalamic damage has been shown to occur following ILF occlusion of 60 minutes or more generating a hyperthermic response (Li et al., 1999). Hyperthermia can exacerbate neuronal cell death (Chen et al., 1991, Azzimondi et al., 1995, Kim et al., 1996), which means that fluctuations in temperature induced by the ILF method may produce a source of variability in infarct size. In comparison,

ischaemic damage induced by the DD MCAO method rarely causes damage to the hypothalamus and thus does not induce a hyperthermic response. The size of the lesions produced using the DD method are relatively small, encompassing approximately 5-20% of the ipsilateral hemisphere. This is relevant to clinical findings as human stroke sizes have been shown to range from 28-80cm^3, which translates to 5-14% of the ipsilateral hemisphere (Carmichael, 2005).

Perfusion-diffusion mismatch data collected from previous in-house MRI studies (Tarr, 2012), and from the MRI study in Chapter 5, suggests that there is substantial penumbra tissue (~20-130mm^3) produced following permanent MCAO induced using the DD method. This is greater in comparison to perfusion-diffusion mismatch data from studies using the ILF method of MCAO where the volume of penumbra tissue in WKY rats during the acute 1-4 hours post MCAO ranged from 22-65mm^3 (Reid et al., 2012). The potentially salvageable, hypoperfused tissue within the ischaemic penumbra is the region where any acute therapy is likely to have the greatest impact and is also the location where hyperglycaemia is likely to have the greatest influence and thus using a model in which there is substantial penumbra will benefit future studies.

Taken together, the evidence from previous in-house glucose studies indicates that the distal diathermy method of MCAO is a suitable method of MCAO for studying the effects of hyperglycaemia in experimental stroke. This method will therefore be used in all future studies assessing the pathological mechanisms by which hyperglycaemia exacerbates ischaemia damage.

3.4.1.2 Glucose levels were not clinically relevant pre- or post-MCAO

The blood glucose data (Figure 3.1B) indicates that a rodent model with clinically relevant blood glucose levels was not successfully produced in Study 1. In rats that received glucose treatment blood glucose levels in individual rats ranged from 13.5-21.0mmol/L with an average of 18mmol/L during the first hour of MCAO. This level of hyperglycaemia is high in comparison to values previously recorded in this strain of rat following identical glucose treatment (Tarr, 2012), and compared to values typically seen in patients (Gray et al., 2007). In rats that received vehicle treatment blood glucose levels remained around baseline levels with values ranging from 7-12mmol/L in individual rats. Blood glucose

levels in normoglycaemic stroke patients typically range from 4-6mmol/L (Gray et al., 2007), and normal values in fasted SD rats have been shown to range from 4-7mmol/L (Tarr, 2012, Saha et al., 2005). Values above this can therefore be considered hyperglycaemic and thus within the vehicle group there were animals that were potentially hyperglycaemic. Also, the glucose values measured at baseline (Figure 3.1A) were >8.0mmol/L in all rats from both treatment groups. These values are high compared to previous baseline blood glucose data from SD rats, where values range from 5-7mmol/L, and this suggests that rats in the present study were hyperglycaemic at baseline. The rats in the present study were from the same supplier as those from the previous study and therefore steps were taken to try to identify the cause of the hyperglycaemia that may have developed in the SD strain. After contacting the animal supplier and speaking with staff in the animal unit a change in diet was ruled out. In order to reduce any influence from environmental stress, experiments were not performed on the day when cages were cleaned. There were no issues with the blood glucose meter or plasma glucose analyser, both of which were calibrated daily to ensure they were reading glucose levels correctly. Regardless of the steps taken, baseline blood glucose values measured in SD rats remained elevated. Further contact with the animal supplier revealed that the Sprague Dawley rats used in Study 1 were from a single breeding colony of Sprague Dawley rats (SDF). The animal supplier had two different breeding colonies and offered to supply rats from each, asking for a copy of the blood glucose data from the two colonies in return. Consequently, blood glucose levels from both strains were analysed pre- and post-MCAO in a second study (Study 2). Rats from two different normotensive rat strains: Wistar and Fischer-344 rats were also included in this study.

3.4.2 Glucose levels were clinically relevant pre- and post-MCAO in Wistar rats (Study 2)

Blood glucose values were measured in two different colonies of Sprague Dawley rat: SDF and SDG, Wistar and Fisher-344 rats at baseline (20 minutes pre-MCAO) and 60 minutes post-MCAO (Figure 3.3). At baseline, out of the four groups, blood glucose levels tended to be lower in Fischer-344 rats with a mean blood glucose level of 6.9mmol/L. In SDF, SDG and Wistar rats blood glucose levels at baseline were >8.0mmol but there were no statistically significant differences

between any of the groups. Published glucose values from normoglycaemic Sprague Dawley, Wistar and Fischer-344 strains measured pre-MCAO are presented in Table 3.2. Compared with published glucose levels, the glucose values reported in the present study for Sprague Dawley rats are almost double, indicating possible hyperglycaemia in this strain. The blood glucose values measured in Wistar rats are slightly higher than published values and those in Fischer-344 rats are in close agreement with published values.

At 60 minutes post-MCAO blood glucose values in the SDF and SDG rats were similar to baseline levels (>8.0mmol/L) but blood glucose values in Fischer-344 rats and Wistar rats were shown to be <7.0mmol/L. These results suggested that either Fischer-344 or Wistar rats could provide an alternative normotensive strain to the SD strain for future studies. Duverger et al (1988), investigated the influence of rat strain on the quantification of cerebral infarction following permanent focal cerebral ischaemia induced by proximal MCAO (using an adaptation of the method by Tamura et al (1981)), and reported that out of the three normotensive rat strains included in their study (Fischer-344, WKY and SD), infarct size was most standardised and reproducible in the Fischer-344 strain (Duverger and MacKenzie, 1988). In contrast, Dittmar et al 2006 reported that Fischer-344 rats are not a suitable strain for experimental stroke studies, in particular those using the filament MCAO model. They experienced more surgical complications and a higher incidence of subarachnoid haemorrhage in Fischer-344 rats compared to other strains. Using magnetic resonance angiography they found that internal carotid arteries from Fishcer-344 rats had more “kinks” compared to arteries from Wistar rats which could explain the surgical difficulties experienced with Fischer-344 rats. From my own personal experience, Fischer-344 rats were easily stressed and difficult to handle in comparison to Wistar and Sprague Dawley rats. There was also a higher degree of mortality with this strain, in particular mortality soon after the induction of anaesthesia. It was therefore decided not to use Fischer-344 rats for future experiments.

As some Wistar rats at baseline and all Wistar rats at 60 minutes post-MCAO displayed blood glucose levels within the target range of 4-7mmol/L blood glucose levels were investigated in a separate group of Wistar rats.

Rat strain	Glucose (mmol/L, source)	Reference
Sprague Dawley	4.3 (blood)	(Kittaka et al., 1996)
Sprague Dawley	4.5 (blood)	(Wei et al., 2003)
Sprague Dawley	6.1 (blood)	(Quast et al., 1997)
Wistar	7.3 (plasma)	(Nedergaard et al., 1987)
Wistar	5.2 (blood)	(Toung et al., 2000)
Wistar	7.2 (plasma)	(Pulsinelli et al., 1982)
Fischer-344	8.3 (plasma)	(Duverger and MacKenzie, 1988)
Fischer-344	6.1 (plasma)	(Li et al., 2004)

Table 3.2. Published glucose values measured pre-MCAO in Sprague Dawley, Wistar and Fischer-344 rats.

Baseline blood glucose levels of all the Wistar rats within this group were within the target blood glucose range. Following a single IP injection of a 15% glucose solution blood glucose values in Wistar rats rose to a mean level of approximately 12mmol/L and remained at this elevated level for 4 hours post-MCAO. In comparison to blood glucose levels reported in previous studies investigating hyperglycaemia in animal models of MCAO, blood glucose levels in hyperglycaemic Wistar rats were relevant to the typical values observed in patients with PSH. As a result it was decided to use rats from the Wistar strain in future studies assessing hyperglycaemia in experimental ischaemic stroke.

3.4.3 Summary

The results from the studies presented in this Chapter demonstrate that administering a 15% glucose solution IP to Wistar rats, 10 minutes prior to MCAO, produces clinically relevant levels of hyperglycaemia that were maintained for 4 hours post-MCAO. This model of hyperglycaemia and rat strain will be carried forward for future studies.

Infarct volume data from this study demonstrates that permanent occlusion of the MCA using the intraluminal filament model produces large ischaemic lesions with considerable variation in size. Large lesions have the potential to mask the effects of a relatively small insult, such as acute hyperglycaemia, on infarct size. It was therefore decided that for future studies investigating the effects of hyperglycaemia in experimental stroke the distal diathermy model would be used which produces smaller and more reproducible ischaemic lesions.

Chapter 4 - The effect of hyperglycaemia on the severity of ischaemia 1 hour after MCAO

4.

4.1 Introduction

4.1.1 Hyperglycaemia and cerebral blood flow

Following ischaemic stroke, the severity of the blood flow deficit is one of the main determinants of acute brain damage and anything that reduces CBF further could increase this damage. Evidence from rodent studies suggests that hyperglycaemia may augment ischaemic brain injury by increasing the perfusion deficit in the acute stage of ischaemic stroke (Duckrow et al., 1985, Duckrow et al., 1987, Kawai et al., 1998). If hyperglycaemia does increase the perfusion deficit this could potentiate other pathophysiological mechanisms known to increase ischaemic brain damage and could help to explain why hyperglycaemia results in larger infarct sizes. In preclinical studies hyperglycaemia has been shown to reduce CBF in both the normal, non-ischaemic rat brain (Duckrow et al., 1985, Duckrow, 1995, Mayhan and Patel, 1995, Wang et al., 2008), and during global and focal ischaemia (Yura, 1991, Kawai et al., 1997a, Kawai et al., 1998). In addition, regional CBF has been shown to be reduced within cerebral regions of interest in hyperglycaemic patients with diabetes, compared to normoglycaemic controls (Vazquez et al., 1999). The triggers for such hyperglycaemia-induced reductions in CBF have yet to be elucidated. Several mechanisms have been proposed from animal studies which include: an osmotic mechanism resulting in a higher brain water content and increased cerebral vascular resistance (Duckrow, 1995); impairment of nitric oxide-dependent dilatation of cerebral arterioles via the activation of protein kinase C (Mayhan and Patel, 1995); and a cooperative effect of hyperglycaemia and cortical spreading depression on CBF (Wang et al., 2008). As with much of the previous research regarding hyperglycaemia in experimental stroke the effects of hyperglycaemia on CBF were investigated in studies using glucose levels that far exceed those seen clinically in patients with PSH. Since the extent of brain injury is governed by the severity of the blood flow deficit during ischaemic stroke it is important to determine first of all if clinically-relevant levels of blood glucose increase ischaemic damage by increasing the reduction in cerebral blood flow. Using a rodent model of permanent focal cerebral ischaemia, Tarr et al, (2013) reported that hyperglycaemia (~12mmol/L) accelerated acute

lesion growth and increased infarct volume compared to normoglycaemia (~6mmol/L). The effects of hyperglycaemia on lesion growth were evident at the earliest time point examined in the study, 1 hour post-MCAO, suggesting that the detrimental impact of hyperglycaemia is rapid. The aim of the present chapter was to determine if hyperglycaemia accelerates acute lesion growth by increasing the severity the CBF deficit at 1 hour post-MCAO using the animal model established in the previous chapter.

4.1.2 Measuring CBF *in vivo* using autoradiography

There are various different techniques which have been developed for the assessment of cerebral blood flow *in vivo*. Commonly used techniques for the clinical assessment of CBF include PET, perfusion computed tomography and MRI. In order for a technique to be suitable for use in routine clinical practice it must be capable of assessing CBF through the intact skull. However, for the assessment of CBF in rodents more invasive techniques are available. For example, autoradiography using the radioactive substance ^{99m}Tc-HMPAO can be used experimentally to assess CBF in animals. ^{99m}Tc-HMPAO is a lipophilic, low molecular weight radiotracer which, following intravenous injection, freely crosses the blood brain barrier. Once in the brain ^{99m}Tc-HMPAO rapidly converts to a non-diffusible hydrophilic species causing entrapment in the brain proportional to regional CBF (Lassen et al., 1988). For this reason ^{99m}Tc-HMPAO autoradiography has been widely used to measure CBF in animal stroke studies (Bullock et al., 1991, Gartshore et al., 1997, Lythgoe et al., 1999). Although this technique is terminal, allowing measurement of CBF at a single time point, the main advantage of using autoradiography to assess CBF is that it produces autoradiograms with high spatial resolution as demonstrated in Figure 4.1. Also, compared with other CBF tracers, such as [^{14}C]-iodoantipyrine (IAP) and ^{133}Xenon, ^{99m}Tc-HMPAO has several advantages such as the short 6-hour half-life of the radionucleotide ^{99m}Tc, and its stable in vivo binding, which lasts for several hours.

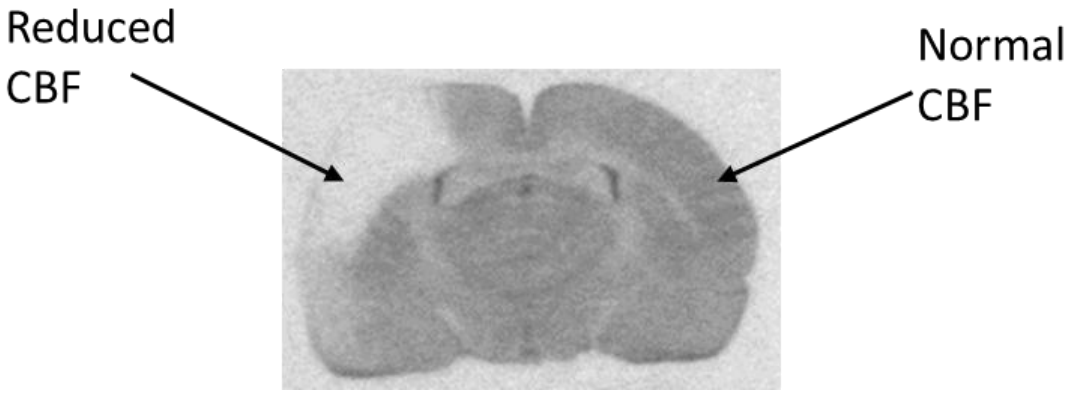

Figure 4.1 Representative ^{99m}Tc-HMPAO autoradiogram of a rat brain section (Level 4, 0.8mm posterior to Bregma). The pale region indicates a region of reduced CBF induced by 1 hour of permanent, distal MCAO.

One of the main disadvantages of ^{99m}Tc-HMPAO autoradiography is that quantitative assessment of CBF is challenging. This is because for quantitative assessment of CBF the arterial activity of the lipophilic complex must be known but it is difficult to measure this due to the rapid conversion of ^{99m}Tc-HMPAO from a lipophilic to hydrophilic form in the blood. Despite this, the use of ^{99m}Tc-HMPAO autoradiography for semi-quantitative assessment of CBF in a rodent stroke model has been validated against quantitative autoradiography methods ([^{14}C]-IAP) and was shown to accurately represent CBF 0.5-72 hours after acute cerebral ischaemia (Bullock et al., 1991). Therefore in the present study a semi-quantitative assessment of CBF 1 hour post-MCAO was obtained using ^{99m}Tc-HMPAO blood flow autoradiography.

4.1.3 Study aim and hypothesis:

To determine the effect of hyperglycaemia on the severity of the blood flow deficit at 1 hour following the induction of cerebral ischaemia using ^{99m}Tc-HMPAO blood flow autoradiography. It was hypothesised that the reduction in CBF induced by 1 hour of permanent MCAO would be greater in hyperglycaemic compared with normoglycaemic rats.

4.2 Methods

4.2.1 Animals

This study used adult male Wistar rats (280-360g) obtained from Harlan Laboratories (UK). Animals were housed in an animal care facility at the University of Glasgow and maintained on a 12:12 hour light/dark cycle. Rats were allowed free access to food and water until the night before the experiment when rats were fasted overnight with free access to water.

4.2.2 Sample size calculation and blinding

To calculate the number of animals required for each group a sample size calculation (Snedecor and Cochran, 1989, Figure 4.2A), was performed using ADC data acquired from a previous in-house MRI study. The calculation was based on the change in ADC derived lesion volume, at 1 hour post-MCAO, exhibited in WKY rats that were hyperglycaemic compared to normoglycaemic controls (Tarr et al., 2013). ADC lesion volume was used for the sample size calculation as there was no CBF data available and therefore ADC lesion volume provided the best approximation. The difference in ADC-derived lesion volume observed at 1 hour post-MCAO between normo- and hyperglycaemic WKY rats was 50.8mm^3. The standard deviation for the normoglycaemic and hyperglycaemic groups was 36.5 and 12.5 respectively. The sample size calculation was based on an 80% power ($1- \beta = 0.8$) and a 95% significance level ($\alpha = 0.05$) and therefore according to Figure 4.2B the C value was 7.85. The number of animals per group was calculated to be 8.5. From this it was decided that the optimum group size would be 10 rats per group. Rats were randomly assigned to a vehicle or glucose treatment group using an online randomization plan generator. A colleague was given a copy of the randomization plan and presented me with a syringe containing the correct treatment for each rat. Blinding presented a problem in the case of rat mortality and in order to account for this it was decided to assign 13 animals to each group and these animals were included in the randomization protocol (Figure 4.3).

A

$$n = 1 + 2C\left(\frac{s}{d}\right)^2$$

B

1-β \ α	0.05	0.01
0.8	7.85	11.68
0.9	10.51	14.88

Figure 4.2. Sample size calculation. A. Equation used to compute sample size for continuous variables (Snedecor & Cochran, 1989), where *d* is the difference to be detected based on previous findings, *s* is the standard deviation and *C* is a constant derived from the power and significance level. B. Table for determining the value of C for the sample size calculation where α is the significance level (95% or 99%) and 1-β = power (80% or 90%).

A Randomization Plan

from

http://www.randomization.com

Rat ID	Treatment	Rat ID	Treatment
1	Vehicle	13	Vehicle
2	Glucose	14	Vehicle
3	Vehicle	15	Glucose
4	Glucose	16	Vehicle
5	Vehicle	17	Vehicle
6	Glucose	18	Vehicle
7	Glucose	19	Glucose
8	Vehicle	20	Vehicle
9	Vehicle	21	Glucose
10	Glucose	22	Glucose
11	Vehicle	23	Glucose
12	Glucose	24	Glucose

Figure 4.3. Randomization plan for ^{99m}Tc-HMPAO blood flow autoradiography study where 13 rats were assigned to each group. The randomization plan was generated from www.randomization.com.

4.2.3 Surgical Procedures

Rats were anaesthetised initially in an anaesthetic chamber with 5% isoflurane delivered in a nitrous oxide: oxygen mixture (70:30). A tracheotomy was then performed and animals were artificially ventilated with 2.5% isoflurane in the same gas mixture described above. The right femoral artery was cannulated for continuous recording of MABP and monitoring of blood pH, $PaCO_2$ and PaO_2 as described in Chapter 2.2.2. The right femoral vein was also cannulated for intravenous administration of ^{99m}Tc-HMPAO. Body temperature was maintained at 37±0.5°C using an external heat source and recorded using a rectal thermometer. Permanent focal cerebral ischaemia was achieved using the distal diathermy model of MCAO as described in Chapter 2.3.2.

4.2.4 Induction of hyperglycaemia and glucose measurements

Animals were randomly assigned (see section 4.2.2) to vehicle or glucose treatment groups. Glucose treated rats received an IP injection of a 15% glucose solution (10ml/kg) in distilled water, 10 minutes prior to induction of cerebral ischaemia. Vehicle treated rats received an equivalent IP injection of distilled water. Arterial blood glucose was measured 20 minutes prior to MCAO to obtain a baseline measurement, at the onset of MCAO (0 minutes) and at 30 and 60 minutes after MCAO as described in Chapter 2.4. The surgeon (LR) was blind to group identity of each animal.

4.2.5 Assessment of CBF using ^{99m}Tc-HMPAO autoradiography

^{99m}Tc-HMPAO was prepared as described in Chapter 2.6. At 1 hour post-MCAO 225 MBq ^{99m}Tc-HMPAO in ~0.6ml saline was injected via the femoral vein catheter over 30 seconds. Approximately five minutes following the administration of ^{99m}Tc-HMPAO, the rat was euthanised by decapitation and the brain was removed and immediately frozen in isopentane at -45°C. The brain was sectioned (20µm) in a cryostat maintained at -20°C. Sections spanning the entire MCA territory, over ten coronal levels (rostral to caudal), were mounted on to glass slides and dried on a hotplate set at 60°C for 5 minutes. Autoradiograms were prepared from these sections by exposing them, alongside pre-calibrated ^{14}C standards (21-174x10^3 nCi/g ^{99m}Tc tissue equivalent for 20µm

thick sections), to autoradiographic film for 1 hour. The autoradiograms were then developed using an automatic film processor.

4.2.5.1 Analysis of autoradiograms

Autoradiograms were analysed for their ^{99m}Tc tissue concentration using an MCID Basic image analysis system (7.0 Rev 1.0, build 207; Imaging Research Inc). For each autoradiogram a density calibration was established to construct a standard curve that compared the MCID system's internal optical density measurement unit (measured grey levels) to the ^{14}C standard values (21-174x10^3 nCi/g ^{99m}Tc tissue equivalents). The density calibration was then applied to the autoradiograms which allowed the ^{99m}Tc-HMPAO tissue concentration to be expressed in relative units of nCi/g. The concentration of ^{99m}Tc-HMPAO was considered to be proportional to CBF. A semi-quantitative assessment of CBF was made by measuring the concentration of ^{99m}Tc-HMPAO using two different analyses as described below.

Threshold analysis

A thresholding approach was used to classify CBF in the ipsilateral cortex into different levels of severity relative to the homologous region of the contralateral hemisphere: most severe (0-15%), severe (0-43%), moderate (43-75%) and mild (75-100%). These thresholds were chosen to reflect tissue with severely, moderately and mildly reduced blood flow (Tamura et al., 1981b, Shen et al., 2003, Hossmann, 1994). Autoradiographic images of ten coronal levels were captured for threshold analysis (Figure 4.4).

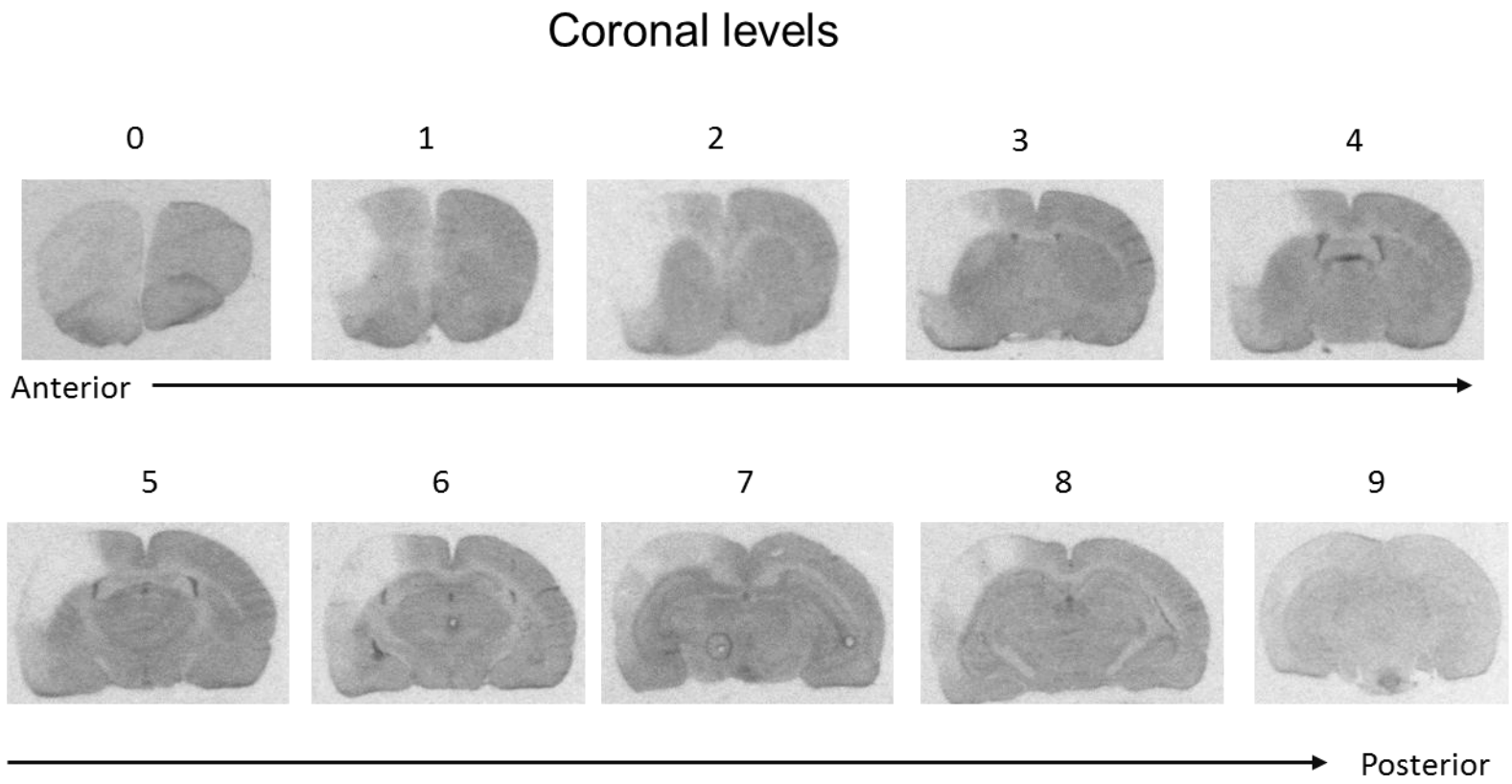

Figure 4.4. Autoradiographic images from a representative animal showing the ten coronal levels (0-9) analysed. The pale regions are areas of reduced ^{99m}Tc-HMPAO tissue concentration and represent areas where blood flow has been reduced by distal diathermy MCAO.

The stereotaxic co-ordinates for each level were defined using a rat brain atlas (Paxinos and Watson, 2007). Each level and its position in relation to Bregma are provided in Table 4.1.

Level	Distance from Bregma (mm)
0	4.7
1	3.2
2	1.2
3	- 0.3
4	-0.8
5	-1.8
6	-3.1
7	-4.8
8	-6.3
9	-8.0

Table 4.1. Ten coronal levels and their position relative to Bregma (mm). Levels with positive values lie anterior to Bregma and levels with negative values lie posterior to Bregma.

After applying a density calibration, the outline drawing tool on the MCID basic programme was used to manually delineate the ipsilateral and contralateral cortex of each coronal level. The tissue concentration of ^{99m}Tc-HMPAO (nCi/g) in the contralateral cortex was measured and values representing 15%, 43% and 75% of this were calculated. A threshold was applied to the ipsilateral cortex using the scan area tool and setting the segmentation range to the ^{99m}Tc-HMPAO values corresponding to that threshold (Figure 4.5). The area of the ipsilateral cortex at each threshold was measured and expressed as a percentage of the area of the ipsilateral cortex. For each coronal level the concentration of ^{99m}Tc-HMPAO was measured in three sections and the average was taken.

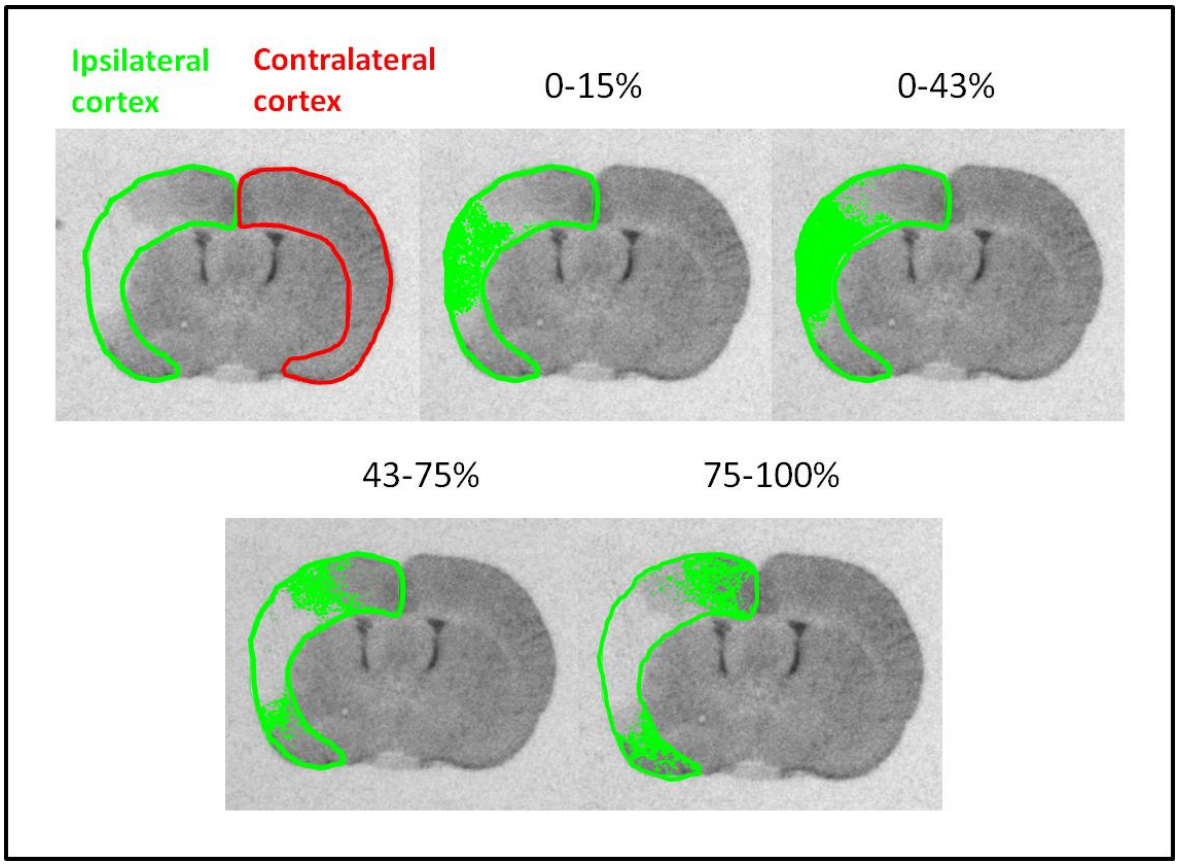

Figure 4.5. Representative autoradiograms depicting threshold analysis. The ipsilateral cortex (outlined in green) and contralateral cortex (red) were manually delineated (top left). The pale region in the ipsilateral cortex represents an area with no uptake of ^{99m}Tc-HMPAO indicating reduced CBF induced by MCAO. In subsequent images the green pixels represent the area of the ipsilateral cortex where ^{99m}Tc-HMPAO uptake was within 0-15%, 0-43%, 43-75% and 75-100% of the contralateral cortex.

Region of interest (ROI) analysis

A list of 22 distinct brain structures was derived from a previous ^{14}C-iodoantipyrine autoradiography study (Tamura et al 1981). Like the threshold analysis, autoradiographic images depicting the uptake of ^{99m}Tc-HMPAO within selected brain sections were captured for ROI analysis. A rat brain atlas (Paxinos and Watson, 2007) was used to identify the 22 brain structures in the autoradiograms. The rectangle drawing tool on the MCID Basic system was used to place a box over each structure (ROI) in the ipsilateral hemisphere and the ^{99m}Tc-HMPAO tissue concentration (nCi/g) was measured (Figure 4.6). The same tool was used to place an identical sized box over the equivalent ROI in the contralateral hemisphere to measure the concentration there. The ^{99m}Tc-HMPAO tissue concentration from the ROI in the ipsilateral hemisphere was then expressed as a percentage of that in the contralateral hemisphere. For each ROI examined, the ^{99m}Tc-HMPAO concentration was measured on three sections and the average was taken.

Some of the threshold analysis (0-15%) and all of the ROI analysis was performed by MRes student Kathleen Macdonald (KM) under supervision by Lisa Roy. For all of the analysis the investigators (LR and KM) were blinded to group identity.

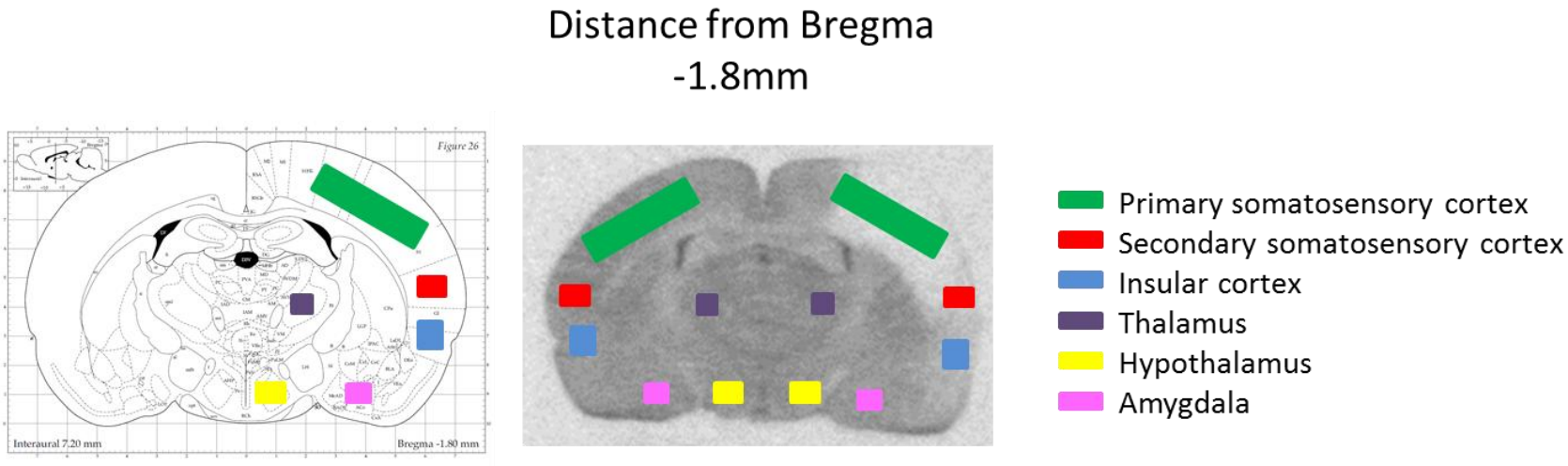

Figure 4.6. Example of the ROI analysis in an autoradiographic section (1.8mm posterior to Bregma). A stereotaxic rat brain atlas (left) was used to identify structures in the autoradiographic image (right). Identical sized boxes were placed over each brain structure in both the ipsilateral and contralateral hemispheres and the ^{99m}Tc-HMPAO tissue concentration in each was measured. Values measured in the ipsilateral cortex were expressed as a percentage of those in the contralateral cortex.

4.2.6 Study exclusion criteria

Animals were excluded from the study if they died during the surgery to induce focal cerebral ischaemia and also if there were any signs of intracerebral haemorrhage development in the brain during cryostat cutting, resulting in extensive subcortical ischaemia on the autoradiograms.

4.2.7 Statistical analysis

Physiological variables, scatterplots of 0-43% threshold data, and CBF ROI measurements were analysed using an unpaired Student's t-test. Blood glucose level data and line graphs of the threshold analysis data were analysed using a 2-way ANOVA with Bonferroni's multiple comparisons post-hoc test. Data are expressed as mean ± standard deviation or scatterplots with the mean indicated.

4.3 Results

4.3.1 Mortality and excluded animals

A total of 26 animals were initially entered into the study. Out of the 26 rats 5 were excluded: 2 rats from the glucose treatment group and 3 rats from the vehicle treatment group. Three of the five rats died due to significant blood loss during the diathermy step of MCAO. One of the rats died during the injection of ^{99m}Tc-HMPAO and one rat was excluded from analysis due to a haemorrhage in the brain which was detected as it was being sectioned. Therefore the final group sizes for analysis were n=10 in the vehicle group and n=11 in the glucose group.

4.3.2 Physiological variables

Physiological variables were monitored throughout the surgical period and the measured variables were all within the normal physiological range (except PaO_2 due to the concentration of oxygen used to deliver the anaesthetic). There were no significant differences in body weight, MABP, temperature, blood gasses and pH between the two groups (Table 4.2).

Group	Weight (g)	MABP (mmHg)	$PaCO_2$ (mmHg)	PaO_2 (mmHg)	pH	Temperature (°C)
Vehicle (n=10)	313 ± 23	85 ± 4	39 ± 6	125 ± 13	7.4 ± 0.1	37 ± 0.2
Glucose (n=11)	322 ± 29	90 ± 4	40 ± 4	120 ± 15	7.4 ± 0.1	37 ± 0.2

Table 4.2. Physiological variables for ^{99m}Tc-HMPAO study. Body weight was measured prior to MCAO. Mean arterial blood pressure (MABP), temperature, pH, PaO_2 and $PaCO_2$ were measured approximately every 30 minutes during surgery and the data are expressed as the mean ± standard deviation over the entire surgical period. There were no significant differences in any of the variables between the two groups (unpaired Student's t-test).

4.3.3 Administration of glucose resulted in clinically relevant hyperglycaemia in the glucose treatment group

The blood glucose measurements taken 20 minutes prior to MCAO, before the IP administration of glucose or vehicle, were 7.3mmol/L and 7.1mmol/L in the vehicle and glucose treatment groups respectively (Figure 4.7). Therefore the two groups were comparable, with no significant difference in blood glucose levels prior to MCAO ($P>0.5$).

Rats received an IP injection of a vehicle or 15% glucose solution 10 minutes before MCAO and blood glucose levels were measured at 0, 30 and 60 minutes post-MCAO. At each time point blood glucose levels were significantly greater in the rats that received glucose treatment compared with those that received vehicle treatment. Following MCAO blood glucose levels were approximately 13mmol/L in rats that received glucose treatment and remained close to the blood glucose values measured at baseline (6-7mmol/L) in the vehicle treatment group.

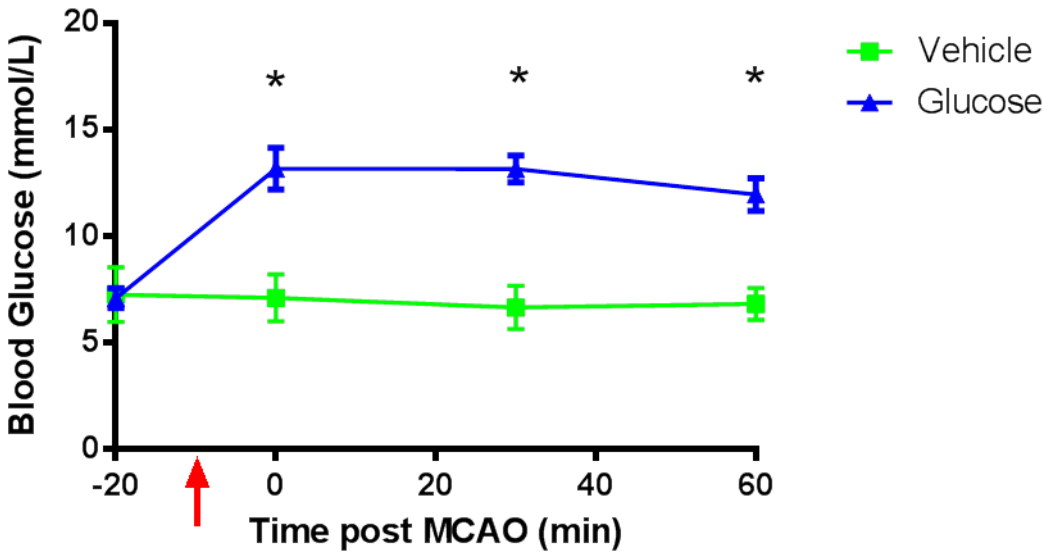

Figure 4.7. Blood glucose data for ^{99m}Tc-HMPAO study. Blood glucose values measured at baseline (-20 minutes) and at subsequent time points over the first hour of MCAO in vehicle (n=10) and glucose (n=11) treated rats. The red arrow indicates the time of vehicle or glucose administration. Data are presented as mean ± standard deviation. *, p<0.0001 compared with vehicle group using 2-way-ANOVA with Bonferroni's post-hoc test.

4.3.4 Hyperglycaemia did not exacerbate the reduction in CBF 1 hour after MCAO

4.3.4.1 Threshold analysis results

For each autoradiogram different thresholds were applied to the ipsilateral cortex of ten coronal levels in order to grade the severity of ischaemia into four categories: most severely (0-15%), severely (0-43%), moderately (43-75%) and mildly (75-100%) reduced relative to the contralateral cortex. The area of the ipsilateral cortex at each threshold, at each coronal level, was measured and expressed as a percentage of the area of the ipsilateral cortex (Figure 4.8). In order to test the hypothesis that there were differences between vehicle and glucose treated animals the data at each threshold were analysed using a 2-way ANOVA with Bonferroni's post-test. The differences between groups were not statistically significant at any of the thresholds examined. However, scrutiny of the results from the 0-43% threshold revealed there to be a small difference between the two groups at every level, with the glucose treatment group tending to have a greater % area of the ipsilateral cortex with a severe reduction in CBF. To investigate this in more detail scatterplots of individual rats were produced for coronal levels 3, 4 and 5 (0.3mm, 0.8mm and 1.8mm posterior to Bregma) at this threshold (Figure 4.9). These levels were selected as there was an observable difference between the two groups at the 0-43% threshold in Figure 4.8. At coronal level 4 the difference between vehicle and glucose treated rats was statistically significant (P=0.046) but the difference between groups at levels 3 (P=0.1), and 5 (P=0.07) was not. From close examination of the autoradiograms by eye there was no obvious difference between any of the groups at these three levels (Figure 4.10), and because the difference at level 4 was small and only marginally significant (P=0.046) no conclusions were drawn from this result.

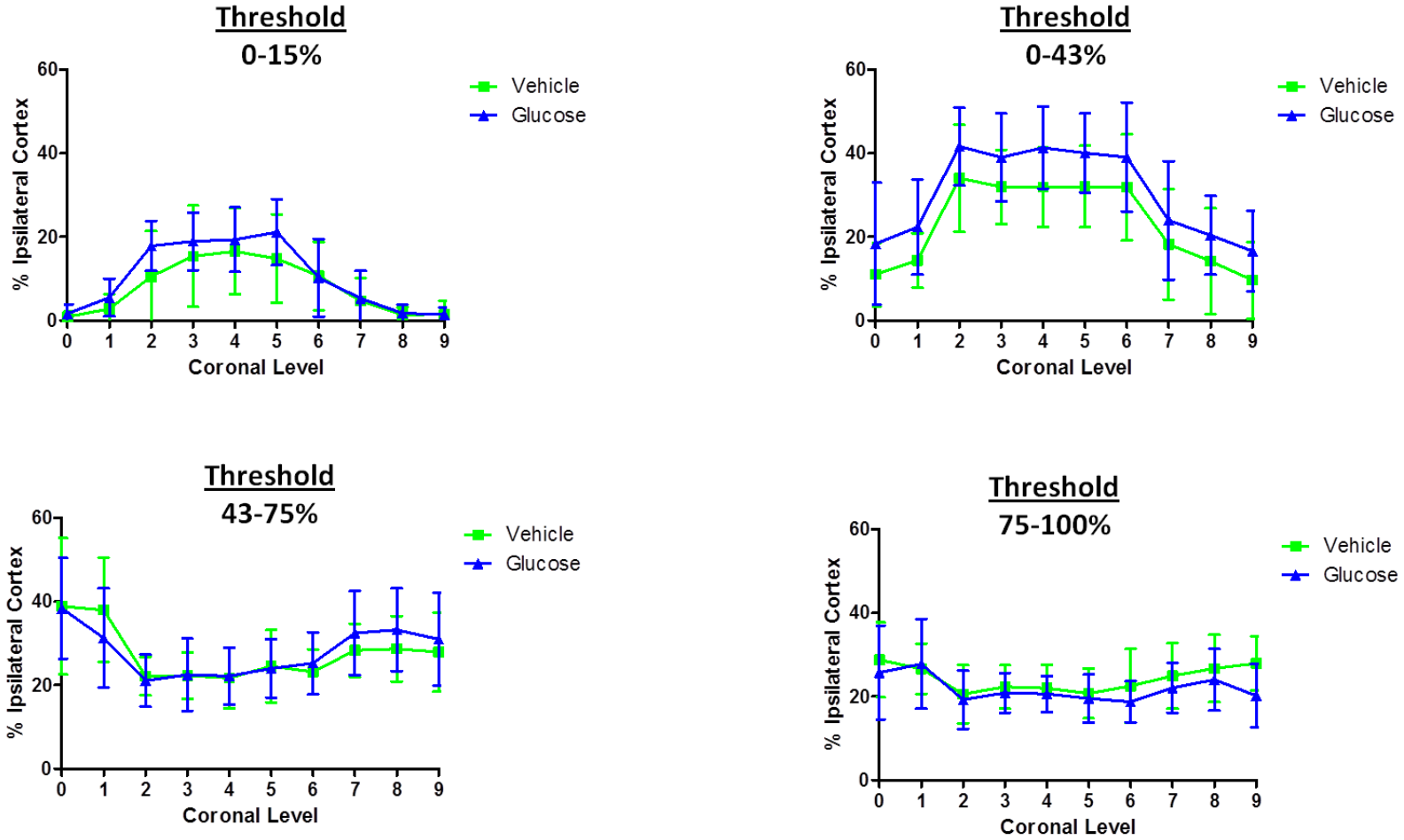

Figure 4.8. Threshold analysis results. The line graphs illustrate the % area of the ipsilateral cortex, across ten coronal levels (rostral to caudal), with CBF that is: most severely (0-15%) severely (0-43%), moderately (43-75%) and mildly (75-100%) reduced relative to the contralateral cortex in vehicle (n=10) and glucose (n=11) treated rats. Data are presented as mean ± standard deviation. Differences between groups are not statistically significant: 2-way-ANOVA with Bonferroni's post-test

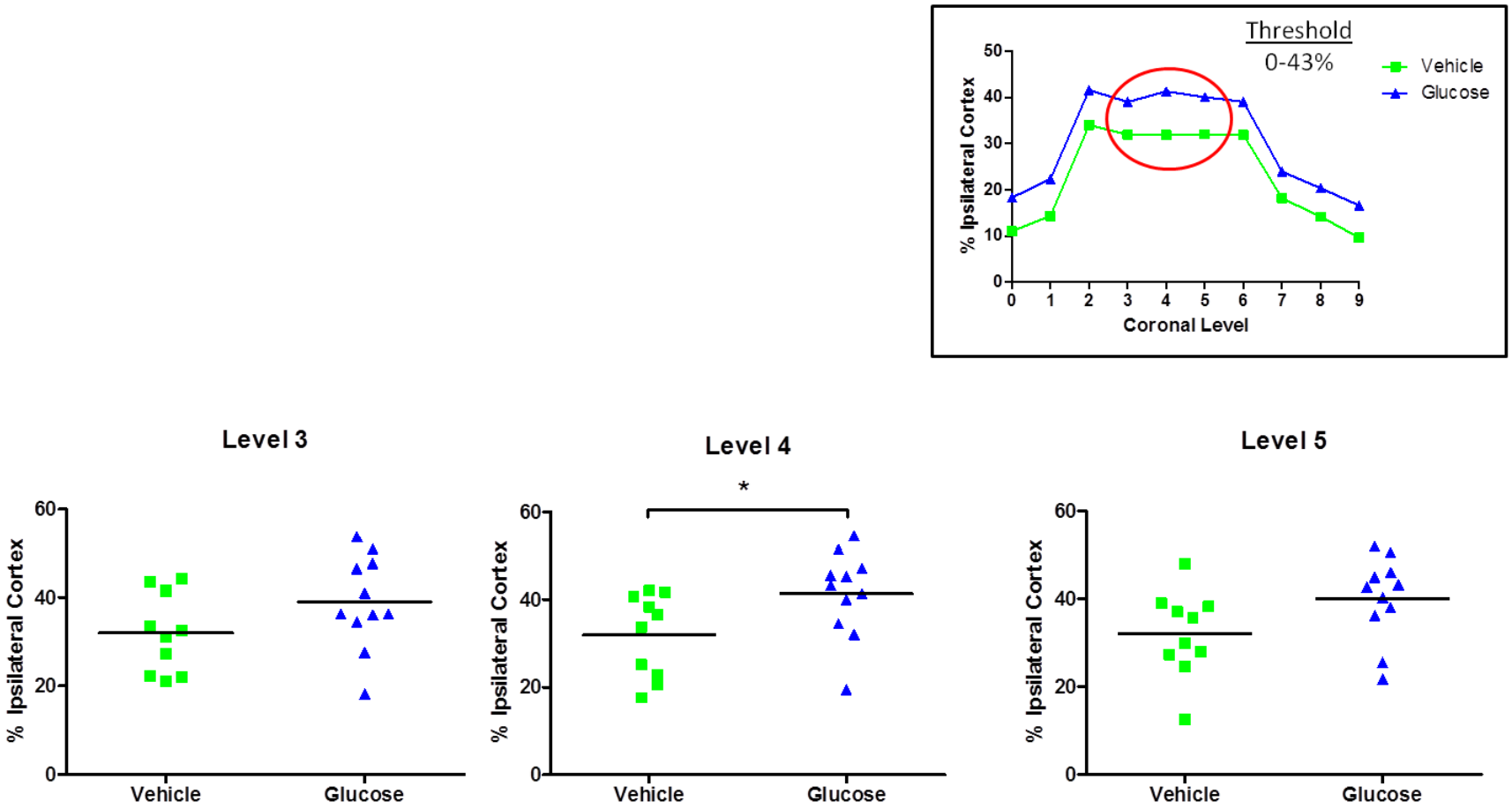

Figure 4.9. Threshold analysis 0-43% threshold. Individual scatterplots illustrating the % area of the ipsilateral cortex at coronal levels 3, 4 and 5 from within the 0-43% threshold (top inset). The line on the scatterplots represents the mean. There was no difference between groups at levels 3 and 5. At level 4, the difference between groups was statistically significant. *P<0.05, using unpaired Student's t-test.

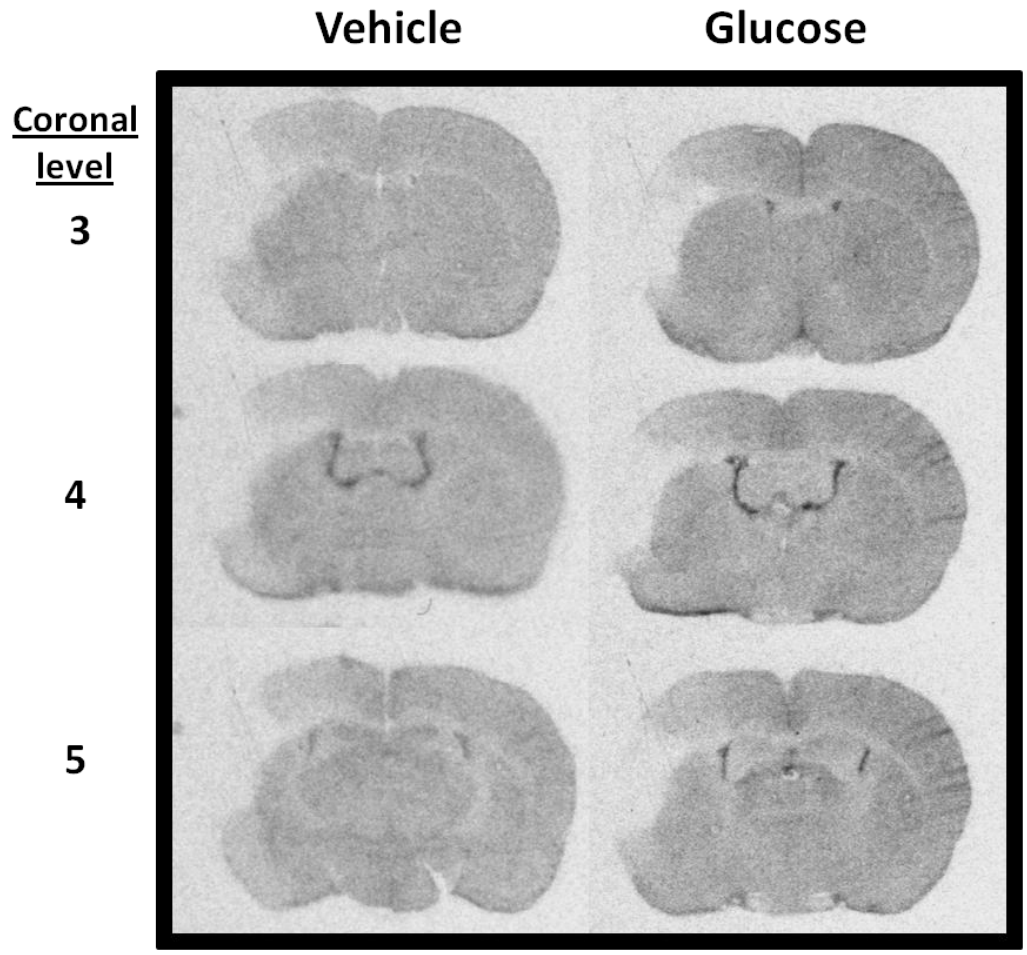

Figure 4.10. Autoradiograms showing the ^{99m}Tc-HMPAO concentration in coronal levels 3, 4 and 5, from a representative vehicle and glucose treated rat. Ischaemia is visible topographically within the ipsilateral cortex in both groups to a similar extent.

4.3.4.2 ROI analysis results

A semi-quantitative assessment of ^{99m}Tc-HMPAO tissue concentration in 22 different brain regions was achieved by measuring the concentration in the ipsilateral hemisphere and expressing this as a percentage of that in the contralateral hemisphere (Normalised ^{99m}Tc-HMPAO concentration, Table 4.3). As expected, there were notable decreases in ^{99m}Tc-HMPAO measurements in the ipsilateral cerebral cortex, brain structures supplied by the distal branches of the MCA, within both groups. There were no statistically significant differences in mean ^{99m}Tc-HMPAO tissue concentrations in any of the 22 structures in the ipsilateral hemisphere between groups. In addition, there were no differences in mean ^{99m}Tc-HMPAO tissue concentrations in brain structures in the hemisphere contralateral to the occluded vessel between vehicle and glucose treated groups (Table 4.4).

Scatterplots of individual rats were produced for some of the ipsilateral brain structures expected to show a considerable reduction in CBF induced by distal MCAO (Figure 4.11A). Normalised ^{99m}Tc-HMPAO values were lower, indicating low CBF, in regions within the ipsilateral cerebral cortex. For example mean ^{99m}Tc-HMPAO concentrations in the primary somatosensory cortex were 18% and 12% of the contralateral regions in vehicle and glucose treated rats respectively. Other areas within the cerebral cortex with notable reductions in ^{99m}Tc-HMPAO concentrations were the secondary somatosensory cortex and motor cortex (Figure 4.11B&C). Across the entire ipsilateral cortex, ^{99m}Tc-HMPAO concentrations ranged from 12-96% of the contralateral region. There was notable variation in values from within the cerebral cortex of both groups. This is evident in both the scatterplots in Figure 4.11 and from the standard deviation values in Table 4.3. This variation could result from biological variation of the branching pattern of the MCA between animals leading to slightly different occlusions for each animal. To minimise this potential source of variation rats from a single strain were used.

In ROI's outside the cerebral cortex there was less variation in ^{99m}Tc-HMPAO concentration measurements. ^{99m}Tc-HMPAO concentrations for every rat were close to 100% of the contralateral region in the globus pallidus, hypothalamus

and thalamus structures (Figure 4.12), and this was the case for most subcortical structures (Table 4.3).

A few regions of the brain displayed a slight increase in blood flow, most notably the globus pallidus and substantia nigra which displayed mean CBF values of 111% and 105-111% of the contralateral regions respectively (Table 4.3). Hyperperfusion within these regions has previously been described in a rodent model of focal cerebral ischaemia (Tamura et al., 1981b) and may be explained by an increase in metabolic demand in these structures following acute ischaemic injury.

% Contralateral Region			
Region	**Vehicle (mean ± SD)**	**Glucose (mean ± SD)**	**P**
Motor cortex	57 ± 18	60 ± 26	0.81
Auditory cortex	54 ± 28	53 ± 28	0.89
Visual cortex	50 ± 15	63 ± 23	0.43
Primary somatosensory cortex	18 ± 15	12 ± 5	0.22
Secondary somatosensory cortex	35 ± 19	25 ± 18	0.42
Anterior cingulate cortex	77 ± 16	81 ± 18	0.53
Medial cingulate cortex	96 ± 15	87 ± 21	0.29
Lateral orbital cortex	60 ± 28	62 ± 22	0.88
Insular cortex	68 ± 28	55 ± 19	0.21
Prelimbic cortex	78 ± 21	80 ± 18	0.80
Piriform cortex	89 ± 21	94 ± 19	0.56
Caudate Putamen Medial	95 ± 17	95 ± 9	0.87
Caudate Putamen Lateral	103 ± 20	98 ± 26	0.60
Hippocampus	106 ± 14	102 ± 5	0.31
Globus pallidus	112 ± 13	111 ± 11	0.85
Nucleus accumbens	99 ± 12	99 ± 10	0.92
Amygdala	105 ± 15	105 ± 12	0.95
Hypothalamus	99 ± 10	98 ± 5	0.88
Thalamus	103 ± 5	101 ± 7	0.40
Substantia nigra	105 ± 8	110 ± 11	0.20
Septum	98 ± 7	99 ± 6	0.56
Corpus callosum	100 ± 8	89 ± 10	0.40

Table 4.3. Normalised ^{99m}Tc-HMPAO concentration (% contralateral region) in 22 distinct structures for vehicle (n=10) and glucose (n=11) treated rats 1 hour after MCAO. There were no significant differences between groups in any region (P> 0.05). Data are presented as mean ± standard deviation.

^{99m}Tc-HMPAO Tissue Concentration (nCi/g)			
Contralateral Region	**Vehicle (mean ± SD x10^3)**	**Glucose (mean ± SD x10^3)**	**P**
Motor cortex	69 ± 21	76 ± 26	0.45
Auditory cortex	65 ± 21	67 ± 31	0.88
Visual cortex	61 ± 20	65 ± 30	0.70
Primary somatosensory cortex	73 ± 21	83 ± 26	0.37
Secondary somatosensory cortex	67 ± 23	67 ± 32	0.94
Anterior cingulate cortex	64 ± 15	66 ± 23	0.90
Medial cingulate cortex	68 ± 20	84 ± 38	0.17
Lateral orbital cortex	74 ± 21	79 ± 25	0.64
Insular cortex	66 ± 19	72 ± 25	0.48
Prelimbic cortex	64 ± 15	69 ± 23	0.55
Piriform cortex	78 ± 25	79 ± 21	0.87
Caudate putamen medial	80 ± 22	84 ± 25	0.69
Caudate putamen lateral	77 ± 22	86 ± 27	0.42
Hippocampus	85 ± 23	86 ± 33	0.85
Globus pallidus	64 ± 23	68 ± 26	0.75
Nucleus accumbens	79 ± 23	82 ± 25	0.71
Amygdala	79 ± 21	83 ± 23	0.73
Hypothalamus	82 ± 21	87 ± 24	0.84
Thalamus	83 ± 20	90 ± 24	0.45
Substantia nigra	81 ± 20	83 ± 32	0.99
Septum	73 ± 19	79 ± 25	0.61
Corpus callosum	48 ± 20	60 ± 25	0.23

Table 4.4. ^{99m}Tc-HMPAO tissue concentrations (nCi/g) of brain structures within the hemisphere contralateral to the occluded MCA. There were no significant differences between groups in any region (P> 0.05). Data are presented as mean ± standard deviation (values x10^3).

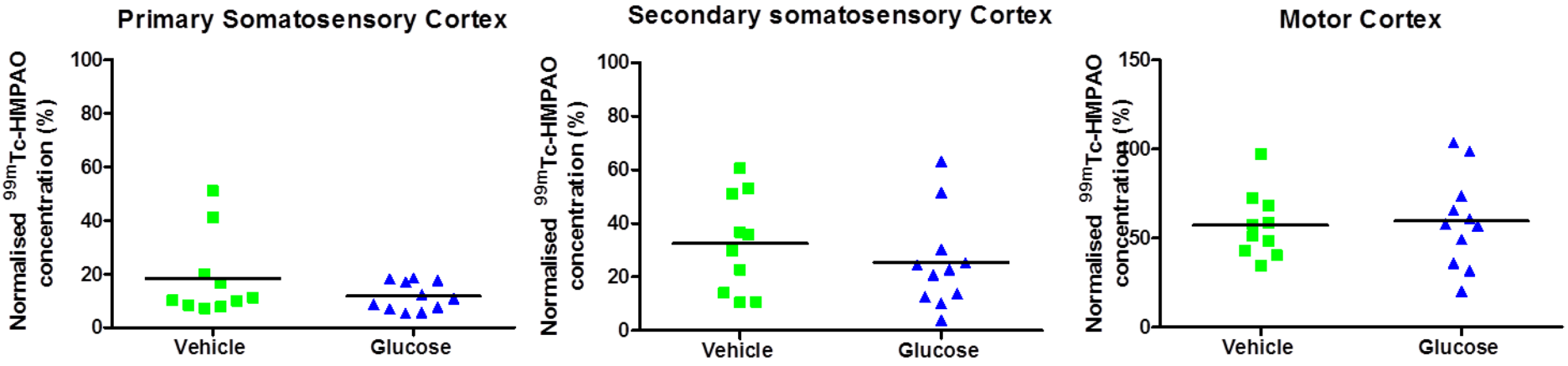

Figure 4.11. ROI analysis results for primary somatosensory cortex, secondary somatosensory cortex and motor cortex. Scatterplots illustrating normalised ^{99m}Tc-HMPAO concentration (% of contralateral region) in cortical brain regions: primary somatosensory cortex, secondary somatosensory cortex and motor cortex from vehicle (n=10) and glucose treated rats (n=11). The line represents the mean. There were no statistically significant differences between groups (unpaired Student's t-test).

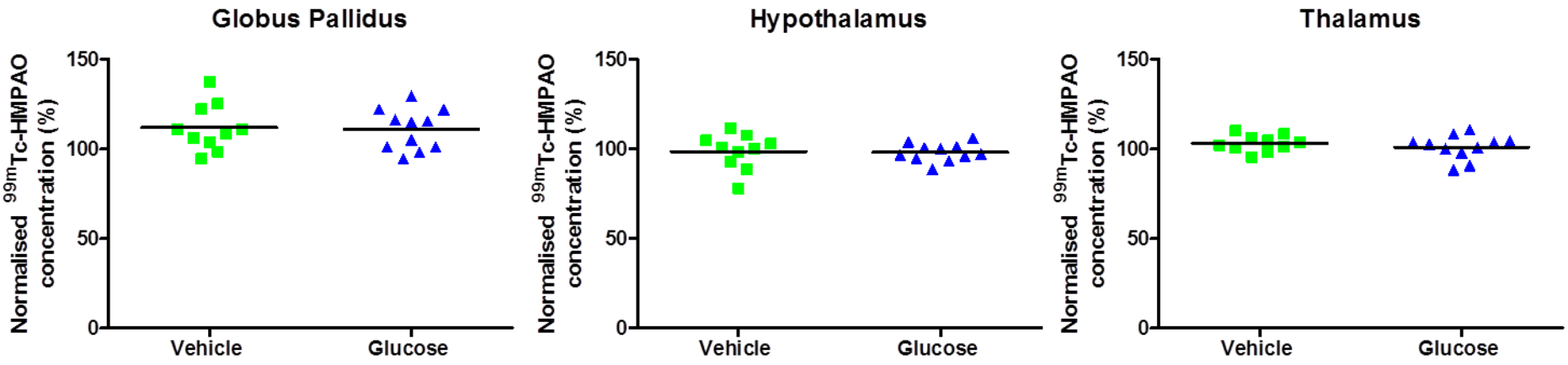

Figure 4.12. ROI analysis results for globus pallidus, hypothalamus and thalamus. Scatterplots illustrating normalised ^{99m}Tc-HMPAO concentration (% of contralateral region) in the thalamus, hypothalamus and globus pallidus, from vehicle (n=10) and glucose treated rats (n=11). The line represents the mean. There were no statistically significant differences between groups (unpaired Student's t-test).

4.4 Discussion

The pathophysiological mechanisms underlying the harmful effects of hyperglycaemia during ischaemic stroke are poorly understood. Hyperglycaemia has been shown to reduce CBF in the normal rat brain (Duckrow et al., 1985) and since the severity of the blood flow deficit is one of the main determinants of acute brain damage it was essential to determine if hyperglycaemia exacerbates the early reduction in CBF induced by MCAO. The purpose of the current study was therefore to assess the effect of hyperglycaemia, at clinically relevant levels, on the severity of the CBF deficit, induced after 1 hour MCAO, using ^{99m}Tc-HMPAO autoradiography. Thorough analysis of the ^{99m}Tc-HMPAO blood flow data using two different methods: threshold and ROI based analyses showed that there were no significant differences in the CBF deficit between hyperglycaemic and normoglycaemic rats. This suggests that the harmful effects of hyperglycaemia during ischaemia may not be caused by an increase in the CBF deficit.

Using two different methods to analyse the ^{99m}Tc-HMPAO blood flow autoradiography data was valuable for two reasons. Firstly it demonstrates that the results are robust as both methods produced the same result. Secondly, the data from the ROI analysis helped to confirm the use of the thresholds selected for the threshold analysis. There is a lack of consensus on where to set thresholds to define severely, moderately and mildly hypoperfused tissue in experimental models of stroke and those used here were based on CBF data from MRI (Shen et al., 2003) and [^{14}C]-IAP autoradiography (Tamura et al., 1981b) studies in rats and therefore might not be appropriate when applied to ^{99m}Tc-HMPAO blood flow maps. The MCA was occluded distally in the present study and by doing so blood flow to regions within the frontal and parietal cortex will be most affected. Thus as expected, the somatosensory cortex displayed the most severe reduction in CBF with values that ranged from 12-35% of the contralateral region. This range closely fits within the 0-43% threshold used in the threshold analysis to calculate the area with severely reduced blood flow. In regions with moderately reduced blood flow, such as the motor cortex, insular cortex and auditory cortex, CBF was approximately 60% of the contralateral region and this was within the threshold range used to define moderately hypoperfused regions (43-75%).

Overall the results from the ROI analysis suggest that the thresholds selected for the threshold analysis were appropriate and could be applied in future studies utilising the ^{99m}Tc-HMPAO blood flow autoradiography technique. However, the thresholds used in this chapter are in slight disagreement with CBF data from a quantitative autoradiography study. Tamura et al (1981) measured CBF 30 minutes after proximal MCAO and found that regions with severe and modest reductions in CBF had levels that were 15-20% and 20-40% of that in the contralateral hemisphere respectively. However, in the present study regions with severe and modest reductions in CBF had levels that were 12-35% and 35-60% of that in the contralateral hemisphere respectively. The differences between studies could partly be explained by the different autoradiographic methods used to measure CBF (quantitative [^{14}C]-IAP vs semi-quantitative ^{99m}Tc-HMPAO) and also by differences in the MCAO model (proximal vs distal MCAO) and rat strain (Sprague-Dawley vs Wistar rat).

4.4.1 Clinically relevant blood glucose levels were observed in normo- and hyperglycaemic rats

Although there was no difference in the severity of the CBF deficit between the two groups in the current study, there were statistically significant differences in the blood glucose values measured between the two groups at 1 hour post-MCAO. The glucose levels measured in both the vehicle and glucose treatment groups closely resembled those seen in normoglycaemic (4-7mmol/L) and hyperglycaemic (6-17mmol/L) ischaemic stroke patients respectively (Gray et al., 2007). Also, the blood glucose data collected in the Wistar rat strain in this study is comparable to that from the previous chapter and reinforces the decision to change from the Sprague-Dawley rat strain to the Wistar rat strain for the study of hyperglycaemia in experimental stroke.

The fact that hyperglycaemia did not increase the severity of the CBF deficit in this study could be explained by the magnitude of the blood glucose increments induced relative to those in previous reports. Experimental studies reporting decreases in CBF had glucose increments of 28 and 29mM above control (Ginsberg et al., 1980, Duckrow et al., 1985). Such high increments in glucose levels are rarely seen in patients with PSH. In clinical trials investigating insulin treatment for PSH blood glucose levels on admission ranged from ~7-10mmol/L

(Gray et al., 2007, Johnston et al., 2009). Blood glucose values in normoglycaemic patients typically range from 4-6mmol/L and therefore only minor increments in blood glucose levels (~1-6mmol/L) are observed in patients with PSH. In the present study the blood glucose increment between vehicle and glucose treated rats was ~6mmol/L which resembles that seen clinically. The present study therefore shows that hyperglycaemia, at clinically relevant levels, does not exacerbate the decrease in CBF induced by 1 hour of MCAO.

4.4.2 Interpretation of results

The findings from the present study are in agreement with results reported previously from studies using animal models of stroke (Gisselsson et al., 1999, Siemkowicz et al., 1982, Venables et al., 1985, Marsh et al., 1986, Quast et al., 1997). Gisselsson and colleagues investigated the influence of hyperglycaemia (20mmol/L) on tissue damage and CBF in rats during and after transient MCAO. In hyperglycaemic rats tissue damage after 30 minutes MCAO was significantly greater compared to normoglycaemic rats but there was no difference in CBF (determined by ^{14}C-IAP autoradiography). Similarly, Venables et al (1985) compared the effects of saline or glucose infusions (achieving blood glucose levels ~10 and 20mmol/L in saline and glucose treatment groups respectively) on changes in CBF during and after transient MCAO in cats. They found that there was no difference in the severity of the CBF deficit after MCAO between saline or glucose treatment groups (Venables et al., 1985).

The results reported here also agree with those from a recent clinical study of 80 acute ischaemic stroke patients where the perfusion deficit, determined by CT perfusion imaging, was found to be similar between patients with and without hyperglycaemia on admission (Luitse et al., 2013). In this study the infarct core area was also measured using CT and the authors found no difference in the size of the infarct core area between hyperglycaemic and normoglycaemic patient groups. A point of criticism of their study however is that only a single measure of the perfusion deficit area and infarct core area was reported by Luitse et al (2013). Both were obtained within 24 hours of admission with a median time between the onset of symptoms and CT imaging of 102 and 104 minutes for normoglycaemic and hyperglycaemic patients respectively. The ischaemic lesion can continue to evolve for several hours following the onset of

symptoms and therefore by measuring the perfusion deficit and infarct core size at a single time point Luitse et al (2013) may have missed an effect of hyperglycaemia. Likewise, a potential limitation of the present study might be that hyperglycaemia does increase the severity of ischaemia but not at the time point examined. Consideration to this was given when designing this thesis and an acute MRI study was proposed that would permit serial measurements of the perfusion deficit over the acute 1-4 hours post-MCAO as well as the evolution of the acute ischaemic lesion. A limiting factor in the study by Luitse and colleagues is the relatively small number of patients included in their study. This is further complicated by the inclusion of patients with and without a history of diabetes. There is evidence that patients without a history of diabetes have a worse outcome after ischaemic stroke than patients with a known history of the condition (Capes et al., 2001). Preclinical studies support this (Tarr et al., 2013) and it has been suggested that the design of future clinical trials of glucose lowering therapies in acute ischaemic stroke should include only those that have no history of diabetes or other co-morbidities.

Although the results from the present suggest that hyperglycaemia doesn't exacerbate ischaemic damage by increasing the perfusion deficit, it is still possible the hyperglycaemia enhances ischaemic brain injury via an effect on the cerebrovasculature. There is evidence that hyperglycaemia can impair reperfusion after global (Ginsberg et al., 1980, Kagstrom et al., 1983) and focal ischaemia (Venables et al., 1985, Kawai et al., 1997b). Results from a study by Kawai et al (1997) indicate that hyperglycaemia has a profound effect on reperfusion during transient MCAO, with blood flows returning to only 50% of those found in normoglycaemic rats. Another potential indicator for a vascular effect of hyperglycaemia is haemorrhage. Hyperglycaemia is consistently associated with a greater incidence of haemorrhagic transformation on reperfusion in animal studies (Kawai et al., 1997b, Decourtenmyers et al., 1989). There is also a higher incidence of haemorrhage following reperfusion with t-PA in hyperglycaemic patients (Alvarez-Sabin et al., 2003). The effects of hyperglycaemia during reperfusion were not examined in this thesis but may be examined in future studies by this department. This would be valuable to the pre-clinical stroke literature as there are few studies, if any, that have

investigated the effects of clinically relevant hyperglycaemia during transient MCAO.

4.4.3 Summary

The present study has shown that hyperglycaemia, at clinically-relevant blood levels, did not exacerbate the CBF deficit induced by 1 hour of permanent MCAO. Hyperglycaemia may exert an effect on CBF at a later time-point than that investigated in this study and subsequent chapters will use MRI to examine the temporal evolution of the perfusion deficit.

Chapter 5 – Imaging the acute effects of hyperglycaemia on the temporal evolution of ischaemic damage and CBF using MRI

5.

5.1 Introduction

Data in the previous chapter demonstrated that hyperglycaemia did not exacerbate the reduction in CBF at 1 hour post-MCAO. However, it is possible that in the previous study an effect of hyperglycaemia did exist but was not detected since the reduction in CBF was measured at only a single time point. In this chapter MRI was used to acquire repeated measurements of the perfusion deficit at hourly intervals over the first 4 hours after MCAO using the non-invasive method of PI, pCASL. Using MRI meant that concurrent DWI could also be performed to assess the acute evolution of ischaemic damage. By performing PI in combination with DWI it was possible to calculate the volume of perfusion-diffusion mismatch tissue during the first four hours after MCAO. PI-DWI mismatch tissue, which is typically represented by an area of abnormal perfusion surrounding an area of abnormal diffusion, is widely used to identify the ischaemic penumbra – hypoperfused, yet viable tissue that is destined to progress to infarction unless perfusion is restored. To my knowledge, no previous animal studies have investigated the effect of hyperglycaemia on PI-DWI mismatch tissue following MCAO. However MRI studies in acute ischaemic stroke patients have shown that larger infarct sizes in patients with admission hyperglycaemia are associated with reduced penumbral salvage (Parsons et al., 2002, Rosso et al., 2011). Parsons et al (2002), examined the association between admission hyperglycaemia and the ischaemic penumbra using acute perfusion-diffusion mismatch MRI. They found that in patients with evidence of perfusion-diffusion mismatch hyperglycaemia was correlated with reduced penumbral salvage, larger final infarct sizes and worse functional outcomes. In patients without PI-DWI mismatch (non-mismatch patients) hyperglycaemia did not correlate with outcome imaging or clinical measures. The difference in outcome between patients with and without mismatch in relation to glycaemic status suggests that PI-DWI mismatch tissue might be highly susceptible to hyperglycaemia through the accelerated conversion of hypoperfused at-risk tissue to infarction. It was therefore interesting to compare the volume of perfusion-diffusion mismatch tissue and the loss of this tissue over time between glucose and vehicle treated rats in the present study to determine if hyperglycaemia exerts an adverse effect on the ischaemic penumbra.

The detrimental effect of hyperglycaemia on infarct volume at 24 hours post-MCAO, which was reported in other rat strains (Tarr et al., 2013), has not yet been confirmed in the Wistar strain used in this thesis. Therefore following acute MRI scanning, animals were recovered for 24 hours post-MCAO, at which time infarct volume was assessed using T_2-weighted MRI. From T_2-weighted images the extent of ipsilateral hemispheric swelling between groups could also be assessed by measuring and comparing the volumes of the ipsilateral and contralateral hemispheres. Hyperglycaemia has been reported to increase cerebral oedema in acute ischaemic stroke patients (Berger and Hakim, 1986) and following experimental stroke in rodents (Kawai et al., 1997a). It was therefore interesting to determine if glucose treatment is associated with increased cerebral oedema in this animal model.

5.1.1 MRI perfusion and diffusion thresholds

In the present Chapter perfusion and diffusion thresholds were applied to quantitative CBF and ADC maps respectively in order to calculate the perfusion deficit, ADC lesion volume and subsequent PI-DWI mismatch. There is currently no consensus on where to set the perfusion and diffusion thresholds to accurately define perfusion and diffusion lesions in rodent models of focal cerebral ischaemia (Campbell and Macrae, 2015). This is particularly important for pre-clinical studies of neuroprotective agents targeting the ischaemic penumbra. If the thresholds applied are too high or too low this could lead to over- or underestimations of the amount of perfusion-diffusion mismatch tissue, leading to the false identification of neuroprotective/neurotoxic agents or exclusion of potentially efficacious agents.

Shen et al (2003) established absolute ADC and CBF thresholds below which pixels within respective ADC and CBF maps are destined to become infarcted following permanent MCAO (intraluminal filament method). The ADC threshold was established from quantitative ADC maps acquired from DWI scans performed at 3 hours post-MCAO. Likewise, the CBF threshold was derived from CBF maps acquired using continuous arterial spin labelling scans performed at 3 hour post-MCAO. To generate ADC and CBF thresholds Shen et al (2003) adjusted the ADC and CBF values on respective ADC and CBF maps until the ADC- and CBF-defined lesion volumes were numerically equal to TTC-derived infarct volumes measured

at 24 hours post-MCAO. The absolute ADC and CBF thresholds established in the study by Shen et al (2003) were 0.53 x 10^{-3} mm^2/sec and 0.3mL.g^{-1}.min^{-1} (30ml/100g/min) respectively. In a similar manner Reid et al (2012), established absolute ADC and CBF viability thresholds for the Wistar Kyoto (WKY) and spontaneously hypertensive stroke prone (SHRSP) rat strains by adjusting ADC and CBF thresholds until the ADC-derived and CBF-derived lesion volumes at 4 hours post-MCAO were numerically equal to infarct volumes measured at 24 hours post-MCAO by T_2-weighted imaging. In WKY rats the ADC and CBF thresholds were 0.61±0.03 x 10^{-3} mm^2/sec and 23±8ml/100g/min respectively. The ADC and CBF threshold values for SHRSP rats were 0.59±0.03 x 10^{-3} mm^2/sec and 36±13ml/100g/min. In the study by Shen et al (2003) the ADC and CBF thresholds were established in Sprague Dawley rats, a normotensive rat strain, whereas Reid et al (2012), used hypertensive SHRSP rats and their control strain, WKY rats. The results from these studies suggest that ADC and CBF viability thresholds can vary depending on rat strain and therefore may be strain specific. In addition to this, an acute MRI study reported differences in the temporal evolution of acute ADC lesion volume between different rat strains (Bardutzky et al., 2005). Consequently ADC-derived lesion volumes could be significantly underestimated if an absolute ADC threshold established in a rat strain where the lesion has fully evolved is applied to define ADC lesion volume in a different strain where the lesion has not fully evolved. It is therefore important that viability perfusion and diffusion thresholds are established for each rat strain used in experimental stroke studies. Currently there are no published ADC or CBF thresholds to define perfusion and diffusion lesions for the Wistar rat strain; the strain used in this thesis. It is also not clear from the literature if ADC and CBF viability thresholds vary depending on the method of MCAO. Both Shen et al (2003) and Reid et al (2012) established thresholds following permanent MCAO induced by the intraluminal filament model. However the distal portion of the MCA was occluded by diathermy in the present study and there could be differences in the temporal evolution of ischaemic damage between different methods. Therefore the perfusion and diffusion data from the present study were used to establish CBF and ADC viability thresholds for the Wistar rat strain following permanent distal diathermy MCAO.

5.1.2 Study Aims

The main aims of this study were to:

1. Establish strain-specific diffusion and perfusion thresholds for Wistar rats that could be applied to quantitative diffusion and perfusion data in order to measure the perfusion and diffusion deficit over the acute 1-4 hours after permanent MCAO.

2. Determine the effect of hyperglycaemia on the early development of ischaemic damage using DWI and the perfusion deficit using pCASL.

3. Investigate the effect of hyperglycaemia on the acute evolution of penumbra tissue using the MRI perfusion-diffusion mismatch model.

4. Assess the effect of hyperglycaemia on infarct volume at 24 hours post-MCAO using T_2 weighted imaging.

5.2 Methods

5.2.1 Animals

Adult male Wistar rats (280-360g) were used in this study. Water and food were freely available except from the night before surgery when rats were fasted overnight with free access to water.

5.2.2 Sample size calculation, randomisation and blinding

To calculate the number of animals required per group a sample size calculation was performed based on the mean and standard deviation values of ADC lesion volume data and the effect size of glucose administration acquired from a previous MRI study using WKY rats (Tarr et al., 2013). The sample size calculation was based on an 80% power and 95% significance level as described in Chapter 4.2.2. The number of animals per group was calculated to be 10. All animals were randomised to treatment groups using an online randomisation plan generator (www.randomization.com). Administration of treatment during surgery was carried out blind to treatment groups with a colleague not involved in the study preparing the appropriate syringe on day of surgery. Similarly, all data analysis was carried out in a blinded manner. Due to the 20% mortality/exclusion rate from the previous study it was decided to include 12 animals per group in the randomisation plan (Figure 5.1). A further 3 rats were later randomised into the study due to the exclusion of some animals.

5.2.3 Surgical procedures

Animals were initially anaesthetised in an anaesthetic chamber with 5% isoflurane in a 70% nitrous oxide and 30% oxygen mixture. Oral intubation was performed and animals were artificially ventilated with 2.5% isoflurane in a nitrous oxide: oxygen mixture (70:30). The right femoral artery was cannulated for continuous recording of MABP and monitoring of blood pH, $PaCO_2$ and PaO_2 as described in Chapter 2.2.2. Body temperature was maintained at 37±0.5°C using an external heat source and recorded using a rectal thermometer. Permanent focal cerebral ischaemia was achieved using the distal diathermy method of MCAO as described in Chapter 2.3.2.

A Randomization Plan

from

http://www.randomization.com

1	Vehicle	13	Vehicle
2	Glucose	14	Vehicle
3	Vehicle	15	Glucose
4	Glucose	16	Vehicle
5	Vehicle	17	Vehicle
6	Glucose	18	Vehicle
7	Glucose	19	Glucose
8	Vehicle	20	Vehicle
9	Vehicle	21	Glucose
10	Glucose	22	Glucose
11	Vehicle	23	Glucose
12	Glucose	24	Glucose

Figure 5.1. Randomization plan for MRI study where 12 rats were assigned to each group. The randomization plan was generated from www.randomization.com.

5.2.4 Induction of hyperglycaemia and blood glucose measurements

Rats were randomly assigned to glucose and vehicle treatment groups. A single dose of a 15% glucose solution (10ml/kg) or the equivalent volume of the vehicle solution (distilled water) was administered IP to glucose and vehicle treated rats, respectively, 10 minutes prior to MCAO. Arterial blood glucose levels were measured 20 minutes prior to MCAO to obtain a baseline glucose reading, at the time of MCAO (0 minutes post-MCAO) and at each hour for four hours post-MCAO as described in Chapter 2.4.

5.2.5 MRI scanning protocol

MRI scanning was performed as described in Chapter 2.7. For all MRI scans, after transferring the animal to the MRI rat cradle, anaesthesia was maintained with 2-2.5% isoflurane in a nitrous-oxide: oxygen mixture (70:30) and the rat's physiology was monitored as described in Chapter 2.7.2. Before the cradle was placed inside the scanner a phased array surface receiver coil was placed on the rat's head. The rat cradle was then secured inside the scanner and a pilot sequence was obtained to ensure the geometry was correct.

To assess the early evolution of ischaemic damage DWI scans were obtained at 1 hour post-MCAO and at each subsequent hour for four hours post-MCAO using the sequence described in Chapter 2.7.3. DWI scans consisted of 8 contiguous coronal slices (1.5mm thick) and quantitative ADC maps were generated for each slice.

Perfusion images were acquired at each hour for 4 hours post-MCAO to assess the acute evolution of the perfusion deficit. A form of pseudo continuous arterial spin labelling was used to generate non-invasive cerebral blood flow measurements on 6 contiguous coronal slices (1.5mm thick) as described in Chapter 2.7.4.

Unlike the DWI scan which took approximately 2 minutes to generate an ADC map of 8 coronal slices, pCASL scans took approximately 7 minutes per coronal slice. A T_1 map, across 8 coronal slices was also performed each hour (for quantifying CBF maps) and this took approximately 10 minutes. Therefore within each hour pCASL scans could only be generated for 6 coronal slices and

the 6 slices which were spatially identical to slices 2-7 of the DWI scan were selected.

5.2.6 Animal Recovery

At the end of the MRI scanning protocol the rat cradle was removed from the MRI scanner and after removing the water jacket, rectal thermocouple and ECG leads, the rat was disconnected from the ventilator and blood pressure monitor and transferred to the operating theatre. Once in the operating theatre the rat was reconnected to the ventilator and anaesthesia was maintained with 2% isoflurane in a nitrous oxide: oxygen mixture (70:30). Rats were then recovered for 24 hours as described in Chapter 2.3.4.

5.2.7 Infarct volume assessment and collection of brain tissue

At 24 hours post-MCAO, a RARE T_2-weighted MRI scan was carried out to allow calculation of infarct volume (Chapter 2.7.5). Following T_2-weighted imaging the animals were deeply anaesthetised by increasing the isoflurane concentration to 5% for five minutes. Animals were then removed from the MRI scanner and killed by decapitation. The brain was rapidly removed from the skull and placed on a chilled glass plate. The cerebellum and olfactory bulbs were removed and a scalpel blade was used to divide the remaining cerebrum into a left (ischaemic) hemisphere and right (non-ischaemic) hemisphere. Each hemisphere was further dissected into cortical and subcortical tissue and all samples were snap frozen in liquid nitrogen and stored at -80˚C. Brain tissue lysates were prepared from the ischaemic cortex tissue samples for protein analysis by western blotting (Chapter 6).

A timeline summarising the MRI scanning protocol and experimental design is presented in Figure 5.2.

Group	Treatment	n
Vehicle	dH2O (10ml/Kg)	10
Glucose	15% glucose (10ml/kg)	10

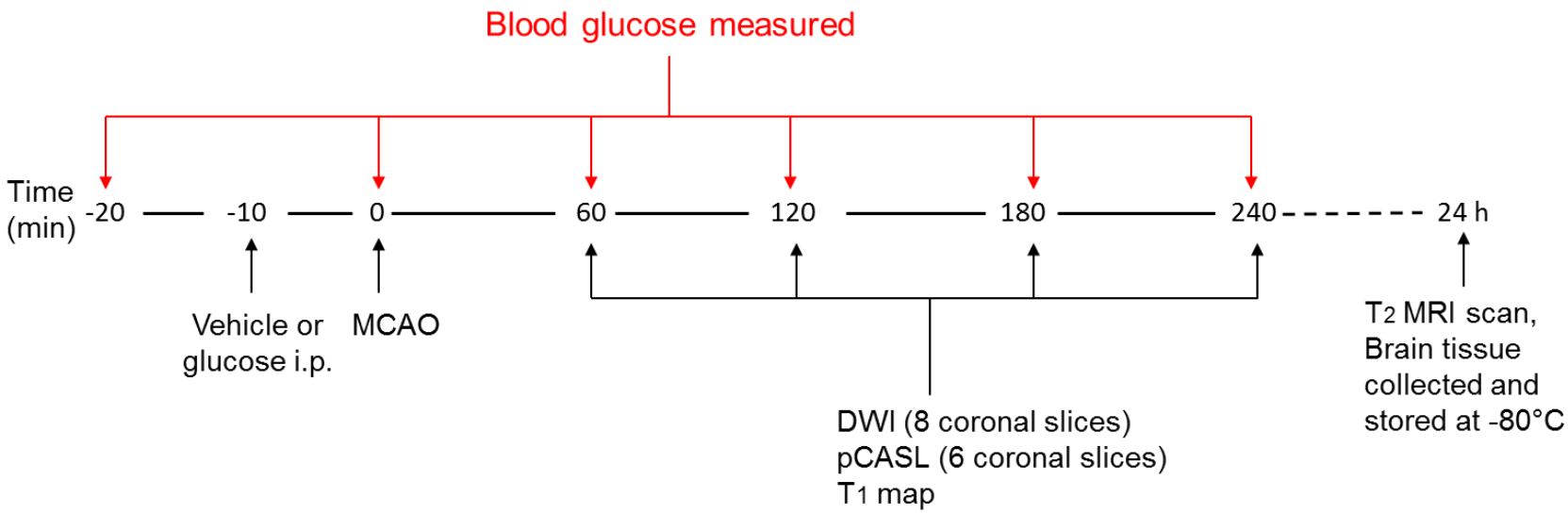

Figure 5.2. Timeline for MRI study. Rats were randomized to vehicle (n=10) and glucose (n=10) treatment groups using an online randomisation plan generator. The vehicle or 15% glucose solution was administered IP 10 minutes prior to MCAO. Following MCAO rats were transferred to the small animal scanner and DWI, pCASL and T_1–weighted scans were performed each hour for 4 hours. Blood glucose levels were measured 20 minutes before MCAO to obtain a baseline reading, at the onset of MCAO (0 minutes) and at hourly intervals for 4 hours. At the end of the 4 hour scanning period animals were recovered for 24 hours. After this time a T_2-weighted MRI scan was performed to assess infarct volume. The animals were then killed and brain was removed and the tissue was collected, snap frozen in liquid nitrogen and stored at -80°C.

5.2.8 MRI data analysis

5.2.8.1 Generation of MRI diffusion and perfusion thresholds for the Wistar strain of rat

For each animal included in the analysis a diffusion (ADC) threshold was established by applying a range of absolute ADC threshold values (0-2 x 10^{-3} mm^2/sec with 0.01 mm^2/sec increments) to the quantitative ADC map generated at 4 hours post-MCAO until the ADC-defined lesion volume was within ±5mm^3 of the oedema corrected T_2-derived lesion volume (Reid, 2012). The 4 hour time point was selected as the ADC-derived lesion volume has been shown to be fully evolved after this time (Li et al., 2000a, Reith et al., 1995).

In a similar manner a perfusion threshold was established for each animal in the study. A range of increasing CBF thresholds (−100-400ml/100g/min with 1 ml/100g/min increments) were applied to the pCASL CBF maps acquired at 4 hours post-MCAO until the pCASL derived lesion volume was within ±10mm^3 of the T_2-derived infarct volume at 24 hours post-MCAO. Negative perfusion values were generated in many of the pixels within the ischaemic cortex where there was zero or low CBF. These negative values resulted from the subtraction step during pCASL image processing (Chapter 2.7.4), where the signal difference was comparable to image noise. Negative perfusion values were assumed to represent zero CBF.

5.2.8.2 Calculation of ADC lesion volume and perfusion deficit volume

To calculate ADC lesion volume an absolute ADC threshold of 0.53 x 10^{-3} mm^2/sec was applied to the ADC maps generated at each hour post-MCAO. This threshold represented the mean ADC threshold generated from all of the animals included in this study and matched the ADC threshold for Sprague-Dawley rats (Shen et al., 2003).

The perfusion threshold generated in this study was not used to calculate the perfusion deficit as this threshold tended to underestimate the perfusion deficit as described in the results. Instead, the volume of tissue with a perfusion deficit was calculated by applying an absolute perfusion threshold of 30ml/100g/min to all CBF maps. This threshold was chosen because it was the absolute CBF

threshold derived by Shen et al (2003) to define the perfusion deficit following permanent MCAO in Sprague-Dawley rats using arterial spin labelling. Also, in a study in which CBF was measured 30 minutes post-MCAO using [^{14}C]-IAP autoradiography, mean CBF within the cerebral cortex was found to be ~30ml/100g/min (Tamura et al., 1981b).

5.2.8.3 Calculation of perfusion-diffusion mismatch

Spatial assessment of the perfusion-diffusion mismatch was carried out on each of the 6 coronal slices of the CBF maps. ImageJ software was used to apply a perfusion threshold of 30ml/100g/min and a diffusion threshold of 0.53 x 10^{-3} mm^2/sec to quantitative CBF maps and ADC maps respectively. The ADC-derived lesion was then superimposed onto the thresholded CBF map and the remaining perfusion deficit (mismatch tissue) was manually delineated and the area of mismatch tissue was calculated. The mismatch area on each of the 6 slices was summed and multiplied by the slice thickness (1.5mm) to obtain the volume of mismatch tissue. This was repeated for each time point after MCAO.

5.2.9 Study exclusion criteria

Animals were excluded from the study if they died during surgery to induce focal cerebral ischaemia, during the MRI scanning protocol or before the 24 hour MRI scans. Animals were also excluded if there were any signs of intracerebral haemorrhage or subdural haematoma (Figure 5.3) development in the brain during T_2-weighted imaging and/or tissue collection.

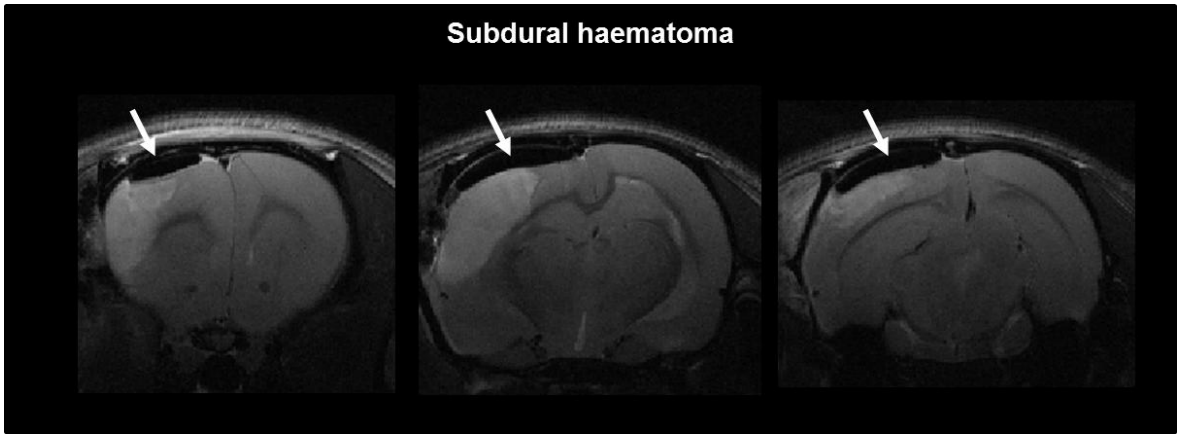

Figure 5.3. T_2 weighted images from an excluded animal which had a subdural haematoma (white arrow). The subdural haematoma appears hypointense on T_2 images.

5.2.10 Statistical analysis

Physiological variables, T_2-weighted lesion volumes, ADC threshold values, CBF threshold values, T_2-derived infarct volume, ipsilateral hemispheric swelling were assessed using a Student's unpaired t-test. Blood glucose values, ADC lesion volumes, perfusion deficit volumes, contralateral hemisphere CBF, PI-DWI mismatch and ADC-defined penumbra volumes were assessed using a repeated measures two-way analysis of variance (RM 2-way ANOVA) with Bonferroni's post-test. Differences between groups were considered to be statistically significant when $P<0.05$. Data are expressed as mean ± standard deviation or scatterplots with the mean indicated. Where images are presented from the median animal of each group these are the median animals from the T_2-derived infarct volume results.

5.3 Results

5.3.1 Mortality and excluded animals

A total of 27 animals were included in this study. Four animals died (3 vehicle treated rats and 1 glucose treated rat) during or after the MRI scanning protocol and these animals were excluded. Three further rats (all glucose treated) were excluded from the study due to the presence of subdural haematomas on T_2-weighted images. The final group sizes for analysis were n=10 for the vehicle treatment group and n=10 for the glucose treatment group.

5.3.2 Physiological variables

Physiological variables were measured throughout the duration of the experiment. Body weight was measured on the day of surgery and there were no differences in body weight measurements between vehicle and glucose treated rats (321±25g & 326±17g respectively, P=0.6). MABP, body temperature and blood $PaCO_2$, PaO_2 and pH were monitored throughout the surgical period to keep them within normal physiological range. Baseline values, measured 20 minutes before MCAO, and the values at 1-4 hours post-MCAO are presented in Table 5.1. For each physiological parameter, except PaO_2, mean values were within normal physiological range. PaO_2 values were above the normal physiological range due to the elevated percentage of inspired oxygen used to maintain physiological stability during general anaesthesia. There were no differences in any of the physiological parameters between the two groups at any of the time points measured.

5.3.3 Blood glucose

Blood glucose values were measured at baseline and at each hour for four hours following MCAO. There was no significant difference in baseline blood glucose levels between vehicle and glucose treatment groups, with values of 4.9±0.9mmol/L and 5.9±1.1mmol/L respectively. Following a single IP injection of either the vehicle or 15% glucose solution (10ml/kg) blood glucose levels remained stable around baseline values in the vehicle group but rose to a mean level of 12.6mmol/L in the glucose group (Figure 5.4). Blood glucose values in

the glucose treatment group remained at this elevated level for the duration of the 4 hour study.

Physiological parameter	Baseline	1 hour	2 hours	3 hours	4 hours
Vehicle (n=10)					
MABP (mmHg)	92 ± 9	91 ± 10	89.5 ± 10	90 ±7.6	89 ± 6.4
$PaCO_2$ (mmHg)	35 ± 10	36 ± 10	41.1 ± 11.3	40.8 ± 10.8	39 ± 5
PaO_2 (mmHg)	126 ± 17	125 ± 16	121 ± 16	131 ± 26	123 ± 30
pH	7.41 ± 0.1	7.38 ± 0.04	7.39 ± 0.04	7.40 ± 0.03	7.35 ± 0.04
Temperature (°C)	37.0 ± 0.3	37.4 ± 0.4	37.3 ± 0.5	37.3 ± 0.3	37.1 ± 0.1
Glucose (n=10)					
MABP (mmHg)	97 ± 10	88 ± 5.1	86.8 ± 10.7	84.5 ±11.2	89 ± 7.0
$PaCO_2$ (mmHg)	37 ± 11	38 ± 6	37.1 ± 8.9	35.9 ± 5.4	41 ± 9
PaO_2 (mmHg)	132 ± 22	123 ± 21	122 ± 14	131 ± 24	132 ± 28
pH	7.47 ± 0.04	7.37 ± 0.1	7.35 ± 0.07	7.37 ± 0.1	7.37 ± 0.04
Temperature (°C)	37.0 ± 0.2	37.2 ± 0.4	37.1 ± 0.6	37.4 ± 0.4	37.2 ± 0.6

Table 5.1. Physiological variables for MRI study. Body weight was measured prior to MCAO. MABP, temperature, pH, PaO_2 and $PaCO_2$ were measured at baseline (20 minutes before MCAO) and at each hour for 4 hours post-MCAO. The data are expressed as mean ± standard deviation. There were no significant differences in any of the variables, at any time point, between vehicle and glucose treated rats (Student's unpaired t-test).

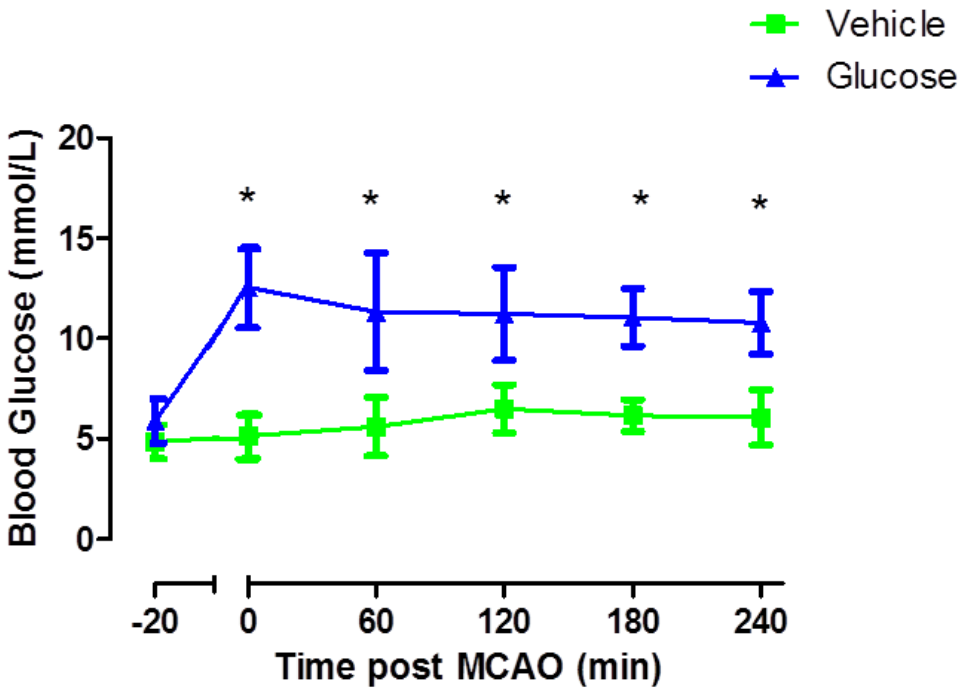

Figure 5.4. Blood glucose data for MRI study. Blood glucose values measured at baseline (-20 minutes) and at each hour for four hours post-MCAO in vehicle (n=10) and glucose (n=10) treated rats. Glucose or vehicle solution was administered 10 minutes before MCAO. *P<0.0001 compared with vehicle using RM 2-way-ANOVA with Bonferroni's post-test. Data are presented as mean ± standard deviation.

5.3.4 Establishing strain specific diffusion and perfusion thresholds

The mean ADC threshold values of the vehicle and glucose treatment groups were 0.51±0.05 and 0.56±0.03 x 10^{-3} mm^2/sec respectively (Figure 5.5A). The difference in ADC threshold values between groups was statistically significant (P=0.03). There was no difference in mean ADC values in the contralateral hemisphere between groups at 4 hours post-MCAO, with values of 0.75 and 0.76 x 10^{-3} mm^2/sec (P=0.1) in vehicle and glucose treated rats respectively. The mean ADC threshold value for all 20 rats in the study was 0.53±0.05 x 10^{-3} mm^2/sec (30% reduction from contralateral hemisphere ADC values, Figure 5.5B). Due to the observed difference in the mean ADC threshold between groups it was decided to use the mean ADC threshold established for all 20 rats, 0.53 x 10^{-3} mm^2/sec, to calculate ADC lesion volume for all rats.

The mean CBF viability threshold values calculated for the vehicle and glucose treatment groups were 3±14 and 8±14ml/100g/min respectively (Figure 5.6A). The difference between groups was not statistically significant (P=0.5). The mean CBF threshold for all rats included in the analysis was 6±14ml/100g/min (Figure 5.6B). By examining the CBF thresholds values for individual rats it was found that more than half had CBF thresholds near to or below 0ml/100g/min, with thresholds of -14 and -13ml/100g/min calculated in some animals (Figure 5.6B). Negative CBF values resulted from the subtraction step during pCASL image processing (Chapter 2.7.4) and are assumed to represent zero flow. Therefore by assuming all negative CBF thresholds are 0ml/100g/min the mean CBF threshold for all 20 animals became 8±11ml/100g/min (Figure 5.6C). However, when using this threshold to define the perfusion deficit on quantitative CBF maps (top row of Figure 5.7) the area of the perfusion deficit on the thresholded CBF map did not match spatially with the region of hypoperfused blood flow on the non-thresholded CBF map (middle row of Figure 5.7). If this threshold was then applied to all animals the perfusion deficit could be underestimated in many animals. When a CBF threshold of 30ml/100g/min was applied to define the perfusion deficit at 4 hours there was better spatial agreement between the perfusion deficit on the thresholded CBF map and the hypoperfused region on the non-thresholded CBF map (bottom row of Figure 5.7). This absolute CBF threshold of 30ml/100g/min has been used to define the perfusion deficit following 3 hours of permanent MCAO in Sprague Dawley rats

(Shen et al., 2003) and is in close agreement with pCASL derived perfusion thresholds generated in-house for WKY (23ml/100g/min) and SHRSP (36ml/100g/min) rats (Reid et al., 2012). Therefore for calculation of the perfusion deficit it was decided to use a threshold of 30ml/100g/min.

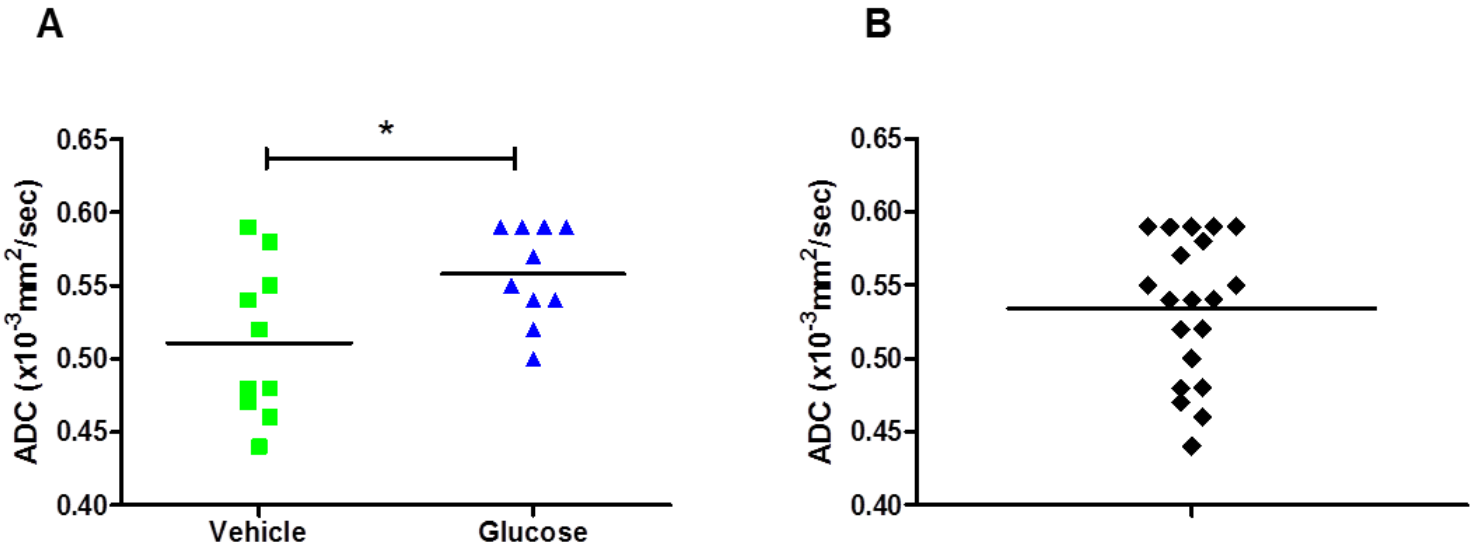

Figure 5.5. ADC thresholds for Wistar rat strain. A. ADC thresholds calculated for vehicle (n=10) and glucose (n=10) treated Wistar rats following MCAO. B. ADC threshold values for all rats (n=20). The ADC thresholds were generated by adjusting the ADC values on quantitative ADC maps acquired at 4 hours post-MCAO until the ADC derived lesion volume matched the T_2-derived infarct volume at 24 hours post-MCAO. Data are presented as scatterplots with the line indicating the mean. *P<0.05 compared with vehicle group using Student's unpaired t-test.

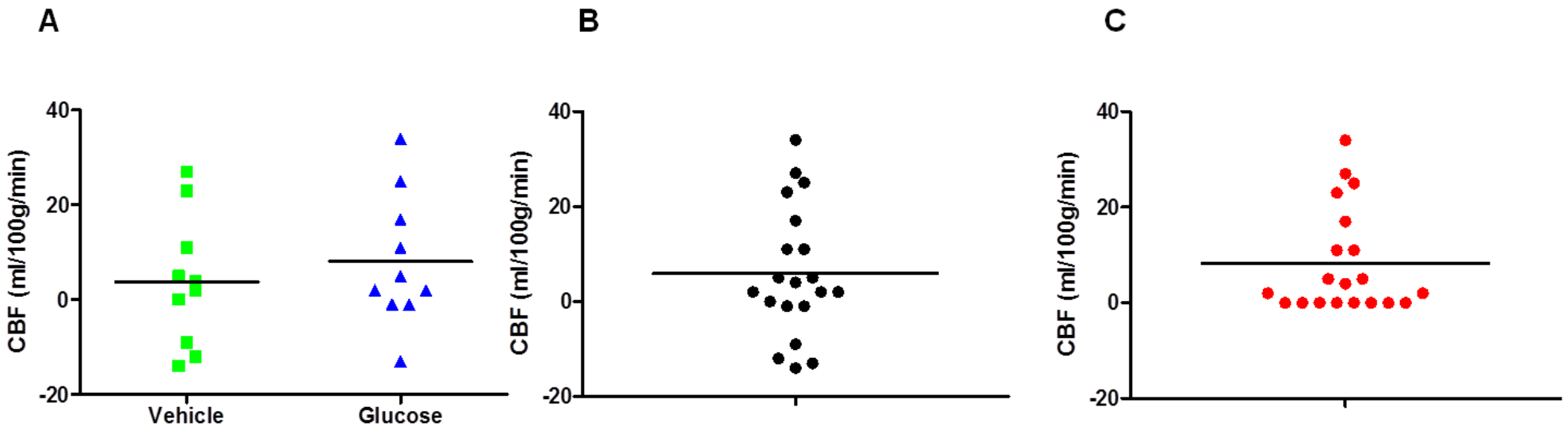

Figure 5.6. pCASL derived CBF thresholds. A. CBF thresholds calculated for vehicle (n=10) and glucose (n=10) treated Wistar rats following MCAO. B. CBF thresholds for all rats (n=20). C. CBF thresholds for each rat with all negative values assumed to be 0ml/100g/min. CBF thresholds were generated by adjusting the CBF values on quantitative blood flow maps acquired at 4 hours post-MCAO until the volume of the perfusion deficit matched the T_2-derived infarct volume at 24 hours post-MCAO. Data are presented as scatterplots with the line indicating the mean.

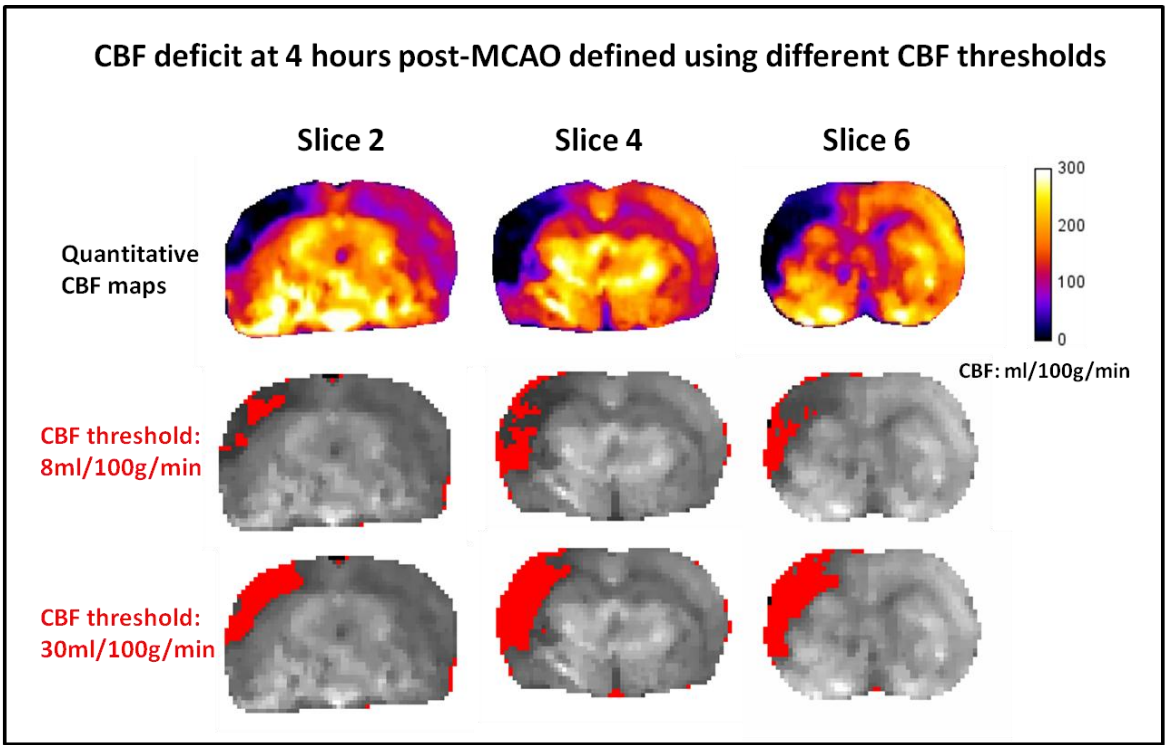

Figure 5.7. CBF deficit at 4 hours post-MCAO defined using different CBF thresholds. Quantitative CBF maps at 4 hours post-MCAO in slices 2, 4 and 6 (caudal to rostral) from a representative animal (top row). Perfusion deficit (red) on the same CBF maps defined using a threshold of 8ml/100g/min (middle row) or 30ml/100g/min (bottom row). 8ml/100g/min represents the mean CBF threshold established in the present study for the Wistar strain and 30ml/100g/min represents the perfusion threshold calculated in Sprague Dawley rats (Shen et al., 2003). The perfusion deficit defined by an absolute threshold of 8ml/100g/min tended to underestimate the hypoperfused region on quantitative CBF maps whereas the perfusion deficit defined by a threshold of 30ml/100g/min threshold tended to match this region.

5.3.5 Apparent diffusion coefficient lesion volume

At 1 hour after MCAO, the earliest time point examined, there was no statistically significant difference in the mean ADC lesion volume between groups (Figure 5.8). At all other time points after MCAO the mean ADC lesion volume was significantly larger in glucose treated rats compared to vehicle treated rats.

The ADC-derived lesion volume increased significantly over the four hour time course in both groups. In the glucose treatment group the mean ADC lesion volume increased significantly from 60±13mm^3 at 1 hour to 81±29mm^3 at 4 hours post-MCAO (P=0.02). In the vehicle treatment group mean ADC lesion volume also increased significantly between 1 and 4 hours but the difference was small with values of 50±11mm^3 and 56±12mm^3 at 1 and 4 hours post-MCAO respectively (P=0.03).

The spatial profiles of the ADC lesions at 1 and 4 hours post-MCAO from the median animal of each group are presented in Figure 5.9. The ADC lesion at 1 hour (white region) was superimposed on the ADC lesion at 4 hours (red) across 8 coronal slices. In most slices the ADC lesion at 4 hours post-MCAO was greater than that at 1 hour post-MCAO in both the vehicle and glucose treated rat. In the glucose treated rat the ADC lesion was anatomically more widespread compared to the vehicle treated rat. To examine this further the ADC lesion area on each of the 8 ADC map slices was plotted for each group at 1 and 4 hours post-MCAO (Figure 5.10). At both time points the most pronounced differences in the lesion area between groups were observed in the more caudal slices (ADC slices 2-3).

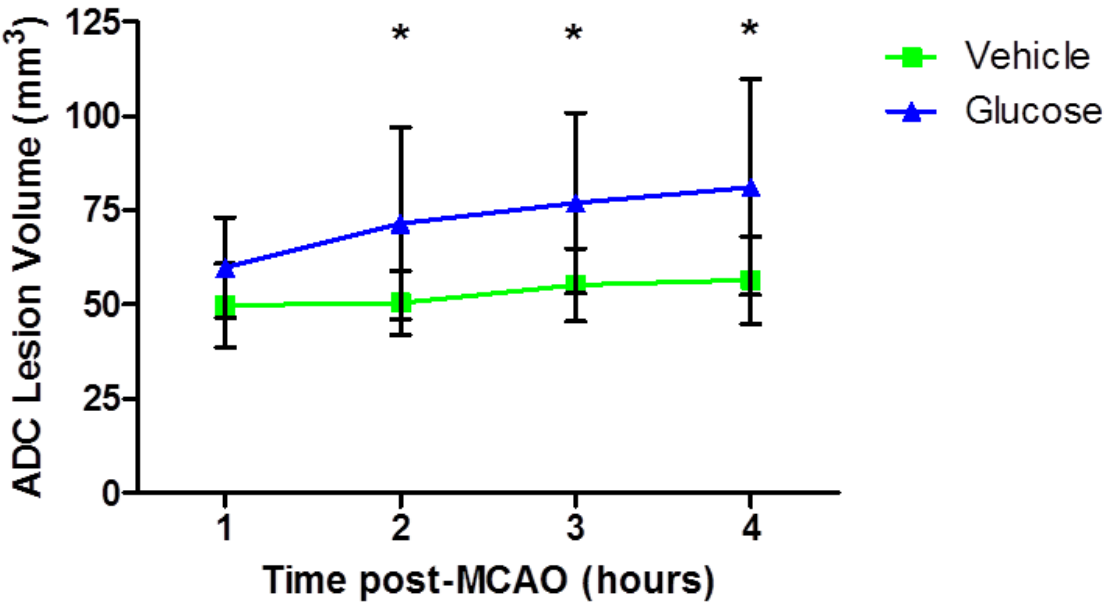

Figure 5.8. ADC-derived lesion volume measured 1-4 hours after MCAO. ADC lesion volume was calculated by applying an abnormal diffusion threshold of 0.53 x10^{-3} mm^2/sec. Data are presented as mean ± standard deviation. *P<0.05 compared with vehicle rats using a repeated measures 2-way-ANOVA with Bonferroni's post-test.

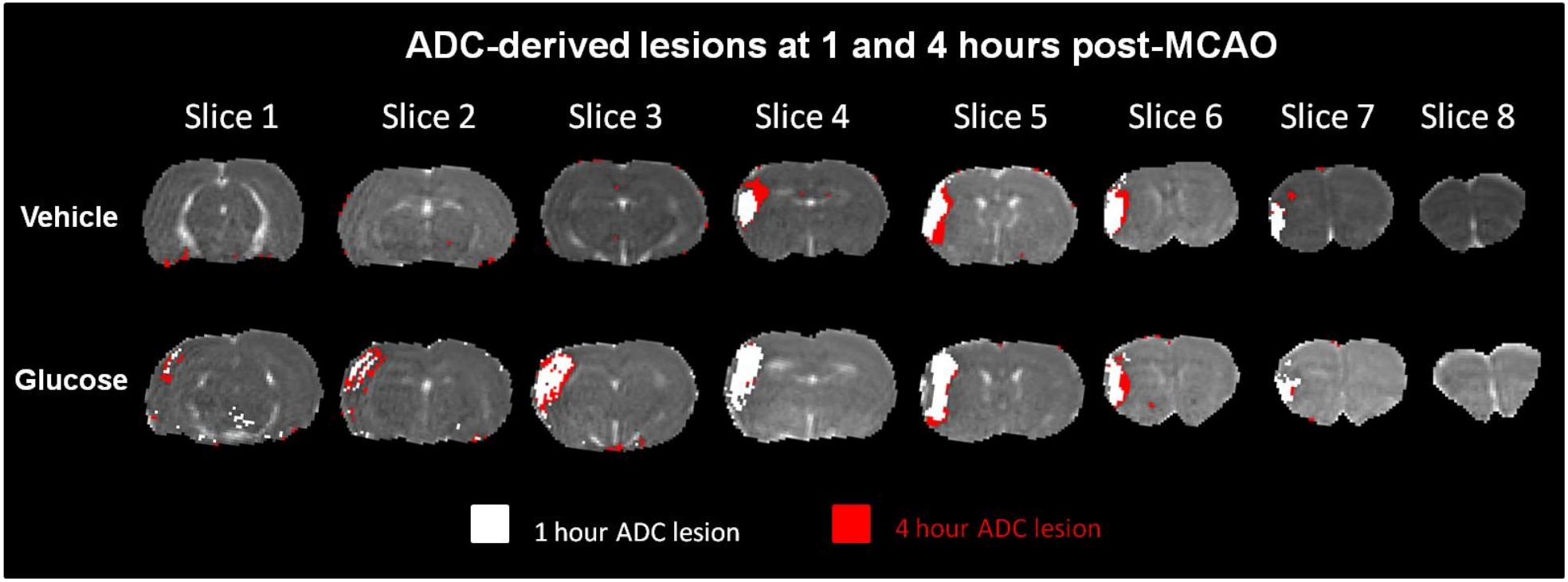

Figure 5.9. ADC-derived lesions at 1 and 4 hours post-MCAO, across 8 coronal slices, from the median animal of each group. The white region depicts the ADC lesion at 1 hour post-MCAO and the red region depicts the ADC lesion at 4 hours post MCAO. ADC lesions at 1 and 4 hours post-MCAO appear to be quite similar in size in these examples but overall there was a significant increase in ADC-derived lesion volume between 1 and 4 hours post-MCAO in both vehicle (n=10) and glucose (n=10) treatment groups. In the glucose treated rat the ADC lesion encompassed nearly all 8 coronal slices whereas in the vehicle treated rat the ACD lesion affected only a few coronal slices.

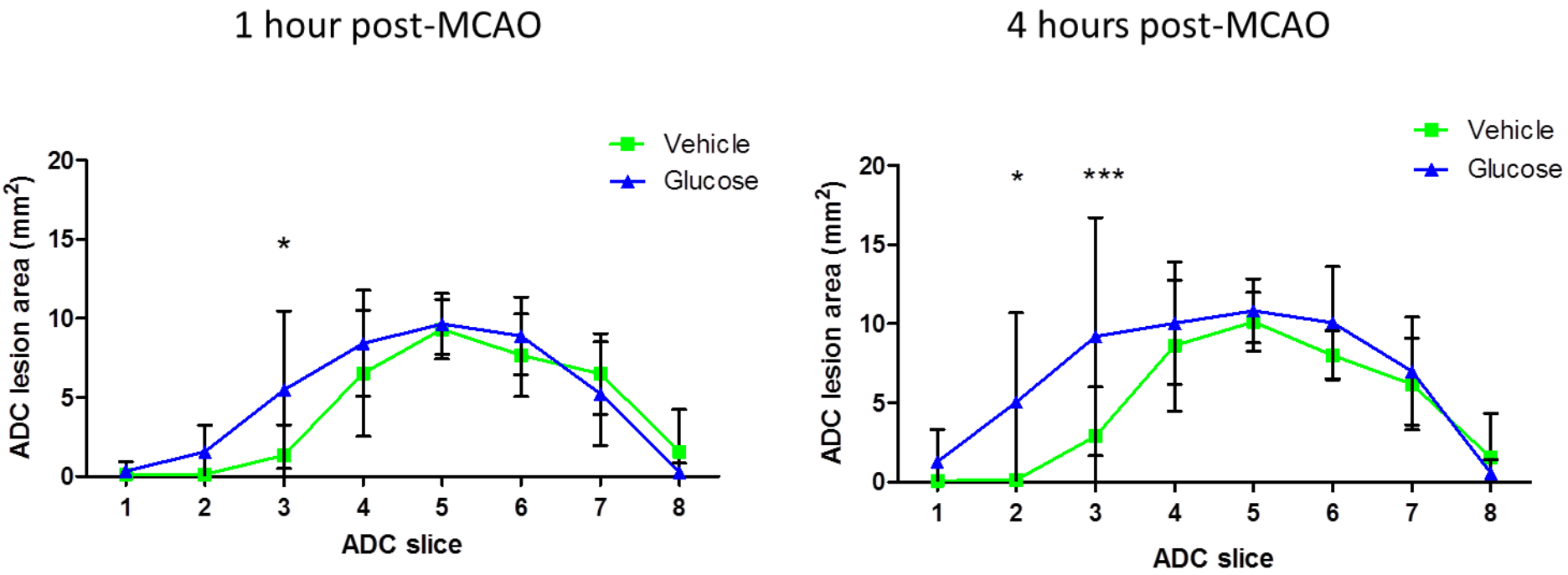

Figure 5.10. The caudal-rostral profile of the ADC lesion at 1 hour and 4 hours post-MCAO. Slices 1-8 refer to the 8 ADC slices depicted in Figure 5.9. Data are presented as mean ± standard deviation for vehicle (n=10) and glucose (n=10) treated rats. *P<0.05, ***P<0.001, compared with vehicle rats using a 2-way-ANOVA with Bonferroni's post-test.

5.3.6 Perfusion deficit volume

An absolute threshold of 30ml/100g/min was applied to quantitative CBF maps acquired 1-4 hours post-MCAO to determine the acute evolution of the perfusion deficit for each group. At all time points after MCAO the mean perfusion deficit volume tended to be larger in the glucose treatment group compared to the vehicle treatment group (Figure 5.11), but the difference between groups was not statistically significant.

The volume of the perfusion deficit tended to increase over time in both groups. In vehicle treated rats the perfusion deficit increased from 140mm^3 at 1 hour post-MCAO to 151mm^3 at 4 hours but the difference was not statistically significant (P=0.5). Similarly, in glucose treated rats the perfusion deficit increased from 164mm^3 to 192mm^3 between 1 and 4 hours post-MCAO respectively (P=0.2). Quantitative CBF maps acquired at 1 and 4 hours post-MCAO from the median animal of each group are presented in Figure 5.12. Darker regions on the CBF maps represent regions of reduced CBF and the region of reduced blood flow induced by MCAO was detected in the ipsilateral cortex of all 6 coronal slices in both groups, at both time points.

Mean contralateral CBF was not significantly different between vehicle and glucose treated rats at any time point after MCAO (Figure 5.13). CBF in the contralateral hemisphere tended to decrease over the 4 hour time period in both groups. In vehicle treated rats mean CBF in the contralateral hemisphere was 116±25ml/100g/min at 1 hour and 92±23ml/100g/min at 4 hours post MCAO. Similarly in glucose treated rats CBF in the contralateral hemisphere decreased from 105±29ml/100g/min at 1 hour to 86±23ml/100g/min at 4 hours post-MCAO. The decrease in mean contralateral CBF in each group over the course of the 4 hour experiment was not significant (P=0.08 and P=0.05 in vehicle and glucose groups respectively).

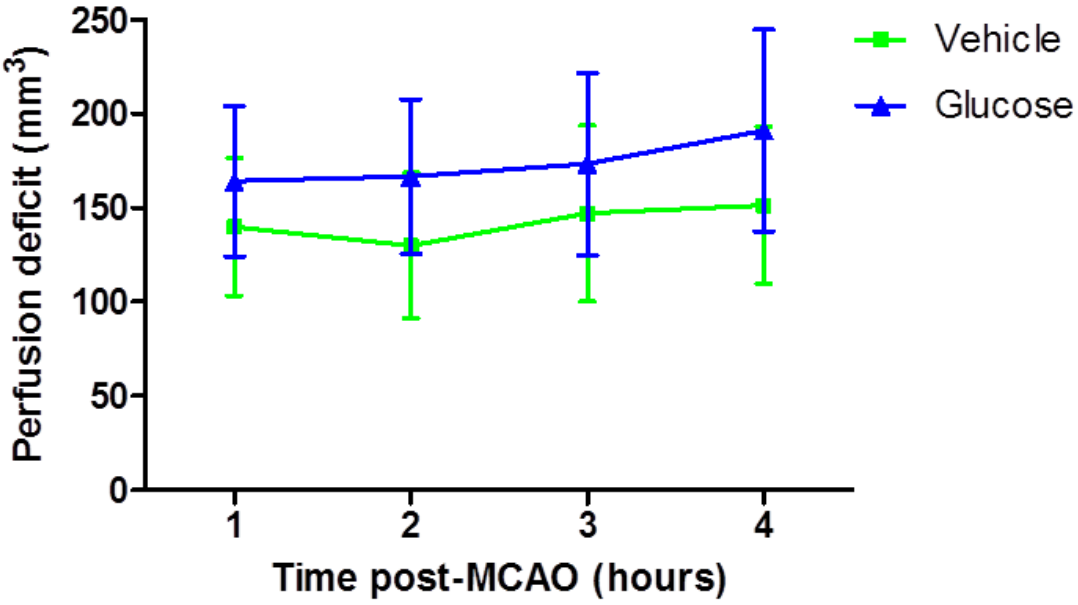

Figure 5.11. Temporal evolution of the perfusion deficit 1-4 hours after MCAO. The perfusion deficit volume was calculated by applying an abnormal perfusion threshold of 30 ml/100g/min to CBF maps. Data are presented as mean ± standard deviation. Differences between groups are not statistically significant: RM 2-way-ANOVA with Bonferroni's post-test.

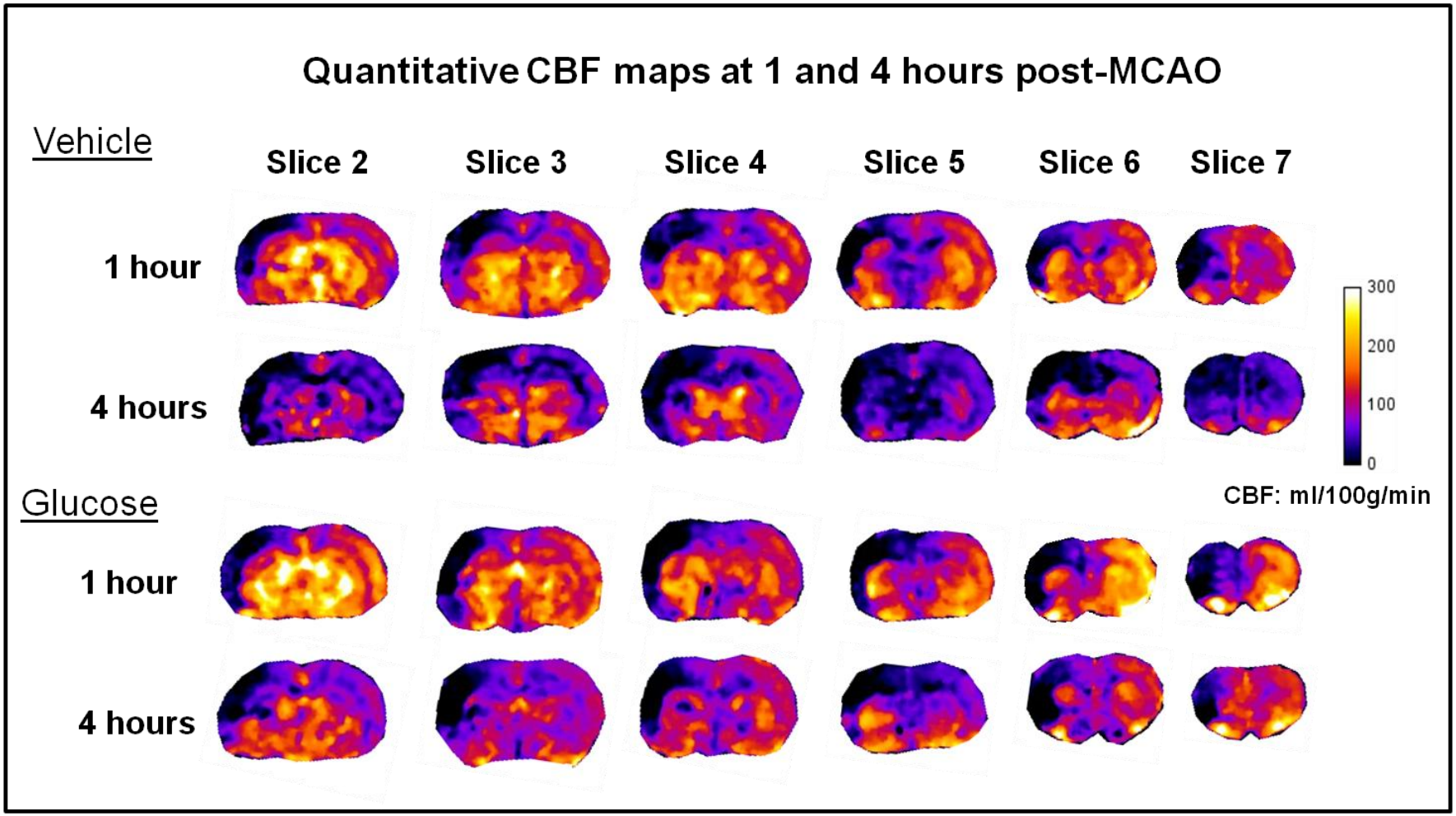

Figure 5.12. Quantitative pCASL derived CBF maps. CBF maps (ml/100g/min) displaying hypoperfused tissue at 1 and 4 hours post-MCAO, across 6 coronal slices, from the median animal of the vehicle and glucose treatment groups. The darker regions represent areas with reduced CBF and these were predominantly found in the ipsilateral cortex, as a result of distal MCAO.

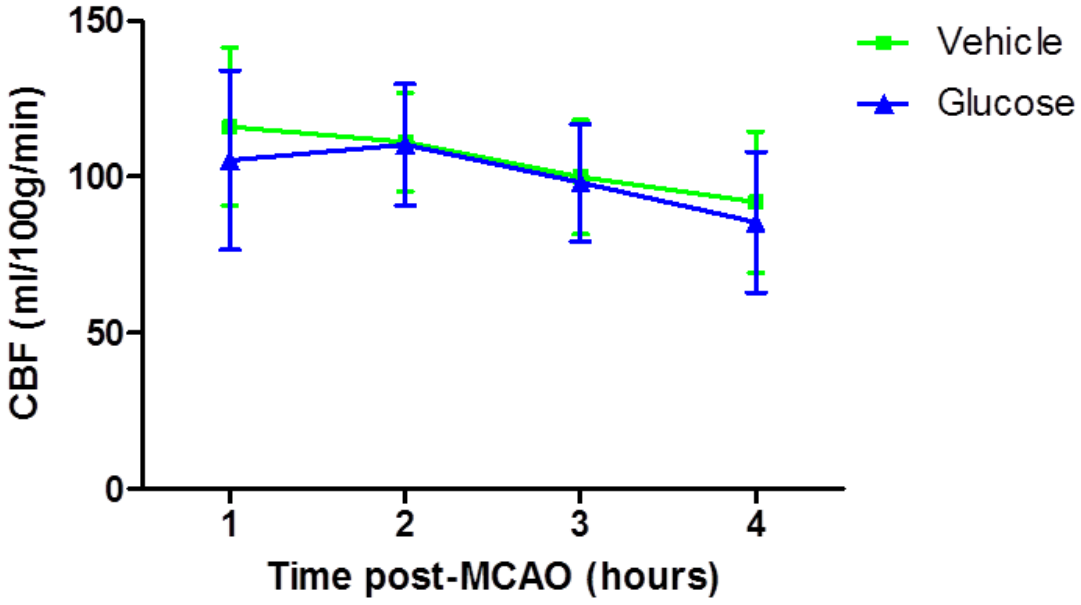

Figure 5.13. Mean CBF, measured by pCASL, in the contralateral hemisphere 1-4 hours after MCAO. Data are presented as mean ± standard deviation. Differences between groups are not statistically significant: RM 2-way-ANOVA with Bonferroni's post-test.

5.3.7 Perfusion-diffusion mismatch volume

The volume of tissue with perfusion-diffusion mismatch, an estimate of the ischaemic penumbra, was comparable between groups at each time point post-MCAO (Figure 5.14). The mean perfusion-diffusion mismatch volume at 1 hour post-MCAO was 103±31mm^3 and 117±36mm^3 in vehicle and glucose treated rats respectively. The volume of perfusion-diffusion mismatch tissue did not change significantly over time in either group as the mismatch volume at 4 hours post-MCAO was 108mm^3 and 130mm^3 in vehicle and glucose treated rats respectively.

The spatial distribution of the perfusion-diffusion mismatch tissue across 6 coronal slices at 1 and 4 hours after permanent MCAO is presented in Figure 5.15. In coronal slices 2 and 3 of the representative vehicle treated animal there was a perfusion deficit but no ADC lesion. In such instances the perfusion deficit was considered to be mismatch tissue.

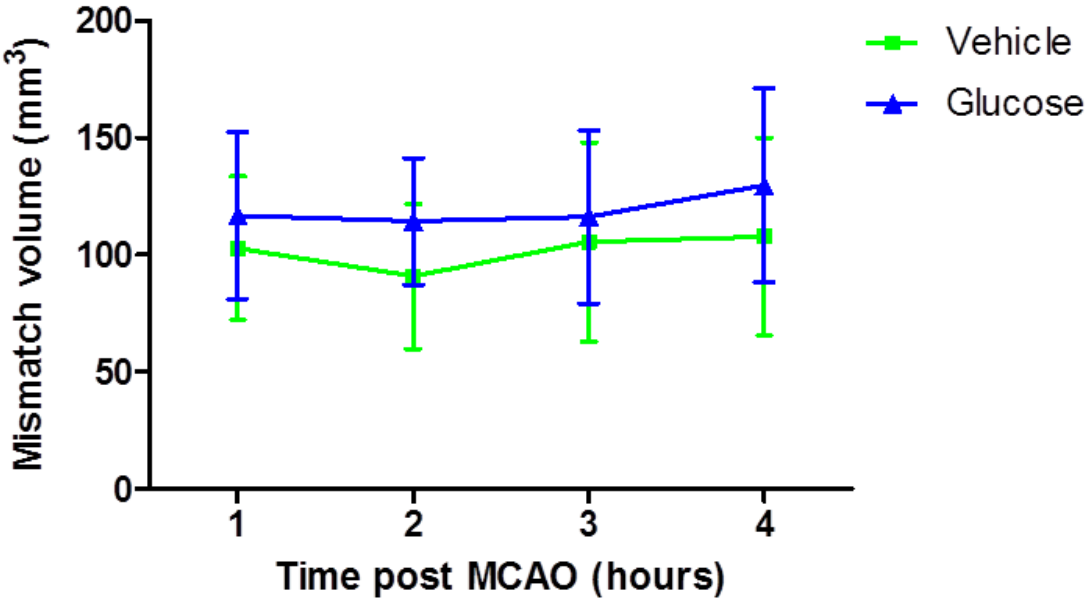

Figure 5.14. Penumbra defined using MRI perfusion-diffusion mismatch. Perfusion-diffusion mismatch volume in vehicle (n=10) and glucose (n=10) treated rats following MCAO. Mismatch volume was calculated by superimposing ADC-derived lesion volumes onto respective CBF maps and manually delineating the remaining perfusion deficit. Data are presented as mean ± standard deviation. Differences between groups are not statistically significant: RM 2-way-ANOVA with Bonferroni's post-test.

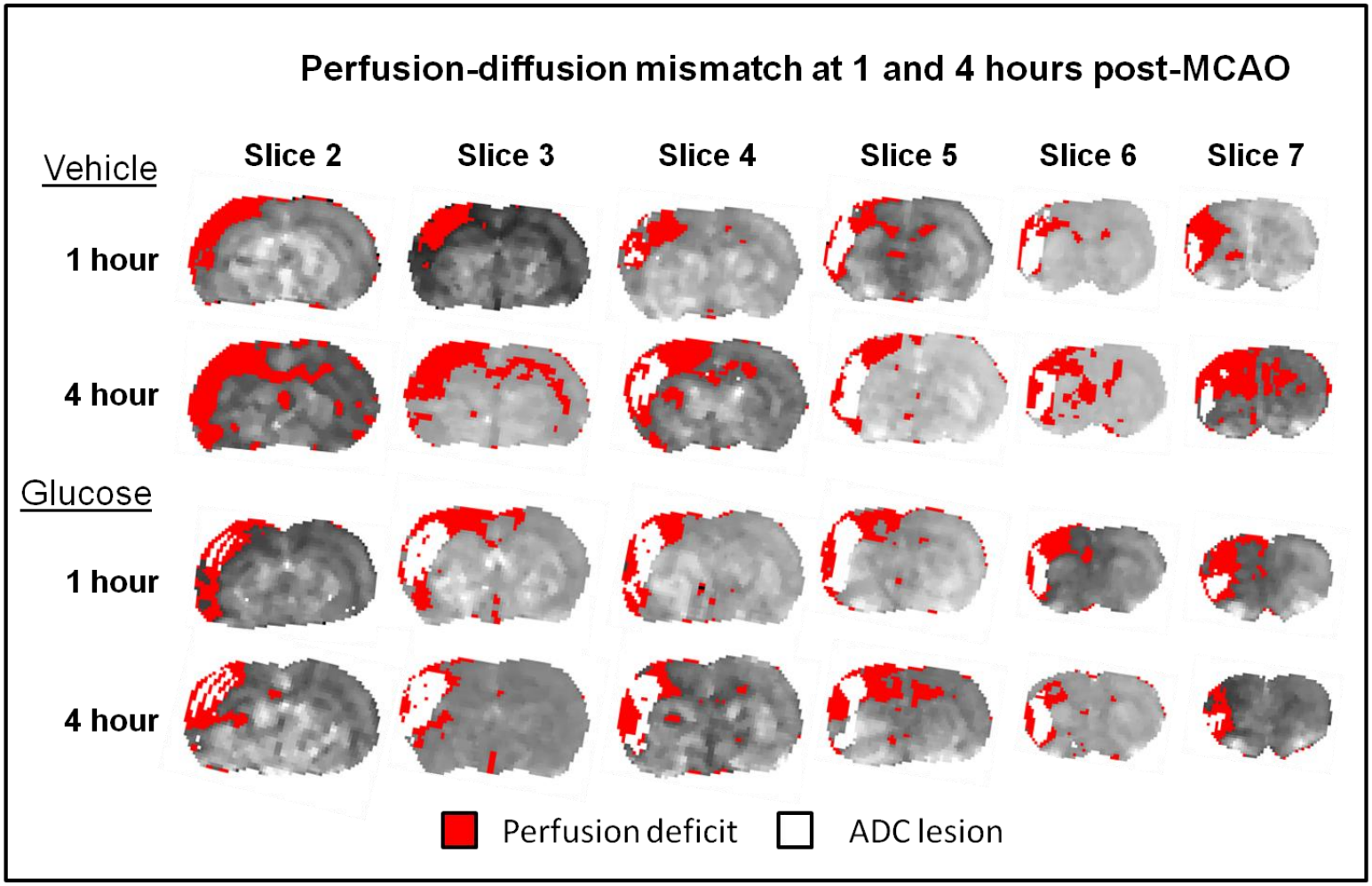

Figure 5.15. Spatial distributions of perfusion-diffusion mismatch tissue across 6 coronal slices (caudal to rostral) at 1 and 4 hours after MCAO. The data displayed are from the median animal of each group. The red region depicts the perfusion deficit defined by applying an absolute threshold of 30ml/100g/min. The white region depicts the ADC lesion defined by applying an ADC threshold of 0.53 x10^{-3} mm^2/sec. On slices where there was a perfusion deficit but no ADC lesion the perfusion deficit area was considered as mismatch tissue.

5.3.8 T_2-weighted infarct volume

T_2-derived infarct volume (corrected for oedema using equations in Chapter 2.7.5) measured 24 hours after permanent MCAO was significantly greater in glucose compared to vehicle treated rats (P=0.002, Figure 5.16A). The mean T_2-derived infarct volume was 57±22mm^3 and 90±19mm^3 in vehicle and glucose treated rats respectively. The correlation between T_2-derived infarct volume at 24 hours post-MCAO and blood glucose levels at 4 hours post-MCAO was also assessed (Figure 5.16C) and a significant correlation was found (R^2=0.37, P=0.004). To assess the extent of ipsilateral hemispheric swelling between groups at 24 hours post-MCAO the volume of the ipsilateral and contralateral hemispheres for each rat were measured from the T_2 map and hemispheric swelling was calculated using the following equation: ipsilateral hemispheric swelling = (volume of ipsilateral hemisphere – volume of contralateral hemisphere)/volume of contralateral hemisphere)(Wali et al., 2012). Hemispheric swelling tended to be greater in glucose treated rats but the difference between groups was not significant (P=0.07, Figure 5.16B).

5.3.9 Penumbra volume derived from ADC lesion expansion

In addition to the perfusion-diffusion mismatch model, the penumbra can also be assessed retrospectively by subtracting the ADC lesion volume measured at each hour from the T_2-derived infarct volume measured at 24 h post-MCAO. Using this method, the volume of the penumbra in the vehicle treatment group was 7±22mm^3 at 1 hour and decreased in size to 0±16mm^3 at 4 hours post-MCAO (Figure 5.17, P=0.03). In glucose treated rats, penumbra volume was 31±16mm3 at 1 hour, declining significantly over time to 9±21mm^3 at 4 hours post-MCAO (Figure 5.17, P=0.02). Penumbra volume was significantly higher in the glucose compared to vehicle treatment groups at 1 hour post-MCAO (7±22mm^3 vs 31±16mm^3, for vehicle and glucose treatment groups respectively (P<0.05, Figure 5.17), but was not significantly different between the groups at later time points.

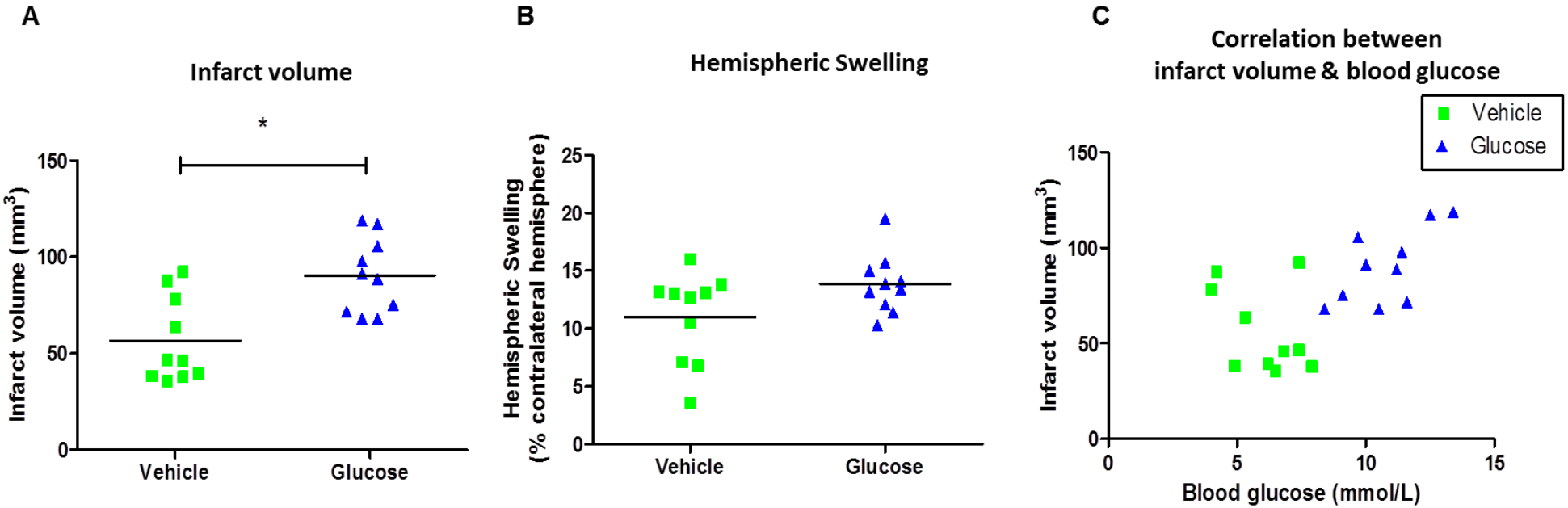

5.16. T_2 derived infarct volume, correlation between infarct volume and blood glucose and hemispheric swelling at 24 hours post-MCAO. Scatter plots showing T_2-derived infarct volume data measured 24 hours after MCAO in each rat (A) and ipsilateral hemispheric swelling (B). The line on each scatter plot represents the mean. *P<0.05 compared with vehicle group using a Student's unpaired t-test. C. The correlation between the T_2-derived infarct volume and blood glucose measured at 4 hours post-MCAO from all rats in the study. There was a significant correlation between T_2-derived infarct volume and blood glucose (R^2 = 0.37, P=0.004)

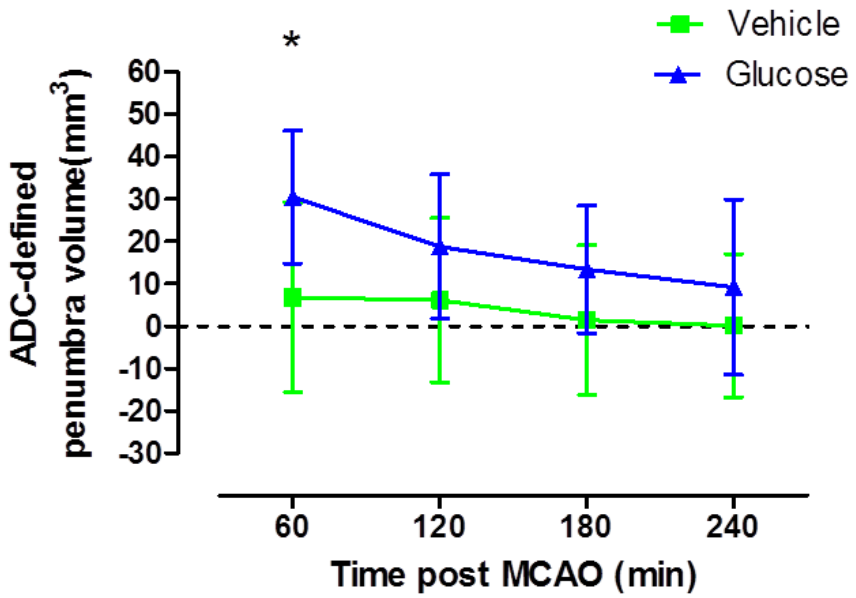

Figure 5.17. ADC-defined penumbra. The ADC-defined penumbra volume as determined by subtracting the ADC lesion volume at each hour post-MCAO from the oedema corrected T_2-derived infarct volume. Data are presented as mean ± standard deviation, n = 10 per group. *P<0.05, RM 2-way-ANOVA with Bonferroni's post-test.

5.4 Discussion

The data from the MRI study presented in the present Chapter demonstrates that clinically relevant hyperglycaemia significantly increases the acute evolution of ischaemic damage and infarct volume in a rodent model of ischaemic stroke. The increase in acute ischaemic damage did not correspond with an increase in the evolution of the acute perfusion deficit, suggesting that the detrimental effects of hyperglycaemia are not mediated by a corresponding reduction in CBF. One of the proposed mechanisms by which hyperglycaemia may be harmful during ischaemic stroke is by accelerating the conversion of the ischaemic penumbra to infarction. The MRI data in this study show that there was no difference in the volume of penumbra tissue, defined by the MRI perfusion-diffusion mismatch model, between hyperglycaemic and normoglycaemic rats. However retrospective analysis of the penumbra using the ADC lesion (ADC-defined penumbra) revealed that there was a considerable volume of ADC-defined penumbra tissue in hyperglycaemic rats at 1 hour after stroke compared to normoglycaemic animals. This suggests that in hyperglycaemic animals there may be a window of opportunity to intervene and alter the progression of the infarct.

5.4.1 Glucose treatment increased the threshold to define ADC-derived ischaemic damage

The strain of rat used in this study was Wistar and to my knowledge this is the first study to define MRI diffusion thresholds for this strain. The mean ADC threshold for all of the Wistar rats included in this study was 0.53 x 10^{-3} mm^2/sec, which was associated with a 30% reduction in ADC from control. This absolute threshold is identical to that established by Shen et al (2003) to define ADC derived ischaemic damage in Sprague-Dawley rats. Shen and colleagues also reported a 30% reduction in ADC from control and similarly, Foley et al (2010) reported a reduction in ADC values of 30% compared to control in Sprague-Dawley rats (Foley et al., 2010). Both Wistar and Sprague-Dawley rats are normotensive rat strains and as such the ADC threshold was predicted to be similar. In comparison to normotensive rat strains, absolute ADC viability thresholds established for hypertensive SHRSP rats and their control strain, WKY rats, were higher with values of 0.59 and 0.61 x 10^{-3} mm^2/sec respectively (23%

and 21% reduction in ADC from control) (Reid et al., 2012). The data from these studies suggests that thresholds to define ischaemic damage may be different between strains. The higher ADC thresholds in WKY and SHRSP strains may reflect the increased sensitivity to ischaemic injury reported in hypertensive compared to normotensive rat strains (Coyle and Jokelainen, 1983, Carswell et al., 1999).

Unlike any of the other studies that have established ADC viability thresholds in rodents, a confounding factor in the establishment of the ADC thresholds in the present study was that rats received either vehicle or glucose treatment. When ADC thresholds were compared between treatment groups it was found that the mean ADC threshold was higher in glucose compared to vehicle treated rats. It is not clear if there is any biological significance in this finding and since the difference between groups was only small (P=0.03) and there was considerable overlap in the data points between groups it seems unlikely that there will be. However the higher ADC threshold may indicate that hyperglycaemic rats are more sensitive to reductions in ADC values and this could help to explain, in part, the larger infarct volumes observed in hyperglycaemic compared to normoglycaemic rats.

5.4.2 Glucose treatment did not influence the pCASL-derived perfusion deficit

Glucose treatment had no significant effect on the volume of tissue with a perfusion deficit (CBF <30ml/100g/min) 1-4 hours after MCAO compared to vehicle treatment. This result is in agreement with the results from the previous Chapter which showed that glucose treatment had no effect on the reduction in CBF at 1 hour post-MCAO, determined by ^{99m}Tc-HMPAO autoradiography. However, in both of the treatment groups in the present study there was a substantial perfusion deficit, at all time points after MCAO, with volumes ranging from 130-192mm^3. The perfusion deficit data for each group is presented in Figure 5.18 alongside the ADC lesion volume data and the T_2-derived infarct volume. It is obvious from this graph that the perfusion deficit was far greater than the ADC lesion volume and this explains why there were such high volumes of perfusion-diffusion mismatch tissue in both groups.

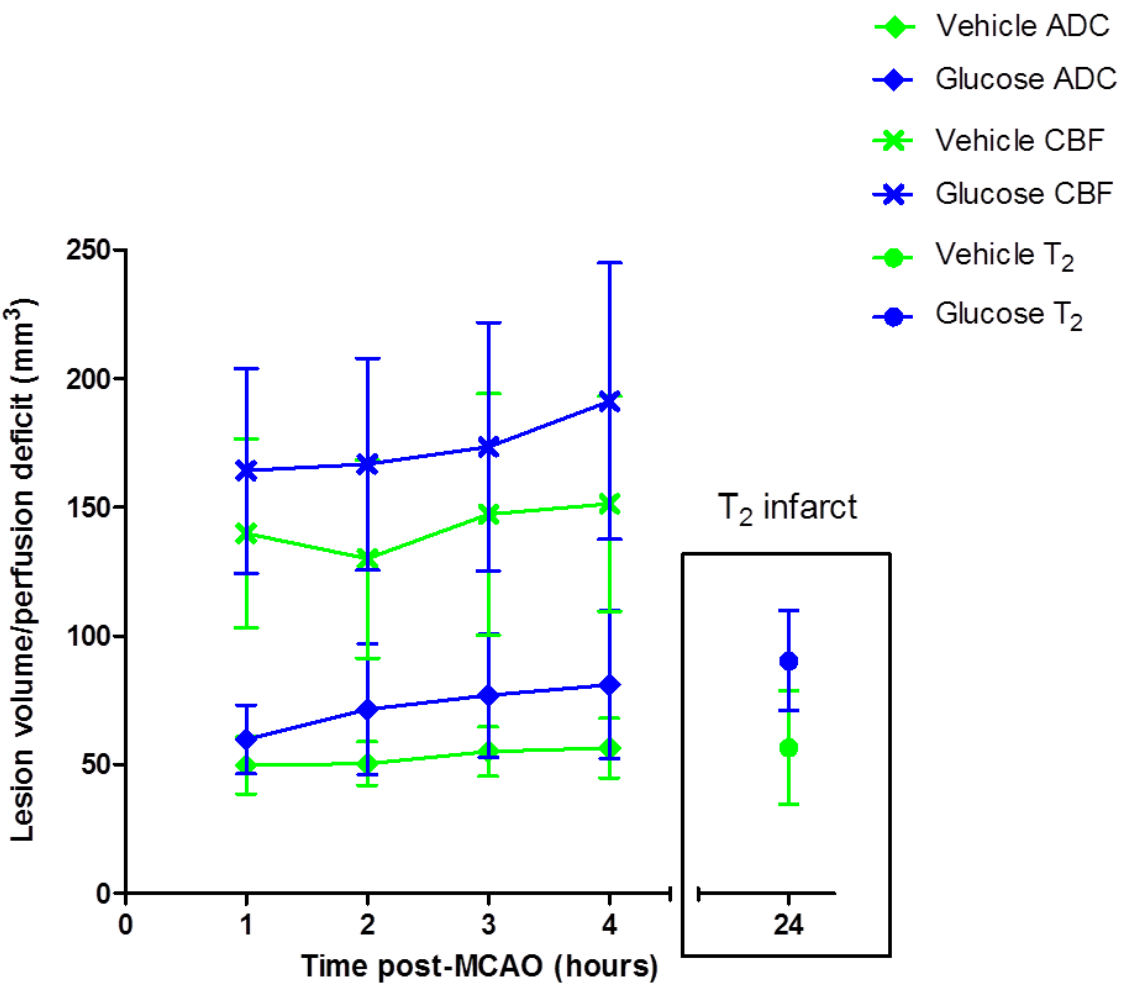

Figure 5.18. Graph summarising the ADC-derived lesion volume, pCASL-derived perfusion deficit and infarct volume data. For both groups: diamonds indicate ADC lesion volume, crosses indicate perfusion deficit (CBF) volume and circles indicate T_2-derived infarct volume measured at 24 hours post-MCAO. Data are presented as mean ± standard deviation.

Despite such a large perfusion deficit at the last measured time point (4 hours post-MCAO), infarct volumes measured 24 hours after MCAO were similar in size to the ADC-derived lesion volume at 4 hours, indicating that most of the tissue with a perfusion deficit at 4 hours was not incorporated into the infarct at 24 hours. A potential explanation for this may be due to the increase in blood pressure that occurs on withdrawal of anaesthesia. Withdrawal of isoflurane, which is known to have a cardio-depressant effect (Schappert et al., 1992) will inevitably lead to a rise in blood pressure as animals regain consciousness. This increase in blood pressure will cause an increase in CBF within the ischaemic hemisphere which reduces the volume of the perfusion deficit and prevents the progression of the hypoperfused at-risk tissue to infarction.

The large perfusion deficit observed in both treatment groups in the present study could be partly due to applying an inappropriate CBF threshold. Voxels within the ipsilateral hemisphere of CBF maps with CBF below 30ml/100g/min were considered to represent hypoperfused tissue. This is the absolute threshold established by Shen et al (2003) to define the perfusion deficit in Sprague Dawley rats and not the absolute threshold established in the present study (8ml/100g/min). The latter threshold did not match spatially with the perfusion deficit visualised on quantitative CBF maps and this was presumed to be due to the high number of voxels with negative CBF values on the quantitative CBF maps that arose during pCASL image processing. Although the applied CBF threshold of 30ml/100g/min matched spatially with the hypoperfused region on quantitative CBF maps, some of the tissue below this threshold could have recovered spontaneously (benign oligaemia) resulting in an overestimation of the perfusion deficit and subsequently perfusion-diffusion mismatch tissue. Nevertheless results from studies assessing CBF autoradiographically support the use of this threshold (Hoehn-Berlage et al, 1995). In their study, Hoehn-Berlage and colleagues measured ADC changes over the first 2 hours following permanent MCAO in Wistar rats. At 2 hours following the onset of MCAO regional CBF was measured by quantitative [^{14}C]-IAP autoradiography and ATP depletion and tissue pH were determined by bioluminescence and fluorescence techniques respectively. Hoehn-Berlage et al (1995) defined the ischaemic penumbra as a hypoperfused region within the ADC lesion with tissue acidosis but normal ATP levels and showed that this region

corresponded to a CBF threshold of 31±11 ml/100g/min (Hoehn-Berlage et al., 1995). This value is almost identical to the threshold of 30ml/100g/ml used in the present study to identify hypoperfused at-risk tissue.

Within both the treatment groups the volume of tissue with a perfusion deficit did not change significantly over time. This data is consistent with previously published data from acute MRI studies characterising the time course of the perfusion deficit after permanent MCAO in normotensive rat strains (Shen et al., 2003, Meng et al., 2004, Bratane et al., 2009). In contrast, the perfusion deficit has been shown to increase significantly over time in hypertensive rat strains (Reid et al., 2012) and this may be due to impaired collateral blood flow after stroke. The stable volume of tissue with a perfusion deficit in normotensive rat strains, such as the Wistar strain used in this thesis, could be explained by tight physiological monitoring of the animals under anaesthesia.

5.4.3 Hyperglycaemia did not influence the temporal profile of mismatch tissue

The mismatch between perfusion and diffusion-weighted MR images is presumed to approximate the ischaemic penumbra. In patients with evidence of perfusion diffusion mismatch tissue, hyperglycaemia was associated with reduced salvage of mismatch tissue from infarction which suggests that the ischaemic penumbra may be susceptible to hyperglycaemic ischaemia. It was therefore interesting to examine the amount of tissue with perfusion-diffusion mismatch at each time point after MCAO in the present study. The results showed that glucose treatment did not influence the volume of perfusion-diffusion mismatch tissue over the first four hours after MCAO. This may have important clinical implications because if the amount of penumbral tissue is similar between normo- and hyperglycaemic patients there may be a window of opportunity for therapeutic intervention to prevent the harmful effects of hyperglycaemia during ischaemia. The ADC lesion volume data predicts the optimal time window for intervention to be within the acute 0-2 hours after stroke onset and future clinical trials of glucose lowering therapies may only see a benefit by targeting treatment to this early time-window.

The volume of perfusion-diffusion mismatch tissue in both groups was approximately 100mm^3 at 1 hour post-MCAO and the absolute volume did not change over time. The volume of mismatch tissue observed was comparable to values reported in published studies in which permanent MCAO was induced by the intraluminal filament model (Shen et al., 2003, Bardutzky et al., 2005, Meng et al., 2004, Bratane et al., 2009). However previous studies reported a decrease in the amount of perfusion-diffusion mismatch tissue over time which correlated with an increase in the acute ADC lesion. Such findings were not observed in the present study. For example in the glucose treatment group the volume of the ADC lesion increased from 1 to 4 hours post-MCAO but the volume of mismatch tissue remained constant over this time. This could be due to a number of factors. Firstly, the thresholds used to define perfusion-diffusion mismatch by Shen et al (2003) were established by applying increasing ADC and CBF thresholds to respective ADC and CBF maps acquired 3 hours post-MCAO until lesion volumes matched the TTC derived infarct volume at 24 hours post-MCAO. By doing this the authors have essentially forced both the CBF and ADC lesions at 3 hours to equal the TTC infarct and therefore it is no surprise that perfusion-diffusion mismatch decreases over time. The authors state that the acute 3 hour time point was selected as the ADC lesion volume has been shown to stop evolving after this time although they did not go on to show this. Therefore Shen et al (2003) may have introduced inaccuracies in their results as they assume that both the ADC lesion and the CBF deficit do not evolve beyond 3 hours. The same is true of the present study as it was assumed that the ADC lesion does not continue to evolve after 4 hours, yet this was not proven. Images were not acquired beyond this time as this would have increased the length of time that the animals were under anaesthesia which could have compromised animal recovery.

Secondly, differences between the evolution and extent of ischaemic brain damage induced by different methods of MCAO might explain the temporal differences in perfusion-diffusion mismatch observed in different studies. To my knowledge there are no previously published studies that have investigated the evolution of the acute perfusion deficit in a rodent stroke model other than the intraluminal filament model of MCAO. Insertion of the intraluminal filament to occlude the origin of the MCA produces a severe reduction in CBF that results in

widespread ischaemic damage, incorporating both cortical and subcortical brain structures. With such extensive ischaemic damage it is inevitable that the collateral blood supply will be unable to maintain perfusion of the hypoperfused at-risk tissue which will rapidly progress to infarction over time. Conversely, occluding the distal portion of the MCA by diathermy, the method used in this thesis, largely restricts ischaemic damage to the ipsilateral cortex and therefore the ischaemic damage induced is not as extensive compared to that induced by the intraluminal filament method. Collateral supply from pial blood vessels could help to maintain perfusion of the hypoperfused at-risk tissue surrounding ischaemic lesions induced by the distal diathermy method of MCAO, resulting in the stable volume of perfusion-diffusion mismatch tissue observed in the present study. It is important to mention here that although the volume of mismatch tissue measured at each hour after the onset of MCAO doesn't significantly change between 1 and 4 hours in each group, the tissue within the penumbra will inevitably change over time. Some of the tissue with perfusion-diffusion mismatch will become incorporated into the infarct and this is supported by the fact that the ADC lesion increased over time in both vehicle and glucose treatment groups. Also, as collateral blood supply decreases over time (supported by the decrease in CBF observed in the contralateral hemisphere Figure 5.12), some of the benign oligaemic tissue will become incorporated into the ischaemic penumbra. Therefore although the volume doesn't changed over time the tissue contributing to the perfusion-diffusion mismatch would have.

5.4.4 Hyperglycaemia increased the ADC-defined penumbra volume at 1 hour post-MCAO

In addition to the perfusion-diffusion mismatch model, tissue at risk of infarction may also be determined retrospectively from the growth of the acute ADC lesion into the final infarct. Using this method, it was established that there was only a small volume of penumbra tissue (~7mm^3) in vehicle treated animals at 1 hour post-MCAO, but a considerable volume of penumbra tissue (~30mm^3) in glucose treated animals at this same time. In the vehicle treatment group, there was little expansion of the ADC lesion volume over time, indicating that the amount of ischaemic damage was almost maximal at 1 hour post-stroke (Figure 5.17). In contrast, there was greater expansion of the ADC lesion volume in the glucose treatment group, which corresponded with a decrease in the ADC-defined

penumbra volume over time. This data suggests that in the hyperglycaemic group there was more tissue at risk of infarction and thus there may be a window of opportunity for early therapeutic intervention to recover this tissue. However, without intervention, hyperglycaemia could continue to exacerbate ischaemic damage resulting in the evolution of brain injury and larger final infarcts. Although this method of defining the penumbra is not applicable for the acute assessment of the penumbra in stroke patients it has many useful research applications, for example in determining if there are differences in the optimal time window for therapeutic intervention.

5.4.5 MRI perfusion deficit data confirms previous findings

Previous studies in this thesis demonstrated that glucose treatment had no effect on the reduction in CBF at 1 hour post-MCAO measured by ^{99m}Tc-HMPAO blood flow autoradiography, suggesting that hyperglycaemia does not exacerbate ischaemic damage by altering CBF. Assessment of ischaemic damage was not feasible in the study reported in Chapter 4 due to the nature of the autoradiographic procedure. Interestingly the MRI data in this chapter revealed no difference in ADC lesion volume between vehicle and glucose treatment groups at 1 hour after MCAO. However, glucose treatment significantly increased ADC-derived lesion volume from 2-4 hours after MCAO compared to vehicle treated rats. The increase in ADC lesion volume at these time points was not associated with a larger perfusion deficit as there was no difference in the pCASL defined perfusion deficit at 2-4 hours between groups. This supports the findings from the autoradiographic study in Chapter 4 and suggests that the adverse effects of hyperglycaemia during focal cerebral ischaemia are not caused by exacerbating the reduction in CBF. These results also support those reported previously in both clinical (Luitse et al., 2013) and animal studies (Gisselsson et al., 1999) where poor functional outcomes in patients and larger infarct sizes in hyperglycaemic animals could not be explained by larger perfusion deficits. Together this data suggests that the detrimental effects of hyperglycaemia are not predominantly mediated in the cerebrovasculature. Alternatively, they may take place within the brain tissue. To determine whether the adverse effects of hyperglycaemia on infarct size are associated with greater tissue injury the brain tissue collected in this study was processed for protein analysis by Western blotting and is presented in Chapter 6.

The vascular effects of hyperglycaemia during ischaemic stroke however, cannot be entirely excluded. Firstly, hyperglycaemia is associated with an increased risk of haemorrhagic transformation (HT) in ischaemic stroke patients (Paciaroni et al., 2009). HT can occur as a natural consequence of ischaemic stroke and is especially common after thrombolytic therapy due to bleeding from ischaemically injured blood vessels. Indeed, numerous studies have reported that there was a greater risk for HT in hyperglycaemic ischaemic stroke patients receiving rt-PA (Hill and Buchan, 2005, Demchuk et al., 1999, Bruno et al., 2002, Poppe et al., 2009, Putaala et al., 2011). The association between hyperglycaemia and an increased HT is supported by experimental data. Won et al (2011) demonstrated a relationship between hyperglycaemia and the increased risk of haemorrhage in an animal model of rt-PA stroke treatment. The authors reported that the increased risk of haemorrhage after 90 minutes of focal ischaemia in hyperglycaemic rats was associated with an increase in superoxide production by NADPH oxidase (Won et al., 2011). Increased superoxide production and its interaction with nitric oxide, producing reactive nitrogen species such as peroxynitrite, is thought to play an important role in vascular disease pathophysiology (Guzik et al., 2000).

Secondly, hyperglycaemia could act on the cerebral microvasculature to alter CBF following ischaemic stroke. Pericytes are contractile cells found in almost all capillaries as well as arterioles and veins. They are small cells found on the outside of the capillary between the endothelial cell layer and the brain parenchyma and have an important range of functions in angiogenesis, endothelial cell regulation and maintenance of the blood brain barrier (Lai and Kuo, 2005, Hirschi and D'Amore, 1996). Pericytes may also have an important role in capillary blood flow regulation. In a recent study Hall et al (2014) demonstrated that during neuronal activity, in response to excitatory neurotransmitters, pericytes relax their grip on capillaries causing them to vasodilate and increase blood supply to active neurons. This pericyte-mediated dilation of capillaries has been shown to occur before arterioles and is estimated to produce 84% of the resulting blood flow increase (Hall et al., 2014). Thus pericytes seem to be major regulators of cerebral blood flow under normal physiological conditions. Evidence from in vitro studies suggests that pericytes have a profound effect on CBF under ischaemic conditions. Hall et al (2014) also

carried out live imaging of cerebral cortical slices in response to simulated ischaemia (oxygen-glucose deprivation, OGD) and found that 15 minutes of OGD caused constriction of capillaries in regions near to pericytes. OGD resulted in the rapid death of these capillaries and it was reported that approximately 90% of pericytes died within 1 hour. This effect was shown to be halved by blocking AMPA/kainate or NMDA receptors and suggests that ischaemia-induced excitotoxicity may contribute to pericyte cell death. Death of pericytes during ischaemia is thought to irreversibly constrict capillaries, which in turn leads to a decrease in cerebral blood flow and promotes brain damage (Hall et al., 2014). Constriction of capillaries by pericytes has also been shown to occur *in vivo* following transient MCAO (Yemisci et al., 2009) and after the onset of simulated retinal ischaemia (Peppiatt et al., 2006). In the former study, Yemisci et al (2009) reported that suppression of oxidative/nitrative stress relieved pericyte contraction and restored microvascular patency after transient cerebral ischaemia followed by reperfusion. This suggests that reactive oxygen and nitrogen species formation may also contribute to pericyte constriction of capillaries during ischaemia.

There is evidence to suggest that high glucose concentrations lead to pericyte cell death. *In vitro* studies revealed that high glucose concentrations (~40mM) increased the rate of respiration and ROS production in mouse cerebral pericytes which led to pericyte cell death by apoptosis (Shah et al., 2013). Hyperglycaemia was also found to increase pericyte death in retinal pericytes through a protein kinase C-δ dependent signalling pathway (Geraldes et al., 2009). These findings implicate pericytes as potential mediators for the injurious effects of chronic hyperglycaemia on the microvasculature in diabetic retinopathy. Such high glucose levels are scarcely seen in ischaemic stroke patients with PSH and therefore the effects, if any, of clinically relevant hyperglycaemia during ischaemia on capillary constriction and pericyte death remains to be elucidated. Future studies investigating the effects of acute hyperglycaemia on the microvasculature could reveal important information on the pathophysiological mechanisms underlying the detrimental effects of hyperglycaemia in ischaemic stroke.

5.4.6 Summary

The data from the MRI study presented in this chapter demonstrates that hyperglycaemia at the time of MCAO exacerbates early ischaemic damage and infarct volume at 24 hours. In addition, retrospective assessment of the penumbra revealed that there was evidence of a considerable volume of ADC-define penumbra tissue in hyperglycaemic rats at 1 hour after stroke compared to normoglycaemic animals, implicating that in hyperglycaemic animals there may be a window of opportunity to intervene and limit further damage. The data from this study also demonstrates that the damaging effects of hyperglycaemia did not correspond with an exacerbation of the acute perfusion deficit following permanent MCAO and this suggests that the adverse effects of hyperglycaemia in ischaemic stroke are not due to an increase in the severity of the ischaemic insult. The alternative is that detrimental mechanisms operate in the brain parenchyma. In the next Chapter the brain tissue samples collected from the experiment reported above, and from 2 hours after MCAO, were used to determine if specific proteins associated with ischaemic damage are altered in hyperglycaemic versus normoglycaemic brain tissue.

Chapter 6 – The effects of glucose treatment on calpain-mediated proteolysis of αII-spectrin and MAP2 after permanent MCAO

6.

6.1 Introduction

Although hyperglycaemia is associated with poor functional outcomes and increased mortality in ischaemic stroke patients (Kiers et al., 1992a, Berger and Hakim, 1986, Melamed, 1976), the mechanism(s) of hyperglycaemia-induced harm are poorly understood. In the previous Chapter it was demonstrated that hyperglycaemia exacerbates acute ischaemic damage over the initial few hours and leads to larger infarcts in a rodent model of permanent MCAO. These results are in agreement with previous animal studies (Tarr et al., 2013, Huang et al., 1996a), and suggest that the detrimental effects of hyperglycaemia occur early following the onset of ischaemic stroke. In Chapter 5, using perfusion MRI, it was shown that exacerbation of ischaemic damage by elevated blood glucose levels was not associated with more severe initial reductions in cerebral blood flow. From this it was hypothesised that the detrimental effects of hyperglycaemia predominantly take place within the brain tissue rather than at the level of the cerebral vasculature. To test this hypothesis, brain tissue was collected from vehicle and glucose treated rats following 2 hours and 24 hours of permanent distal MCAO and processed for Western blot analysis of proteins that are known to be markers of ischaemic tissue damage.

6.1.1 Calpain-mediated brain injury

Increased extracellular glutamate levels during ischaemia leads to the activation of calcium permeable NMDA receptors, resulting in a massive influx of calcium into the cell. One of the damaging effects of this calcium overload is the excessive activation of calpain, a cysteine protease which has a wide range of important physiological functions including long-term potentiation, neurite outgrowth and synaptic remodelling (Sorimachi et al., 1997, Denny et al., 1990). The excessive activation of calpain during ischaemia leads to the unregulated proteolysis of calpain substrates and calpain-mediated neuronal death (Neumar et al., 2001). Further to this, studies have shown that calpain inhibitors are neuroprotective during focal cerebral ischaemia, indicating that calpains are important mediators of ischaemic brain damage (Hong et al., 1994a, Hong et al., 1994b, Li et al., 1998). Evidence from *in vitro* studies suggests that calpain

activation may be an important intracellular mediator of glutamate excitoxicity. For example, Siman et al (1989) demonstrated that neuronal damage induced by intensive glutamate receptor stimulation, results in calpain activation, manifested as increased levels of the break down products of one of calpains substrates, spectrin (Siman et al., 1989). This is supported by *in vivo* studies which show that blocking NMDA receptors reduces the proteolytic activity of calpain during transient forebrain ischaemia (Seubert et al., 1988). In addition to the cytoskeletal protein spectrin, calpain has a number of other substrates including microtubule-associated proteins (MAPs), kinases, phosphatases and membrane receptors and transporters. Of these, microtubule associated protein 2 (MAP2) has been widely studied in animal models of stroke. MAP2 protein levels and immunoreactivity have been reported to decrease over-time after MCAO and therefore MAP2 degradation is regarded as a reliable marker of ischaemic brain injury (Pettigrew et al., 1996, Dawson and Hallenbeck, 1996, Popp et al., 2009).

6.1.2 Does hyperglycaemia exacerbate the proteolytic activity of calpain?

The possibility that hyperglycaemia exaggerates ischaemic injury by increasing excitotoxic brain damage has been studied in rodent stroke models using microdialysis (Li et al., 2000c, Choi et al., 2010, Wei and Quast, 1998). Li et al, (2000) used microdialysis coupled with high-performance liquid chromatography techniques to measure extracellular glutamate and other excitatory amino acid concentrations in normo- and hyperglycaemic rats subjected to 15 minutes of transient forebrain ischaemia. They found that pre-ischaemic hyperglycaemia (target blood glucose level: 20mmol/L) enhanced extracellular glutamate release in the cerebral cortex which correlated with exaggerated neuronal damage in this region. Hyperglycaemia (~26mM) also increased extracellular glutamate levels in brain dialysate samples collected during ischaemia in a transient MCAO stroke model (Wei and Quast, 1998). The increased glutamate levels during ischaemia in hyperglycaemic rats correlated with increased brain injury, determined by diffusion weighted imaging. Based on the results from these microdialysis studies, it was postulated that the increase in early ischaemic damage and infarct sizes observed in hyperglycaemic rats following permanent MCAO in the previous Chapter may be caused by an enhancement of

glutamate-mediated excitotoxicity. Since calpain activation has been shown to occur during excitotoxic brain damage it was hypothesised that hyperglycaemia, at the time of focal cerebral ischaemia, would significantly increase extracellular glutamate levels, and consequently the proteolytic activity of calpain, compared to a normoglycaemic model.

6.1.3 Study aims

In the previous study brain tissue from the ipsilateral cortex was collected from vehicle and glucose treated rats 24 hours after permanent MCAO. Infarct volume, determined by T_2-weighted MRI, was found to be significantly greater in glucose compared to vehicle treated rats. The aim of the present study was to determine if the larger infarct sizes at 24 hours post-MCAO in the glucose treatment group was associated with an increase in the proteolytic activity of calpain, manifested as an increase in levels of spectrin breakdown products (SBDPs) and a greater extent of MAP2 degradation.

From the previous MRI study in Chapter 5 the earliest time point at which glucose treatment was found to have a harmful effect was 2 hours after MCAO. In order to gain a better understanding of the mechanisms of hyperglycaemia-induced harm at this earlier time point, separate groups of vehicle and glucose treated rats were generated in which the MCA was occluded permanently for 2 hours. As with the 24 hour MCAO tissue, the levels of αII-spectrin and MAP2 protein were assessed in the 2 hour MCAO tissue to determine if hyperglycaemia exacerbates the proteolytic activity of calpain at this earlier time point.

6.2 Methods

6.2.1 Brain tissue samples

6.2.1.1 Preparation of 2 hour permanent MCAO samples

Adult male Wistar rats (310-420grams) were fasted overnight prior to stroke surgery. Anaesthesia was induced in an induction chamber with 5% isoflurane in nitrous-oxide: oxygen (70:30). A tracheotomy was performed for artificial ventilation and the right femoral artery was cannulated for blood gas and glucose measurements as described in Chapter 2.2. Permanent focal cerebral ischaemia was induced by occluding the left MCA using the distal diathermy MCAO method as described in detail in Chapter 2.3. Rats were randomly assigned to vehicle (n=7) or glucose (n=7) treatment groups using an online randomization plan generator and treatments were administered 10 minutes before MCAO as described in Chapter 2.4. Blood glucose levels were measured 20 minutes before MCAO to obtain a baseline glucose reading, at the onset of MCAO and at subsequent time points after MCAO. Body weight was measured prior to surgery and arterial blood gases were measured before MCAO, at the onset of MCAO and at 2 hours post-MCAO.

After 2 hours of ischaemia the rat was killed by an overdose of anaesthetic and the brain was rapidly removed and placed onto a chilled glass plate. The olfactory bulbs, cerebellum and brainstem were removed and the remaining cerebrum was dissected into 4 sub-sections: ipsilateral cortex, contralateral cortex, ipsilateral subcortex and contralateral subcortex. All samples were placed into sterile Eppendorf tubes, snap-frozen in liquid nitrogen and stored at -80°C.

The brain tissue from animals used in the previous chapter was collected in an identical manner at 24 hours post-MCAO and processed alongside the 2 hour MCAO tissue. Brain tissue collected from a naive rat (adult, male, Wistar) was used as a control.

6.2.1.2 Preparation of cytosolic and membrane fractions

Brain tissue lysates were prepared from the ipsilateral cortex tissue samples collected from each rat as described in Chapter 2.8.2. The whole of the ipsilateral cerebral cortex was homogenised as the previous MRI study in Chapter 5 showed that the ischaemic lesion was present on coronal brain slices throughout the MCA territory.

The centrifugation protocol used separated the tissue lysates into crude membrane and cytosolic fractions. The proteins of interest; αII-spectrin and MAP2 are cell membrane skeletal proteins and thus are expected to be found within the membrane fraction. However, it was decided to analyse both the membrane and cytosolic fractions as MCAO is known to cause cell membrane disruption and therefore proteins typically found in membrane fractions could be released into the cytosol.

6.2.2 Protein analysis

6.2.2.1 Protein concentration and protein loading determination

The protein concentration of the cytosolic and membrane fractions for each rat was determined using a BCA assay as described in Chapter 2.8.3. To determine the optimum amount of protein to load for Western blotting experiments a standard curve of protein load versus band optical density (OD) was produced for each antibody (Figure 6.1). The standard curves were prepared using different amounts of protein from both the membrane and cytosolic fractions of three vehicle treated rats (24 hour MCAO tissue). Protein bands were most consistent and were not oversaturated when loading 10μg of protein, in each of the standard curves. In addition, 10μg protein generated sharp, well defined protein bands when assessed by Coomassie blue staining, indicating that the gels were not overloaded. Therefore 10μg of protein was loaded in all other Western blots in this Chapter.

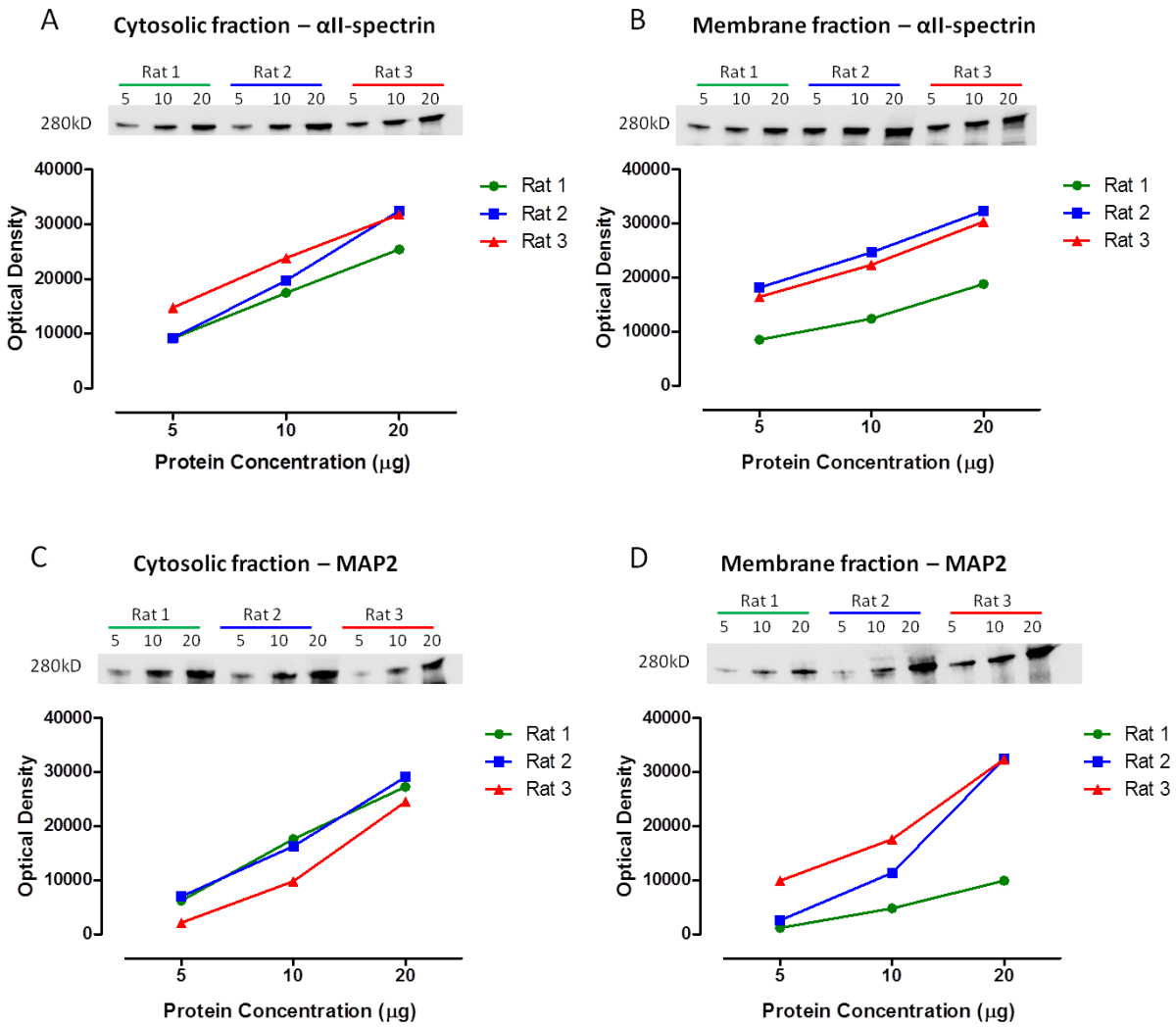

Figure 6.1. Standard curves of protein load versus protein band OD in three vehicle treated rats. Standard curves A (cytosolic fraction) and B (membrane fraction) were produced from Western blots probed with an antibody against αII-spectrin and curves C (cytosolic fraction) and D (membrane fraction) from blots probed with an antibody against MAP2. A consistent, non-saturated signal was produced in each of the curves when 10µg of protein was loaded therefore 10µg of each sample was loaded on to gels for all Western blots.

6.2.2.2 SDS-PAGE

For SDS-PAGE, samples were prepared as described in Chapter 2.8.4 and loaded into pre-cast gels. This study was conducted blind and the vehicle and glucose groups were allocated a code A and B. Samples were loaded onto the gel by alternating between groups. Each gel included a molecular weight reference sample and a naive rat brain to serve as a positive Western blot control for each gel. Data from this sample was not used for analysis.

6.2.2.3 Coomassie blue staining

The Coomassie blue stain (SimplyBlueTM SafeStain, Invitrogen, UK) was used to assess the protein loading between samples, and the profile of each sample used to identify any sample degradation (see Chapter 2.8.5 for details of gel staining). Protein loading between groups was comparable at 2 hours (Figure 6.2: left) but more variable at 24 hours (Figure 6.2: right). At 2 hours, there did not appear to be any evidence of gross protein degradation, which would be indicated by the accumulation of low molecular weight proteins. There were some changes at 24 hours although a consistent pattern was observed when these gels were repeated using fresh aliquots.

6.2.2.4 Western blots

Western blots were performed with primary antibodies against mouse anti-spectrin (MAB1622, Millipore) and rabbit anti-MAP2 (ab32454, Abcam), both at a dilution of 1/200,000, as described in Chapter 2.8.6. Following enhanced chemiluminescence signal detection the OD of the protein bands on each Western blot were measured using ImageJ (Chapter 2.8.7). An example of the calpain proteolysis of spectrin into 150kD and 155kD fragments is illustrated in Figure 6.3. The fragment at 150kD is reported to be specific to cleavage by calpain but the fragment at 155kD can be produced by either calpain or caspase-3 cleavage (Nath et al., 1996).

All Western blots were re-probed with a ß-acting loading control antibody to ensure that the lanes on each gel were loaded evenly with sample.

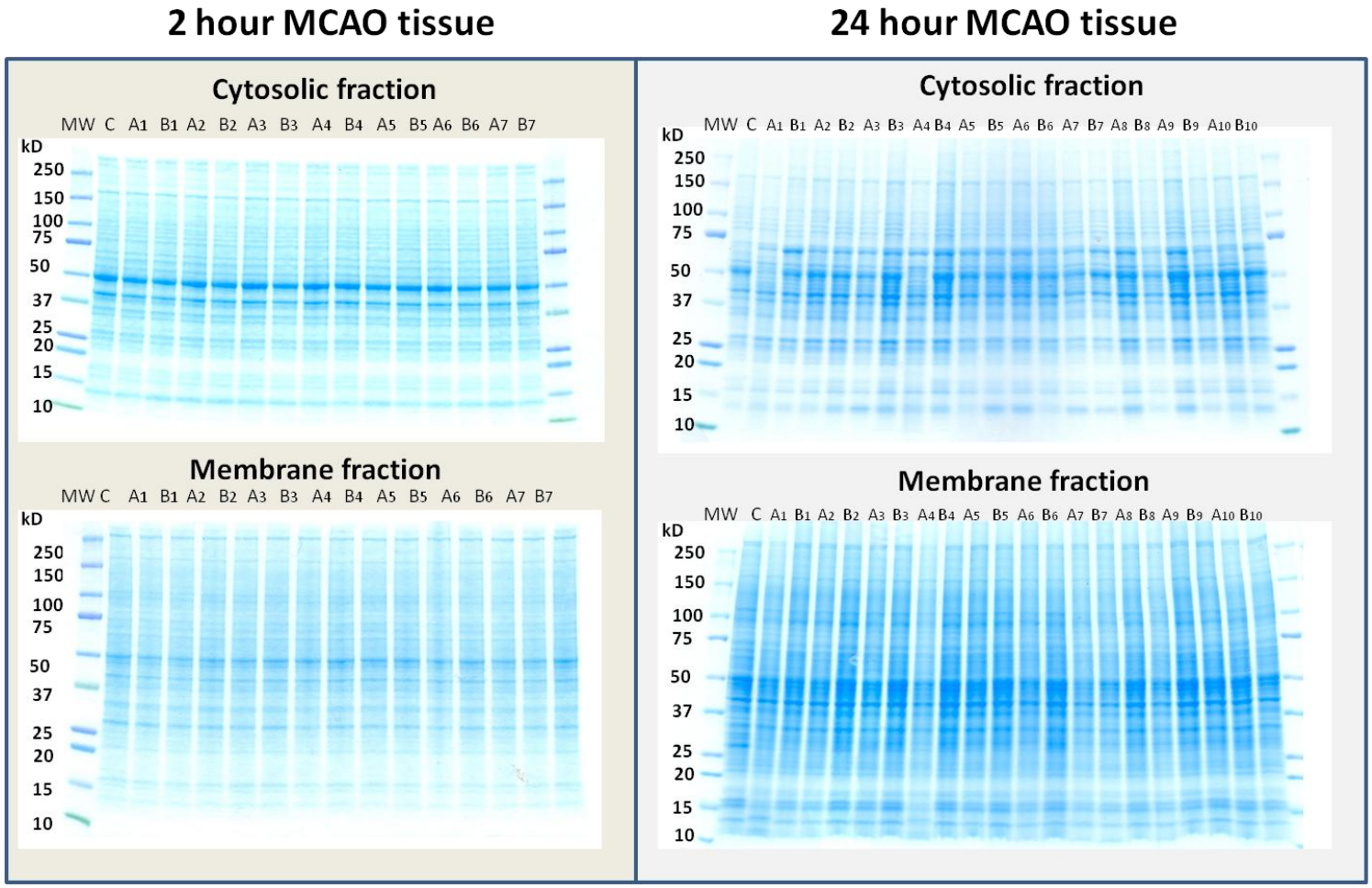

Figure 6.2. Coomassie blue stained gels of proteins from the cytosolic and membrane fractions of brain tissue from the ipsilateral cortex collected 2 hours and 24 hours after MCAO. In each gel 10ug of each sample was loaded per well. MW = molecular weight marker, C = control sample, A and B are the codes given to the different groups for blinding purposes.

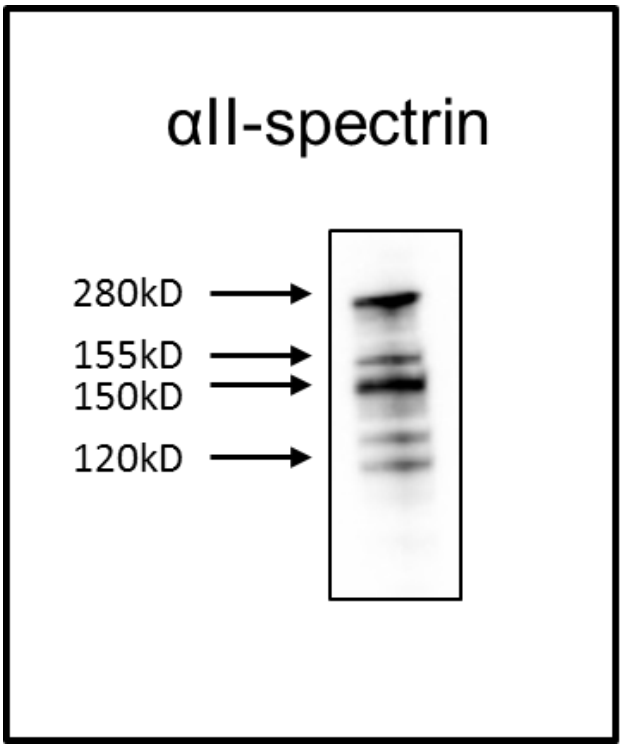

Figure 6.3. Western blot illustrating calpain-mediated proteolysis of αII-spectrin in ischaemic brain tissue collected 24 hours after permanent MCAO. Calpain cleaves αII-spectrin (280kD) producing two spectrin breakdown products at 150kD and 155kD. The breakdown product at 150kD is exclusively the result of calpain action and the fragment at 155kD can result from either calpain or caspase-3 cleavage. In this example bands can also be observed at approximately 120-125kD. These may result from caspase-3 mediated proteolysis of αII-spectrin which has been shown to produce a fragment at 120kD.

Blots were re-probed with the loading control antibody at least 24 hours after the ECL detection step of the Western blot protocol to allow sufficient time for the ECL signal to decrease. For the re-probing step, blots were washed 3 times, for 5 minutes each, in 1xT-TBS followed by a 30 minute incubation in blocking solution (5% milk powder in 1x T-TBS) at room temperature. Blots were then incubated overnight at 4°C in a mouse anti-beta actin primary antibody (ab8224, Abcam) diluted 1/400,000 in blocking solution. The following day blots were washed 3 times, for 10 minutes each in 1xT-TBS and then incubated for 1 hour at room temperature in a HRP conjugated anti-mouse secondary antibody (Dako, UK) diluted 1/10,000 in blocking solution. Blots were then washed 3 times, for 10 minutes each, in 1x T-TBS followed by ECL signal detection and quantification as described in Chapter 2.8.7. Relative protein levels of αII-spectrin and MAP2 were calculated by dividing the OD values of the αII-spectrin and MAP2 bands by the OD values of the ß-actin band.

The Western blots for MAP2 were performed by BMedSci student Michael Burns (2 hour MCAO tissue) and MRes student Evelina Avizaite (24 hour MCAO tissue) under my supervision.

6.2.3 Statistical Analysis

Blood glucose level data in the 2 hour MCAO rats were analysed using a 2-way ANOVA with Bonferroni's multiple comparisons post-hoc test. Physiological variables, scatterplots of relative αII-spectrin and MAP2 protein level data and scatterplots of ß-actin band OD data were analysed using an unpaired Student's t-test.

6.3 Results

6.3.1 Blood glucose & physiological data for rats exposed to 2 hour MCAO

Blood glucose levels measured 20 minutes pre-MCAO (baseline) were comparable between vehicle and glucose treated rats, with mean values of 8.2±1.4mmol/L and 7.8±1.4mmol/L, respectively (Figure 6.4). Following a single IP injection of a vehicle (distilled water) or 15% glucose solution, 10 minutes before MCAO, blood glucose levels at the onset of MCAO and at subsequent time points after MCAO remained close to baseline blood glucose levels in vehicle treated rats. In rats that received glucose treatment blood glucose levels increased, with mean blood glucose levels of 18.5±3.1mmol/L at the onset of MCAO and 14.4±2.1mmol/L at 2 hours post-MCAO.

Physiological variables of the 2 hour MCAO rats are presented in Table 6.1. Body weight was measured on the day of MCAO surgery before the induction of anaesthesia. All other physiological variables were monitored throughout the surgical period. The mean values measured at 2 hours post-MCAO for each group are presented in Table 6.1. The differences between groups were not statistically significant for any physiological variable measured.

Group	Weight (g)	MABP (mmHg)	$PaCO_2$ (mmHg)	PaO_2 (mmHg)	pH	Temperature (°C)
Vehicle (n=7)	370 ± 30	92 ± 7	46 ± 5	107 ± 12	7.349 ± 0.04	37 ± 0.2
Glucose (n=7)	367 ± 36	87 ± 7	42 ± 9	126 ± 25	7.395 ± 0.05	37 ± 0.3

Table 6.1. Table of physiological variables for 2 hour MCAO animals. Body weight was measured prior to MCAO. The MABP, temperature, pH, PaO_2 and $PaCO_2$ data presented are the mean ± standard deviation values measured at 2 hours post-MCAO. There were no significant differences in any of the variables between the two groups (unpaired Student's t-test).

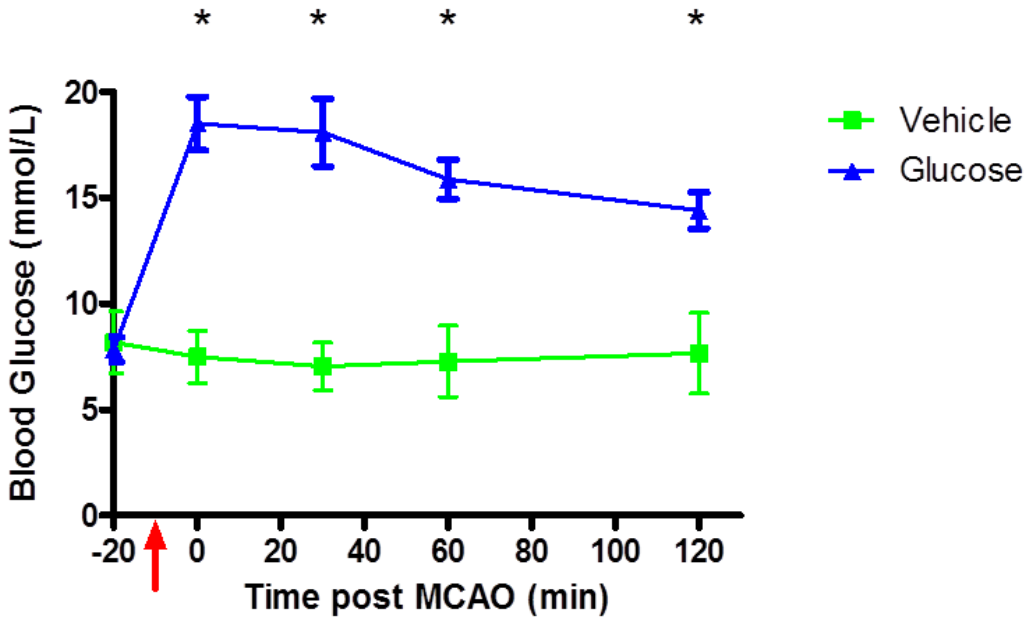

Figure 6.4. Blood glucose values of 2 hour MCAO rats. Blood glucose levels were measured 20 minutes before permanent MCAO in all rats to obtain a baseline value and at subsequent time points after MCAO in vehicle (n=7) and glucose (n=7) treated rats. The red arrow indicates the time of vehicle or glucose administration. Data are presented as mean ± standard deviation. *, P<0.0001 compared to vehicle group using 2-way ANOVA with Bonferroni's multiple comparisons post-hoc test.

6.3.2 Western blot results

Following western blot analysis the groups were de-coded. In Western blots from the 2 hour MCAO tissue samples V_{1-7} and G_{1-7} represent vehicle and glucose treated animals respectively. Similarly, in Western blots from the 24 hour tissue samples V_{1-10} and G_{1-10} represent vehicle and glucose treated animals respectively.

6.3.2.1 - 2 hour MCAO

Cytosolic fraction - αII-spectrin

Calpain cleaves αII-spectrin (280kD) producing two spectrin breakdown products (SBDPs) at approximately 150kD and 145kD. A band representing intact full-length spectrin was observed at approximately 280kD in all samples (Figure 6.5A). There were no differences in the relative protein levels of this band between vehicle and glucose treatment groups (P =0.4, Figure 6.7A). A doublet band was observed at 150-155kD in most samples (except one – G_1, with a single band at 155kD) representing SBDPs (Figure 6.5B). After re-probing the blot with the loading control antibody against ß-actin a band was observed at 42kD in all samples (Figure 6.5C). To estimate the amount of ß-actin in each sample the OD of the ß-actin band for each animal was measured and the values for each group are presented as a scatterplot. There were no significant differences between groups (P=0.4), indicating that there were no sample loading differences (Figure 6.5C). To determine if there was a difference in calpain-mediated proteolysis of αII-spectrin between vehicle and glucose treatment groups the OD value of the SBDP doublet band (150-155kD) was expressed as a ratio of the ß-actin band to give relative SBDP protein levels (Figure 6.5D). The difference in relative SBDP protein levels between vehicle and glucose treatment groups was not statistically significant (P= 0.09), indicating that there was no difference in the proteolytic activity of calpain at 2 hours post-MCAO in the cytosolic fraction. In addition to measuring the amount of SBDPs, the ratio of the intact αII-spectrin to the specific spectrin breakdown products has been shown to be a reliable indicator of calpain proteolytic activity (Sebe et al., 2013, Schoch et al., 2012). However in this analysis there was no significant difference in the ratio of intact αII-spectrin to SBDPs between vehicle and glucose treatment groups (P=0.3).

Membrane fraction - αII-spectrin

The Western blot from the membrane fraction of the 2 hour MCAO tissue was similar to that of the cytosolic fraction. Bands representing intact spectrin and SBDPs were observed at 280kD and 150-155kD respectively (Figure 6.6A). In comparison to the cytosolic fraction, a doublet band representing SBDPs was not observed in all fractions, with only a single band at 155kD in most samples (Figure 6.6A). After reprobing the blot with the loading control antibody, bands representing β-actin were observed at 42kD (Figure 6.6B). In a pattern similar to the cytosolic fraction analysis, there was no difference in β-actin (Figure 6.6B), relative SBDP (Figure 6.6C) and αII-spectrin (Figure 6.7B) protein levels between vehicle and glucose treatment groups ($P=0.3$, $P=1.0$ and $P = 0.7$ respectively). There was also no significant difference in the ratio of intact spectrin to SBDPs between groups ($P=0.9$), indicating that there was no difference in the proteolytic activity of calpain at 2 hours post-MCAO in the membrane fraction.

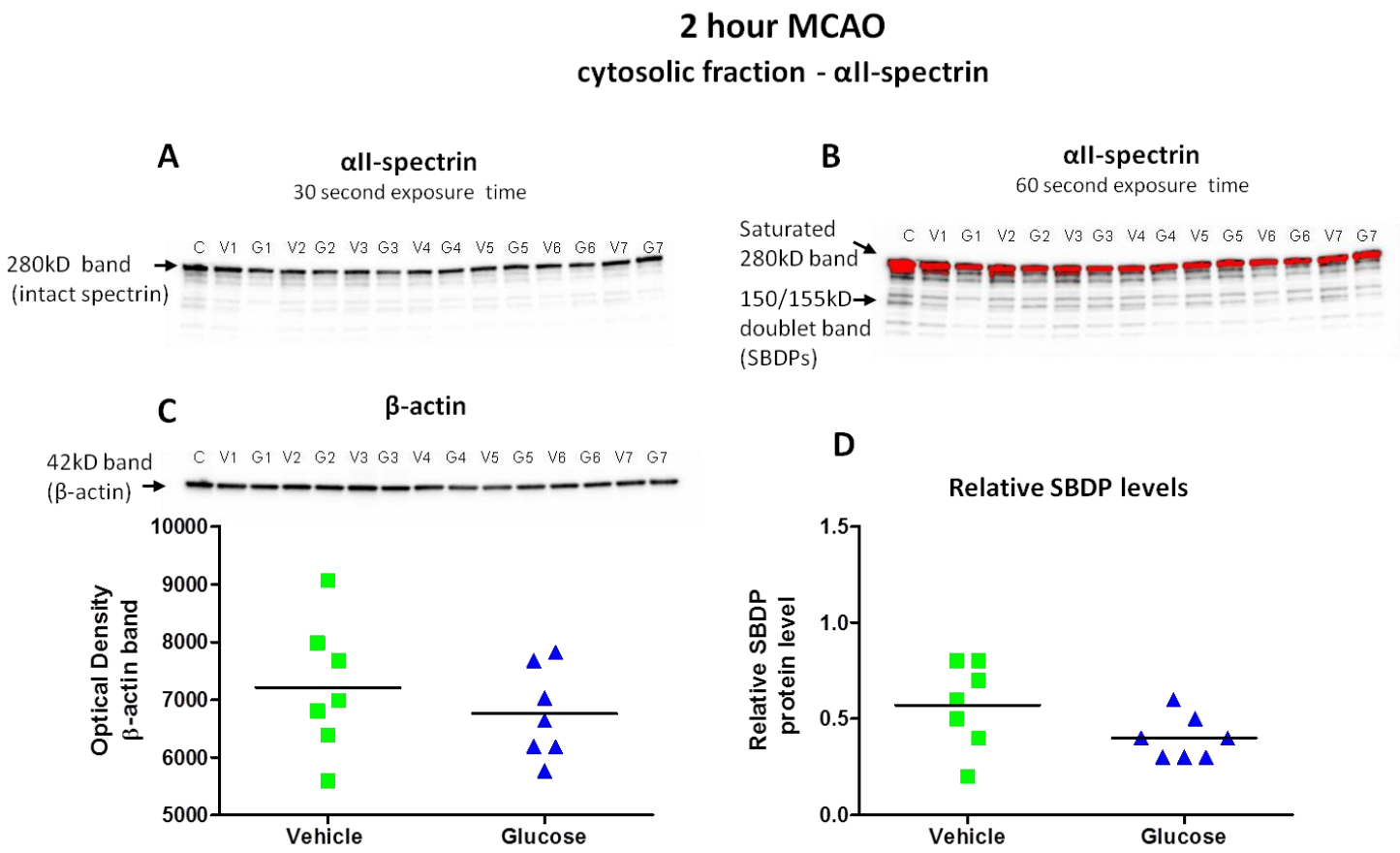

Figure 6.5. αII-spectrin Western blot analysis from cytosolic fraction of 2 hour MCAO tissue. A. Bands representing intact αII-spectrin were observed at 280kD. Sample C = control, naive brain tissue sample. B. Doublet bands representing SBDPs, resulting from calpain mediated cleavage of intact spectrin, were observed at 150-155kD. The exposure time was increased for SBDP analysis which resulted in saturation of the 280kD bands (highlighted in red). C. After re-probing the blot with a β-actin loading control antibody, a band was observed at 42kD in each sample. There was no significant difference in OD values of the β-actin bands between the vehicle and glucose groups (unpaired Student's t-test). D. The OD value of the SBDP band was expressed as a ratio of the β-actin band for each animal to give the relative SBDP protein levels. There was no significant difference in relative SBDP protein levels between the two groups (unpaired Student's t-test).

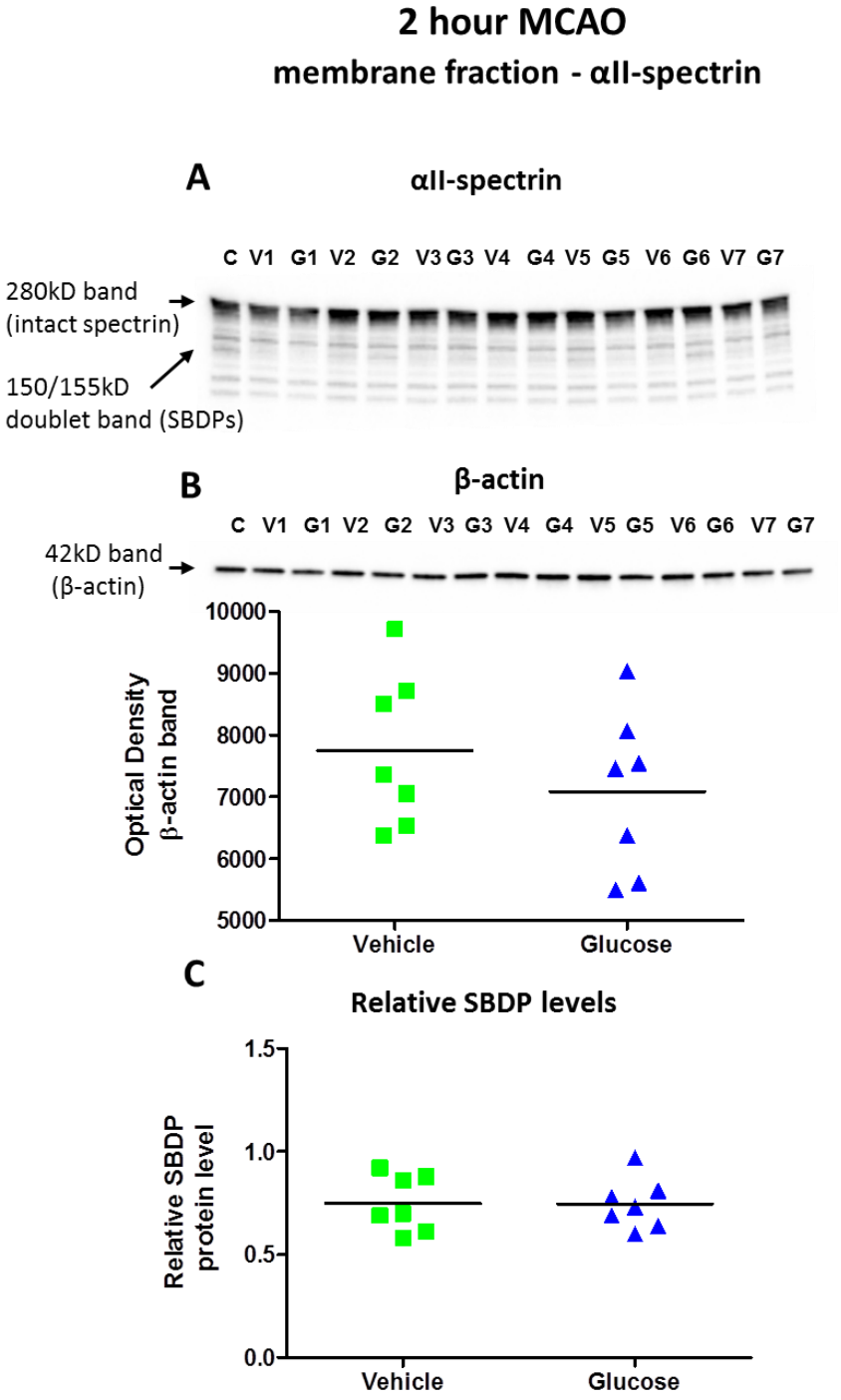

Figure 6.6. αII-spectrin Western blot analysis from membrane fraction of 2 hour MCAO tissue. A. Bands representing intact αII-spectrin and SBDPs were observed at 280kD and 150-155kD respectively. B. After re-probing the blot with β-actin, a band was observed at 42kD in each sample. There was no significant difference in OD values of the β-actin bands between vehicle (n=7) and glucose (n=7) treated rats (unpaired Student's t-test). C. The OD value of the SBDP band was expressed as a ratio of the β-actin band for each animal to give the relative SBDP protein levels. There was no significant difference in relative SBDP protein levels between the two groups (unpaired Student's t-test).

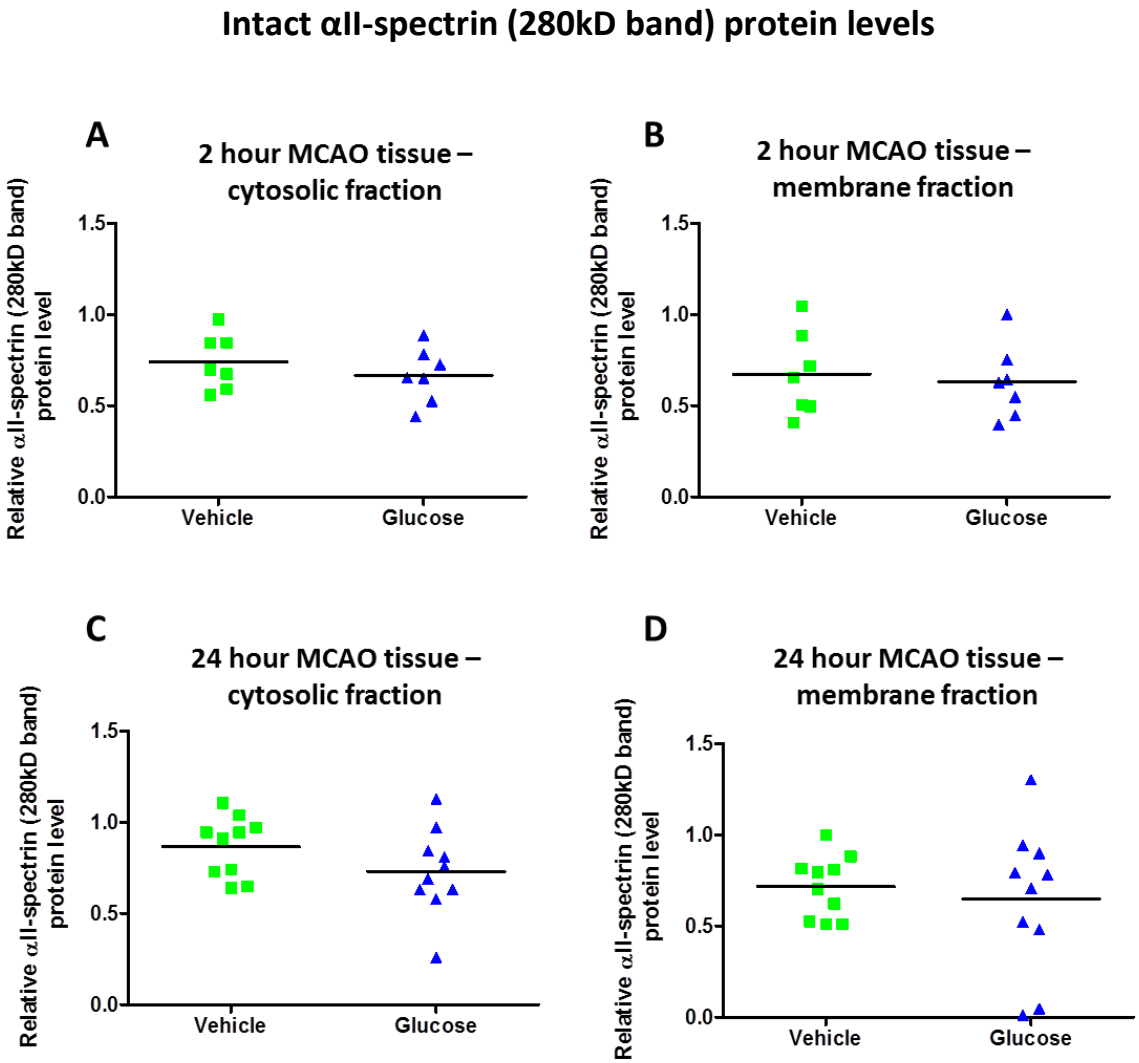

Figure 6.7. Intact αII-spectrin protein levels. In all αII-spectrin Western blots the OD values of the intact αII-spectrin bands (280kD) were expressed as a ratio of the β-actin bands to give the relative αII-spectrin protein levels for each animal. There was no significant difference in relative αII-spectrin protein levels between vehicle and glucose treated rats in either the cytosolic or membrane fractions in ischaemic cortex tissue collected at both 2 and 24 hours after MCAO (unpaired Student's t-test).

Cytosolic fraction – MAP2

There are four isoforms of MAP2 in the mammalian brain: two high molecular weight (HMW) isoforms: MAP2A (280kD) and MAP2B (270kD) that are specifically expressed in neurons (dendrites) and two low molecular weight isoforms: MAP2C (70kD) and MAP2D (75kD) that are present in glial cells (Dehmelt and Halpain, 2005). In all of the 2 hour MCAO cytosolic samples a band was observed at 270-280kD representing HMW MAP2 expression (Figure 6.8A). In the control sample (C) it was assumed that there would be limited MAP2 degradation since this sample was prepared rapidly following brain extraction with a cocktail of protease inhibitors present. Therefore as the intensity of the MCAO samples is similar to that of the control it appears that there was minimal MAP2 degradation at 2 hours post-MCAO across the samples. The intensity of the ß-actin band was also comparable between samples and there was no significant difference in ß-actin expression levels between groups (P=0.7, Figure 6.8B). To account for sample loading errors the OD value of the HMW MAP2 band was expressed as a ratio of the ß-actin band to give the relative MAP2 protein levels (Figure 6.8C). There were no significant differences in relative MAP2 protein levels between vehicle and glucose treated rats (P=0.8).

Membrane fraction – MAP2

The expression of MAP2 in the membrane fraction of the 2 hour MCAO tissue was similar to that of the cytosolic fraction. A band representing HWM MAP2 was observed at 270-280kD (Figure 6.9A) in all samples. MAP2 (and spectrin) is subject to calpain-mediated proteolysis under physiological conditions (Chan and Mattson, 1999b, Fischer et al., 1991) however, under ischaemic conditions the level of proteolysis of MAP2 is considered to be extreme. The level of calpain-mediated proteolysis of MAP2 in the 2 hour tissue samples appeared to be minimal since the band intensities of the ischaemic tissue samples were similar to that of the control sample, in which it was assumed that the level of proteolysis would be at a physiological level. When comparing vehicle and glucose treated animals there was no significant difference in the relative MAP2 protein levels between groups (P=0.4, Figure 6.9C). There were some notable differences in ß-actin protein levels within a couple of the samples (Figure 6.9B), suggesting some potential sample loading errors. The most obvious difference was observed in sample V4, in which the intensity of the ß-actin band

at 42kD was less than the others. It is this sample which is responsible for the outlier in the vehicle group of the scatterplots in Figures 6.9B&C. When this sample was included in the MAP2 analysis there were no significant differences in MAP2 protein levels between the vehicle or glucose treatment groups (P=0.4, Figure 6.9C). Similarly, when omitted from analysis there was still no significant change (P=0.07).

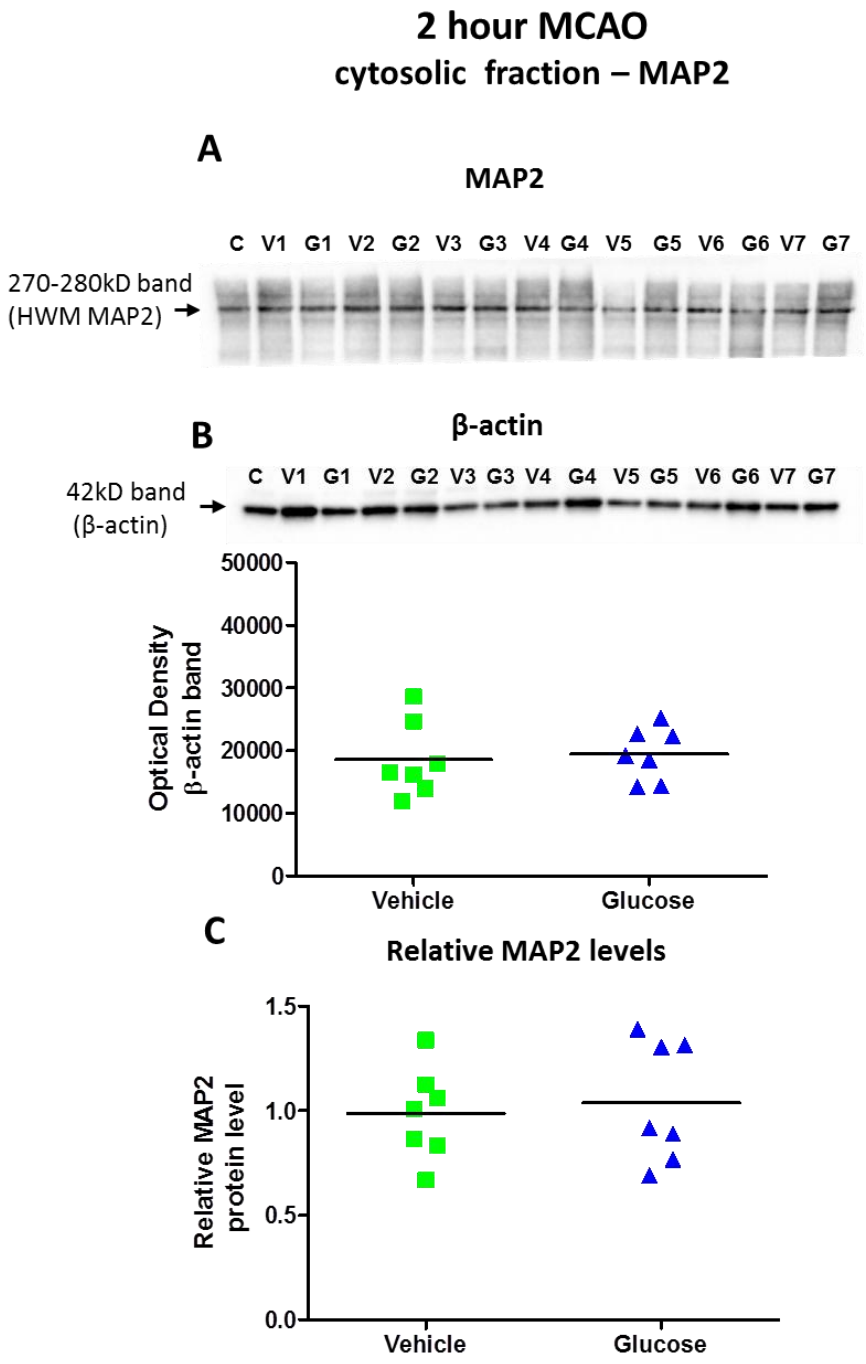

Figure 6.8. MAP2 Western blot analysis from the cytosolic fraction of the 2 hour MCAO tissue. A. Bands representing HMW MAP2 protein were observed at approximately 270-280kD. Sample C = control sample from a naive rat brain. B. The expression levels of β-actin were comparable between samples and there was no significant difference between vehicle and glucose treated rats (unpaired Student's t-test). C. The relative MAP2 protein level for each rat was calculated by dividing the OD value of the HMW MAP2 band by that of the β-actin band. There was no significant difference in relative MAP2 protein levels between vehicle and glucose treated rats (unpaired Student's t-test).

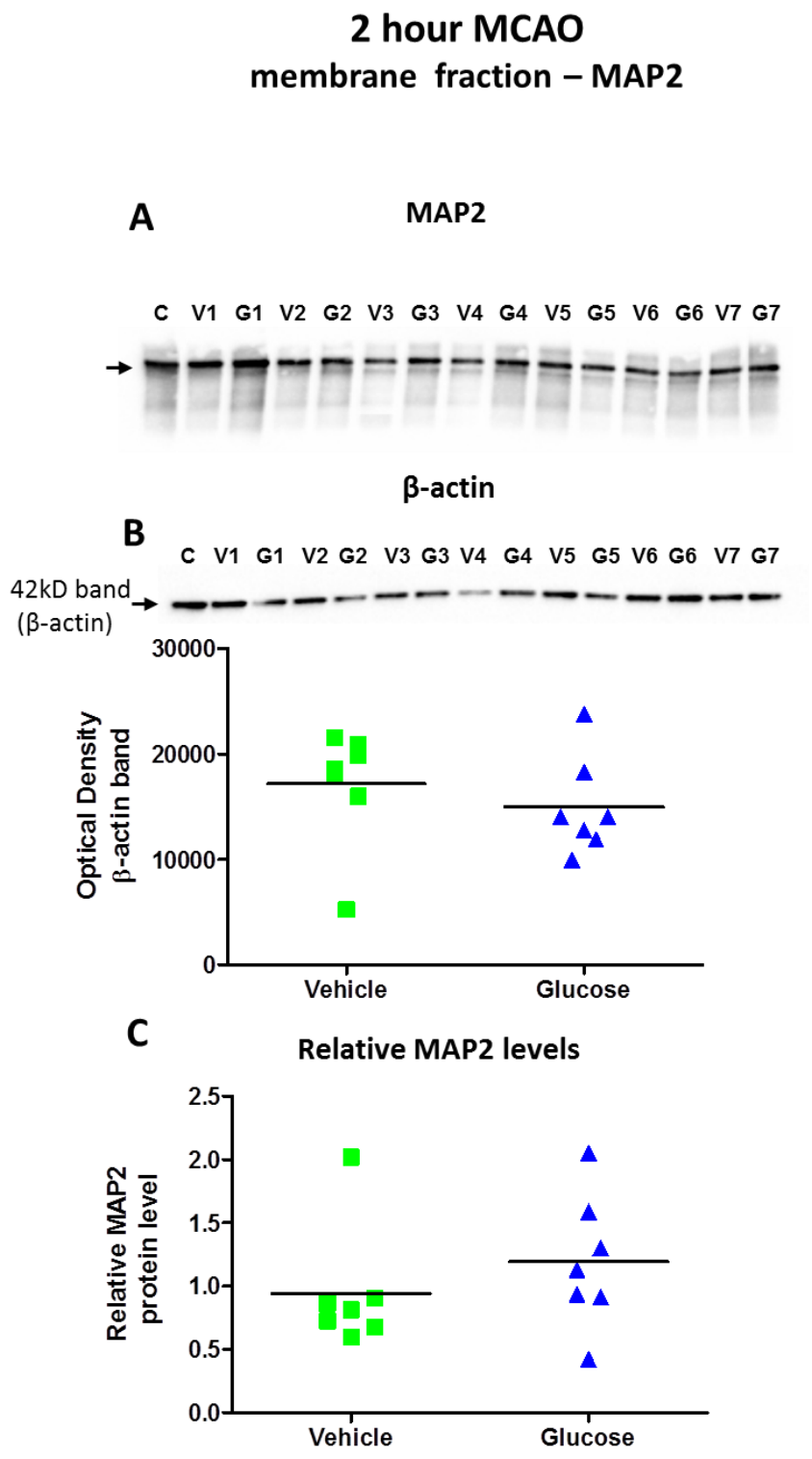

Figure 6.9. MAP2 Western blot analysis from the membrane fraction of the 2 hour MCAO tissue. A. Bands were observed at approximately 270-280kD representing HMW MAP2. Sample C = control, naive brain tissue sample. B. The expression levels of β-actin were comparable between samples and there was no significant difference between vehicle and glucose treated rats (unpaired Student's t-test). C. The relative MAP2 protein level for each rat was calculated by dividing the OD value of the MAP2 band by that of the β-actin band. There was no significant difference in relative MAP2 protein levels between vehicle and glucose treated rats (unpaired Student's t-test).

6.3.2.2 - 24 hour MCAO tissue

Cytosolic fraction - αII-spectrin

In all of the 24 hour MCAO tissue samples from the cytosolic fraction a doublet band was observed at 280kD (Figure 6.10A). This doublet band may have formed from the intact α (280kD) and ß (247-460kD) spectrin subunits but was taken to represent intact αII-spectrin. A doublet band was also observed at 150-155kD in all samples representing calpain mediated SBDPs. In the control, naive tissue sample the intensity of the doublet band at 280kD was greater than the 150/155kD doublet band indicating only a small (physiological) amount of calpain proteolysis. Among the ischaemic tissue samples most displayed a similar band intensity pattern to the control sample however, in some of the samples from glucose treated rats (G1 and G4) the intensity of the band at 280kD was less than the band at 150-155kD, indicating a greater extent of spectrin breakdown in these samples. Although the intensity of the 280kD was less in these samples there was no statistical difference in the intensity of the intact αII-spectrin band between groups (Figure 6.7C).

There was no difference in ß-actin expression between vehicle and glucose treated rats (P=0.5, Figure 6.10B). To determine if the amount of SBDPs differed between vehicle and glucose treated rats the OD values of the SBDP bands were expressed as a ratio of the ß-actin loading control band (Figure 6.10C). There tended to be more SBDPs in glucose treated rats compared to vehicle treated rats but the difference between groups was not statistically significant (P=0.08). However, there was a significant difference in the ratio of intact αII-spectrin to SBDPs between vehicle and glucose treatment groups, with values of 1.3±0.5 and 0.9±0.3 respectively (P=0.03). In the glucose treatment group the ratio of intact, full length αII-spectrin to the amount of SBDPs was less than the vehicle group suggesting that there was more SBDPs and more calpain proteolysis in the glucose treatment group.

Membrane fraction - αII-spectrin

The Western blot from the membrane fraction produced similar results to the blot from the cytosolic samples (Figure 6.11A). A doublet band representing intact spectrin was observed at 280kD. This band was present in all samples from the vehicle treatment group but was not observed in two rats from the

glucose treatment group (G_1 and G_4). Despite this, there was no difference in the relative expression of the 280kD αII-spectrin band between groups (Figure 6.7D). A doublet band representing calpain mediated SBDPs was observed at 150-155kD in all rats. In the two glucose treated rats, in which a band at 280kD was not observed (G_1 and G_4), an intense band at 150kD was observed suggesting a greater extent of calpain-mediated spectrin breakdown in these samples. Despite the observed differences in the intensity of the 280kD and 150-155kD band intensities between samples, there was no difference in the amount of ß-actin between groups ((P=0.7), Figure 6.11B). When the OD values of the SBDP bands were expressed as a ratio of the ß-actin bands, to account for sample loading differences, the protein levels of SBDPs were significantly greater in glucose compared to vehicle treated rats (P=0.03, Figure 6.11C), suggesting that glucose treatment increased calpain-mediated αII-spectrin breakdown in the membrane fraction. In addition, the amount of calpain proteolysis was significantly greater in the glucose treatment group as measured by the ratio of intact αII-spectrin to SBDPs, with mean values of 1.6±0.9 and 0.9±0.5 in vehicle and glucose treatment groups respectively (P=0.03).

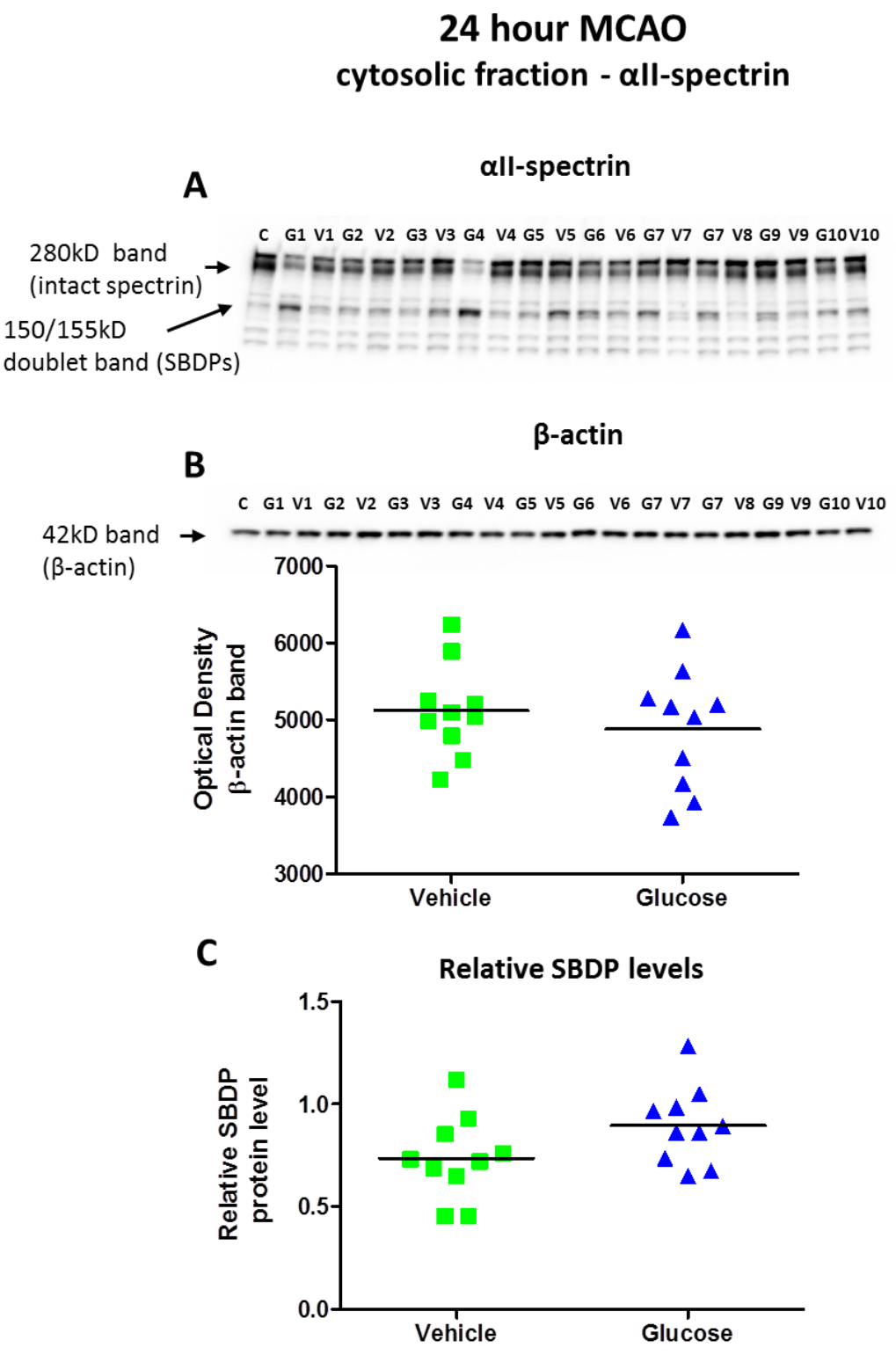

Figure 6.10. αII-spectrin Western blot analysis from the cytosolic fraction of ipsilateral cortex tissue acquired 24 hours after permanent MCAO. Bands representing intact αII-spectrin and SBDPs were observed at 280kD and 150/155kD respectively. Sample C = control, naive brain tissue sample. B. After re-probing the blot with a β-actin, a band was observed at 42kD in each sample. There was no significant difference in OD values of the β-actin bands between vehicle and glucose treated rats (unpaired Student's t-test). C. The OD value of the SBDP band was expressed as a ratio of the β-actin band for each animal to give the relative SBDP protein levels. There was no significant difference in relative SBDP protein levels between the two groups (unpaired Student's t-test).

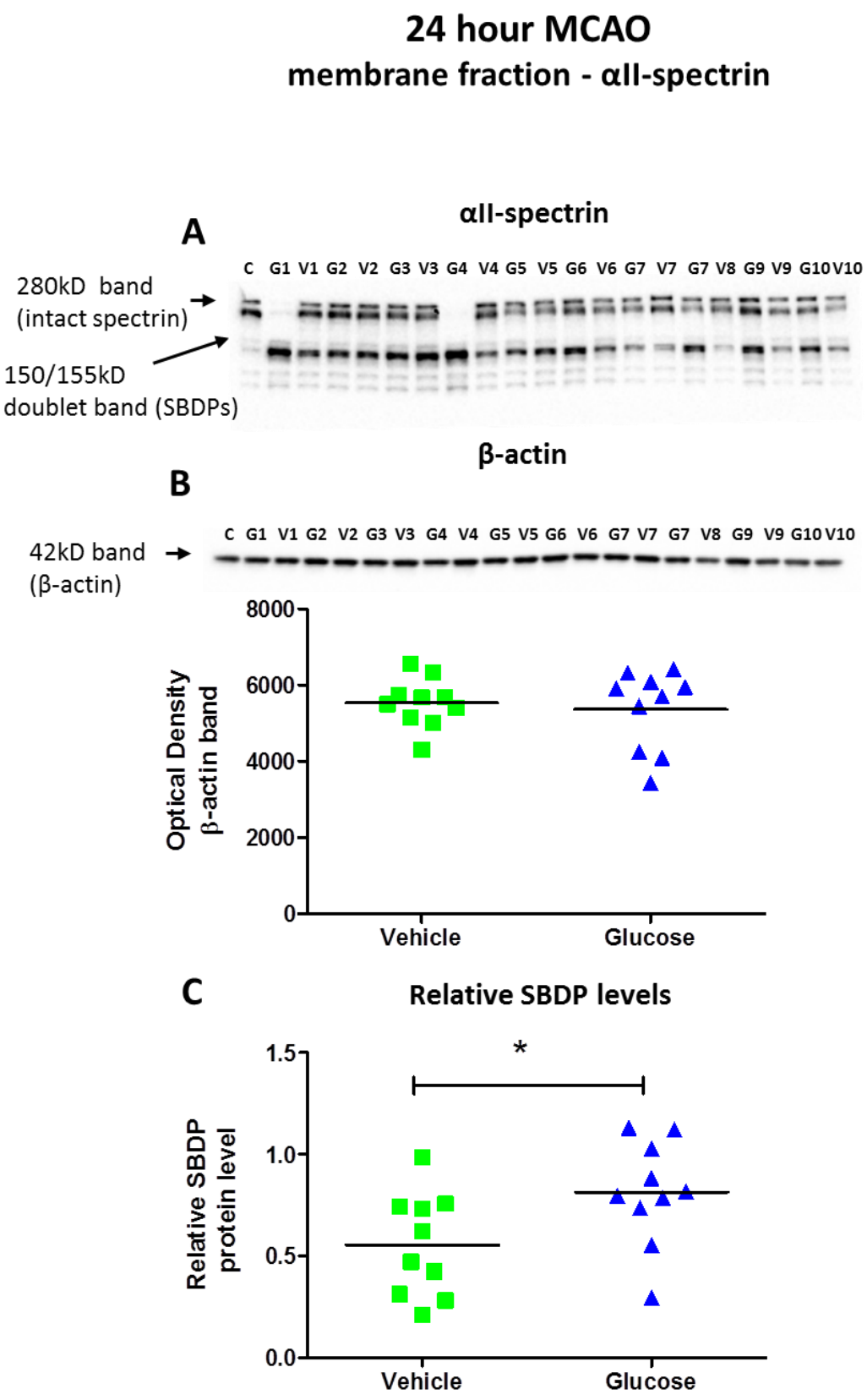

Figure 6.11. αII-spectrin Western blot analysis from the membrane fraction of ipsilateral cortex tissue acquired 24 hours after permanent MCAO. A. Bands representing intact αII-spectrin and SBDPs were observed at 280kD and 150-155kD respectively. Sample C = control, naive brain tissue sample. B. There was no significant difference in OD values of the β-actin bands between vehicle and glucose treated rats (unpaired student's t-test). C. The OD value of the SBDP band was expressed as a ratio of the β-actin band for each animal to give the relative SBDP protein levels. *, P<0.05 compared to vehicle group using an unpaired Student's t-test.

Cytosolic fraction – MAP2

In the 24 hour MCAO samples from the cytosolic fraction a HMW MAP2 band was observed at approximately 270-280kD in a few samples (Figure 6.12A). However, in the majority of samples this band was absent, indicating MAP2 degradation, and this is highlighted in the scatterplot (Figure 6.12C) as the relative MAP2 protein levels are zero in almost half of the rats from each group. The difference in relative MAP2 protein levels between groups was not statistically significant (P=0.7). In most samples within the cytosolic fraction a band was observed at approximately 150kD (Figure 6.12A), the identity of which is not known. There was no difference in ß-actin expression levels between vehicle and glucose treatment groups (P=0.4, Figure 6.12B) indicating that there was no sample loading differences in this Western blot.

Membrane fraction – MAP2

In samples from the membrane fraction of 24 hour MCAO tissue a band representing HMW MAP2 was observed at approximately 270-280kD in most samples (Figure 6.13A). The intensity of the HMW MAP2 band varied among samples indicating differing amounts of MAP2 degradation. The intensity was greatest in the control sample (C) where MAP2 proteolysis was expected to be minimal. There was no difference in ß-actin expression (P=0.9, Figure 6.13B) or relative MAP2 protein levels (P=0.05, Figure 6.13C) between glucose and vehicle treatment groups although relative MAP2 protein levels in glucose treated rats tended to be lower than vehicle treated rats.

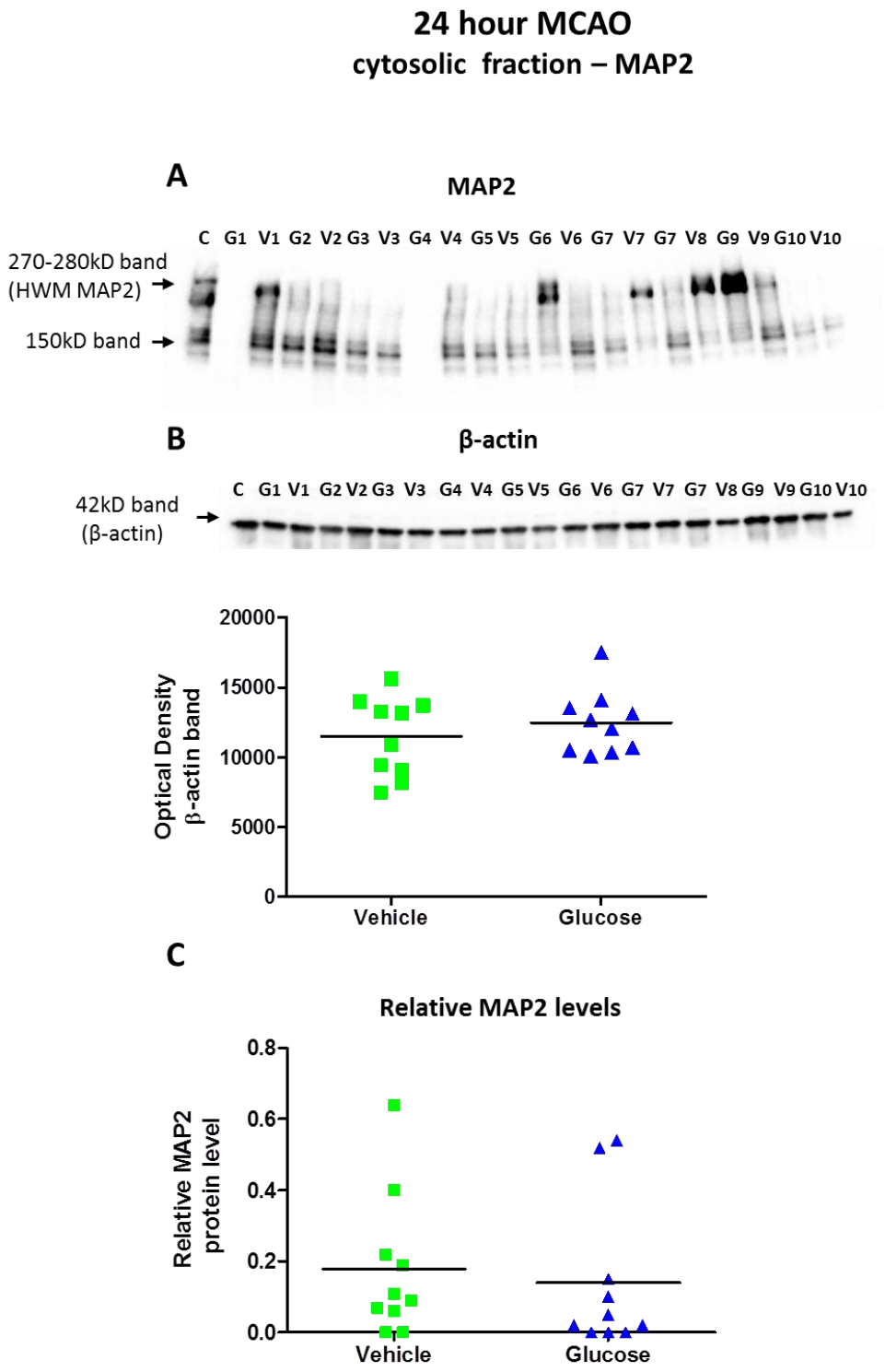

Figure 6.12. MAP2 Western blot analysis from the cytosolic fraction of ipsilateral cortex brain tissue samples collected 24 hours after permanent MCAO. A. Bands were observed at approximately 270-280kD representing HMW MAP2. The identity of the band observed at approximately 150kD in not known. Sample C = control, naive brain tissue sample. B. The expression levels of β-actin were comparable between samples and there was no significant difference between vehicle and glucose treated rats (unpaired student's t-test). C. The relative MAP2 protein level for each rat was calculated by dividing the OD value of the MAP2 band by that of the β-actin band. There was no significant difference in relative MAP2 protein levels between vehicle and glucose treated rats (unpaired Student's t-test).

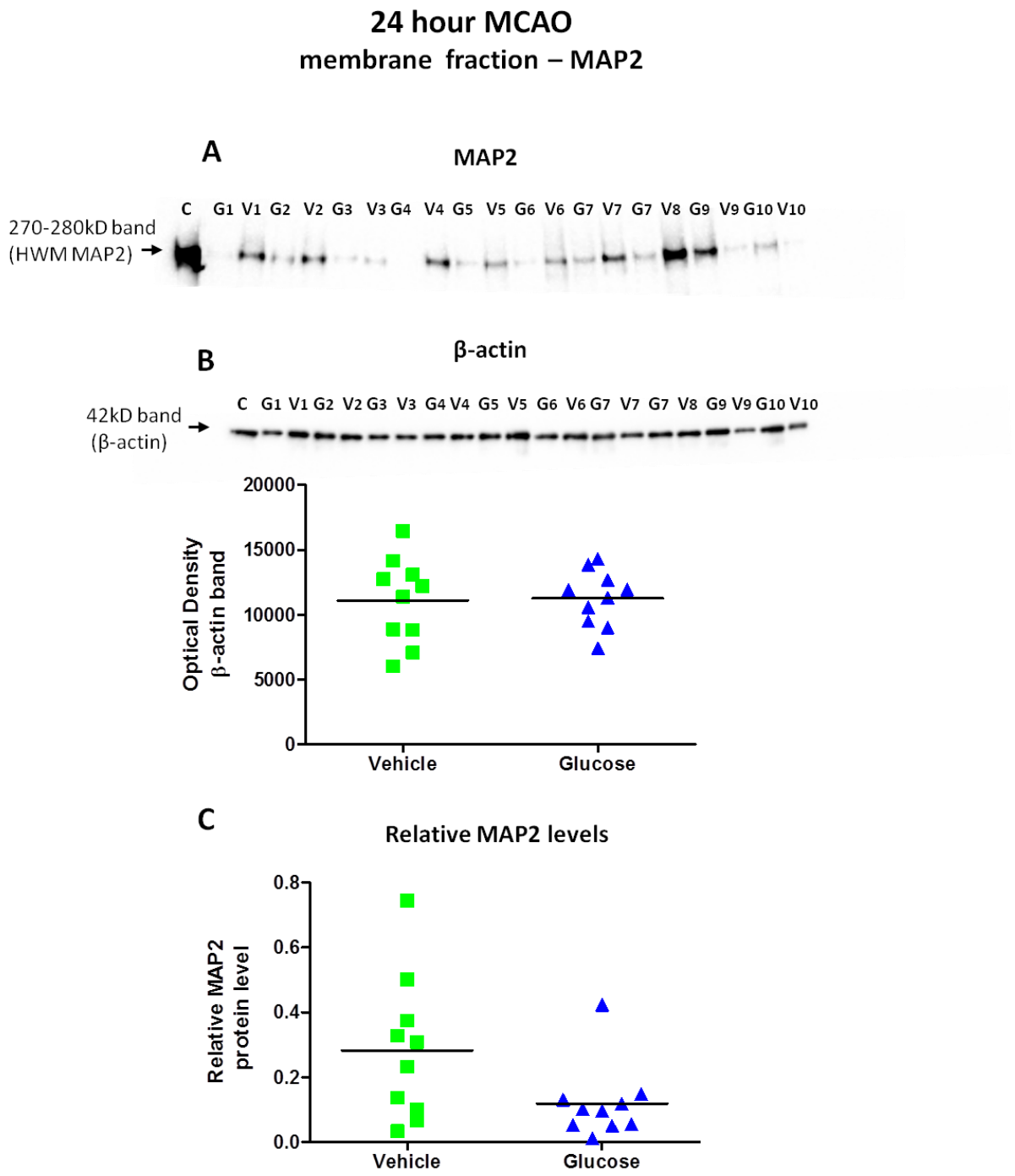

Figure 6.13. MAP2 Western blot analysis from the membrane fraction of ipsilateral cortex brain tissue samples collected 24 hours after permanent MCAO. A. Bands were observed at approximately 270-280kD representing HMW MAP2. Sample C = control, naive brain tissue sample. B. The expression levels of β-actin were comparable between samples and there was no significant difference between vehicle and glucose treated rats (unpaired student's t-test). C. The relative MAP2 protein level for each rat was calculated by dividing the OD value of the MAP2 band by that of the β-actin band. There was no significant difference in relative MAP2 protein levels between vehicle and glucose treated rats (unpaired Student's t-test).

6.4 Discussion

To obtain insight into the possible damaging effects of hyperglycaemia within the brain tissue the degradation of αII-spectrin and MAP2, known markers of calpain-mediated brain injury, were analysed in ipsilateral cortex tissue from vehicle and glucose treated rats using Western blotting. It was hypothesised that there would be greater tissue injury in glucose compared to vehicle treated animals, manifested as greater amounts of SBDPs and MAP2 degradation in brain tissue samples from the glucose treatment group.

In the tissue collected 2 hours after MCAO there was no difference in the levels of SBDPs or MAP2 degradation, between vehicle or glucose treatment groups suggesting that glucose treatment did not influence the proteolytic activity of calpain at this time. In each Western blot a sample from a naive rat brain was included as a positive control for each antibody. Both αII-spectrin and MAP2 have been shown to be expressed in normal rat brain tissue lysates (Nakajima et al., 2011, Pettigrew et al., 1996) and as such this was accepted as an appropriate control. It was assumed that there would be minimal (physiological) calpain proteolysis in the control sample and therefore the levels of intact αII-spectrin and MAP2 would be higher in the control compared to ischaemic tissue samples. Although no formal comparison between the OD values of the control and MCAO samples could be made, visually there were no obvious differences in the levels of αII-spectrin, SBDPs and MAP2 protein between control and MCAO samples, which suggests that at 2 hours after MCAO the levels of calpain proteolysis were similar to physiological levels. The fact that only a single breakdown product at 155kD was observed in most of the MCAO samples on the αII-spectrin blots at 2 hours also suggests that there was minimal evidence of calpain mediated proteolysis at this time. This is because the 155kD fragment has been reported to be produced when αII-spectrin is cleaved by calpain and caspase-3 (Nath et al., 1996). However, the fragment at 150kD is reported to be specific to cleavage by calpain and this is absent in some samples, most notably within samples from membrane fraction. Conversely, the calpain specific breakdown product at 150kD is present within all the samples at 24 hours (and to a greater extent than the 155kD product) and thus there was clear evidence of calpain's proteolytic activity in the 24 hour MCAO tissue. Compared to the expression of αII-spectrin and MAP2 in the control brain sample, αII-spectrin

break down products and MAP2 degradation were clearly visible on Western blots from the 24 hour MCAO tissue. There was evidence of a significant effect of glucose treatment on the proteolytic activity of calpain on αII-spectrin in the membrane fraction of the 24 hour MCAO tissue as the relative levels of SBDPs were significantly greater in rats that received glucose treatment compared to those that received vehicle treatment. In addition, the ratio of intact spectrin to SBDPs, another method of assessing the proteolytic activity of calpain, was lower in the glucose- compared to vehicle treatment group in both the membrane and cytosolic fractions at 24 hours which suggests that there was an increase in calpain proteolysis in the glucose treatment group. Taken together the results from the present study demonstrate an association between glucose treatment and an increase in protein markers of neuronal injury in the 24 hour infarcted tissue but not the acute 2 hour ischaemic tissue. The failure to detect an association at 2 hours after MCAO may reflect the limitations of adopting a biochemical approach (see below), but may also result from the potential for hyperglycaemia to influence multiple pathophysiological mechanisms simultaneously that combine to exacerbate ischaemic damage.

6.4.1 Study limitations

There are a number of limitations in the present study which could have impacted on the results. Firstly, assessment of the protein levels of SBDPs and MAP2 in the same animal at two time different time points is not possible and therefore direct comparisons between the 2 hour and 24 hour time points could not be made. Observationally, the results showed evidence of calpain-mediated proteolysis of αII-spectrin and MAP2 at 24 hours but not at 2 hours. This is in agreement with results from Western blotting experiments reported by Pettigrew et al (1996), who investigated the time-course of αII-spectrin and MAP2 following permanent MCAO in the rat. They showed that after 1 hour of permanent MCAO the expression of αII-spectrin and MAP2 in ischaemic brain tissue was similar to that in the unaffected hemisphere, with pronounced changes in the expression of both proteins observed after 6 and 24 hours permanent MCAO (Pettigrew et al., 1996). Therefore, it might not be possible to detect the degradation of αII-spectrin and MAP2 2 hours after MCAO using Western blotting. Further experiments are needed to determine if the

detrimental effects of hyperglycaemia during the initial hours of ischaemia take place predominantly within the brain tissue.

Secondly, when investigating the time-related neuronal changes in SBDPs after permanent MCAO, Bartus and colleagues dissected out 1-mm blocks of tissue from the ipsilateral striatum and cortex for Western blot analysis (Bartus et al., 1995). In contrast, the entire ipsilateral cortex was dissected for Western blot analysis in the present study. By doing so it is possible that any significant changes that occurred in the ischaemic tissue have been diluted. Future studies might benefit from dissecting out smaller regions of the cortex associated with ischaemic damage for analysis. Although it could be argued that if hyperglycaemia does indeed have a profound effect it might have been possible to detect it in the large (diluted) samples.

Another limitation of the present study was that direct comparisons between different Western blots could not be made. This is because the measured OD value for each protein band on a blot is an arbitrary unit which only has meaning within the context of the OD values of other bands within that blot. This therefore impacts on the amount of samples that can be analysed together and subsequently the questions that can be asked. For example, whether glucose treatment increases the proteolytic activity of calpain in the ipsilateral cortex, relative to that in the contralateral cortex, compared to vehicle treatment was not investigated. The expression of αII-spectrin and MAP2 in the contralateral cortex was not examined at any stage in the present study. The important question that this study set out to answer was whether there was a difference between vehicle or glucose treatment on ischaemic tissue injury and due to the limited number of samples that could be loaded on a single gel it was important to select the brain region where ischaemic injury would take place.

6.4.2 Summary

By measuring the proteolytic activity of calpain on two of its substrates in ischaemic brain tissue the aim was to gain an indirect measurement of hyperglycaemia on glutamate excitotoxicity. This is because *in vivo* microdialysis studies have shown that hyperglycaemia increases extracellular glutamate levels during ischaemia (Li et al., 2000c, Wei and Quast, 1998, Choi et al., 2010), and

there is evidence that stimulation of glutamate receptors *in vitro* leads to calpain activation and subsequent substrate proteolysis (Siman et al., 1989). The Western blot results reported in the present study suggest there might be an association between the harmful outcomes of acute hyperglycaemia and enhanced calpain proteolysis 24 hours after permanent MCAO. However, there was no association at 2 hours after MCAO. This was identified as the earliest time point where glucose treatment significantly increased acute lesion volume in the previous study. It was important to include this earlier time point as hyperglycaemia has been shown to accelerate acute ischaemic damage and therefore establishing the acute pathological mechanisms of hyperglycaemia induced damage are essential in terms of therapeutic intervention.

It is therefore still not clear why hyperglycaemia is harmful during ischaemia. The most likely explanation is that a moderate glucose insult affects many different pathological mechanisms simultaneously, that cumulatively exacerbate ischaemic damage. Of these many mechanisms, the anaerobic metabolism of glucose through the lactic acid cycle was the first and is the most persistent hypothesis used to explain the relationship between hyperglycaemia and worse clinical outcomes from ischaemic stroke. In the absence of oxygen glucose is metabolised anaerobically producing lactate as a by-product. Elevated lactate levels can acidify cells and the surrounding environment leading to tissue acidosis. This is potentially damaging and can lead to the production of free radicals and mitochondrial dysfunction (Anderson et al., 1999, Rehncrona et al., 1989), both of which would be detrimental during ischaemia. Both clinical and experimental studies have revealed an association between hyperglycaemia and increased brain lactate levels. Furthermore elevated lactic acid concentrations have been shown to correlate with worse outcomes (Parsons et al., 2000, Anderson et al., 1999, LaManna et al., 1992). Although there appears to be strong evidence indicating increased lactate as an important mediator of hyperglycaemia induced brain damage, the fact that lactate metabolism is important for ATP production during ischaemia (Pellerin and Magistretti, 1994) and that inhibiting lactate production during ischaemia exacerbates, rather than reduces, ischaemic damage (Cassady et al., 2001) suggests that it is not the only contributor. Nevertheless it would have been interesting to compare the lactate levels in glucose and vehicle treated rats in this thesis. Magnetic resonance

spectroscopy can be used to assess brain lactate levels during ischaemia and lactate measurements were considered as part of the previous MRI study. Unfortunately this could not be achieved due to MR signal inference from the craniectomy required for occlusion of the distal portion of the MCA by diathermy. Future studies could consider investigating the effect of glucose or vehicle treatment on brain lactate levels using a subset of animals in which the MCA is occluded by an alternative method that does not require a craniectomy.

Chapter 7 – General Discussion

7. General Discussion

Hyperglycaemia at the onset of ischaemic stroke is strongly associated with worse clinical outcomes (Baird et al., 2003, Capes et al., 2001, Bruno et al., 1999, Candelise et al., 1985). Despite this, the pathophysiological mechanisms underlying this association are poorly understood. An increase in the severity of the blood flow deficit following ischaemic stroke has been implicated in hyperglycaemia-induced brain damage (Duckrow, 1995, Kawai et al., 1998, Wang et al., 2008). However, the studies in this thesis demonstrate that an increase in the severity of ischaemia is not the primary mechanism by which hyperglycaemia exacerbates ischaemic damage following permanent MCAO. This suggests that the detrimental effects of hyperglycaemia are not predominantly mediated in the cerebrovasculature. Alternatively, the damaging effects of hyperglycaemia may occur within the brain parenchyma. However, additional studies are required to confirm this.

The studies reported in this thesis represent one of the few to examine hyperglycaemia at levels typically encountered in acute ischaemic stroke, demonstrating that hyperglycaemia exacerbates acute lesion volume and infarct volume in a normotensive rat strain. Furthermore, the damaging effects of hyperglycaemia were found to occur early after the onset of cerebral ischaemia, suggesting that hyperglycaemia accelerates the evolution of ischaemic damage. The findings from this thesis will now be put into clinical context to discuss the pathophysiological mechanisms that relate hyperglycaemia to poor clinical outcomes. Some of the future strategies for pre-clinical stroke research along with the current practices for managing hyperglycaemia in acute ischaemic stroke patients will also be discussed. Firstly some of the limitations of this research will be considered.

7.1.1 Study limitations

One of the primary aims of this thesis was to establish a clinically relevant animal model for studying the effects of hyperglycaemia during experimental ischaemic stroke. To induce hyperglycaemia a single IP injection of a 15% glucose solution was administered 10 minutes prior to permanent MCAO. A limitation of this approach is that it does not model all of the features of human

PSH. The clinical presentation of PSH is far more complex in terms of the etiology of hyperglycaemia and the temporal profile of hyperglycaemia seen in acute ischaemic stroke patients. However in terms of the preclinical picture of PSH, the studies reported in this thesis are novel as they are one of the very few to report that hyperglycaemia, at levels comparable to those in patients presenting with PSH, increases acute ischaemic damage and infarct size in a rodent model of ischaemic stroke. The results from previous preclinical stroke studies investigating the effects of hyperglycaemia on infarct size have been inconsistent and the glucose levels induced in hyperglycaemic animals greatly exceed those seen clinically. The animal model described in this thesis is therefore an important addition to the preclinical literature and could be used in the future to study the effects of glucose lowering therapies

The necessary use of anaesthetics in animal models may also be a limiting factor in this research because anaesthetic agents have the potential to induce hyperglycaemia. Saha et al (2005) demonstrated that anaesthetics such as isoflurane and ketamine/xylazine (KX) induced acute hyperglycaemia in fed rats. In contrast, neither agents were found to induce hyperglycaemia in rats that had been fasted for 18 hours. The authors investigated the mechanism of KX induced hyperglycaemia in fed rats and showed that the effect was mediated through the modulation of glucoregulatory hormones (insulin, growth hormone and corticosterone) via stimulation of α2-adrenergic receptors (Saha et al., 2005). To reduce any influence of isoflurane anaesthesia on blood glucose levels all of the animals reported in this thesis were fasted for 18 hours prior to the induction of anaesthesia. However isoflurane may have had some influence on blood glucose levels in glucose treated rats. For instance in experiments where rats were maintained under anaesthesia for 4 hours, blood glucose levels in glucose treated rats increased and remained elevated for 4 hours. This is a longer time than predicted for an acute glucose insult and therefore it seems that isoflurane, like KX-induced anaesthesia, may influence the glucoregulatory hormones that would normally act to normalise blood glucose levels. However this does not present a disadvantage to the model as blood glucose levels in patients with admission hyperglycaemia can remain elevated for several hours after symptom onset (Yong and Kaste, 2008).

The use of distilled water as a vehicle solution in this thesis also presents a potential limitation. IP injections of water can alter the concentration of electrolytes in the intraperitoneum which can potentially be cytotoxic leading to tissue fibrosis (Levine and Saltzman, 2001). Although the volume administered in a single injection was unlikely to have a significant effect on fluid balance it would be preferable to use isotonic saline as the vehicle in future studies.

7.1.2 Pathophysiology of PSH

Hyperglycaemia-associated reduction in cerebral blood flow

Evidence from clinical studies suggests that hyperglycaemia during ischaemic stroke is particularly detrimental in patients without a history of diabetes (Capes et al., 2001, Shimoyama et al., 2014). Recent in-house studies support this as hyperglycaemia increased infarct volume in rats without features of the metabolic syndrome such as hypertension and insulin resistance (Tarr, 2012, Tarr et al., 2013). In light of these findings a standard normotensive rat strain was selected for studying the mechanisms by which hyperglycaemia exacerbates ischaemic damage. It was essential to establish from the outset whether clinically relevant hyperglycaemia induces a reduction in cerebral perfusion. This is because any further reduction in CBF during MCAO could increase the volume of hypoperfused tissue leading to larger infarcts and greater penumbral loss. The blood flow data generated from the autoradiography study in Chapter 4 and the MRI study in Chapter 5 demonstrate that hyperglycaemia does not exacerbate ischaemic damage by increasing the perfusion deficit. It should be mentioned here that if hyperglycaemia increased the perfusion deficit it would have been important to determine the effects of glucose treatment on plasma osmolality. This is because the treatment groups in this thesis did not control for differences in osmotic load between vehicle and glucose treated rats and studies have shown that an increase in plasma osmolality can reduce regional CBF (Duckrow, 1995, Duckrow et al., 1985). Therefore if hyperglycaemia increased the perfusion deficit it would have been difficult to exclude the influence of an osmotic mechanism.

Clinically, few studies have investigated the influence of admission hyperglycaemia on the severity of the perfusion deficit after ischaemic stroke. In one recent study, Luitse et al (2013) reported that patients with admission

hyperglycaemia did not have larger perfusion deficits compared to normoglycaemic patients during the acute stage of ischaemic stroke. These results are in agreement with the findings from this thesis and suggest that the detrimental effects of hyperglycaemia in ischaemic stroke are not associated with larger perfusion deficits. However, they found that patients with admission hyperglycaemia had worse functional outcomes (Luitse et al., 2013), an outcome measure that was not examined in this thesis. The association between hyperglycaemia and poor functional outcomes observed in their study might be explained by the fact that ~50% of patients in each group were treated with intravenous thrombolysis and there is an increased risk of intracerebral haemorrhage with thrombolysis treatment in patients with PSH (Bruno et al., 2002, Bruno et al., 1999). From personal correspondence with the authors of this study I learned that they found no difference in the size of the perfusion deficit between normo- and hyperglycaemic patients that were not treated with thrombolysis, although it was noted that the group sizes were relatively small. This was of interest because the animal model established in this thesis is most relevant to that particular subset of patients. Whether hyperglycaemia exacerbates the perfusion deficit in ischaemic stroke patients needs to be examined in a larger patient cohort and Luitse and colleagues recognise this as they are planning to perform a larger, prospective study examining perfusion deficits in patients with and without admission hyperglycaemia.

If hyperglycaemic patients do have larger perfusion deficits this could lead to larger infarcts and reduced penumbral salvage. To date, only a few clinical studies have investigated the effects of hyperglycaemia on the penumbral tissue (Parsons et al 2002, Rosso et al 2011). These studies demonstrated that the volume of tissue-at-risk that progressed to infarction was larger in hyperglycaemic compared to normoglycaemic patients groups and suggests that the ischaemic penumbra is particularly vulnerable during hyperglycaemic ischaemia. In contrast, the data presented in Chapter 5 demonstrate that hyperglycaemia does not influence the volume of the perfusion-diffusion mismatch-defined ischaemic penumbra. Therefore, the observed increase in acute lesion volume in hyperglycaemic rats did not correspond with a smaller volume of mismatch tissue in the acute phase after MCAO. This could have important clinical implications because the ischaemic penumbra is the target of

most therapeutic interventions. Therefore, if there are equal amounts of penumbral tissue in normoglycaemic and hyperglycaemic patients there might be a window of opportunity for therapeutic intervention in patients with PSH. In addition, calculation of the ADC-defined penumbra in Chapter 5 demonstrated that hyperglycaemic rats may have a greater amount of penumbra following the onset of ischaemia in comparison to normoglycaemic rats, suggesting that there may be a window of opportunity for therapeutic intervention in hyperglycaemic ischaemia. Further pre-clinical studies are needed to clarify the effects of hyperglycaemia on the tissue within the ischaemic penumbra. Together, with the results from this thesis, these studies would help to inform the design of future clinical trials investigating the treatment of PSH.

Other mechanisms of hyperglycaemia-mediated brain injury

There are many different ways in which hyperglycaemia could be harmful during ischaemia. Some of the possible mechanisms proposed from animal studies include: changes in cerebral metabolism (Folbergrova et al., 1992), increased local oedema (Berger and Hakim, 1986), an increase in NMDA receptor mediated calcium entry into neurons (Li et al., 2000b) and an increase in glucose mediated oxidative stress and inflammation (Mohanty et al., 2000, Dhindsa et al., 2004). Although the findings from this thesis do not implicate a definitive mechanism, it is clear from the MRI data presented in Chapter 5 that the harmful effects of hyperglycaemia occurred during the acute 1-2 hours after the onset of cerebral ischaemia. During this acute time period glutamate-mediated neuronal excitotoxicity contributes to ischaemic brain damage (Brouns and De Deyn, 2009). Therefore it is possible that hyperglycaemia could exacerbate ischaemic damage by increasing glutamate-mediated excitotoxicity. The study presented in Chapter 6 aimed to measure this mechanism indirectly by estimating the protein levels of αII-spectrin and MAP2. These proteins are well-defined markers of neuronal brain injury and are also substrates for calpain, the activity of which has been reported to increase *in vivo* during experimental ischaemic stroke (Neumar et al., 2001, Pettigrew et al., 1996, Bartus et al., 1995) and *in vitro* following glutamate receptor stimulation (Seubert et al., 1988). The data in Chapter 6 suggested that hyperglycaemia might increase the amount of calpain proteolysis. Future studies in our laboratory will continue to determine if hyperglycaemia exacerbates excitotoxic ischaemic damage by examining

whether neuronal death, induced by intracerebral injection of NMDA, is increased by hyperglycaemia. This model of neuronal brain injury has been widely used to test the protective effects of pharmacological agents against an excitotoxic brain insult and could provide important information on the effects of a clinically relevant glucose insult during excitotoxic processes.

It is conceivable that acute hyperglycaemia, at the levels induced in this thesis, could exacerbate some, if not all of the proposed pathophysiological mechanisms of hyperglycaemia during ischaemia to a small degree that only when combined together have a significant effect on infarct size. This might be true of the studies in this thesis. In Chapter 5 glucose treated rats tended to have a larger volume of tissue with a perfusion deficit compared to normoglycaemic rats. Likewise, in Chapter 6 ischaemic brain tissue from hyperglycaemic rats tended to have more spectrin break down products than normoglycaemic rats, which could indicate a greater amount of calpain activity resulting from an increase in calcium influx during neuronal excitotoxicity. Neither the perfusion deficit data nor western blot data alone is sufficient to explain the significant increase in acute ADC lesion volume and infarct size observed in hyperglycaemic rats, yet a combination of these different mechanisms might. This could be a problem for future pre-clinical mechanistic studies as it may never be possible to pin point a single definitive pathophysiological mechanism.

7.1.3 Future investigation of hyperglycaemia in experimental stroke

The studies performed in this thesis, as well as previous in-house studies (Tarr, 2012), demonstrated the effects of hyperglycaemia on acute lesion volume and infarct size using identical methods to induce hyperglycaemia and focal cerebral ischaemia. Although our results appear to be reproducible they are only applicable to a single stroke model which may be a limiting factor. Further studies are therefore needed to determine if hyperglycaemia has the same effect on lesion volume in alternative stroke models. Consideration should be given to the embolic stroke model. This model more closely mimics human stroke but it is seldom used as it produces ischaemic lesions that are more variable in size and location than other MCAO models. This makes it difficult for assessing neuroprotective therapies as large group sizes are required to

overcome this inherent variation. Despite this, the embolic model is the most suitable for assessing the safety and efficacy of antithrombotic drugs and combination therapies. As such, the embolic model would be the most suitable model for assessing the detrimental impact of hyperglycaemia during thrombolyisis. Clinical studies have demonstrated an association between admission hyperglycaemia and an increased risk of haemorrhage with rt-PA induced thrombolysis (Bruno et al., 2002, Alvarez-Sabin et al., 2003, Kase et al., 2001, De Silva et al., 2010). This is supported by the observation that hyperglycaemia induces rt-PA induced haemorrhage after focal cerebral ischaemia in rodents. Since thrombolyisis with rt-PA is currently the only licensed treatment for ischaemic stroke patients it is important to determine the mechanisms underlying this association. Further to this, it is important that novel therapies for PSH are tested in combination with rt-PA to determine whether such therapies can reduce the risk of haemorrhage associated with rt-PA. Fan et al (2013) recently investigated the feasibility of early glycaemic control with insulin combined with rt-PA thrombolysis in a focal embolic stroke model of type 1 diabetic rats. They demonstrated that a combination therapy with insulin and rt-PA significantly reduced brain infarction and swelling and ameliorated rt-PA-associated haemorrhagic transformation 24 hours after stroke (Fan et al., 2013). Similar studies are needed to assess the outcome of hyperglycaemia and rt-PA in non-diabetic rats.

Further studies are also required to assess the impact of hyperglycaemia on CBF in animal models with pre-diabetic status. This is essential because although the effects of hyperglycaemia during ischaemic stroke are reported to be worse in non-diabetic patients, at follow-up many of these patients are found to have underlying dysglycaemia such as impaired glucose tolerance and insulin resistance (Kernan et al., 2005, Matz et al., 2006, Vancheri et al., 2005). Similar to diabetes, these pre-diabetic conditions could lead to changes in the cerebrovasculature that may influence vascular tone and integrity which can ultimately affect CBF and the magnitude of ischaemic injury.

7.1.4 Clinical management of post-stroke hyperglycaemia

Current European and American guidelines for the management of PSH recommend intervention with insulin to treat hyperglycaemia. The European

Stroke Initiative guidelines recommend treatment of hyperglycaemia with insulin when blood glucose levels exceed 10mmol/L (European Stroke Organisation Executive and Committee, 2008), whereas the American Stroke Association state that it is reasonable to treat hyperglycaemia in acute ischaemic stroke to achieve blood glucose levels in the range 140-180mg/dL (7.8-10mmol/L)(Jauch et al., 2013). Despite these recommendations, there is limited evidence from clinical trials that treatment of PSH with insulin improves patient outcome. To date, the GIST-UK trial is the only large-scale trial that has prospectively investigated the influence of glycaemic control on clinical outcome after stroke. The results from GIST-UK show that there was no influence of insulin infusion therapy on the primary outcome measure: 90-day mortality rate, compared to saline infusion although there were several limitations to the study. Firstly GIST-UK enrolled only 933 patients out of the original target of 2355 and was therefore underpowered to enable accurate conclusions about clinical outcome to be made. Secondly, the study enrolled a heterogeneous population of patients, including patients, with lacunar and haemorrhagic strokes as well as patients with a wide range of comorbidities including those with a history of diabetes, hypertension and previous stroke. Lastly, insulin treatment was administered for 24 hours, with the median time to treatment beginning approximately 13 hours after the onset of stroke symptoms. By including such a heterogeneous population the GIST-UK trial could have diluted any treatment effect as studies have shown that the relationship between hyperglycaemia and patient outcome differs between stroke subtypes and the absence or presence of existing comorbidities (Uyttenboogaart et al., 2007, Capes et al., 2001, Kruyt et al., 2008). Furthermore, the results presented in this thesis suggest that insulin treatment in GIST-UK may have been initiated outside the therapeutic time-window. By using MRI we found that the harmful effects of hyperglycaemia occurred during the acute 1-2 hours after stroke onset. If future glucose lowering protocols are to be effective, studies should aim to initiate treatment within this time-window. Although this is a challenging target to meet, if hyperglycaemia does indeed accelerate ischaemic brain damage there will be no benefit of glucose lowering/neuroprotective therapies if they are administered after the damage has been done.

Although the results from GIST-UK were neutral the trial did provide useful data that will aid the design of future clinical trials of which a large multicentre, randomized controlled trial for PSH is currently ongoing. Stroke Hyperglycaemia Insulin Network Effort (SHINE) was established to evaluate the safety and efficacy of targeted glucose control (intravenous insulin with target 4-7mmol/L) versus control therapy (subcutaneous insulin plus basal insulin with a target blood glucose <10mmol/L) in patients with diabetes or admission hyperglycaemia (>6.0mmol/L) within 12 hours of symptom onset. The primary outcome of the trial is functional outcome at 3 months as measured by the modified Rankin Scale score. This trial is in the process of enrolling patients at present and the results won't be available until 2018. The results from SHINE are expected to have a considerable impact on the management of stroke patients with hyperglycaemia. The eligibility criteria for SHINE will result in a stroke population that is less heterogeneous compared to GIST-UK. In addition, the trial also recommends that insulin therapies are given within 3 hours of admission. Therefore subsequent post-hoc analyses from the trial could provide valuable information on the importance of this early time window for treatment. SHINE will also administer insulin treatment for 72 hours after symptom onset. Increasing the length of time that insulin is administered for in comparison to GIST-UK could benefit patients with persistent hyperglycaemia. Blood glucose levels have been reported to decline during the first 24 hours after stroke (Gray et al., 2007, Yong and Kaste, 2008), but can rise again after 24 to 88 hours, regardless of diabetic status (Allport et al., 2006). Administering insulin therapy beyond 24 hours could therefore benefit a wider range of patients. However, active treatment in the acute phase can only be successful as long as there is viable tissue. At present it is still unclear how long the ischaemic penumbra exists for in stroke patients, and whether this time window is influenced by high glucose levels. Therefore although the administration of insulin for 72 hours may lower blood glucose levels it may not have any benefit if there is no viable tissue to salvage. Thus, future clinical trials of glucose lowering therapies for PSH could consider recruiting only patients with evidence of a penumbra, as determined by either perfusion CT or MRI perfusion-diffusion mismatch techniques.

7.1.5 Future strategies for preclinical stroke research:

Experimental stroke research

To date, the neuroprotective effects of more than 1000 interventions for experimental stroke have been published. Of these, only 1 pharmacological treatment: thrombolysis with rt-PA, has successfully translated from the bench to bedside (Figure 7.1, (O'Collins et al., 2006)). There are a number of experimental factors which may explain why so many neuroprotective agents showed efficacy *in vivo* but failed to translate to the human stroke population. Differences between the complexity of the human stroke population and animal populations in experimental stroke studies may be an important factor. Preclinical studies usually involve MCAO in young, healthy animals under anaesthesia with tightly controlled temperature, blood pressure and blood gasses. In contrast, clinical trials permit multiple stroke subtypes and elderly patients with a range of associated variables that can affect prognosis including: comorbidities such as diabetes and hypertension, prior strokes, polypharmacy and poor collateral circulation. Future preclinical studies could address some of these issues by including older animals with comorbidities. For example, an 18 month old rat with diabetes and hypertension would provide a more accurate representation of the clinical stroke population than the 3-4 month old healthy rats used in many previous studies. As well as the need to include aged animals, pre-clinical studies should also incorporate more female animals as the susceptibility and responses to stroke can be different between genders (Wiszniewska et al., 2011, Liu et al., 2009). Females are highly underrepresented in experimental stroke research despite the fact that there are more total incidences of stroke and a higher 30-day mortality rate in woman compared to men (Roger, 2011). In addition to the appropriateness of the experimental animals, discrepancies between the stroke model (transient or permanent), outcome measures (histology vs functional outcomes), study quality (randomization, blinding, consideration of statistical power) therapeutic windows and drug-dosing schedules have also been linked to the failure of neuroprotection strategies to translate from the laboratory to the clinical setting (O'Collins et al., 2006)

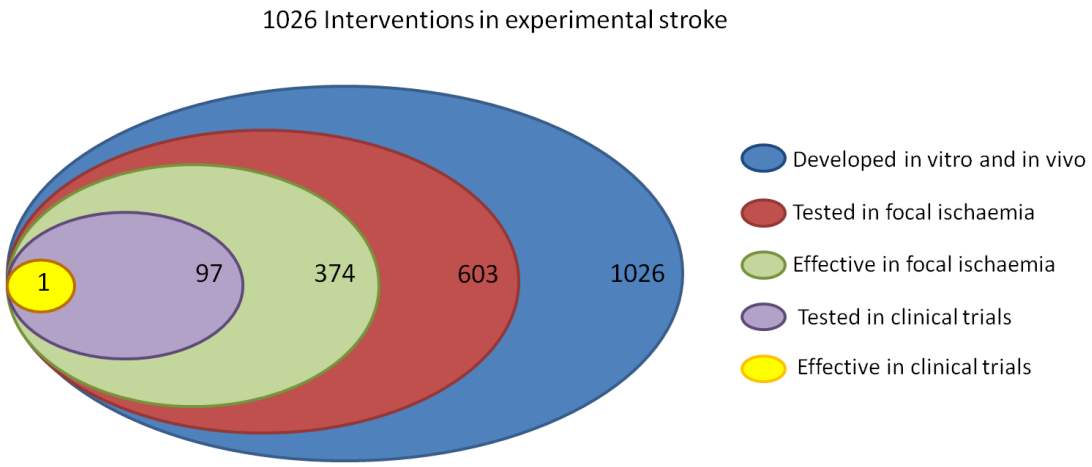

Figure 7.1. 1026 interventions in experimental stroke. A review of pre-clinical stroke studies identified 1026 interventions which had been tested in *in vitro* and *in vivo* experimental stroke models (O'Collins et al., 2006). Of these, 603 were tested in focal ischaemia. 374 were effective in focal ischaemia and of these 97 were tested in clinical trials. To date, only one intervention, thrombolysis with rtPA, has been approved for the treatment of ischaemic stroke (Figure adapted from (Dirnagl, 2015)).

In particular, the higher proportion of studies using transient rather than permanent MCAO models may have contributed significantly to the failure to translate neuroprotective therapies from the bench to bedside. The evolution of ischaemic injury is very different between transient and permanent or gradually reversed focal ischaemia models (embolic MCAO occlusion). In permanent MCAO or gradually reversed focal ischaemia models the evolution of injury follows a similar pattern to that observed clinically. Damage to the core ischaemic region is irreversible but the progression of the penumbra to infarction can be prevented by intervention, but only within a short therapeutic time window of approximately 3 hours after the onset of focal ischaemia (Hossmann, 2012). However in transient focal ischaemia models some damage to the core ischaemic region can recover following prompt reperfusion, but is followed by delayed secondary injury or reperfusion injury that occurs after an interval of as long as 6 to 12 hours (Hossmann, 2012). Intervention within this interval can reduce ischaemic injury but this longer therapeutic time-window is not clinically relevant (Saver et al., 2010). This could explain the failure of many clinical trials which have been designed on the basis of transient MCAO studies and therefore have a therapeutic window which is far too long. For example, a meta-analysis of pre-clinical studies investigating the effects of NXY-59, a neuroprotective drug that showed promise in animal studies but not in the Stroke–Acute Ischaemic NYX Treatment I (SAINT I) trial, reported that the design of SAINT I was heavily biased on successful studies which used transient focal ischaemia models and treatment delays ranging from 15 minutes to 5 hours after ischaemia/reperfusion (Bath et al., 2009).

The poor translational power of preclinical stroke studies led to the establishment of the Stroke Therapy Academic Industry Roundtable (STAIR), which issues guidelines to improve the quality of pre-clinical stroke research ((STAIR), 1999). Some of the recommendations from STAIR highlight the importance of study design factors such as randomization, blinding and sample size calculations as many neuroprotection studies appeared to show selection bias by not including or reporting randomization of treatments and blinding of investigators (van der Worp et al., 2005).

These recommendations from STAIR were considered when designing the experiments in this thesis. For example, rats were randomized to glucose or

vehicle treatment groups using an online randomization plan generator and the investigator was blinded to the treatment groups in each study. Despite this it is possible that some degree of bias was introduced as it was obvious which group received glucose from taking regular blood glucose measurements.

It has also been recognised that many neuroprotective studies using animal models of stroke may have been underpowered to detect the effect they report, as most studies use group sizes with fewer than 10 animals per group (Howells et al., 2014). Power calculations were performed to calculate the number of rats required to determine the effects of hyperglycaemia on the ^{99m}Tc-HMPAO blood flow deficit after MCAO in Chapter 4 and on acute lesion volume in Chapter 5. These calculations were based on the standard deviation and change in infarct volume between glucose and vehicle treated WKY rats from previous in-house studies as this data set was considered the most appropriate.

In order to overcome the translational problems encountered in pre-clinical stroke research (in fact, pre-clinical research as a whole as many of the translational issues in stroke research also apply to other research fields) effort is required, not just from the research community, but also from funding bodies and publishers. If they do not advocate strict adherence to the STAIR guidelines, and continue to fund and publish research which does not adhere to these recommendations, the problem will only continue.

Practical solutions to overcoming the translational failures are being taken and one of these is the establishment of Multi-PART, the first randomized controlled pre-clinical trial network. The key objective of Multi-PART is to bring the rigour of the randomized, controlled, multicentre clinical trial design to the pre-clinical setting. Such a design will help to reduce biases related to individual laboratory practises and conditions and ultimately provide strong, evidence based criteria to inform the decision on whether to move a novel therapeutic into clinical development.

7.1.6 Conclusion

Post-stroke hyperglycaemia is common and associated with worse clinical outcomes. The pathophysiology underlying this association is poorly understood

and most of the proposed pathophysiological mechanisms have been inferred from animal models which are clinically irrelevant. The findings reported in this thesis demonstrated, using a clinically relevant model of PSH, that hyperglycaemia does not exacerbate ischaemic damage by increasing the severity of the ischaemic insult. Therefore the mechanism by which hyperglycaemia exacerbates acute ischaemic damage remains to be determined. The results further demonstrate that hyperglycaemia is harmful to the ischaemic brain during the acute 1-2 hours after the onset of ischaemia, which indicates that there may be a narrow window of opportunity for the treatment of PSH. Future pre-clinical and clinical studies are needed to confirm this as the effects of glucose-lowering therapies given after this time-window could provide no benefit, only the risk of further damage by inducing hypoglycaemia.

List of References

(SSNAP), S. S. N. A. P. 2014. Sentinel Stroke National Audit Programme (SSNAP) Acute Organisational Audit Report 2014.

(STAIR), S. T. A. I. R. 1999. *Stroke,* 30**,** 2752-2758.

AHA/ASA. 2012. *Stroke Risk Factors* [Online]. Available: http://www.strokeassociation.org/STROKEORG/AboutStroke/UnderstandingRisk/Understanding-Stroke-Risk_UCM_308539_SubHomePage.jsp [Accessed 13th September 2015].

AIR, E. L. & KISSELA, B. M. 2007. Diabetes, the metabolic syndrome, and ischemic stroke: epidemiology and possible mechanisms. *Diabetes Care,* 30**,** 3131-40.

ALBERS, G. W., THIJS, V. N., WECHSLER, L., KEMP, S., SCHLAUG, G., SKALABRIN, E., BAMMER, R., KAKUDA, W., LANSBERG, M. G., SHUAIB, A., COPLIN, W., HAMILTON, S., MOSELEY, M. & MARKS, M. P. 2006. Magnetic resonance imaging profiles predict clinical response to early reperfusion: the diffusion and perfusion imaging evaluation for understanding stroke evolution (DEFUSE) study. *Ann Neurol,* 60**,** 508-17.

ALICKE, B. & SCHWARTZ-BLOOM, R. D. 1995. Rapid down-regulation of GABAA receptors in the gerbil hippocampus following transient cerebral ischemia. *J Neurochem,* 65**,** 2808-11.

ALLPORT, L., BAIRD, T., BUTCHER, K., MACGREGOR, L., PROSSER, J., COLMAN, P. & DAVIS, S. 2006. Frequency and temporal profile of poststroke hyperglycemia using continuous glucose monitoring. *Diabetes Care,* 29**,** 1839-1844.

ALLPORT, L. E., BUTCHER, K. S., BAIRD, T. A., MACGREGOR, L., DESMOND, P. M., TRESS, B. M., COLMAN, P. & DAVIS, S. M. 2004. Insular cortical ischemia is independently associated with acute stress hyperglycemia. *Stroke,* 35**,** 1886-1891.

ALVAREZ-SABIN, J., MOLINA, C. A., MONTANER, J., ARENILLAS, J. F., HUERTAS, R., RIBO, M., CODINA, A. & QUINTANA, M. 2003. Effects of admission hyperglycemia on stroke outcome in reperfused tissue plasminogen activator--treated patients. *Stroke,* 34**,** 1235-41.

ANDERSON, R. E., TAN, W. K., MARTIN, H. S. & MEYER, F. B. 1999. Effects of glucose and PaO2 modulation on cortical intracellular acidosis, NADH redox state, and infarction in the ischemic penumbra. *Stroke,* 30**,** 160-70.

ARBOIX, A. 2010. Cardioembolic infarction: a renewed topic of interest. *Curr Cardiol Rev,* 6**,** 137.

ARBOIX, A. 2014. Stroke of Cardioembolic origin: What have we learnt in the past 10 years? *Journal of Cardiology and Therapy,* 1**,** 98-101.

AUWERX, J., BOUILLON, R., COLLEN, D. & GEBOERS, J. 1988. Tissue-type plasminogen activator antigen and plasminogen activator inhibitor in diabetes mellitus. *Arteriosclerosis,* 8**,** 68-72.

AZZIMONDI, G., BASSEIN, L., NONINO, F., FIORANI, L., VIGNATELLI, L., RE, G. & D'ALESSANDRO, R. 1995. Fever in acute stroke worsens prognosis. A prospective study. *Stroke,* 26**,** 2040-3.

BACK, T., GINSBERG, M. D., DIETRICH, W. D. & WATSON, B. D. 1996. Induction of spreading depression in the ischemic hemisphere following experimental middle cerebral artery occlusion: effect on infarct morphology. *J Cereb Blood Flow Metab,* 16**,** 202-13.

BAIRD, A. E., BENFIELD, A., SCHLAUG, G., SIEWERT, B., LOVBLAD, K. O., EDELMAN, R. R. & WARACH, S. 1997. Enlargement of human cerebral

ischemic lesion volumes measured by diffusion-weighted magnetic resonance imaging. *Ann Neurol,* 41**,** 581-9.

BAIRD, T. A., PARSONS, M. W., PHAN, T., BUTCHER, K. S., DESMOND, P. M., TRESS, B. M., COLMAN, P. G., CHAMBERS, B. R. & DAVIS, S. M. 2003. Persistent poststroke hyperglycemia is independently associated with infarct expansion and worse clinical outcome. *Stroke,* 34**,** 2208-14.

BANO, D., YOUNG, K. W., GUERIN, C. J., LEFEUVRE, R., ROTHWELL, N. J., NALDINI, L., RIZZUTO, R., CARAFOLI, E. & NICOTERA, P. 2005. Cleavage of the plasma membrane Na+/Ca2+ exchanger in excitotoxicity. *Cell,* 120**,** 275-85.

BARAZZONI, R., ZANETTI, M., DAVANZO, G., KIWANUKA, E., CARRARO, P., TIENGO, A. & TESSARI, P. 2000. Increased fibrinogen production in type 2 diabetic patients without detectable vascular complications: correlation with plasma glucagon concentrations. *J Clin Endocrinol Metab,* 85**,** 3121-5.

BARDUTZKY, J., SHEN, Q., HENNINGER, N., BOULEY, J., DUONG, T. Q. & FISHER, M. 2005. Differences in ischemic lesion evolution in different rat strains using diffusion and perfusion imaging. *Stroke,* 36**,** 2000-5.

BARON, J. C., BOUSSER, M. G., REY, A., GUILLARD, A., COMAR, D. & CASTAIGNE, P. 1981. Reversal of focal "misery-perfusion syndrome" by extra-intracranial arterial bypass in hemodynamic cerebral ischemia. A case study with 15O positron emission tomography. *Stroke,* 12**,** 454-9.

BARON, J. C., ROUGEMONT, D., SOUSSALINE, F., BUSTANY, P., CROUZEL, C., BOUSSER, M. G. & COMAR, D. 1984. Local interrelationships of cerebral oxygen consumption and glucose utilization in normal subjects and in ischemic stroke patients: a positron tomography study. *J Cereb Blood Flow Metab,* 4**,** 140-9.

BARTUS, R. T., DEAN, R. L., CAVANAUGH, K., EVELETH, D., CARRIERO, D. L. & LYNCH, G. 1995. Time-Related Neuronal Changes Following Middle Cerebral-Artery Occlusion - Implications for Therapeutic Intervention and the Role of Calpain. *Journal of Cerebral Blood Flow and Metabolism,* 15**,** 969-979.

BASKERVILLE, T. A., MCCABE, C., WEIR, C. J., MACRAE, I. M. & HOLMES, W. M. 2012. Noninvasive MRI measurement of CBF: evaluating an arterial spin labelling sequence with 99mTc-HMPAO CBF autoradiography in a rat stroke model. *J Cereb Blood Flow Metab,* 32**,** 973-7.

BATH, P. M., GRAY, L. J., BATH, A. J., BUCHAN, A., MIYATA, T., GREEN, A. R. & INVESTIGATORS, N. X. Y. E. M.-A. I. I. A. W. S. 2009. Effects of NXY-059 in experimental stroke: an individual animal meta-analysis. *Br J Pharmacol,* 157**,** 1157-71.

BEDERSON, J. B., PITTS, L. H., GERMANO, S. M., NISHIMURA, M. C., DAVIS, R. L. & BARTKOWSKI, H. M. 1986. Evaluation of 2,3,5-triphenyltetrazolium chloride as a stain for detection and quantification of experimental cerebral infarction in rats. *Stroke,* 17**,** 1304-8.

BELL, M. A. & BALL, M. J. 1981. Morphometric Comparison of Hippocampal Microvasculature in Aging and Demented People - Diameters and Densities. *Acta Neuropathologica,* 53**,** 299-318.

BERGER, L. & HAKIM, A. M. 1986. The Association of Hyperglycemia with Cerebral Edema in Stroke. *Stroke,* 17**,** 865-871.

BOMONT, L. & MACKENZIE, E. T. 1995. Neuroprotection after focal cerebral ischaemia in hyperglycaemic and diabetic rats. *Neuroscience Letters,* 197**,** 53-6.

BRATANE, B. T., BOULEY, J., SCHNEIDER, A., BASTAN, B., HENNINGER, N. & FISHER, M. 2009. Granulocyte-colony stimulating factor delays PWI/DWI mismatch evolution and reduces final infarct volume in permanent-suture and embolic focal cerebral ischemia models in the rat. *Stroke,* 40**,** 3102-6.

BROUNS, R. & DE DEYN, P. P. 2009. The complexity of neurobiological processes in acute ischemic stroke. *Clinical Neurology and Neurosurgery,* 111**,** 483-495.

BRUNO, A., BILLER, J., ADAMS, H. P., JR., CLARKE, W. R., WOOLSON, R. F., WILLIAMS, L. S. & HANSEN, M. D. 1999. Acute blood glucose level and outcome from ischemic stroke. Trial of ORG 10172 in Acute Stroke Treatment (TOAST) Investigators. *Neurology,* 52**,** 280-4.

BRUNO, A., KENT, T. A., COULL, B. M., SHANKAR, R. R., SAHA, C., BECKER, K. J., KISSELA, B. M. & WILLIAMS, L. S. 2008. Treatment of hyperglycemia in ischemic stroke (THIS) a randomized pilot trial. *Stroke,* 39**,** 384-389.

BRUNO, A., LEVINE, S. R., FRANKEL, M. R., BROTT, T. G., LIN, Y., TILLEY, B. C., LYDEN, P. D., BRODERICK, J. P., KWIATKOWSKI, T. G. & FINEBERG, S. E. 2002. Admission glucose level and clinical outcomes in the NINDS rt-PA Stroke Trial. *Neurology,* 59**,** 669-74.

BULLOCK, R., PATTERSON, J. & PARK, C. 1991. Evaluation of 99mTc-hexamethylpropyleneamine oxime cerebral blood flow mapping after acute focal ischemia in rats. *Stroke,* 22**,** 1284-90.

CAMPBELL, B. C. & MACRAE, I. M. 2015. Translational perspectives on perfusion-diffusion mismatch in ischemic stroke. *Int J Stroke,* 10**,** 153-62.

CANDELISE, L., LANDI, G., ORAZIO, E. N. & BOCCARDI, E. 1985. Prognostic significance of hyperglycemia in acute stroke. *Arch Neurol,* 42**,** 661-3.

CAPES, S. E., HUNT, D., MALMBERG, K., PATHAK, P. & GERSTEIN, H. C. 2001. Stress hyperglycemia and prognosis of stroke in nondiabetic and diabetic patients: a systematic overview. *Stroke,* 32**,** 2426-32.

CARMICHAEL, S. T. 2005. Rodent models of focal stroke: size, mechanism, and purpose. *NeuroRx,* 2**,** 396-409.

CARSWELL, H. V. O., ANDERSON, N. H., CLARK, J. S., GRAHAM, D., JEFFS, B., DOMINICZAK, A. F. & MACRAE, I. M. 1999. Genetic and gender influences on sensitivity to focal cerebral ischemia in the stroke-prone spontaneously hypertensive rat. *Hypertension,* 33**,** 681-685.

CASSADY, C. J., PHILLIS, J. W. & O'REGAN, M. H. 2001. Further studies on the effects of topical lactate on amino acid efflux from the ischemic rat cortex. *Brain Res,* 901**,** 30-7.

CASTILLO, J., RAMA, R. & DAVALOS, A. 2000. Nitric oxide-related brain damage in acute ischemic stroke. *Stroke,* 31**,** 852-7.

CHAN, P. H. 2001. Reactive oxygen radicals in signaling and damage in the ischemic brain. *Journal of Cerebral Blood Flow and Metabolism,* 21**,** 2-14.

CHAN, S. L. & MATTSON, M. P. 1999a. Caspase and calpain substrates: roles in synaptic plasticity and cell death. *J Neurosci Res,* 58**,** 167-90.

CHAN, S. L. & MATTSON, M. P. 1999b. Caspase and calpain substrates: Roles in synaptic plasticity and cell death. *J Neurosci Res,* 58**,** 167-190.

CHEN, H., CHOPP, M. & WELCH, K. M. 1991. Effect of mild hyperthermia on the ischemic infarct volume after middle cerebral artery occlusion in the rat. *Neurology,* 41**,** 1133-5.

CHOI, S., KANG, S. W., LEE, G. J., CHOI, S. K., CHAE, S. J., PARK, H. K. & CHUNG, J. H. 2010. Real-time ischemic condition monitoring in normoglycemic and hyperglycemic rats. *Physiol Meas,* 31**,** 439-50.

COYLE, P. & JOKELAINEN, P. T. 1983. Differential Outcome to Middle Cerebral-Artery Occlusion in Spontaneously Hypertensive Stroke-Prone Rats (Shrsp) and Wistar Kyoto (Wky) Rats. *Stroke,* 14**,** 605-611.

DANDONA, P., JAMES, I. M., NEWBURY, P. A., WOOLLARD, M. L. & BECKETT, A. G. 1978. Cerebral Blood-Flow in Diabetes-Mellitus - Evidence of Abnormal Cerebrovascular Reactivity. *British Medical Journal,* 2**,** 325-326.

DARBY, D. G., BARBER, P. A., GERRATY, R. P., DESMOND, P. M., YANG, Q., PARSONS, M., LI, T., TRESS, B. M. & DAVIS, S. M. 1999. Pathophysiological topography of acute ischemia by combined diffusion-weighted and perfusion MRI. *Stroke,* 30**,** 2043-52.

DAVIS, S. M., DONNAN, G. A., PARSONS, M. W., LEVI, C., BUTCHER, K. S., PEETERS, A., BARBER, P. A., BLADIN, C., DE SILVA, D. A., BYRNES, G., CHALK, J. B., FINK, J. N., KIMBER, T. E., SCHULTZ, D., HAND, P. J., FRAYNE, J., HANKEY, G., MUIR, K., GERRATY, R., TRESS, B. M. & DESMOND, P. M. 2008. Effects of alteplase beyond 3 h after stroke in the Echoplanar Imaging Thrombolytic Evaluation Trial (EPITHET): a placebo-controlled randomised trial. *Lancet Neurol,* 7**,** 299-309.

DAWSON, D. A. & HALLENBECK, J. M. 1996. Acute focal ischemia-induced alterations in MAP2 immunostaining: description of temporal changes and utilization as a marker for volumetric assessment of acute brain injury. *J Cereb Blood Flow Metab,* 16**,** 170-4.

DE SILVA, D. A., EBINGER, M., CHRISTENSEN, S., PARSONS, M. W., LEVI, C., BUTCHER, K., BARBER, P. A., BLADIN, C., DONNAN, G. A., DAVIS, S. M. & THROMBOLYTIC, E. I. 2010. Baseline Diabetic Status and Admission Blood Glucose Were Poor Prognostic Factors in the EPITHET Trial. *Cerebrovascular Diseases,* 29**,** 14-21.

DECOURTENMYERS, G., MYERS, R. E. & SCHOOLFIELD, L. 1988. Hyperglycemia Enlarges Infarct Size in Cerebrovascular Occlusion in Cats. *Stroke,* 19**,** 623-630.

DECOURTENMYERS, G. M., KLEINHOLZ, M., WAGNER, K. R. & MYERS, R. E. 1989. Fatal Strokes in Hyperglycemic Cats. *Stroke,* 20**,** 1707-1715.

DEHMELT, L. & HALPAIN, S. 2005. The MAP2/Tau family of microtubule-associated proteins. *Genome Biol,* 6**,** 204.

DEMCHUK, A. M., MORGENSTERN, L. B., KRIEGER, D. W., LINDA CHI, T., HU, W., WEIN, T. H., HARDY, R. J., GROTTA, J. C. & BUCHAN, A. M. 1999. Serum glucose level and diabetes predict tissue plasminogen activator-related intracerebral hemorrhage in acute ischemic stroke. *Stroke,* 30**,** 34-9.

DENNY, J. B., POLAN-CURTAIN, J., GHUMAN, A., WAYNER, M. J. & ARMSTRONG, D. L. 1990. Calpain inhibitors block long-term potentiation. *Brain Res,* 534**,** 317-20.

DHINDSA, S., TRIPATHY, D., MOHANTY, P., GHANIM, H., SYED, T., ALJADA, A. & DANDONA, P. 2004. Differential effects of glucose and alcohol on reactive oxygen species generation and intranuclear nuclear factor-kappaB in mononuclear cells. *Metabolism,* 53**,** 330-4.

DIABETES.CO.UK. *Blood Sugar Level Range* [Online]. Available: http://www.diabetes.co.uk/diabetes_care/blood-sugar-level-ranges.html [Accessed 05/02/2016.

DIABETES.CO.UK. *Convert whole blood glucose results to plasma readings* [Online]. Available: http://www.diabetes.co.uk/whole-blood-readings-to-plasma-converter.html [Accessed 15/02/2015.

DIRNAGL, U. 2015. Is preclinical stroke research broken, and if so, how can we fix it? UK Preclinical Stroke Symposium.

DIRNAGL, U., IADECOLA, C. & MOSKOWITZ, M. A. 1999. Pathobiology of ischaemic stroke: an integrated view. *Trends Neurosci,* 22**,** 391-7.

DONNAN, G. A., BARON, J., DAVIS, S. & SHARP, F. R. 2007. *The Ischaemic Penumbra,* New York, Informa Healthcare.

DUCKROW, R. B. 1995. Decreased cerebral blood flow during acute hyperglycemia. *Brain Res,* 703**,** 145-50.

DUCKROW, R. B., BEARD, D. C. & BRENNAN, R. W. 1985. Regional cerebral blood flow decreases during hyperglycemia. *Ann Neurol,* 17**,** 267-72.

DUCKROW, R. B., BEARD, D. C. & BRENNAN, R. W. 1987. Regional cerebral blood flow decreases during chronic and acute hyperglycemia. *Stroke,* 18**,** 52-8.

DUVERGER, D. & MACKENZIE, E. T. 1988. The Quantification of Cerebral Infarction Following Focal Ischemia in the Rat: Influence of Strain, Arterial Pressure, Blood Glucose Concentration, and Age. *J Cereb Blood Flow Metab,* 8**,** 449-461.

ENDRES, M., NAMURA, S., SHIMIZU-SASAMATA, M., WAEBER, C., ZHANG, L., GOMEZ-ISLA, T., HYMAN, B. T. & MOSKOWITZ, M. A. 1998. Attenuation of delayed neuronal death after mild focal ischemia in mice by inhibition of the caspase family. *J Cereb Blood Flow Metab,* 18**,** 238-47.

EUROPEAN STROKE ORGANISATION EXECUTIVE, C. & COMMITTEE, E. S. O. W. 2008. Guidelines for management of ischaemic stroke and transient ischaemic attack 2008. *Cerebrovasc Dis,* 25**,** 457-507.

FAN, X., NING, M. M., LO, E. H. & WANG, X. Y. 2013. Early Insulin Glycemic Control Combined With tPA Thrombolysis Reduces Acute Brain Tissue Damages in a Focal Embolic Stroke Model of Diabetic Rats. *Stroke,* 44**,** 255-259.

FINFER, S., BLAIR, D., BELLOMO, R., MCARTHUR, C., MITCHELL, I., MYBURGH, J. & AL., E. 2009. Intensive versus Conventional Glucose Control in Critically Ill Patients. *New England Journal of Medicine,* 360**,** 1283-1297.

FISCHER, I., ROMANO-CLARKE, G. & GRYNSPAN, F. 1991. Calpain-mediated proteolysis of microtubule associated proteins MAP1B and MAP2 in developing brain. *Neurochem Res,* 16**,** 891-8.

FOLBERGROVA, J., MEMEZAWA, H., SMITH, M. L. & SIESJO, B. K. 1992. Focal and perifocal changes in tissue energy state during middle cerebral artery occlusion in normo- and hyperglycemic rats. *J Cereb Blood Flow Metab,* 12**,** 25-33.

FOLEY, L. M., HITCHENS, T. K., BARBE, B., ZHANG, F., HO, C., RAO, G. R. & NEMOTO, E. M. 2010. Quantitative temporal profiles of penumbra and infarction during permanent middle cerebral artery occlusion in rats. *Transl Stroke Res,* 1**,** 220-9.

GARG, R., CHAUDHURI, A., MUNSCHAUER, F. & DANDONA, P. 2006. Hyperglycemia, insulin, and acute ischemic stroke: a mechanistic justification for a trial of insulin infusion therapy. *Stroke,* 37**,** 267-73.

GARTSHORE, G., PATTERSON, J. & MACRAE, I. M. 1997. Influence of ischemia and reperfusion on the course of brain tissue swelling and blood-brain barrier permeability in a rodent model of transient focal cerebral ischemia. *Exp Neurol,* 147**,** 353-60.

GERALDES, P., HIRAOKA-YAMAMOTO, J., MATSUMOTO, M., CLERMONT, A., LEITGES, M., MARETTE, A., AIELLO, L. P., KERN, T. S. & KING, G. L. 2009. Activation of PKC-delta and SHP-1 by hyperglycemia causes vascular cell apoptosis and diabetic retinopathy. *Nat Med,* 15**,** 1298-306.

GERRIETS, T., STOLZ, E., WALBERER, M., MULLER, C., KLUGE, A., BACHMANN, A., FISHER, M., KAPS, M. & BACHMANN, G. 2004. Noninvasive

quantification of brain edema and the space-occupying effect in rat stroke models using magnetic resonance imaging. *Stroke,* 35**,** 566-71.

GIBSON, B. R., GALIATSATOS, P., RABIEE, A., EATON, L., ABU-HAMDAH, R., CHRISTMAS, C., MILNER, S. M., ANDERSEN, D. K. & ELAHI, D. 2009. Intensive insulin therapy confers a similar survival benefit in the burn intensive care unit to the surgical intensive care unit. *Surgery,* 146**,** 922-930.

GILL, R., ANDINE, P., HILLERED, L., PERSSON, L. & HAGBERG, H. 1992. The effect of MK-801 on cortical spreading depression in the penumbral zone following focal ischaemia in the rat. *J Cereb Blood Flow Metab,* 12**,** 371-9.

GINSBERG, M. D., PRADO, R., DIETRICH, W. D., BUSTO, R. & WATSON, B. D. 1987. Hyperglycemia reduces the extent of cerebral infarction in rats. *Stroke,* 18**,** 570-4.

GINSBERG, M. D., WELSH, F. A. & BUDD, W. W. 1980. Deleterious effect of glucose pretreatment on recovery from diffuse cerebral ischemia in the cat. I. Local cerebral blood flow and glucose utilization. *Stroke,* 11**,** 347-54.

GISSELSSON, L., SMITH, M. L. & SIESJO, B. K. 1999. Hyperglycemia and focal brain ischemia. *J Cereb Blood Flow Metab,* 19**,** 288-97.

GO, A. S. 2009. The ACTIVE pursuit of stroke prevention in patients with atrial fibrillation. *N Engl J Med,* 360**,** 2127-9.

GOLL, D. E., THOMPSON, V. F., LI, H., WEI, W. & CONG, J. 2003. The calpain system. *Physiological Reviews,* 83**,** 731-801.

GRAY, C. S., HILDRETH, A. J., SANDERCOCK, P. A., O'CONNELL, J. E., JOHNSTON, D. E., CARTLIDGE, N. E., BAMFORD, J. M., JAMES, O. F. & ALBERTI, K. G. 2007. Glucose-potassium-insulin infusions in the management of post-stroke hyperglycaemia: the UK Glucose Insulin in Stroke Trial (GIST-UK). *Lancet Neurol,* 6**,** 397-406.

GRAY, C. S., SCOTT, J. F., FRENCH, J. M., ALBERTI, K. G. & O'CONNELL, J. E. 2004. Prevalence and prediction of unrecognised diabetes mellitus and impaired glucose tolerance following acute stroke. *Age Ageing,* 33**,** 71-7.

GRIFFITH, D. N., SAIMBI, S., LEWIS, C., TOLFREE, S. & BETTERIDGE, D. J. 1987. Abnormal cerebrovascular carbon dioxide reactivity in people with diabetes. *Diabet Med,* 4**,** 217-20.

GUZIK, T. J., WEST, N. E., BLACK, E., MCDONALD, D., RATNATUNGA, C., PILLAI, R. & CHANNON, K. M. 2000. Vascular superoxide production by NAD(P)H oxidase: association with endothelial dysfunction and clinical risk factors. *Circ Res,* 86**,** E85-90.

HACKE, W., ALBERS, G., AL-RAWI, Y., BOGOUSSLAVSKY, J., DAVALOS, A., ELIASZIW, M., FISCHER, M., FURLAN, A., KASTE, M., LEES, K. R., SOEHNGEN, M. & WARACH, S. 2005. The Desmoteplase in Acute Ischemic Stroke Trial (DIAS): a phase II MRI-based 9-hour window acute stroke thrombolysis trial with intravenous desmoteplase. *Stroke,* 36**,** 66-73.

HACKE, W., KASTE, M., BLUHMKI, E., BROZMAN, M., DAVALOS, A., GUIDETTI, D., LARRUE, V., LEES, K. R., MEDEGHRI, Z., MACHNIG, T., SCHNEIDER, D., VON KUMMER, R., WAHLGREN, N., TONI, D. & INVESTIGATORS, E. 2008. Thrombolysis with alteplase 3 to 4.5 hours after acute ischemic stroke. *N Engl J Med,* 359**,** 1317-29.

HAKIM, A. M., EVANS, A. C., BERGER, L., KUWABARA, H., WORSLEY, K., MARCHAL, G., BIEL, C., POKRUPA, R., DIKSIC, M., MEYER, E. & ET AL. 1989. The effect of nimodipine on the evolution of human cerebral infarction studied by PET. *J Cereb Blood Flow Metab,* 9**,** 523-34.

HALL, C. N., REYNELL, C., GESSLEIN, B., HAMILTON, N. B., MISHRA, A., SUTHERLAND, B. A., O'FARRELL, F. M., BUCHAN, A. M., LAURITZEN, M. & ATTWELL, D. 2014. Capillary pericytes regulate cerebral blood flow in health and disease. *Nature,* 508**,** 55-60.

HANKEY, G. J. & WARLOW, C. I. 1999. Treatment and secondary prevention of stroke: evidence, costs, and effects on individuals and populations. *Lancet,* 354**,** 1457-1463.

HASEGAWA, Y., FISHER, M., LATOUR, L. L., DARDZINSKI, B. J. & SOTAK, C. H. 1994. MRI diffusion mapping of reversible and irreversible ischemic injury in focal brain ischemia. *Neurology,* 44**,** 1484-90.

HEISS, W.-D. 2000. Ischemic Penumbra[colon] Evidence From Functional Imaging in Man. *J Cereb Blood Flow Metab,* 20**,** 1276-1293.

HEISS, W. D. 2003. Best measure of ischemic penumbra: positron emission tomography. *Stroke,* 34**,** 2534-5.

HEISS, W. D., HUBER, M., FINK, G. R., HERHOLZ, K., PIETRZYK, U., WAGNER, R. & WIENHARD, K. 1992. Progressive derangement of periinfarct viable tissue in ischemic stroke. *J Cereb Blood Flow Metab,* 12**,** 193-203.

HEISS, W. D., KRACHT, L., GROND, M., RUDOLF, J., BAUER, B., WIENHARD, K. & PAWLIK, G. 2000. Early [(11)C]Flumazenil/H(2)O positron emission tomography predicts irreversible ischemic cortical damage in stroke patients receiving acute thrombolytic therapy. *Stroke,* 31**,** 366-9.

HILL, M. D. 2014. Stroke and diabetes mellitus. *Handb Clin Neurol,* 126**,** 167-74.

HILL, M. D. & BUCHAN, A. M. 2005. Thrombolysis for acute ischemic stroke: results of the Canadian Alteplase for Stroke Effectiveness Study. *CMAJ,* 172**,** 1307-12.

HIRSCHI, K. K. & D'AMORE, P. A. 1996. Pericytes in the microvasculature. *Cardiovasc Res,* 32**,** 687-98.

HOEHN-BERLAGE, M., NORRIS, D. G., KOHNO, K., MIES, G., LEIBFRITZ, D. & HOSSMANN, K. A. 1995. Evolution of regional changes in apparent diffusion coefficient during focal ischemia of rat brain: the relationship of quantitative diffusion NMR imaging to reduction in cerebral blood flow and metabolic disturbances. *J Cereb Blood Flow Metab,* 15**,** 1002-11.

HONG, S. C., GOTO, Y., LANZINO, G., SOLEAU, S., KASSELL, N. F. & LEE, K. S. 1994a. Neuroprotection with a calpain inhibitor in a model of focal cerebral ischemia. *Stroke,* 25**,** 663-9.

HONG, S. C., LANZINO, G., GOTO, Y., KANG, S. K., SCHOTTLER, F., KASSELL, N. F. & LEE, K. S. 1994b. Calcium-activated proteolysis in rat neocortex induced by transient focal ischemia. *Brain Res,* 661**,** 43-50.

HOSSMANN, K. A. 1994. Viability thresholds and the penumbra of focal ischemia. *Ann Neurol,* 36**,** 557-65.

HOSSMANN, K. A. 2012. The two pathophysiologies of focal brain ischemia: implications for translational stroke research. *J Cereb Blood Flow Metab*.

HOWELLS, D. W., SENA, E. S. & MACLEOD, M. R. 2014. Bringing rigour to translational medicine. *Nat Rev Neurol,* 10**,** 37-43.

HUANG, N. C., WEI, J. & QUAST, M. J. 1996a. A comparison of the early development of ischemic brain damage in normoglycemic and hyperglycemic rats using magnetic resonance imaging. *Exp Brain Res,* 109**,** 33-42.

HUANG, N. C., WEI, J. & QUEST, M. J. 1996b. Acomparison of the early development of ischaemic brain damage in normoglycaemic and hyperglycaemic rats using magentic resonance imaging. *Experimental Brain Research,* 109**,** 33-42.

IADECOLA, C. & DAVISSON, R. L. 2008. Hypertension and cerebrovascular dysfunction. *Cell Metabolism,* 7**,** 476-484.

ISD_SCOTLAND 2014. Scottish Stroke Care Audit, 2014 National Report.

JAUCH, E. C., SAVER, J. L., ADAMS, H. P., JR., BRUNO, A., CONNORS, J. J., DEMAERSCHALK, B. M., KHATRI, P., MCMULLAN, P. W., JR., QURESHI, A. I., ROSENFIELD, K., SCOTT, P. A., SUMMERS, D. R., WANG, D. Z., WINTERMARK, M., YONAS, H., AMERICAN HEART ASSOCIATION STROKE, C., COUNCIL ON CARDIOVASCULAR, N., COUNCIL ON PERIPHERAL VASCULAR, D. & COUNCIL ON CLINICAL, C. 2013. Guidelines for the early management of patients with acute ischemic stroke: a guideline for healthcare professionals from the American Heart Association/American Stroke Association. *Stroke,* 44**,** 870-947.

JICKLING, G. C., STAMOVA, B., ANDER, B. P., ZHAN, X., TIAN, Y., LIU, D., XU, H., JOHNSTON, S. C., VERRO, P. & SHARP, F. R. 2011. Profiles of lacunar and nonlacunar stroke. *Ann Neurol,* 70**,** 477-85.

JOHNSTON, K. C., HALL, C. E., KISSELA, B. M., BLECK, T. P. & CONAWAY, M. R. 2009. Glucose Regulation in Acute Stroke Patients (GRASP) trial: a randomized pilot trial. *Stroke,* 40**,** 3804-9.

JOU, I. M., TSAI, Y. T., TSAI, C. L., WU, M. H., CHANG, H. Y. & WANG, N. S. 2000. Simplified rat intubation using a new oropharyngeal intubation wedge. *J Appl Physiol (1985),* 89**,** 1766-70.

JUHAN-VAGUE, I., ROUL, C., ALESSI, M. C., ARDISSONE, J. P., HEIM, M. & VAGUE, P. 1989. Increased plasminogen activator inhibitor activity in non insulin dependent diabetic patients--relationship with plasma insulin. *Thromb Haemost,* 61**,** 370-3.

JUNKER, U., JAGGI, C., BESTETTI, G. & ROSSI, G. L. 1985. Basement-Membrane of Hypothalamus and Cortex Capillaries from Normotensive and Spontaneously Hypertensive Rats with Streptozotocin-Induced Diabetes. *Acta Neuropathologica,* 65**,** 202-208.

KAGSTROM, E., SMITH, M. L. & SIESJO, B. K. 1983. Recirculation in the rat brain following incomplete ischemia. *J Cereb Blood Flow Metab,* 3**,** 183-92.

KAMADA, H., YU, F., NITO, C. & CHAN, P. H. 2007. Influence of hyperglycemia on oxidative stress and matrix metalloproteinase-9 activation after focal cerebral ischemia/reperfusion in rats: relation to blood-brain barrier dysfunction. *Stroke,* 38**,** 1044-9.

KANNEL, W. B., D'AGOSTINO, R. B. & BELANGER, A. J. 1987. Fibrinogen, cigarette smoking, and risk of cardiovascular disease: insights from the Framingham Study. *Am Heart J,* 113**,** 1006-10.

KASE, C. S., FURLAN, A. J., WECHSLER, L. R., HIGASHIDA, R. T., ROWLEY, H. A., HART, R. G., MOLINARI, G. F., FREDERICK, L. S., ROBERTS, H. C., GEBEL, J. M., SILA, C. A., SCHULZ, G. A., ROBERTS, R. S., GENT, M. & INVESTIGATORS, P. I. 2001. Cerebral hemorrhage after intra-arterial thrombolysis for ischemic stroke - The PROACT II trial. *Neurology,* 57**,** 1603-1610.

KATSURA, K., KRISTIAN, T. & SIESJO, B. K. 1994. Energy metabolism, ion homeostasis, and cell damage in the brain. *Biochem Soc Trans,* 22**,** 991-6.

KAWAI, N., KEEP, R. F. & BETZ, A. L. 1997a. Effects of hyperglycemia on cerebral blood flow and edema formation after carotid artery occlusion in Fischer 344 rats. *Acta Neurochir Suppl,* 70**,** 34-6.

KAWAI, N., KEEP, R. F. & BETZ, A. L. 1997b. Hyperglycemia and the vascular effects of cerebral ischemia. *Acta Neurochir Suppl,* 70**,** 27-9.

KAWAI, N., KEEP, R. F., BETZ, A. L. & NAGAO, S. 1998. Hyperglycemia induces progressive changes in the cerebral microvasculature and blood-brain

barrier transport during focal cerebral ischemia. *Acta Neurochir Suppl,* 71, 219-21.

KERNAN, W. N., VISCOLI, C. M., INZUCCHI, S. E., BRASS, L. M., BRAVATA, D. M., SHULMAN, G. I. & MCVEETY, J. C. 2005. Prevalence of abnormal glucose tolerance following a transient ischemic attack or ischemic stroke. *Arch Intern Med,* 165, 227-33.

KIDWELL, C. S., SAVER, J. L., MATTIELLO, J., STARKMAN, S., VINUELA, F., DUCKWILER, G., GOBIN, Y. P., JAHAN, R., VESPA, P., KALAFUT, M. & ALGER, J. R. 2000. Thrombolytic reversal of acute human cerebral ischemic injury shown by diffusion/perfusion magnetic resonance imaging. *Ann Neurol,* 47, 462-9.

KIERS, L., DAVIS, S. M., LARKINS, R., HOPPER, J., TRESS, B., ROSSITER, S. C., CARLIN, J. & RATNAIKE, S. 1992a. Stroke topography and outcome in relation to hyperglycaemia and diabetes. *J Neurol Neurosurg Psychiatry,* 55, 263-70.

KIERS, L., DAVIS, S. M., LARKINS, R., HOPPER, J., TRESS, B., ROSSITER, S. C., CARLIN, J. & RATNAIKE, S. 1992b. Stroke Topography and Outcome in Relation to Hyperglycemia and Diabetes. *Journal of Neurology Neurosurgery and Psychiatry,* 55, 263-270.

KIM, Y., BUSTO, R., DIETRICH, W. D., KRAYDIEH, S. & GINSBERG, M. D. 1996. Delayed postischemic hyperthermia in awake rats worsens the histopathological outcome of transient focal cerebral ischemia. *Stroke,* 27, 2274-80; discussion 2281.

KITTAKA, M., WANG, L., SUN, N., SCHREIBER, S. S., SEEDS, N. W., FISHER, M. & ZLOKOVIC, B. V. 1996. Brain capillary tissue plasminogen activator in a diabetes stroke model. *Stroke,* 27, 712-9.

KRAFT, S. A., LARSON, C. P., JR., SHUER, L. M., STEINBERG, G. K., BENSON, G. V. & PEARL, R. G. 1990. Effect of hyperglycemia on neuronal changes in a rabbit model of focal cerebral ischemia. *Stroke,* 21, 447-50.

KRISHNAMURTHI, R. V., FEIGIN, V. L., FOROUZANFAR, M. H., MENSAH, G. A., CONNOR, M., BENNETT, D. A., MORAN, A. E., SACCO, R. L., ANDERSON, L. M., TRUELSEN, T., O'DONNELL, M., VENKETASUBRAMANIAN, N., BARKER-COLLO, S., LAWES, C. M., WANG, W., SHINOHARA, Y., WITT, E., EZZATI, M., NAGHAVI, M., MURRAY, C., GLOBAL BURDEN OF DISEASES, I. R. F. S. & GROUP, G. B. D. S. E. 2013. Global and regional burden of first-ever ischaemic and haemorrhagic stroke during 1990-2010: findings from the Global Burden of Disease Study 2010. *Lancet Glob Health,* 1, e259-81.

KRUYT, N. D., NYS, G. M., VAN DER WORP, H. B., VAN ZANDVOORT, M. J., KAPPELLE, L. J. & BIESSELS, G. J. 2008. Hyperglycemia and cognitive outcome after ischemic stroke. *J Neurol Sci,* 270, 141-7.

LAI, C. H. & KUO, K. H. 2005. The critical component to establish in vitro BBB model: Pericyte. *Brain Research Reviews,* 50, 258-265.

LAMANNA, J. C., GRIFFITH, J. K., CORDISCO, B. R., LIN, C. W. & LUST, W. D. 1992. Intracellular pH in rat brain in vivo and in brain slices. *Can J Physiol Pharmacol,* 70 Suppl, S269-77.

LANSBERG, M. G., STRAKA, M., KEMP, S., MLYNASH, M., WECHSLER, L. R., JOVIN, T. G., WILDER, M. J., LUTSEP, H. L., CZARTOSKI, T. J., BERNSTEIN, R. A., CHANG, C. W., WARACH, S., FAZEKAS, F., INOUE, M., TIPIRNENI, A., HAMILTON, S. A., ZAHARCHUK, G., MARKS, M. P., BAMMER, R., ALBERS, G. W. & INVESTIGATORS, D. S. 2012. MRI profile and response to endovascular reperfusion after stroke (DEFUSE 2): a prospective cohort study. *Lancet Neurol,* 11, 860-7.

LASSEN, N. A., ANDERSEN, A. R., FRIBERG, L. & PAULSON, O. B. 1988. The retention of [99mTc]-d,l-HM-PAO in the human brain after intracarotid bolus injection: a kinetic analysis. *J Cereb Blood Flow Metab,* 8**,** S13-22.

LE, D. A., WU, Y., HUANG, Z., MATSUSHITA, K., PLESNILA, N., AUGUSTINACK, J. C., HYMAN, B. T., YUAN, J., KUIDA, K., FLAVELL, R. A. & MOSKOWITZ, M. A. 2002. Caspase activation and neuroprotection in caspase-3- deficient mice after in vivo cerebral ischemia and in vitro oxygen glucose deprivation. *Proc Natl Acad Sci U S A,* 99**,** 15188-93.

LETOURNEUR, A., ROUSSEL, S., TOUTAIN, J., BERNAUDIN, M. & TOUZANI, O. 2011. Impact of genetic and renovascular chronic arterial hypertension on the acute spatiotemporal evolution of the ischemic penumbra: a sequential study with MRI in the rat. *J Cereb Blood Flow Metab,* 31**,** 504-13.

LEVINE, S. & SALTZMAN, A. 2001. Peritoneal toxicity of water: a model of chronic peritonitis caused by osmotic dysequilibrium in rats. *J Appl Toxicol,* 21**,** 303-6.

LI, F., CARANO, R. A. D., IRIE, K., SOTAK, C. H. & FISHER, M. 2000a. Temporal evolution of average apparent diffusion coefficient threshold to define ischemic abnormalities in a rat permanent occlusion model. *Journal of Stroke and Cerebrovascular Diseases,* 9**,** 1-7.

LI, F., OMAE, T. & FISHER, M. 1999. Spontaneous hyperthermia and its mechanism in the intraluminal suture middle cerebral artery occlusion model of rats. *Stroke,* 30**,** 2464-70; discussion 2470-1.

LI, P. A., HOWLETT, W., HE, Q. P., MIYASHITA, H., SIDDIQUI, M. & SHUAIB, A. 1998. Postischemic treatment with calpain inhibitor MDL 28170 ameliorates brain damage in a gerbil model of global ischemia. *Neuroscience Letters,* 247**,** 17-20.

LI, P. A., SHUAIB, A., MIYASHITA, H., HE, Q. P. & SIESJO, B. K. 2000b. Hyperglycemia enhances extracellular glutamate accumulation in rats subjected to forebrain ischemia. *Stroke,* 31**,** 183-191.

LI, P. A., SHUAIB, A., MIYASHITA, H., HE, Q. P., SIESJO, B. K. & WARNER, D. S. 2000c. Hyperglycemia enhances extracellular glutamate accumulation in rats subjected to forebrain ischemia. *Stroke,* 31**,** 183-92.

LI, W. A., MOORE-LANGSTON, S., CHAKRABORTY, T., RAFOLS, J. A., CONTI, A. C. & DING, Y. 2013. Hyperglycemia in stroke and possible treatments. *Neurol Res,* 35**,** 479-91.

LI, Z. G., BRITTON, M., SIMA, A. A. & DUNBAR, J. C. 2004. Diabetes enhances apoptosis induced by cerebral ischemia. *Life Sci,* 76**,** 249-62.

LIN, B., GINSBERG, M. D., BUSTO, R. & LI, L. 2000. Hyperglycemia triggers massive neutrophil deposition in brain following transient ischemia in rats. *Neurosci Lett,* 278**,** 1-4.

LIN, V. W., BROSGOL, Y., HOMEL, P., HSU, E., ALI, N., CHATTERJEE, M. & PAVLAKIS, S. G. Young Patients with Diabetes Have Decreased Cerebrovascular Reactivity under Hypercapneic Conditions. *Pediatric Neurology*.

LIU, L., WANG, Z., WANG, X., SONG, L., CHEN, H., BEMEUR, C., STE-MARIE, L. & MONTGOMERY, J. 2007. Comparison of two rat models of cerebral ischemia under hyperglycemic conditions. *Microsurgery,* 27**,** 258-62.

LIU, M., DZIENNIS, S., HURN, P. D. & ALKAYED, N. J. 2009. Mechanisms of gender-linked ischemic brain injury. *Restor Neurol Neurosci,* 27**,** 163-79.

LONGA, E. Z., WEINSTEIN, P. R., CARLSON, S. & CUMMINS, R. 1989. Reversible middle cerebral artery occlusion without craniectomy in rats. *Stroke,* 20**,** 84-91.

LUENGO-FERNANDEZ, R., LEAL, J. & GRAY, A. 2015. UK research spend in 2008 and 2012: comparing stroke, cancer, coronary heart disease and dementia. *BMJ Open,* 5**,** e006648.

LUITSE, M. J., VAN SEETERS, T., HORSCH, A. D., KOOL, H. A., VELTHUIS, B. K., KAPPELLE, L. J. & BIESSELS, G. J. 2013. Admission hyperglycaemia and cerebral perfusion deficits in acute ischaemic stroke. *Cerebrovasc Dis,* 35**,** 163-7.

LYNCH, G. & BAUDRY, M. 1984. The Biochemistry of Memory - a New and Specific Hypothesis. *Science,* 224**,** 1057-1063.

LYTHGOE, M. F., WILLIAMS, S. R., BUSZA, A. L., WIEBE, L., MCEWAN, A. J., GADIAN, D. G. & GORDON, I. 1999. The relationship between magnetic resonance diffusion imaging and autoradiographic markers of cerebral blood flow and hypoxia in an animal stroke model. *Magn Reson Med,* 41**,** 706-14.

MACDOUGALL, N. J. & MUIR, K. W. 2011. Hyperglycaemia and infarct size in animal models of middle cerebral artery occlusion: systematic review and meta-analysis. *J Cereb Blood Flow Metab,* 31**,** 807-18.

MALMBERG, K., RYDEN, L., EFENDIC, S., HERLITZ, J., NICOL, P., WALDENSTROM, A., WEDEL, H. & WELIN, L. 1995. Randomized Trial of Insulin-Glucose Infusion Followed by Subcutaneous Insulin-Treatment in Diabetic-Patients with Acute Myocardial-Infarction (Digami Study) - Effects on Mortality at 1 Year. *Journal of the American College of Cardiology,* 26**,** 57-65.

MARKUS, R., REUTENS, D. C., KAZUI, S., READ, S., WRIGHT, P., PEARCE, D. C., TOCHON-DANGUY, H. J., SACHINIDIS, J. I. & DONNAN, G. A. 2004. Hypoxic tissue in ischaemic stroke: persistence and clinical consequences of spontaneous survival. *Brain,* 127**,** 1427-36.

MARSH, W. R., ANDERSON, R. E. & SUNDT, T. M., JR. 1986. Effect of hyperglycemia on brain pH levels in areas of focal incomplete cerebral ischemia in monkeys. *J Neurosurg,* 65**,** 693-6.

MARTIN, A., ROJAS, S., CHAMORRO, A., FALCON, C., BARGALLO, N. & PLANAS, A. M. 2006. Why does acute hyperglycemia worsen the outcome of transient focal cerebral ischemia? Role of corticosteroids, inflammation, and protein O-glycosylation. *Stroke,* 37**,** 1288-1295.

MARTIN, R. L., LLOYD, H. G. & COWAN, A. I. 1994. The early events of oxygen and glucose deprivation: setting the scene for neuronal death? *Trends Neurosci,* 17**,** 251-7.

MATZ, K., KERESZTES, K., TATSCHL, C., NOWOTNY, M., DACHENHAUSEN, A., BRAININ, M. & TUOMILEHTO, J. 2006. Disorders of glucose metabolism in acute stroke patients: an underrecognized problem. *Diabetes Care,* 29**,** 792-7.

MAYHAN, W. G. & PATEL, K. P. 1995. Acute effects of glucose on reactivity of cerebral microcirculation: role of activation of protein kinase C. *Am J Physiol,* 269**,** H1297-302.

MCCABE, C., GALLAGHER, L., GSELL, W., GRAHAM, D., DOMINICZAK, A. F. & MACRAE, I. M. 2009. Differences in the evolution of the ischemic penumbra in stroke-prone spontaneously hypertensive and Wistar-Kyoto rats. *Stroke,* 40**,** 3864-8.

MCCORMICK, M., HADLEY, D., MCLEAN, J. R., MACFARLANE, J. A., CONDON, B. & MUIR, K. W. 2010. Randomized, controlled trial of insulin for acute poststroke hyperglycemia. *Ann Neurol,* 67**,** 570-8.

MCCUSKEY, P. A. & MCCUSKEY, R. S. 1984. In vivo and electron microscopic study of the development of cerebral diabetic microangiography. *Microcirc Endothelium Lymphatics,* 1**,** 221-44.

MELAMED, E. 1976. Reactive hyperglycaemia in patients with acute stroke. *J Neurol Sci,* 29**,** 267-75.

MENG, X., FISHER, M., SHEN, Q., SOTAK, C. H. & DUONG, T. Q. 2004. Characterizing the diffusion/perfusion mismatch in experimental focal cerebral ischemia. *Ann Neurol,* 55**,** 207-12.

MOFFAT, B. A., CHENEVERT, T. L., HALL, D. E., REHEMTULLA, A. & ROSS, B. D. 2005. Continuous arterial spin labeling using a train of adiabatic inversion pulses. *J Magn Reson Imaging,* 21**,** 290-6.

MOHANTY, P., HAMOUDA, W., GARG, R., ALJADA, A., GHANIM, H. & DANDONA, P. 2000. Glucose challenge stimulates reactive oxygen species (ROS) generation by leucocytes. *J Clin Endocrinol Metab,* 85**,** 2970-3.

MONTANER, J., MOLINA, C. A., MONASTERIO, J., ABILLEIRA, S., ARENILLAS, J. F., RIBO, M., QUINTANA, M. & ALVAREZ-SABIN, J. 2003. Matrix metalloproteinase-9 pretreatment level predicts intracranial hemorrhagic complications after thrombolysis in human stroke. *Circulation,* 107**,** 598-603.

MORETON, F. C., MCCORMICK, M. & MUIR, K. W. 2007. Insular cortex hypoperfusion and acute phase blood glucose after stroke: a CT perfusion study. *Stroke,* 38**,** 407-10.

MOSELEY, M. E., COHEN, Y., MINTOROVITCH, J., CHILEUITT, L., SHIMIZU, H., KUCHARCZYK, J., WENDLAND, M. F. & WEINSTEIN, P. R. 1990. Early detection of regional cerebral ischemia in cats: comparison of diffusion- and T2-weighted MRI and spectroscopy. *Magn Reson Med,* 14**,** 330-46.

MOSKOWITZ, M. A., LO, E. H. & IADECOLA, C. 2010. The Science of Stroke: Mechanisms in Search of Treatments. *Neuron,* 67**,** 181-198.

MUIR, K. W., MCCORMICK, M., BAIRD, T. & ALI, M. 2011. Prevalence, Predictors and Prognosis of Post-Stroke Hyperglycaemia in Acute Stroke Trials: Individual Patient Data Pooled Analysis from the Virtual International Stroke Trials Archive (VISTA). *Cerebrovasc Dis Extra,* 1**,** 17-27.

MURTAGH, B. & SMALLING, R. W. 2006. Cardioembolic stroke. *Curr Atheroscler Rep,* 8**,** 310-6.

NAKAJIMA, T., OCHI, S., ODA, C., ISHII, M. & OGAWA, K. 2011. Ischemic preconditioning attenuates of ischemia-induced degradation of spectrin and tau: implications for ischemic tolerance. *Neurol Sci,* 32**,** 229-39.

NAKAMURA, H., STRONG, A. J., DOHMEN, C., SAKOWITZ, O. W., VOLLMAR, S., SUE, M., KRACHT, L., HASHEMI, P., BHATIA, R., YOSHIMINE, T., DREIER, J. P., DUNN, A. K. & GRAF, R. 2010. Spreading depolarizations cycle around and enlarge focal ischaemic brain lesions. *Brain,* 133**,** 1994-2006.

NAKASHIMA, M., NIWA, M., IWAI, T. & UEMATSU, T. 1999. Involvement of free radicals in cerebral vascular reperfusion injury evaluated in a transient focal cerebral ischemia model of rat. *Free Radic Biol Med,* 26**,** 722-9.

NATH, R., RASER, K. J., STAFFORD, D., HAJIMOHAMMADREZA, I., POSNER, A., ALLEN, H., TALANIAN, R. V., YUEN, P., GILBERTSEN, R. B. & WANG, K. K. 1996. Non-erythroid alpha-spectrin breakdown by calpain and interleukin 1 beta-converting-enzyme-like protease(s) in apoptotic cells: contributory roles of both protease families in neuronal apoptosis. *Biochem J,* 319 (Pt 3)**,** 683-90.

NEDERGAARD, M. 1987. Transient focal ischemia in hyperglycemic rats is associated with increased cerebral infarction. *Brain Res,* 408**,** 79-85.

NEDERGAARD, M., GJEDDE, A. & DIEMER, N. H. 1987. Hyperglycaemia protects against neuronal injury around experimental brain infarcts. *Neurol Res,* 9**,** 241-4.

NEUMAR, R. W., MENG, F. H., MILLS, A. M., XU, Y. A., ZHANG, C., WELSH, F. A. & SIMAN, R. 2001. Calpain activity in the rat brain after transient forebrain ischemia. *Exp Neurol,* 170**,** 27-35.

NIIZUMA, K., ENDO, H. & CHAN, P. H. 2009. Oxidative stress and mitochondrial dysfunction as determinants of ischemic neuronal death and survival. *Journal of Neurochemistry,* 109**,** 133-138.

NINDS 1995. Tissue plasminogen activator for acute ischemic stroke. The National Institute of Neurological Disorders and Stroke rt-PA Stroke Study Group. *N Engl J Med,* 333**,** 1581-7.

NTAIOS, G., PAPAVASILEIOU, V., BARGIOTA, A., MAKARITSIS, K. & MICHEL, P. 2014. Intravenous insulin treatment in acute stroke: a systematic review and meta-analysis of randomized controlled trials. *International Journal of Stroke,* 9**,** 489-493.

O'COLLINS, V. E., MACLEOD, M. R., DONNAN, G. A., HORKY, L. L., VAN DER WORP, B. H. & HOWELLS, D. W. 2006. 1,026 experimental treatments in acute stroke. *Ann Neurol,* 59**,** 467-77.

O'DONNELL, M. J., XAVIER, D., LIU, L., ZHANG, H., CHIN, S. L., RAO-MELACINI, P., RANGARAJAN, S., ISLAM, S., PAIS, P., MCQUEEN, M. J., MONDO, C., DAMASCENO, A., LOPEZ-JARAMILLO, P., HANKEY, G. J., DANS, A. L., YUSOFF, K., TRUELSEN, T., DIENER, H. C., SACCO, R. L., RYGLEWICZ, D., CZLONKOWSKA, A., WEIMAR, C., WANG, X. & YUSUF, S. 2010. Risk factors for ischaemic and intracerebral haemorrhagic stroke in 22 countries (the INTERSTROKE study): a case-control study. *Lancet,* 376**,** 112-23.

O'NEILL, P. A., DAVIES, I., FULLERTON, K. J. & BENNETT, D. 1991. Stress hormone and blood glucose response following acute stroke in the elderly. *Stroke,* 22**,** 842-7.

OSTERGAARD, L., JESPERSEN, S. N., MOURIDSEN, K., MIKKELSEN, I. K., JONSDOTTIR, K. Y., TIETZE, A., BLICHER, J. U., AAMAND, R., HJORT, N., IVERSEN, N. K., CAI, C., HOUGAARD, K. D., SIMONSEN, C. Z., VON WEITZEL-MUDERSBACH, P., MODRAU, B., NAGENTHIRAJA, K., RIISGAARD RIBE, L., HANSEN, M. B., BEKKE, S. L., DAHLMAN, M. G., PUIG, J., PEDRAZA, S., SERENA, J., CHO, T. H., SIEMONSEN, S., THOMALLA, G., FIEHLER, J., NIGHOGHOSSIAN, N. & ANDERSEN, G. 2013. The role of the cerebral capillaries in acute ischemic stroke: the extended penumbra model. *J Cereb Blood Flow Metab,* 33**,** 635-48.

PACIARONI, M., AGNELLI, G., CASO, V., COREA, F., AGENO, W., ALBERTI, A., LANARI, A., MICHELI, S., BERTOLANI, L., VENTI, M., PALMERINI, F., BILLECI, A. M., COMI, G., PREVIDI, P. & SILVESTRELLI, G. 2009. Acute hyperglycemia and early hemorrhagic transformation in ischemic stroke. *Cerebrovasc Dis,* 28**,** 119-23.

PANDOLFI, A., GIACCARI, A., CILLI, C., ALBERTA, M. M., MORVIDUCCI, L., DE FILIPPIS, E. A., BUONGIORNO, A., PELLEGRINI, G., CAPANI, F. & CONSOLI, A. 2001. Acute hyperglycemia and acute hyperinsulinemia decrease plasma fibrinolytic activity and increase plasminogen activator inhibitor type 1 in the rat. *Acta Diabetol,* 38**,** 71-6.

PARSONS, M., LI, T., BARBER, P., YANG, Q., DARBY, D., DESMOND, P., TRESS, B. & DAVIS, S. 2000. Acute Hyperglycaemia in stroke leads to increased brain lactate production and greater final infarct size. *Stroke,* 31**,** 2795-2795.

PARSONS, M. W., BARBER, P. A., DESMOND, P. M., BAIRD, T. A., DARBY, D. G., BYRNES, G., TRESS, B. M. & DAVIS, S. M. 2002. Acute hyperglycemia adversely affects stroke outcome: a magnetic resonance imaging and spectroscopy study. *Ann Neurol,* 52**,** 20-8.

PAXINOS, G. & WATSON, C. 2007. *The Rat Brain in stereotaxic coordinates*, London, Elsevier Inc.

PELLERIN, L. 2010. Food for thought: the importance of glucose and other energy substrates for sustaining brain function under varying levels of activity. *Diabetes Metab,* 36 Suppl 3, S59-63.

PELLERIN, L. & MAGISTRETTI, P. J. 1994. Glutamate uptake into astrocytes stimulates aerobic glycolysis: a mechanism coupling neuronal activity to glucose utilization. *Proc Natl Acad Sci U S A,* 91, 10625-9.

PEPPIATT, C. M., HOWARTH, C., MOBBS, P. & ATTWELL, D. 2006. Bidirectional control of CNS capillary diameter by pericytes. *Nature,* 443, 700-4.

PEREIRA, V. M., GRALLA, J., DAVALOS, A., BONAFÉ, A., CASTAÑO, C., CHAPOT, R., LIEBESKIND, D. S., NOGUEIRA, R. G., ARNOLD, M., SZTAJZEL, R., LIEBIG, T., GOYAL, M., BESSELMANN, M., MORENO, A. & SCHROTH, G. 2013. Prospective, Multi-Centre, Single-Arm Study of Mechanical Thrombectomy using Solitaire FR in Acute Ischemic Stroke-STAR. *Stroke; a journal of cerebral circulation,* 44, 2802-2807.

PETTIGREW, L. C., HOLTZ, M. L., CRADDOCK, S. D., MINGER, S. L., HALL, N. & GEDDES, J. W. 1996. Microtubular proteolysis in focal cerebral ischemia. *J Cereb Blood Flow Metab,* 16, 1189-202.

PETTY, G. W., BROWN, R. D., JR., WHISNANT, J. P., SICKS, J. D., O'FALLON, W. M. & WIEBERS, D. O. 2000. Ischemic stroke subtypes : a population-based study of functional outcome, survival, and recurrence. *Stroke,* 31, 1062-8.

POPP, A., JAENISCH, N., WITTE, O. W. & FRAHM, C. 2009. Identification of ischemic regions in a rat model of stroke. *PLoS One,* 4, e4764.

POPPE, A. Y., MAJUMDAR, S. R., JEERAKATHIL, T., GHALI, W., BUCHAN, A. M., HILL, M. D. & CANADIAN ALTEPLASE FOR STROKE EFFECTIVENESS STUDY, I. 2009. Admission hyperglycemia predicts a worse outcome in stroke patients treated with intravenous thrombolysis. *Diabetes Care,* 32, 617-22.

POWERS, W. J., GRUBB, R. L., JR., DARRIET, D. & RAICHLE, M. E. 1985. Cerebral blood flow and cerebral metabolic rate of oxygen requirements for cerebral function and viability in humans. *J Cereb Blood Flow Metab,* 5, 600-8.

PRADO, R., GINSBERG, M. D., DIETRICH, W. D., WATSON, B. D. & BUSTO, R. 1988. Hyperglycemia increases infarct size in collaterally perfused but not end-arterial vascular territories. *J Cereb Blood Flow Metab,* 8, 186-92.

PULSINELLI, W. A., WALDMAN, S., RAWLINSON, D. & PLUM, F. 1982. Moderate hyperglycemia augments ischemic brain damage: a neuropathologic study in the rat. *Neurology,* 32, 1239-46.

PUTAALA, J., SAIRANEN, T., MERETOJA, A., LINDSBERG, P. J., TIAINEN, M., LIEBKIND, R., STRBIAN, D., ATULA, S., ARTTO, V., RANTANEN, K., SILVONEN, P., PIIRONEN, K., CURTZE, S., HAPPOLA, O., MUSTANOJA, S., PITKANIEMI, J., SALONEN, O., SILVENNOINEN, H., SOINNE, L., KUISMA, M., TATLISUMAK, T. & KASTE, M. 2011. Post-thrombolytic hyperglycemia and 3-month outcome in acute ischemic stroke. *Cerebrovasc Dis,* 31, 83-92.

QUAST, M. J., WEI, J., HUANG, N. C., BRUNDER, D. G., SELL, S. L., GONZALEZ, J. M., HILLMAN, G. R. & KENT, T. A. 1997. Perfusion deficit parallels exacerbation of cerebral ischemia/reperfusion injury in hyperglycemic rats. *J Cereb Blood Flow Metab,* 17, 553-9.

READ, S. J., HIRANO, T., ABBOTT, D. F., MARKUS, R., SACHINIDIS, J. I., TOCHON-DANGUY, H. J., CHAN, J. G., EGAN, G. F., SCOTT, A. M., BLADIN, C. F., MCKAY, W. J. & DONNAN, G. A. 2000. The fate of hypoxic tissue on 18F-

fluoromisonidazole positron emission tomography after ischemic stroke. *Ann Neurol,* 48**,** 228-35.

READ, S. J., HIRANO, T., ABBOTT, D. F., SACHINIDIS, J. I., TOCHON-DANGUY, H. J., CHAN, J. G., EGAN, G. F., SCOTT, A. M., BLADIN, C. F., MCKAY, W. J. & DONNAN, G. A. 1998. Identifying hypoxic tissue after acute ischemic stroke using PET and 18F-fluoromisonidazole. *Neurology,* 51**,** 1617-21.

REHNCRONA, S., HAUGE, H. N. & SIESJO, B. K. 1989. Enhancement of iron-catalyzed free radical formation by acidosis in brain homogenates: differences in effect by lactic acid and CO2. *J Cereb Blood Flow Metab,* 9**,** 65-70.

REID, E. 2012. *An examination of ischaemic penumbra in the spontaneously hypertensive stroke-prone rat (SHRSP) using the MRI perfusion-diffusion mismatch model.* Ph.D., University of Glasgow.

REID, E., GRAHAM, D., LOPEZ-GONZALEZ, M. R., HOLMES, W. M., MACRAE, I. M. & MCCABE, C. 2012. Penumbra detection using PWI/DWI mismatch MRI in a rat stroke model with and without comorbidity: comparison of methods. *J Cereb Blood Flow Metab,* 32**,** 1765-77.

REITH, W., HASEGAWA, Y., LATOUR, L. L., DARDZINSKI, B. J., SOTAK, C. H. & FISHER, M. 1995. Multislice diffusion mapping for 3-D evolution of cerebral ischemia in a rat stroke model. *Neurology,* 45**,** 172-7.

RIBO, M., MOLINA, C., MONTANER, J., RUBIERA, M., DELGADO-MEDEROS, R., ARENILLAS, J. F., QUINTANA, M. & ALVAREZ-SABIN, J. 2005. Acute hyperglycemia state is associated with lower tPA-induced recanalization rates in stroke patients. *Stroke,* 36**,** 1705-9.

ROBINSON, R. G., SHOEMAKER, W. J., SCHLUMPF, M., VALK, T. & BLOOM, F. E. 1975. Effect of experimental cerebral infarction in rat brain on catecholamines and behaviour. *Nature,* 255**,** 332-4.

ROGER 2011. Heart Disease and Stroke Statistics-2011 Update: A Report From the American Heart Association (vol 123, pg e18, 2011). *Circulation,* 124**,** E426-E426.

ROHDE, S., HAEHNEL, S., HERWEH, C., PHAM, M., STAMPFL, S., RINGLEB, P. A. & BENDSZUS, M. 2011. Mechanical thrombectomy in acute embolic stroke: preliminary results with the revive device. *Stroke,* 42**,** 2954-6.

ROSE, S. E., JANKE, A. L., GRIFFIN, M., FINNIGAN, S. & CHALK, J. B. 2004. Improved prediction of final infarct volume using bolus delay-corrected perfusion-weighted MRI: implications for the ischemic penumbra. *Stroke,* 35**,** 2466-71.

ROSENBERG, G. A., ESTRADA, E. Y. & DENCOFF, J. E. 1998. Matrix metalloproteinases and TIMPs are associated with blood-brain barrier opening after reperfusion in rat brain. *Stroke,* 29**,** 2189-2195.

ROSSO, C., ATTAL, Y., DELTOUR, S., HEVIA-MONTIEL, N., LEHERICY, S., CROZIER, S., DORMONT, D., BAILLET, S. & SAMSON, Y. 2011. Hyperglycemia and the fate of apparent diffusion coefficient-defined ischemic penumbra. *AJNR Am J Neuroradiol,* 32**,** 852-6.

ROTHWELL, P. M., COULL, A. J., GILES, M. F., HOWARD, S. C., SILVER, L. E., BULL, L. M., GUTNIKOV, S. A., EDWARDS, P., MANT, D., SACKLEY, C. M., FARMER, A., SANDERCOCK, P. A., DENNIS, M. S., WARLOW, C. P., BAMFORD, J. M. & ANSLOW, P. 2004. Change in stroke incidence, mortality, case-fatality, severity, and risk factors in Oxfordshire, UK from 1981 to 2004 (Oxford Vascular Study). *Lancet,* 363**,** 1925-33.

ROTHWELL, P. M. & WARLOW, C. P. 2005. Timing of TIAs preceding stroke - Time window for prevention is very short. *Neurology,* 64**,** 817-820.

SAHA, J. K., XIA, J., GRONDIN, J. M., ENGLE, S. K. & JAKUBOWSKI, J. A. 2005. Acute hyperglycemia induced by ketamine/xylazine anesthesia in rats: mechanisms and implications for preclinical models. *Exp Biol Med (Maywood),* 230**,** 777-84.

SAKA, O., MCGUIRE, A. & WOLFE, C. 2009. Cost of stroke in the United Kingdom. *Age Ageing,* 38**,** 27-32.

SAN ROMAN, L., OBACH, V., BLASCO, J., MACHO, J., LOPEZ, A., URRA, X., TOMASELLO, A., CERVERA, A., AMARO, S., PERANDREU, J., BRANERA, J., CAPURRO, S., OLEAGA, L. & CHAMORRO, A. 2012. Single-center experience of cerebral artery thrombectomy using the TREVO device in 60 patients with acute ischemic stroke. *Stroke,* 43**,** 1657-9.

SAVER, J. L., SMITH, E. E., FONAROW, G. C., REEVES, M. J., ZHAO, X., OLSON, D. M., SCHWAMM, L. H., COMMITTEE, G. W.-S. S. & INVESTIGATORS 2010. The "golden hour" and acute brain ischemia: presenting features and lytic therapy in >30,000 patients arriving within 60 minutes of stroke onset. *Stroke,* 41**,** 1431-9.

SCHAEFER, P. W., BARAK, E. R., KAMALIAN, S., GHARAI, L. R., SCHWAMM, L., GONZALEZ, R. G. & LEV, M. H. 2008. Quantitative assessment of core/penumbra mismatch in acute stroke: CT and MR perfusion imaging are strongly correlated when sufficient brain volume is imaged. *Stroke,* 39**,** 2986-92.

SCHALLER, B. & GRAF, R. 2004. Cerebral ischemia and reperfusion: The pathophysiologic concept as a basis for clinical therapy. *Journal of Cerebral Blood Flow and Metabolism,* 24**,** 351-371.

SCHAPPERT, T., HIMMEL, H. M. & RAVENS, U. 1992. Differences in cardiodepressant effects of halothane and isoflurane after inotropic stimulation in guinea-pig papillary muscles. *Arch Int Pharmacodyn Ther,* 320**,** 43-55.

SCHMID-ELSAESSER, R., ZAUSINGER, S., HUNGERHUBER, E., BAETHMANN, A. & REULEN, H. J. 1998. A critical reevaluation of the intraluminal thread model of focal cerebral ischemia: evidence of inadvertent premature reperfusion and subarachnoid hemorrhage in rats by laser-Doppler flowmetry. *Stroke,* 29**,** 2162-70.

SCHOCH, K. M., EVANS, H. N., BRELSFOARD, J. M., MADATHIL, S. K., TAKANO, J., SAIDO, T. C. & SAATMAN, K. E. 2012. Calpastatin overexpression limits calpain-mediated proteolysis and behavioral deficits following traumatic brain injury. *Exp Neurol,* 236**,** 371-82.

SCOTT, J. F., ROBINSON, G. M., FRENCH, J. M., O'CONNELL, J. E., ALBERTI, K. G. & GRAY, C. S. 1999a. Glucose potassium insulin infusions in the treatment of acute stroke patients with mild to moderate hyperglycemia: the Glucose Insulin in Stroke Trial (GIST). *Stroke,* 30**,** 793-9.

SCOTT, J. F., ROBINSON, G. M., FRENCH, J. M., O'CONNELL, J. E., ALBERTI, K. G. & GRAY, C. S. 1999b. Prevalence of admission hyperglycaemia across clinical subtypes of acute stroke. *Lancet,* 353**,** 376-7.

SEBE, J. Y., BERSHTEYN, M., HIROTSUNE, S., WYNSHAW-BORIS, A. & BARABAN, S. C. 2013. ALLN rescues an in vitro excitatory synaptic transmission deficit in Lis1 mutant mice. *J Neurophysiol,* 109**,** 429-36.

SESHADRI, S., BEISER, A., KELLY-HAYES, M., KASE, C. S., AU, R., KANNEL, W. B. & WOLF, P. A. 2006. The lifetime risk of stroke: estimates from the Framingham Study. *Stroke,* 37**,** 345-50.

SEUBERT, P., LARSON, J., OLIVER, M., JUNG, M. W., BAUDRY, M. & LYNCH, G. 1988. Stimulation of NMDA receptors induces proteolysis of spectrin in hippocampus. *Brain Res,* 460**,** 189-94.

SHAH, G. N., MOROFUJI, Y., BANKS, W. A. & PRICE, T. O. 2013. High glucose-induced mitochondrial respiration and reactive oxygen species in mouse cerebral pericytes is reversed by pharmacological inhibition of mitochondrial carbonic anhydrases: Implications for cerebral microvascular disease in diabetes. *Biochem Biophys Res Commun,* 440**,** 354-8.

SHARDLOW, E. & JACKSON, A. 2011. Cerebral blood flow and intracranial pressure. *Anaesthesia & Intensive Care Medicine,* 12**,** 220-223.

SHEN, Q., MENG, X., FISHER, M., SOTAK, C. H. & DUONG, T. Q. 2003. Pixel-by-pixel spatiotemporal progression of focal ischemia derived using quantitative perfusion and diffusion imaging. *J Cereb Blood Flow Metab,* 23**,** 1479-88.

SHIMOYAMA, T., KIMURA, K., UEMURA, J., SAJI, N. & SHIBAZAKI, K. 2014. Elevated glucose level adversely affects infarct volume growth and neurological deterioration in non-diabetic stroke patients, but not diabetic stroke patients. *Eur J Neurol,* 21**,** 402-10.

SHUAIB, A., BUTCHER, K., MOHAMMAD, A. A., SAQQUR, M. & LIEBESKIND, D. S. 2011. Collateral blood vessels in acute ischaemic stroke: a potential therapeutic target. *Lancet Neurol,* 10**,** 909-21.

SIEMKOWICZ, E., HANSEN, A. J. & GJEDDE, A. 1982. Hyperglycemic ischemia of rat brain: the effect of post-ischemic insulin on metabolic rate. *Brain Res,* 243**,** 386-90.

SIESJO, B. K., KATSURA, K. I., KRISTIAN, T., LI, P. A. & SIESJO, P. 1996. Molecular mechanisms of acidosis-mediated damage. *Acta Neurochir Suppl,* 66**,** 8-14.

SIMAN, R., NOSZEK, J. C. & KEGERISE, C. 1989. Calpain I activation is specifically related to excitatory amino acid induction of hippocampal damage. *J Neurosci,* 9**,** 1579-90.

SLIVKA, A. P. 1991. Hypertension and Hyperglycemia in Experimental Stroke. *Brain Res,* 562**,** 66-70.

SMITH, P. K., KROHN, R. I., HERMANSON, G. T., MALLIA, A. K., GARTNER, F. H., PROVENZANO, M. D., FUJIMOTO, E. K., GOEKE, N. M., OLSON, B. J. & KLENK, D. C. 1985. Measurement of protein using bicinchoninic acid. *Anal Biochem,* 150**,** 76-85.

SMOLOCK, A. R., MISHRA, G., EGUCHI, K., EGUCHI, S. & SCALIA, R. 2011. Protein kinase C upregulates intercellular adhesion molecule-1 and leukocyte-endothelium interactions in hyperglycemia via activation of endothelial expressed calpain. *Arterioscler Thromb Vasc Biol,* 31**,** 289-96.

SOBESKY, J., ZARO WEBER, O., LEHNHARDT, F. G., HESSELMANN, V., NEVELING, M., JACOBS, A. & HEISS, W. D. 2005. Does the mismatch match the penumbra? Magnetic resonance imaging and positron emission tomography in early ischemic stroke. *Stroke,* 36**,** 980-5.

SORIMACHI, H., ISHIURA, S. & SUZUKI, K. 1997. Structure and physiological function of calpains. *Biochem J,* 328 (Pt 3)**,** 721-32.

STROKE.ORG.UK 2015. State of the Nation Stroke Statistics - January 2015.

STRONG, A. J., SMITH, S. E., WHITTINGTON, D. J., MELDRUM, B. S., PARSONS, A. A., KRUPINSKI, J., HUNTER, A. J. & PATEL, S. 2000. Factors influencing the frequency of fluorescence transients as markers of peri-infarct depolarizations in focal cerebral ischemia. *Stroke,* 31**,** 214-221.

SUGAWARA, T. & CHAN, P. H. 2003. Reactive oxygen radicals and pathogenesis of neuronal death after cerebral ischemia. *Antioxid Redox Signal,* 5**,** 597-607.

SWANSON, R. A., MORTON, M. T., TSAO-WU, G., SAVALOS, R. A., DAVIDSON, C. & SHARP, F. R. 1990. A semiautomated method for measuring brain infarct volume. *J Cereb Blood Flow Metab,* 10**,** 290-3.

SYMON, L., LASSEN, N. A., ASTRUP, J. & BRANSTON, N. M. 1977. Thresholds of ischaemia in brain cortex. *Adv Exp Med Biol,* 94**,** 775-82.

TAGAMI, M., NARA, Y., KUBOTA, A., FUJINO, H. & YAMORI, Y. 1990. Ultrastructural-Changes in Cerebral Pericytes and Astrocytes of Stroke-Prone Spontaneously Hypertensive Rats. *Stroke,* 21**,** 1064-1071.

TAMURA, A., GRAHAM, D. I., MCCULLOCH, J. & TEASDALE, G. M. 1981a. Focal cerebral ischaemia in the rat: 1. Description of technique and early neuropathological consequences following middle cerebral artery occlusion. *J Cereb Blood Flow Metab,* 1**,** 53-60.

TAMURA, A., GRAHAM, D. I., MCCULLOCH, J. & TEASDALE, G. M. 1981b. Focal cerebral ischaemia in the rat: 2. Regional cerebral blood flow determined by [14C]iodoantipyrine autoradiography following middle cerebral artery occlusion. *J Cereb Blood Flow Metab,* 1**,** 61-9.

TAN, S., ZHI, P. K., LUO, Z. K. & SHI, J. 2015. Severe instead of mild hyperglycemia inhibits neurogenesis in the subventricular zone of adult rats after transient focal cerebral ischemia. *Neuroscience,* 303**,** 138-48.

TANG, X. N., CAIRNS, B., KIM, J. Y. & YENARI, M. A. 2012. NADPH oxidase in stroke and cerebrovascular disease. *Neurological Research,* 34**,** 338-345.

TARR, D. 2012. *Imaging the effects of acute hyperglycaemia on early ischaemic injury using MRI in an experimental stroke model*. Ph.D., University of Glasgow

TARR, D., GRAHAM, D., ROY, L. A., HOLMES, W. M., MCCABE, C., MHAIRI MACRAE, I., MUIR, K. W. & DEWAR, D. 2013. Hyperglycemia accelerates apparent diffusion coefficient-defined lesion growth after focal cerebral ischemia in rats with and without features of metabolic syndrome. *J Cereb Blood Flow Metab,* 33**,** 1556-63.

TOUNG, T. K., HURN, P. D., TRAYSTMAN, R. J. & SIEBER, F. E. 2000. Estrogen decreases infarct size after temporary focal ischemia in a genetic model of type 1 diabetes mellitus. *Stroke,* 31**,** 2701-6.

TOWNSEND, N., WILLIAMS, J., BHATNAGAR, P., WICKRAMASINGHE, K. & RAYNER, M. 2014. *Cardiovascular disease statistics,* London, British Heart Foundation.

TRACEY, F., CRAWFORD, V. L., LAWSON, J. T., BUCHANAN, K. D. & STOUT, R. W. 1993. Hyperglycaemia and mortality from acute stroke. *Q J Med,* 86**,** 439-46.

TRACEY, F. & STOUT, R. W. 1994. Hyperglycemia in the acute phase of stroke and stress response. *Stroke,* 25**,** 524-5.

TREADWELL, S. D. & THANVI, B. 2010. Malignant middle cerebral artery (MCA) infarction: pathophysiology, diagnosis and management. *Postgraduate Medical Journal,* 86**,** 235-242.

TRUELSEN, T., PIECHOWSKI-JOZWIAK, B., BONITA, R., MATHERS, C., BOGOUSSLAVSKY, J. & BOYSEN, G. 2006. Stroke incidence and prevalence in Europe: a review of available data. *Eur J Neurol,* 13**,** 581-98.

TSURUTA, R., FUJITA, M., ONO, T., KODA, Y., KOGA, Y., YAMAMOTO, T., NANBA, M., SHITARA, M., KASAOKA, S., MARUYAMA, I., YUASA, M. & MAEKAWA, T. 2010. Hyperglycemia enhances excessive superoxide anion radical generation, oxidative stress, early inflammation, and endothelial injury in forebrain ischemia/reperfusion rats. *Brain Res,* 1309**,** 155-63.

URABE, T., WATADA, H., OKUMA, Y., TANAKA, R., UENO, Y., MIYAMOTO, N., TANAKA, Y., HATTORI, N. & KAWAMORI, R. 2009. Prevalence of abnormal

glucose metabolism and insulin resistance among subtypes of ischemic stroke in Japanese patients. *Stroke,* 40**,** 1289-95.

UYTTENBOOGAART, M., KOCH, M. W., STEWART, R. E., VROOMEN, P. C., LUIJCKX, G. J. & DE KEYSER, J. 2007. Moderate hyperglycaemia is associated with favourable outcome in acute lacunar stroke. *Brain,* 130**,** 1626-30.

VAN DER WORP, H. B., DE HAAN, P., MORREMA, E. & KALKMAN, C. J. 2005. Methodological quality of animal studies on neuroprotection in focal cerebral ischaemia. *J Neurol,* 252**,** 1108-14.

VAN KOOTEN, F., HOOGERBRUGGE, N., NAARDING, P. & KOUDSTAAL, P. J. 1993. Hyperglycemia in the acute phase of stroke is not caused by stress. *Stroke,* 24**,** 1129-32.

VANCHERI, F., CURCIO, M., BURGIO, A., SALVAGGIO, S., GRUTTADAURIA, G., LUNETTA, M. C., DOVICO, R. & ALLETTO, M. 2005. Impaired glucose metabolism in patients with acute stroke and no previous diagnosis of diabetes mellitus. *QJM,* 98**,** 871-8.

VAZQUEZ, L. A., AMADO, J. A., GARCIA-UNZUETA, M. T., QUIRCE, R., JIMENEZ-BONILLA, J. F., PAZOS, F., PESQUERA, C. & CARRIL, J. M. 1999. Decreased plasma endothelin-1 levels in asymptomatic type I diabetic patients with regional cerebral hypoperfusion assessed by Spect. *J Diabetes Complications,* 13**,** 325-31.

VENABLES, G. S., MILLER, S. A., GIBSON, G., HARDY, J. A. & STRONG, A. J. 1985. The effects of hyperglycaemia on changes during reperfusion following focal cerebral ischaemia in the cat. *J Neurol Neurosurg Psychiatry,* 48**,** 663-9.

WAGNER, K. R., KLEINHOLZ, M., DE COURTEN-MYERS, G. M. & MYERS, R. E. 1992. Hyperglycemic versus normoglycemic stroke: topography of brain metabolites, intracellular pH, and infarct size. *J Cereb Blood Flow Metab,* 12**,** 213-22.

WALI, B., ISHRAT, T., ATIF, F., HUA, F., STEIN, D. G. & SAYEED, I. 2012. Glibenclamide Administration Attenuates Infarct Volume, Hemispheric Swelling, and Functional Impairments following Permanent Focal Cerebral Ischemia in Rats. *Stroke Res Treat,* 2012**,** 460909.

WANG, Q., TANG, X. N. & YENARI, M. A. 2007. The inflammatory response in stroke. *Journal of Neuroimmunology,* 184**,** 53-68.

WANG, Z., LUO, W., LI, P., QIU, J. & LUO, Q. 2008. Acute hyperglycemia compromises cerebral blood flow following cortical spreading depression in rats monitored by laser speckle imaging. *J Biomed Opt,* 13**,** 064023.

WARACH, S., PETTIGREW, L. C., DASHE, J. F., PULLICINO, P., LEFKOWITZ, D. M., SABOUNJIAN, L., HARNETT, K., SCHWIDERSKI, U. & GAMMANS, R. 2000. Effect of citicoline on ischemic lesions as measured by diffusion-weighted magnetic resonance imaging. Citicoline 010 Investigators. *Ann Neurol,* 48**,** 713-22.

WARLOW, C., SUDLOW, C., DENNIS, M., WARDLAW, J. & SANDERCOCK, P. 2003. Stroke. *Lancet,* 362**,** 1211-1224.

WEI, J., COHEN, D. M. & QUAST, M. J. 2003. Effects of 2-deoxy-d-glucose on focal cerebral ischemia in hyperglycemic rats. *J Cereb Blood Flow Metab,* 23**,** 556-64.

WEI, J., HUANG, N. C. & QUAST, M. J. 1997. Hydroxyl radical formation in hyperglycemic rats during middle cerebral artery occlusion/reperfusion. *Free Radic Biol Med,* 23**,** 986-95.

WEI, J. & QUAST, M. J. 1998. Effect of nitric oxide synthase inhibitor on a hyperglycemic rat model of reversible focal ischemia: detection of

excitatory amino acids release and hydroxyl radical formation. *Brain Res,* 791**,** 146-56.

WEIR, C. J., MURRAY, G. D., DYKER, A. G. & LEES, K. R. 1997. Is hyperglycaemia an independent predictor of poor outcome after acute stroke? Results of a long term follow up study. *British Medical Journal,* 314**,** 1303-1306.

WHO 1988. The World Health Organization MONICA Project (monitoring trends and determinants in cardiovascular disease): a major international collaboration. WHO MONICA Project Principal Investigators. *J Clin Epidemiol,* 41**,** 105-14.

WILLIAMS, D. S., DETRE, J. A., LEIGH, J. S. & KORETSKY, A. P. 1992. Magnetic resonance imaging of perfusion using spin inversion of arterial water. *Proc Natl Acad Sci U S A,* 89**,** 212-6.

WINTERMARK, M., FLANDERS, A. E., VELTHUIS, B., MEULI, R., VAN LEEUWEN, M., GOLDSHER, D., PINEDA, C., SERENA, J., VAN DER SCHAAF, I., WAAIJER, A., ANDERSON, J., NESBIT, G., GABRIELY, I., MEDINA, V., QUILES, A., POHLMAN, S., QUIST, M., SCHNYDER, P., BOGOUSSLAVSKY, J., DILLON, W. P. & PEDRAZA, S. 2006. Perfusion-CT assessment of infarct core and penumbra: receiver operating characteristic curve analysis in 130 patients suspected of acute hemispheric stroke. *Stroke,* 37**,** 979-85.

WISZNIEWSKA, M., NIEWADA, M. & CZLONKOWSKA, A. 2011. Sex Differences in Risk Factor Distribution, Severity, and Outcome of Ischemic Stroke. *Acta Clinica Croatica,* 50**,** 21-28.

WON, S. J., TANG, X. N., SUH, S. W., YENARI, M. A. & SWANSON, R. A. 2011. Hyperglycemia promotes tissue plasminogen activator-induced hemorrhage by Increasing superoxide production. *Ann Neurol,* 70**,** 583-90.

YEMISCI, M., GURSOY-OZDEMIR, Y., VURAL, A., CAN, A., TOPALKARA, K. & DALKARA, T. 2009. Pericyte contraction induced by oxidative-nitrative stress impairs capillary reflow despite successful opening of an occluded cerebral artery. *Nat Med,* 15**,** 1031-7.

YONEDA, Y., TOKUI, K., HANIHARA, T., KITAGAKI, H., TABUCHI, M. & MORI, E. 1999. Diffusion-weighted magnetic resonance imaging: detection of ischemic injury 39 minutes after onset in a stroke patient. *Ann Neurol,* 45**,** 794-7.

YONG, M. & KASTE, M. 2008. Dynamic of hyperglycemia as a predictor of stroke outcome in the ECASS-II trial. *Stroke,* 39**,** 2749-2755.

YURA, S. 1991. Effects of hyperglycemia on ischemic brain damage, local cerebral blood flow and ischemic cerebral edema. *Hokkaido Igaku Zasshi,* 66**,** 1-15.

ZASSLOW, M. A., PEARL, R. G., SHUER, L. M., STEINBERG, G. K., LIEBERSON, R. E. & LARSON, C. P., JR. 1989. Hyperglycemia decreases acute neuronal ischemic changes after middle cerebral artery occlusion in cats. *Stroke,* 20**,** 519-23.

ZHU, C. Z. & AUER, R. N. 2004. Optimal blood glucose levels while using insulin to minimize the size of infarction in focal cerebral ischemia. *J Neurosurg,* 101**,** 664-8.